DISS. ETH NO. 24150

PERTURBATION THEORY FOR STEADY-STATE LAPLACIAN MODELS OF BIOLOGICAL SYSTEMS

A thesis submitted to attain the degree of

DOCTOR OF SCIENCES of ETH ZURICH

(Dr. sc. ETH Zurich)

presented by

PENCHO STEFANOV YORDANOV

M. Sc. in Molecular Life Science, Jacobs University Bremen, Germany

born on 12.10.1987

citizen of
the Republic of Bulgaria

accepted on the recommendation of

Prof. Dr. Jörg Stelling, examiner
Prof. Dr. Mustafa Khammash, co-examiner
Prof. Dr. Jeremy Gunawardena, co-examiner

2017

Summary

A fundamental problem in fields such as systems biology and pharmacology is to determine how biological systems change their dose-response behaviour upon external or natural perturbations. A comprehensive understanding of this relation through the effects of topologies, reactions, and parameters on the response is invaluable when designing, analysing, and identifying biological processes. However, the characterisation of said relation is frequently challenged by the complexity, topological and parametric uncertainty, multiple levels of organisation, and heterogeneity inherent to biology. We address these challenges through the lens of the classical steady-state Laplacian models, which are mathematical models with only zero and (pseudo) first order mass-action reactions. Laplacian models have found countless applications in biology since, frequently, they can be obtained from non-linear models using time-scale separation, and due to their analytical tractability, i.e. that a closed form of their steady-states always exists. Despite their apparent simplicity, Laplacian models suffer from the (super) exponential growth of the size of their steady-state expressions that makes the symbolic analysis of models of even moderate sizes practically impossible.

This thesis develops theory and methods to study how perturbations in steady-state Laplacian models of biological systems translate to dose-response relations, while accounting for biological complexity, uncertainty, and heterogeneity.

First, in Chapter 3, we lay the theoretical groundwork of the thesis by investigating the factorisation properties of an important class of polynomials, the so called Kirchhoff polynomials, which link the topology of Laplacian models, expressed through directed graphs, to their symbolic steady-state expressions. We reveal the intimate connection between combinatorial properties of the digraph representation of Laplacian models and its corresponding Kirchhoff polynomial. Specifically, we devise digraph decomposition rules corresponding to factorisation steps of the Kirchhoff polynomial and provide necessary and sufficient primality conditions for the resulting factors expressed through connectivity properties of the decomposed components. As a result we propose a linear time algorithm for the prime factorisation of Kirchhoff polynomials based on directed graph connectivity properties.

In Chapter 4 we employ the prime factorisation algorithm to develop a framework for the efficient manipulation and generation of expressions of Kirchhoff polynomials, which result from steady-state derivations for Laplacian models. To manipulate such expressions we transform them to a coarse-grained representation which can easily be symbolically handled. To generate such expressions we propose two heuristic algorithms producing compressed Kirchhoff polynomials. Thereby we demonstrate that, contrary to prior belief, Kirchhoff polynomial generation is not restricted by the (super) exponentially growing size of the poly-

nomials but, rather, by the connectivity properties of their corresponding directed graphs.

In Chapter 5 we proceed to study the relative differences between dose-response curves produced by a reference and a perturbed steady-state Laplacian model. We exploit the connectivity properties of the directed graph representation of Laplacian models to identify equivalence classes of models, reliably reject improbable hypothetical models, and determine how perturbations in topology and parameters affect the dose-response, all in a parameter-free manner.

Finally, in Chapter 6 we formulate a framework to search for a minimal model of interferon type I differential signalling. The framework accounts for topological uncertainty by investigating an ensemble of hypothetical models and ranking them with respect to experimental dose-response data using Bayesian model comparison, and for parametric uncertainty by employing Bayesian parameter inference. Each considered model is a simple multi-scale threshold model that incorporates at its core a steady-state Laplacian submodel determining the number of active interferon receptors resulting from interferon stimulation, includes receptor number cell-to-cell variability, and produces the proportion of alive cells in a population resulting from interferon-induced activities. As a result we demonstrate that the minimal sufficient mechanisms explaining differential signalling are receptor assembly, receptor endocytosis and recycling, and inhibition by the factor USP18.

Zusammenfassung

Ein grundlegendes Problem in Fachgebieten wie der Systembiologie und der Pharmakologie ist es zu bestimmen, wie biologische Systeme ihr Dosis-Wirkungs-Verhalten aufgrund äußerer oder natürlicher Störungen ändern. Ein umfassendes Verständnis dieser Beziehung durch den Einfluss von Topologien, Reaktionen und Parametern ist von unschätzbarem Wert, wenn es darum geht, biologische Prozesse zu entwerfen, zu analysieren und zu identifizieren. Jedoch wird die Charakterisierung dieser Beziehung häufig durch die Komplexität, die topologische und parametrische Unsicherheit, die verschiedenen Organisationsstufen und die der Biologie innewohnende Heterogenität in Frage gestellt. Wir begegnen diesen Herausforderungen durch Anwendung von klassischen, stationären Laplace-Modellen, welche mathematischen Modelle mit Massenwirkungsreaktionen von nullter und (pseudo-) erster Ordnung sind. Laplace-Modelle haben unzählige Anwendungen in der Biologie gefunden, da sie häufig aus nichtlinearen Modellen unter Verwendung der Zeitskalen-Trennung erhalten werden können, und aufgrund ihrer analytischen Lösbarkeit, d.h. dass eine geschlossene Form ihres einzigen stationären Zustands immer existiert. Trotz ihrer scheinbaren Einfachheit leiden Laplace-Modelle an (super-) exponentiell wachsenden Steady-State-Ausdrücken, was die symbolische Analyse von Modellen ab moderater Größe praktisch unmöglich macht.

Diese Doktorarbeit entwickelt Theorie und Methoden, um zu untersuchen, wie sich Perturbationen in Steady-State Laplace-Modelle von biologischen Systemen in Dosis-Wirkungs-Beziehungen übersetzen, unter Berücksichtigung der biologischen Komplexität, Ungewissheit und Heterogenität.

Zunächst werden im Kapitel 3 die theoretischen Grundlagen der Arbeit geschaffen, indem wir die Faktorisierungseigenschaften einer wichtigen Klasse von Polynomen untersuchen, die sogenannten Kirchhoff-Polynome, die die Topologie der Laplace-Modelle, dargestellt durch gerichtete Graphen, mit ihren symbolischen Steady-State-Ausdrücken verknüpfen. Wir zeigen die enge Verbindung zwischen kombinatorischen Eigenschaften der Darstellung von Laplace-Modellen als gerichteten Graphen und dementsprechendem Kirchhoff-Polynom. Insbesondere entwickeln wir Zerlegungsregeln für gerichtete Graphen, die den Faktorisierungsschritten des Kirchhoff-Polynoms entsprechen, und liefern notwendige und hinreichende Unreduzierbarkeitbedingungen für die resultierenden Faktoren, die durch die zusammenhängenden Eigenschaften der zersetzten Komponenten repräsentiert werden. Als Ergebnis schlagen wir einen linearen Zeitalgorithmus für die Primfaktorisierung von Kirchhoff-Polynomen basierend auf gerichteten Graphenzusammenhangseigenschaften vor.

Im Kapitel 4 verwenden wir den Primfaktorisierungsalgorithmus, um ein Rahmenkonzept für die effiziente Manipulation und Erzeugung von Ausdrücken von

Kirchhoff-Polynomen zu entwickeln, die aus stationären Ableitungen für Laplace-Modelle resultieren. Um solche Ausdrücke zu manipulieren, verwandeln wir sie in eine grobkörnige Darstellung, die leicht symbolisch gehandhabt werden kann. Um solche Ausdrücke zu generieren, schlagen wir zwei heuristische Algorithmen vor, die komprimierte Kirchhoff-Polynome erzeugen. Dabei zeigen wir, dass die Kirchhoff-Polynomerzeugung, entgegen der bisherigen überzeugung, nicht durch die (super-) exponentiell wachsende Größe der Polynome, sondern durch die Konnektivitätseigenschaften ihrer entsprechenden gerichteten Graphen beschränkt ist.

Im Kapitel 5 werden die relativen Unterschiede zwischen den Dosis-Wirkungs-Kurven, die durch ein Referenz- und ein perturbiertes Steady-State Laplace-Modell erzeugt werden, untersucht. Wir nutzen die Konnektivitätseigenschaften der gerichteten Graphendarstellung von Laplace-Modellen, um äquivalenzklassen von Modellen zu identifizieren, unwahrscheinliche, hypothetische Modelle zuverlässig zurückzuweisen und zu bestimmen, wie Perturbationen von der Topologie und den Parametern die Dosisantwort beeinflussen, und zwar in einer parameter-freien Weise.

Schließlich formulieren wir im Kapitel 6 ein Rahmenkonzept, um nach einem minimalen Modell der Interferon-Typ-I-Differentialsignalisierung zu suchen. Das Modell berücksichtigt topologische Unsicherheit, indem er ein Ensemble von hypothetischen Modellen untersucht und in Bezug auf experimentelle Dosis-Wirkungs-Daten unter Verwendung des Bayes'schen Modellvergleichs und für parametrische Unsicherheit unter Verwendung der Bayes'schen Parameter-Schlußfolgerung klassifiziert. Jedes betrachtete Modell ist ein einfaches mehrstufiges Schwellenmodell, das in seinem Kern ein stationäres Laplace-Submodell enthält, das die Anzahl der aktiven Interferonrezeptoren bei der Interferonstimulation bestimmt, Zell-zu-Zell-Variabilität der Rezeptorenzahl einschließt und den aus Interferon-induzierten Aktivitäten resultierten Anteil der Lebendzellen in einer Population produziert. Als Ergebnis zeigen wir, dass die minimal ausreichenden Mechanismen, die die differentielle Signalisierung erklären, die Rezeptorzusammenstellung, die Rezeptorendozytose und Recycling und die Inhibition durch den Faktor USP18 sind.

Acknowledgements

I dedicate this thesis to my parents Sonya and Stefan, my sisters Yana and Dobromira, my grandparents Yana, Pencho, Dobrina, and Panayot, and my better half Kremena. I heartily thank them for their unfailing support, love, and encouragement to follow my dreams.

I am sincerely grateful to Jörg Stelling for his excellent supervision, personal and professional support, and the opportunity to conduct research in his amazing group. I admire his problem solving abilities and strong work ethic, which have inspired me throughout my doctoral studies. I also highly appreciate the freedom he granted me in developing my own ideas paving my way to become an independent researcher.

I would like to thank Mustafa Khammash and Jeremy Gunawardena for being part of my examination committee, expressing interest in my work, and for the many useful suggestions and comments.

I am particularly grateful to Irene Otero-Muras for supporting, teaching, and encouraging me as a young doctoral student, introducing me to the whole new world of parameter-free approaches to study biological systems, and involving me in her exciting projects.

My sincere thanks goes to Przemysław Uznański and Matúš Mihalák for their enthusiasm to collaborate, immense professionalism, and revealing to me gracious approaches to combinatorial problems.

I wish to express my warm and sincere thanks to all past and current members of the Computational Systems Biology (CSB) group. Throughout the many group meetings, hours in the office, and out in the city they have given me advice, proposed ideas, and have nourished a cheerful and friendly atmosphere. In particular I would like to acknowledge Alberto Giovanni Busetto, Charlotte Ramon, Claude Lormeau, Eleni Karamasioti, Fabian Rudolf, Hans-Michael Kaltenbach, Janina Linnik, Lekshmi Dharmarajan, Lukas Widmer, Mikael Sunnaker, Mikolaj Rybinski, Moritz Lang, Nico Gorbach, Sotiris Dimopoulos, Stefan Bauer, and Thomas Liphardt for insightful discussions concerning my projects. I would also like to thank Sibylle Wohlgemuth and Maurice Langhinrichs for the pleasure to be involved in their supervision.

I gratefully acknowledge financial support from the EU FP7 project IFNAction and all members of the project for stimulating discussions and insight into interferon signalling.

I am also thankful to the Zurich Life Science Graduate School for allowing me to participate in courses and retreats, where I had the honour to meet many amazing and clever people.

I feel very fortunate to have incredible friends in Zurich, in Bulgaria, and around the word, who support me and make my life outside the workplace enjoyable. I

am thankful to Arun Shivanandan, Boris Espinoza-Kalchev, Deyan Ginev, Desislava Valkanova, Emilia Boiadjieva, Georgi Smilyanov, Hristo Stoev, Iva Lelios, Milena Tsenova, Pavlin Mavrodiev, Peter Ivanov, Petia Doytcheva, Rayna Petkova, Rossen Slavov, Theodora Topliyski, Thomas Knöpfel, Tyanko Alexiev, Vladimir Petrov, and Vladimir Vuksanovic for making my PhD student years pleasurable and exciting.

Last, but not least, I am extremely grateful to be a part of the "Ludi Mladi" Bulgarian folk dance group that has been my second family for the last years.

Zurich, January 23, 2017

Pencho Yordanov

Contents

1

Introduction

1.1 Structure to Function Mapping in Biology

One of the most fundamental tenets in biology is that structure and function are tightly coupled. This notion coheres with the principles of evolution that, in general, biological structures are adaptations, that is, they have evolved over time through the process of natural selection to perform functions necessary for survival. The intertwining of structure and function is manifested at all levels of biological self-organization, from the molecular, through the cellular, organismic, and population level, to the ecosystem level. There are plenty of examples in literature demonstrating how molecular structure determines function, one of the classics being the binding of oxygen to haemoglobin. Particularly, upon oxygenation the structure of haemoglobin is stabilised to a high affinity state for subsequent oxygen binding which results in a cooperative behaviour and ultimately to efficient oxygen transportation from the lungs to peripheral tissues (Fersht, 1999). Characterising the causal relationship between structure and function on the molecular level as in the example of haemoglobin is a significant challenge by itself. However, climbing up the ladder of biological organisation, we need to investigate structure and function on a systems level, defined by interactions and dynamics rather than molecular parts in isolation (Kitano, 2002). In doing so we encounter a plethora of challenges, a central one being *emergence* of function, which is best characterised by the famous quote from Aristotle – "The whole is greater than the sum of its parts". More precisely, this is the phenomenon in which smaller and simpler entities combine through interactions to non-trivially produce a larger entity capable of a functionality much richer than the functionalities of the individual parts. An instance of interest for this thesis are biochemical signalling networks, which are composed of a network of interacting molecules with various binding and catalytic properties, but exhibit higher level functions such as integration of signals across multiple time scales and generation of distinct outputs depending on input type, strength, and duration (Bhalla & Iyengar, 1999).

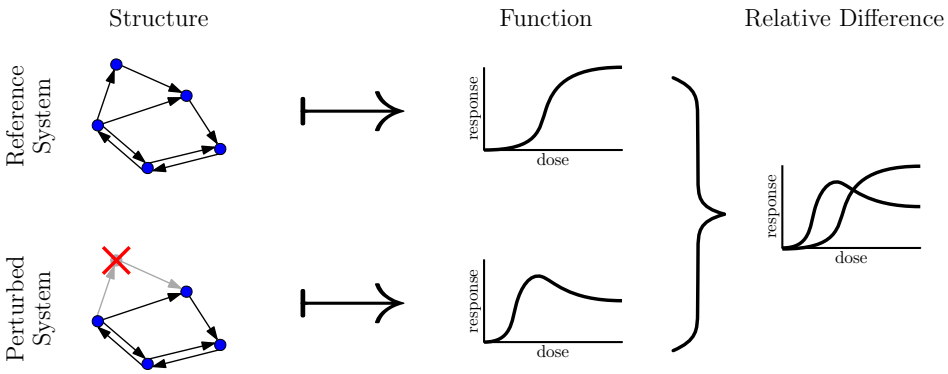

Figure 1.1: The typical process of structure to function mapping in systems biology. The response of a perturbed system is compared to the response of a reference system to determine relative functional changes revealing the functional role of the perturbed entity.

The art of investigating biochemical signalling networks using the system-level approach, as is aimed in the field of *systems biology* (Kitano, 2002), is to thoroughly understand the intimate relation between topology and dynamics of molecular interactions (which we define in this thesis as "structure"), and the signal processing functions they accomplish. The detailed characterisation of this relation would not only quench our thirst for knowledge but also provide means to control, design, and repair signalling networks in our quest to treat complex diseases. The essential tool to study and reverse-engineer structure-function relationships is that of system *perturbation* as illustrated in Figure 1.1. For instance, a biochemical system can be perturbed by changing its environmental stimuli, knocking down a gene, inhibiting a reaction with a drug, or considering the disease state of a cell. Such alterations could lead to a modified function which, when contrasted to the response of the unperturbed system (also called reference), helps us build-up the structure-function mapping from context-specific relative responses. Comparisons between reference and perturbed states are not only a figment of human experimentation but can also serve a "natural" purpose. Notably, cells perform such fold-change comparisons to reliably trigger vital responses despite cellular noise as it has been shown for Wnt signalling (Goentoro & Kirschner, 2009).

1.2 Major Challenges

A single perturbation experiment is usually not sufficient to elucidate the complex structure-function relationships in biochemical systems. Rather, a detailed characterisation requires, as illustrated in Figure 1.2, an iterative process in which the (perturbed) function of a biological entity is measured to produce data, whose interpretation can be used to design new (perturbation) experiments, and so forth, until satisfactory understanding of the structure-function mapping is obtained

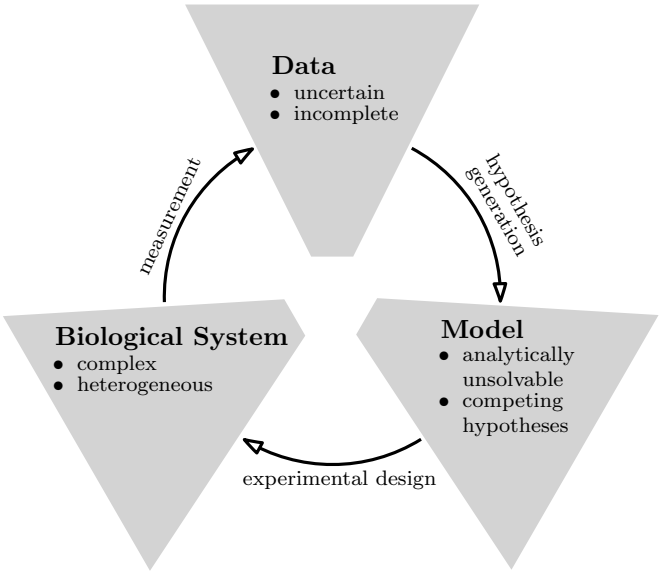

Figure 1.2: The main phases and challenges of the iterative process to gain understanding of structure-function relationships in biological systems.

(Kreutz & Timmer, 2009; Busetto et al., 2013; Molinelli et al., 2013). This process is riddled with challenges due to the inherent complexity of biological systems and their multiple levels of organisation. Namely, complex biochemical networks comprise a multitude of different components which are coupled through dynamic interactions. Additionally, the abundance of components among single cells in a population could greatly vary due to noise of intrinsic or extrinsic origin (Elowitz et al., 2002). With the aid of modern data acquisition techniques, these characteristics of biological systems translate to vast amounts of data. However, the data is generally incomplete since, at present time, many of the components and interactions cannot be measured, and are uncertain due to measurement errors and molecular noise.

To extract the essence of such complex, yet incomplete and uncertain data, and to understand the structural mechanisms that generated it requires adequate mathematical models and formalisms. However, model building and analysis are directly influenced by the quality and quantity of available data. For example, multiple model hypotheses have to be considered to account for incomplete and uncertain data sets. It is not always clear how to generate these hypotheses and frequently they are set up depending on the subjective understanding of the modeller. Another challenge, falls into the domain of model selection, that is, choosing the model hypothesis which offers the best description of a given biological system. Accomplishing this is often computationally expensive and in many model selection approaches heavily depends on the complexity of the likelihood function (a function measuring the support for a model provided by the data for a set of

parameter values) (Kirk et al., 2013). Further, large and complex data sets lead to models which are too complicated for analysis in closed form and heavily rely on computer simulations, which additionally complicates the comparison of the competing hypotheses (Toni & Stumpf, 2010). Large dynamical models of biochemical signalling networks also suffer from a large number of free parameters, and a combinatorial explosion in the number of states they incorporate (Danos et al., 2007). This complicates even their numerical analysis due to the computationally costly exploration of high-dimensional parameter spaces with complex geometry that is necessary for model selection and parameter inference (Zamora-Sillero et al., 2011).

1.3 Context and Motivation

This thesis is devoted to the study of the relationship between biochemical networks' structure, expressed through steady-state models containing a set of biochemical species that interact through reactions with exclusively zero and (pseudo) first order mass-action kinetics (Poland, 1989), which we call *steady-state Laplacian models*, and the dose-response relationships they produce. For instance, dose-response relationships in this context are generated when a ligand with constant concentration modulates the rate constant of a reaction which leads to changes in the steady-state concentration of a biochemical species.

Laplacian models have a long history of success stories staring from the early years of studying enzyme kinetics, when King & Altman (1956) introduced their structural method to derive rate-laws of enzyme-catalysed reactions, going though various applications for allosteric enzymes, G-protein coupled receptors, ion channels, post-translational modification (Gunawardena, 2012), and lasting until the present day, notably in studying non-equilibrium gene-regulation (Ahsendorf et al., 2014; Estrada et al., 2016). Their enormous success is not only due to the analysis power coming with their linearity (no second or higher order kinetics are allowed), but also because they can be obtained from more complicated models by applying the time-scale separation technique (Gunawardena, 2014).

We are interested to obtain a theoretical understanding of how perturbations in the structure of steady-state Laplacian models translate to relative differences in the dose-response relations they generate, and simultaneously to account for the complexity, uncertainty, and heterogeneity inherent to the investigation of biochemical networks and their accompanying data. Laplacian models are suitable for this purpose since they possess a rare property – closed form solutions for their steady-states always exist (Gunawardena, 2012). Thereby, they provide a direct, analytically tractable connection between model structure and the steady-state response it produces. The cornerstone for establishing the aforesaid connection is Tutte's Matrix-Tree Theorem (Tutte, 1948). It reveals the intimate relation between a matrix representation of Laplacian models, the so called *graph Laplacian matrix*, and a graph theoretical representation, that of subgraphs of labelled directed graphs (*digraphs*) called *arborescences* (or also termed rooted directed spanning trees).

Briefly, Laplacian models can be represented as labelled digraphs in which vertices describe model species and edges are reactions with rate constants contained in the corresponding edge labels. The Laplacian matrix representation can be obtained by expressing the dynamics of the model in the Ordinary Differential Equation (ODE) framework, and the steady-state of the model is completely determined by its kernel. On the other hand, when edge labels of the digraph representation are regarded as variables, then the set of all arborescences can be algebraically encoded in a polynomial form, a homogeneous multivariate polynomial called the *Kirchhoff polynomial* (Chung & Yang, 2000). Additionally, the same polynomial can be obtained by symbolically deriving all (j, j)-minors of the graph Laplacian matrix and summing them up, a crucial step for deriving the steady-state of the system (for details see Chapter 2). Thereby, Kirchhoff polynomials become mediators between the structure of a model, in terms of its digraph representation, and its function, expressed through its steady-state.

However, despite their apparent simplicity, Laplacian models are not ready to meet the challenges of complex and uncertain data. The first reason concerns the poor scaling of the available steady-state derivation and analysis techniques. Namely, although closed form solutions always exist, it is often impractical to obtain and manipulate them due to the typically (super) exponential growth in the length of Kirchhoff polynomials, precluding handling of even Laplacian models of moderate size. The second reason relates to the undeveloped integration of Laplacian models with uncertain and heterogeneous data sets. This would require the application of model comparison and parameter inference approaches, as well as, the incorporation of the models into multi-scale models when cell-to-cell variation in a population is studied. The recently introduced mathematical rigour into Laplacian models of biological systems (Gunawardena, 2012; Mirzaev & Gunawardena, 2013) paves the way for further theoretical developments in order to meet these challenges.

With regards to the function generated by biochemical systems modelled in the Laplacian framework, as previously briefly remarked, we consider steady-state dose-response curves in which the dose is a reaction rate constant modulated by an input, e.g. a ligand with a constant concentration, and the response is a quantity, e.g. proportion of alive cells in a population, connected to the steady-state of a model species. Experimentally obtained dose-response curves are a classical and widely used apparatus to study input-output relations in biochemical systems (Tallarida & Jacob, 2012). Usually, a reference dose-response curve, e.g. coming from a control experiment, is compared to the dose-response curve generated by a perturbed system to answer questions as diverse as what the optimal dosage of a drug is by calculating its therapeutic index, and how ligands with similar structure reliably trigger diverse cellular responses (Jaitin et al., 2006). However, traditional methods concentrate on studying and comparing sigmoid dose-response curves, while for non-monotone, or else termed *hormetic*, dose-response relationships which are also common (Mattson & Calabrese, 2009), comparison and analysis methods are still lacking.

1.4 Contributions of This Thesis

In this thesis we develop theoretical and practical tools to characterise the relationship between model structure and produced dose-response in the realm of Laplacian models under perturbation, and in the context of data heterogeneity and uncertainty.

First, in Chapter 2, we formally introduce the main concepts and definitions relevant for this thesis.

In Chapter 3 we show how to obtain the prime factorisation of Kirchhoff polynomials using combinatorial properties of digraphs such as strong connectivity and vertex domination. In particular, we provide digraph decomposition rules that correspond to factorisation steps of the polynomial, and also give necessary and sufficient primality conditions of the resulting factors expressed by connectivity properties of the corresponding decomposed components. Thereby, we obtain a linear time algorithm for decomposing a digraph into components corresponding to factors of the initial polynomial, and a guarantee that no finer factorisation is possible.

In Chapter 4, based on the Kirchhoff polynomial factorisation theory from Chapter 3, we develop a framework for the efficient manipulation and generation of expressions of Kirchhoff polynomials that result from steady-state derivations for Laplacian models. In the manipulation part we devise criteria to efficiently test the equality of Kirchhoff polynomials through their corresponding digraphs. By prime decomposing the digraphs contained in an expression of Kirchhoff polynomials and identifying the digraphs giving rise to equal polynomials, we formulate a coarse-grained variant of the expression which is suitable for symbolic simplification. In the generation part we introduce two heuristic algorithms to explicitly generate individual Kirchhoff polynomials in a compressed form. The algorithms are inspired by algebraic simplification of polynomials but operate on the corresponding digraphs. We demonstrate that Kirchhoff polynomial generation is dependent on digraph connectivity and not, as earlier believed, on the (super) exponentially growing number of arborescences.

The theoretical and practical basis built-up by the previous two chapters allows us, in Chapter 5, to formulate a framework to study the relative differences between reference and perturbed dose-response curves, which we call *differential responses*, generated by Laplacian models. More precisely, we exploit the connectivity properties of the digraphs representing Laplacian systems to address challenges such as to determine the reactions that affect differential responses, to identify equivalence classes of networks, and to reliably reject hypothetical models without needing to know parameter values. We illustrate these direct connections between network structure and function for models of insulin signalling to exemplify applications of the methodology in systems biology and pharmacology.

Finally, in Chapter 6, we make use of the developments from the previous chapters to formulate a minimal model of interferon type I differential signalling on the basis of prior literature knowledge and experimental population-level dose-response data. We construct a simple multi-scale model consisting of an experimentally determined receptor number distribution over a population of cells

which gets transformed to the distribution of active receptors within the population through a Laplacian model of important interferon dose dependent receptor stability mechanisms. An activity threshold then divides the population into dead and alive cells according to their number of active receptors. The resulting dose-response relationship is evaluated against dose-response data, simultaneously accounting for parametric uncertainty by performing Bayesian parameter inference and for model topology uncertainty by exploring an ensemble of possible receptor stability Laplacian models through Bayesian model comparison. As a result we demonstrate that the mechanisms of receptor assembly, endocytosis, and inhibition by the factor USP18 are the minimal sufficient model constituents which can explain the observed differential responses.

2

Background, Definitions, and Notation

2.1 Laplacian Models

We focus on biological reaction networks governed by *Laplacian dynamics*, modelled by ordinary differential equations (ODEs) with zero and (pseudo) first order mass-action kinetics.

Consider the example network in Figure 2.1a in which all reactions follow first order mass-action kinetics. It comprises three species and four reactions: a receptor R can transition to (from) its ligand-bound state RL with rate constant r_1 (r_2), or the receptor can become irreversibly phosphorylated as RLp with rate constant r_3, and RLp can transition to R with rate constant r_4. This system is a simple model of receptor tyrosine kinase activation and its dynamics can be expressed as the ODE system:

$$\frac{d}{dt}\begin{pmatrix} x_R \\ x_{RL} \\ x_{RLp} \end{pmatrix} = \underbrace{\begin{pmatrix} -r_1 & r_2 & r_4 \\ r_1 & -(r_2+r_3) & 0 \\ 0 & r_3 & -r_4 \end{pmatrix}}_{\mathcal{L}} \begin{pmatrix} x_R \\ x_{RL} \\ x_{RLp} \end{pmatrix}, \tag{2.1}$$

where x denotes the concentration of the respective species in the subscript and $\mathcal{L}$ is called the *Laplacian matrix* of the system.

The dynamics of Laplacian models can be represented as a diffusion process on directed graphs (*digraphs*) corresponding to their reaction schemes. Formally, a simple digraph $G = (V, E)$ consists of a set of vertices $V(G)$ and a set of edges (ordered pairs of distinct vertices) $E(G)$; it has no self-loops and no multiple parallel edges. Laplacian models can correspond to *strongly connected* digraphs, that is, digraphs G in which for any two vertices $u, v \in V(G)$ there exists a directed path from u to v and from v to u, or to *non-strongly connected* digraphs in which the strong connectivity condition does not hold. For example, the digraph in Figure 2.1a is strongly connected, whereas the digraph in Figure 2.1d is not.

We consider the reaction scheme in Figure 2.1a as a digraph G with $V(G) = \{v_R, v_{RL}, v_{RLp}\}$, where v denotes the vertex corresponding to the species in the

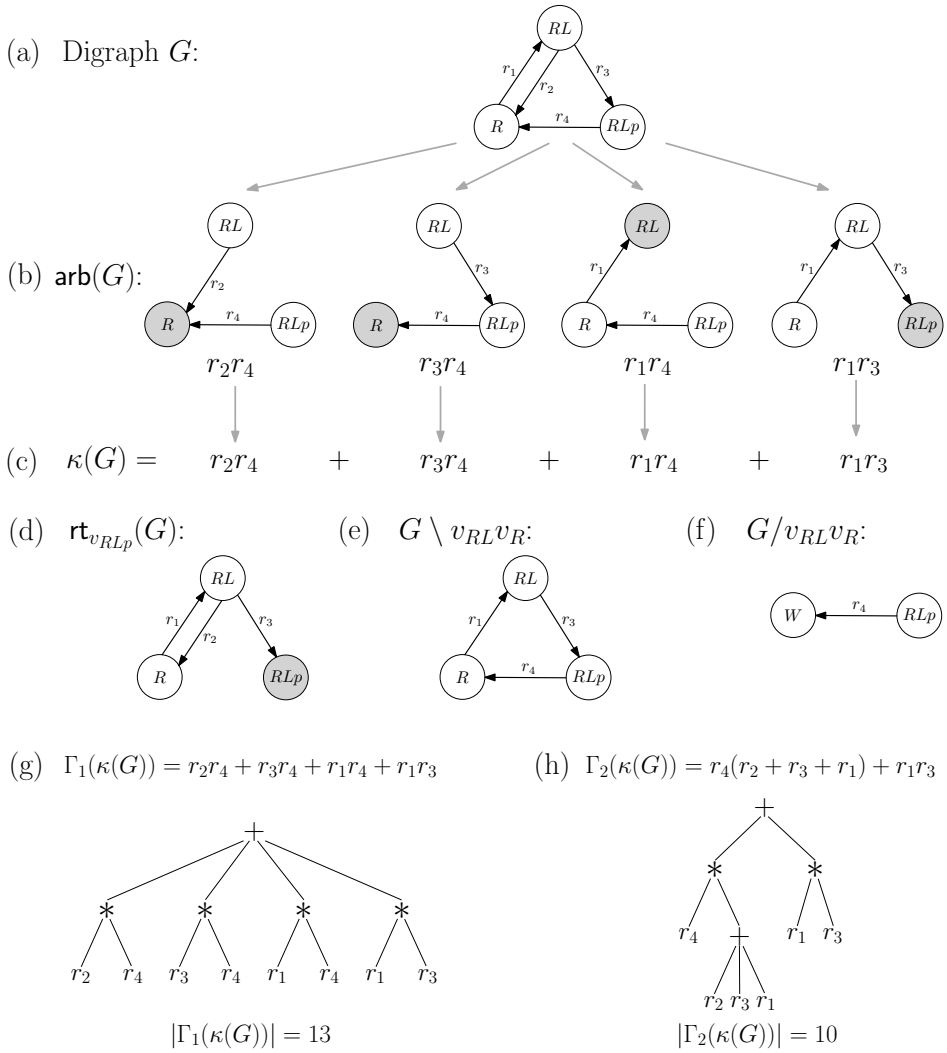

Figure 2.1: Example model of receptor tyrosine kinase activation. (a) Digraph (kinetic scheme) G, (b) all its arborescences rooted at each vertex, and (c) the corresponding Kirchhoff polynomial. (d) The digraph obtained by rooting G at v_{RL}, (e) the edge deleted digraph $G\setminus v_{RL}v_R$, and (f) the edge contracted digraph $G/v_{RL}v_R$. Labels on vertices denote names of species represented by them and W denotes a vertex obtained after the application of digraph operations. Grey vertices are roots of the corresponding arborescence and of all arborescences when rooting a digraph, respectively. In (g) and (h) two algebraically equivalent representations of $\kappa(G)$ are shown together with their expression trees and sizes, i.e. (g) $\Gamma_1(\kappa(G))$ a fully expanded representation and (h) $\Gamma_2(\kappa(G))$ a simplified representation.

subscript, and $E(G) = \{v_R v_{RL}, v_{RL} v_{RLp}, v_{RL} v_R, v_{RLp} v_R\}$. The reaction rate constants are labels of the corresponding edges in G. A label function $\ell : E(G) \mapsto \mathcal{I}$ associates a mathematical (arithmetic, polynomial, or algebraic) expression to each edge of G. For example, $\ell(v_R v_{RL}) = r_1$. Additionally, by $\ell(G)$ we define the *set of all edge labels* of G.

In such a labelled digraph G we can associate each vertex $v_i \in V(G)$ to a non-negative species concentration x_i and each edge to a mass-action reaction with reaction rate constants that are independent of the species concentrations and given by the label function ℓ. Hence, we obtain a dynamical system in which species concentrations hosted on the vertices of G flow in the direction of the edges at rates proportional to the concentrations on the edges' source vertices; proportionality is defined by the edge label expression.

2.2 Closed and Open Models

Laplacian models can be *closed*, not exchanging matter with the environment (as in the illustrative example), or *open*, when synthesis and degradation reactions are present.

In general, the dynamics of closed Laplacian models can be expressed in the form:

$$\frac{dx}{dt} = \mathcal{L}(G)x, \tag{2.2}$$

where $x = (x_1, \ldots, x_n)^T$ is the vector of species' concentrations corresponding to each vertex $v_1, \ldots, v_n \in V(G)$ and $\mathcal{L}(G)$ is the Laplacian matrix of G defined as:

$$\mathcal{L}(G)_{ij} = \begin{cases} \ell(v_j v_i) & \text{if } i \neq j, \\ -\sum_{r \neq j} \ell(v_j v_r) & \text{if } i = j, \end{cases} \tag{2.3}$$

and $\ell(v_j v_i) = 0$ when the $v_j v_i \notin E(G)$. In closed systems the total amount of material x_t is conserved and there is a single conservation law $x_1 + \cdots + x_n = x_t$. The system reaches a unique stable steady-state that can be derived symbolically for any species by obtaining a basis element of the kernel of the Laplacian matrix.

Digraphs G representing open systems are obtained by adding a vertex $v_\varnothing$ representing the environment to a *core digraph* $\overline{G}$ (akin to closed systems, the core digraph is composed of all non-synthesis and non-degradation reactions) and by introducing directed edges from $v_\varnothing$ to the synthesized species in $\overline{G}$ with labels s_i and edges labelled d_i from the degraded species to $v_\varnothing$. The dynamics of open Laplacian models are defined in general form as:

$$\frac{dx}{dt} = \mathcal{L}(\overline{G})x - \Delta x + S,$$

where $\mathcal{L}(\overline{G})$ is the Laplacian matrix of the core digraph, Δ is a diagonal matrix with $\Delta_{ii} = \delta_i$ the degradation rate constants of the species with index i, and S is a vector $S_i = s_i$ comprising the synthesis rate constants for all species. If a species does not have a degradation or a synthesis reaction then $s_i = 0$ or $\delta_i = 0$,

respectively. In open systems, the total amount of matter is not conserved but the rates at which matter enters and leaves the system determine the final distribution of steady-state concentrations. In particular, synthesis and degradation at steady-state are balanced: $\delta_1 x_1 + \ldots + \delta_n x_n = s_1 + \ldots + s_n$. Similarly to closed systems, but assuring that the steady-state concentration at $v_\varnothing$ is always 1, the unique stable steady-state for vertex v_i ($v_i \neq v_\varnothing$) can be symbolically derived.

Note that in this thesis we are primarily interested in closed and open Laplacian models of biological systems corresponding to strongly connected digraphs G (the core digraph $\overline{G}$ in open models can be strongly or non-strongly connected), although this does not limit the generality of the developed theory.

For more details, proofs, and derivations on Laplacian models we refer the reader to Gunawardena (2012); Mirzaev & Gunawardena (2013); Mirzaev & Bortz (2015).

2.3 Arborescences

Steady-states of Laplacian models can always be derived in symbolic form but, in practice, the length of the symbolic steady-state expressions grows (super) exponentially with the size of the digraph G. To cope with this growth, we introduce concepts intimately connected to both the structure of Laplacian digraphs and to the steady-states of Laplacian models: a certain class of *subdigraphs*, so-called *arborescences*, that can be used to generate Kirchhoff polynomials (see next subsection).

Formally, a digraph H is a subdigraph of a digraph G if $V(H) \subseteq V(G)$ and $E(H) \subseteq E(G)$, where every edge in $E(H)$ has its vertices in $V(H)$. For $V' \subseteq V$, $G[V']$ denotes the *induced subdigraph* of G by the set of vertices V'. A strongly connected component (SCC) of G is any largest (w.r.t. vertex inclusion) strongly connected induced subdigraph of G. By definition, no two distinct SCCs can share a vertex and thus the SCCs $G_1, \ldots, G_k$ of a digraph G induce a unique partition $V(G_1), \ldots, V(G_k)$ of $V(G)$. Again, by definition, for two distinct SCCs G_i and G_j there can be a directed path from G_i to G_j, or from G_j to G_i, but not both. The existence of such paths between SCCs naturally induces a unique partial order on the SCCs $G_1, \ldots, G_k$.

An *in-arborescence* A is a subdigraph of G spanning its vertex set such that a root vertex is reachable from all vertices along a unique directed path. In other words, A is a rooted directed spanning tree of G with edges directed towards the root vertex. Similarly, an *out-arborescence* is such a rooted directed spanning tree for which all edges are directed away from a root vertex.

Note that to formally develop the theory in Chapter 3 we work with out-arborescences which is a convention in combinatorics, while in all other chapters we consider in-arborescences which are relevant for Laplacian models. This is not restricting the application of the developed theory since there is a bijection between the in-arborescences of a digraph G and the out-arborescences of the reverse (with all edges reversed) digraph of G. Consequently, statements on out-arborescences can be rewritten for in-arborescences trivially. To avoid confu-

sion, by "arborescences" we refer to both in- and out-arborescences and when a definition is specific to in- or out-arborescences we mention it explicitly.

Thus by $\mathsf{arb}(G)$ we denote the set of all arborescences of G, and by $\mathsf{arb}_v(G)$ the set of all arborescences rooted at vertex v. All in-arborescences of the example digraph are shown in Figure 2.1b: two in-arborescences are rooted at v_R, one is rooted at v_{RL}, and another one at v_{RLp}. Let rt be the digraph *rooting* operation such that $\mathsf{rt}_v(G)$ is the digraph constructed from G by removing all edges outgoing from v (see Figure 2.1d) for in-arborescences and incoming to v for out-arborescences. All arborescences of $\mathsf{rt}_v(G)$ are necessarily rooted at v. We denote the set of all incoming edges to vertex v by $\mathrm{in}_G(v)$ and when it is not ambiguous, simply by $\mathrm{in}(v)$. We will say that a digraph G is *rooted* at a vertex v with respect to in-arborescences if v has no outgoing edges and v is reachable from every other vertex in G, and with respect to out-arborescences when v has no incoming edges and every other vertex is reachable from v. Observe that $\mathsf{arb}_v(G) = \mathsf{arb}(\mathsf{rt}_v(G))$. Note also that an in-(out-)arborescence of G exists iff the partial order of the SCCs has exactly one maximal (minimal) element, i.e. no other SCC is reachable from the maximal SCC (all other SCCs are reachable from the minimal SCC). Such a SCC is called a *terminal SCC* (*initial SCC*).

2.4 Kirchhoff Polynomials and Steady-States of Laplacian Models

An arborescence A of a digraph G with n vertices has $n-1$ edges $e_1, \ldots, e_{n-1} \in E(G)$ (for a concise notation, we denote edges with the symbol e when not referring to the pairs of vertices defining them). An arborescence can also be represented as a monomial $\ell(e_1) \cdot \ell(e_2) \cdots \ell(e_{n-1})$ in the edge labels $\ell(e_1), \ell(e_2), \ldots, \ell(e_{n-1})$ of a *uniquely labelled digraph* G. Correspondingly, one can represent the set of all arborescences in G by a homogeneous multivariate polynomial over the variables $\ell(e_i)$, $e_i \in E(G)$. This polynomial is called the *Kirchhoff polynomial* $\kappa(G)$:

$$\kappa(G) = \sum_{A \in \mathsf{arb}(G)} \prod_{e_i \in A} \ell(e_i). \tag{2.4}$$

The Kirchhoff polynomial with respect to in-arborescences of the example digraph is shown in Figure 2.1c.

We also denote the Kirchhoff polynomial of all arborescences rooted at vertex v by $\kappa_v(G) = \sum_{A \in \mathsf{arb}_v(G)} \prod_{e_i \in E(A)} \ell(e_i)$, where $\kappa_v(G)$ is a shorter notation for $\kappa(\mathsf{rt}_v(G))$. For a Kirchhoff polynomial P, we denote by $\mathrm{var}(P)$ the set of variables appearing in P. We call a Kirchhoff polynomial P a *factor* of another Kirchhoff polynomial Q, if there exists a Kirchhoff polynomial R such that $Q = P \cdot R$. A Kirchhoff polynomial P that is irreducible because it cannot be factorized into non-trivial factors, is called *prime*. We extend these definitions to digraphs by calling G' *a component (a prime component) of* G if $\kappa(G')$ *is a factor (a prime factor) of* $\kappa(G)$. Additionally, observe that if G is disconnected or has more than one terminal SCC for in-arborescences and more than one initial SCC for out-

arborescences then $\kappa(G) = 0$, and if G consists of a single vertex then $\kappa(G) = 1$.

A Kirchhoff polynomial can have multiple *algebraically equivalent representations*. For example, the Kirchhoff polynomial from Figure 2.1c can be written in the following two ways as shown in Figure 2.1g,h:

$$\Gamma_1\left(\kappa(G)\right) = r_2r_4 + r_3r_4 + r_1r_4 + r_1r_3 \quad \text{and} \quad \Gamma_2\left(\kappa(G)\right) = r_4(r_2 + r_3 + r_1) + r_1r_3,$$

where the function $\Gamma_i : \mathbb{R}[\ell(G)] \to \mathbb{T}$ denotes a specific representation of $\kappa(G)$; it relates a given Kirchhoff polynomial $\kappa(G)$ over the set of labels $\ell(G)$ to the set of *expression trees* $\mathbb{T}$ in which the branch vertices represent either the n-ary addition or the n-ary multiplication operation, and leaf vertices are the unique edge labels $\ell(G)$ which are the variables of the Kirchhoff polynomial. In this case $\Gamma_1(\kappa(G))$ denotes a fully expanded representation while $\Gamma_2(\kappa(G))$ is one possible simplified representation.

We define the *size* of a representation of a Kirchhoff polynomial, denoted $|\Gamma(\kappa(G))|$, as the size of its corresponding expression tree. Thus looking at Figure 2.1g we see that $|\Gamma_1\left(\kappa(G)\right)| = 13$ since there is one summation over all monomials, one multiplication per monomial equal to four multiplication vertices in total, and eight expression tree leaves. The size of the other algebraically equivalent representation shown in Figure 2.1h is $|\Gamma_2\left(\kappa(G)\right)| = 10$ since there are two addition vertices, two summation vertices, and six expression tree leaves.

The Kirchhoff polynomials establish a direct connection between model structure, in terms of in-arborescences, and function, in terms of steady-state expressions. Briefly, the unique steady-state of a Laplacian model can be symbolically obtained from a basis element of the kernel of the Laplacian matrix by employing *Tutte's Matrix-Tree Theorem* (Tutte, 1948)[1]. The theorem links the (i, j)-th minors of the Laplacian matrix $\mathcal{L}$, i.e. the symbolic determinants of the sub-matrix obtained from $\mathcal{L}$ by removing its i-th row and j-th column, to the graph theoretical concept of in-arborescences and consequently to their representation as Kirchhoff polynomials (see Gunawardena (2012); Mirzaev & Gunawardena (2013); Mirzaev & Bortz (2015) for details and proofs).

Theorem 2.4.1 (Tutte's Matrix-Tree Theorem)**.** *Let G be a digraph with n vertices then the minors $\mathcal{L}(G)_{(i,j)}$ of its Laplacian matrix can be expressed, up to a sign, by the Kirchhoff polynomial rooted at the vertex v_j corresponding to the j-th column of $\mathcal{L}(G)$ as:*

$$\mathcal{L}(G)_{(i,j)} = (-1)^{n+i+j-1} \sum_{A \in \mathsf{arb}_{v_j}(G)} \prod_{e \in A} \ell(e) = \kappa_{v_j}(G).$$

We are interested in the final results, namely that the steady-state concentration x_i^{SS} of species i in a closed system associated to a vertex v_i can be expressed as

[1] This theorem is itself a generalization of Kirchhoff's Theorem (Kirchhoff, 1847) for undirected graphs.

a fraction of Kirchhoff polynomials:

$$x_i^{SS} = \frac{\kappa_{v_i}(G)}{\kappa(G)} x_t. \tag{2.5}$$

Thus, the steady-state concentration of species RLp associated to vertex v_{RLp} in our example system is (see Figure 2.1b-d):

$$x_{RLp}^{SS} = \frac{\kappa_{v_{RLp}}(G)}{\kappa(G)} x_t = \frac{r_1 r_3}{r_3 r_4 + r_2 r_4 + r_1 r_4 + r_1 r_3} x_t.$$

Correspondingly, for open systems and a vertex $v_i \neq v_\varnothing$ we obtain:

$$x_i^{SS} = \frac{\kappa_{v_i}(G)}{\kappa_{v_\varnothing}(G)}.$$

We observe that the resulting steady-state expressions are expressions of Kirchhoff polynomials. While these expressions look simple, the number of arborescences in a digraph G usually grows exponentially with the size of G (Gabow & Myers, 1978). Symbolic steady-state expressions of Laplacian models as expressed by Kirchhoff polynomials therefore face the problem of combinatorial explosion, which makes manipulation and generation of such expressions challenging.

2.5 Deletion, Contraction, Domination

In this section we introduce additional digraph operations, connectivity definitions, and constructs which are relevant for working with Kirchhoff polynomials.

For a digraph G with $e \in E(G)$ and $v \in V(G)$ we denote *edge deletion* by $G \setminus e$, i.e. the digraph obtained from G by deleting e, and *vertex deletion* by $G \setminus v$, i.e. the digraph obtained from G by deleting v together with all edges in which it participates (see Figure 2.1e for an application of edge deletion to the example digraph).

Further, for a digraph G and an edge $e = v_i v_j \in E(G)$ we denote by G/e the *edge contracted* digraph that is constructed from G, with respect to in-arborescences, by (i) removing the edge $v_j v_i$, if it exists, and all out-going edges from v_i, i.e. $v_i u \in E(G)$; and (ii) fusing vertices v_i and v_j into a single new vertex w (see Figure 2.1f). Edge contractions may result in digraphs with multiple parallel edges between two vertices (multidigraphs) or self-loops. We resolve this by replacing m multiple parallel directed edges $e_1, e_2, \ldots, e_m$ going from u to v with a single edge $e = uv$ such that $\ell(e) = \ell(e_1) + \ell(e_2) + \ldots + \ell(e_m)$ and removing self-loops. Thereby, we transform the multidigraph into a simple digraph whose Kirchhoff polynomial is equal to that of the multidigraph.

Of use will also be a more general definition of contraction with respect to out-arborescences, which applies to contracting a subset of vertices in a digraph.

Definition 2.5.1 (Contraction)**.** *For a subset S of the vertices of a digraph G, and for a vertex $u \in S$, by contracted digraph $G(S \to u)$ we denote the digraph G' constructed from G as follows:*

1. *All edges xy, where $x \in V \setminus S$, $y \in S \setminus \{u\}$ are removed from G.*
2. *All edges within S are removed (i.e., all edges xy, where $x, y \in S$).*
3. *All vertices of S are contracted into a single vertex u.*

Observe that G' has no loops, and if G has no parallel edges incoming to u, then G', as well, has no parallel edges incoming to u. It can, however, happen that u has parallel outgoing edges. Further, for all $z \in V \setminus S$:

- $zu \in E(G')$ if and only if $zu \in E(G)$, and
- for every edge $sz \in E(G)$ such that $s \in S$, there is a corresponding edge $uz \in E(G')$.

The classic *deletion-contraction* formula for an edge $e \in E(G)$ partitions $\mathsf{arb}(G)$ into two sets, one in which e participates in no arborescences and one in which e participates in all arborescences. Equivalently, it decomposes $\kappa(G)$ into a sum of Kirchhoff polynomials (Levine, 2011):

Proposition 2.5.2 (Edge Deletion-Contraction)**.** *Let G be a digraph and $e \in E(G)$ be an arbitrarily chosen edge. Then:*

$$\kappa(G) = \kappa(G \setminus e) + \ell(e)\kappa(G/e).$$

We also define the digraph connectivity concepts of *domination* and *immediate domination* with respect to out-arborescences.

Definition 2.5.3 (Domination)**.** *If G is rooted at v, then we say that vertex u dominates vertex w, if all directed paths from v to w go through vertex u. By $\mathsf{dom}_G(u)$ we denote the set of all vertices of G dominated by u. If $\mathsf{dom}_G(u) \neq \{u\}$ and $u \neq v$, we say that u is a non-trivial dominator.*

Definition 2.5.4 (Immediate Domination)**.** *Let G be rooted at v. Vertex y is called an immediate dominator of vertex z, if $y \neq z$, y dominates z, and for every other vertex x that dominates z, we have that x also dominates y. Equivalently we say that z is immediately dominated by y, and we denote such y as $\mathsf{parent}_G(z)$ (it is easy to see that there can be at most one such vertex). The set of all vertices immediately dominated by vertex y is denoted by $\mathsf{imm}_G(y) = \{z : \mathsf{parent}_G(z) = y\}$.*

Thus, $\mathsf{parent}_G(z)$ taken over all $z \in V$ defines a directed tree $T(G)$ of immediate domination, rooted at the root v of G (note that $\mathsf{parent}_G(v)$ is undefined). Furthermore, for any vertex y, the immediately dominated vertices $z \in \mathsf{imm}_G(y)$ induce the following partition of $\mathsf{dom}_G(y) \setminus \{y\}$: $\{\mathsf{dom}_G(z) : z \in \mathsf{imm}_G(y)\}$.

2.6 Bayesian Parameter Inference and Model Comparison

Bayesian theory offers a prominent approach to account for data and model uncertainty in computational systems biology (Wilkinson, 2007; Geris & Gomez-Cabrero, 2015). It supplies the formal means to infer uncertain parameters and compare competing models on the basis of sparse and noisy experimental data (Vyshemirsky & Girolami, 2008).

Under the Bayesian viewpoint probability is a measure of the *degree of belief* about the occurrence of an event (Bernardo & Smith, 2001). This definition applies to any event regardless the origin of its uncertainty or number of observations. In contrast to the frequentist approach in which events have unknown but fixed probabilities, the Bayesian approach aims to directly incorporate the full uncertainty within the same framework by assigning a probability distribution to all unknown quantities – parameters, data, and competing models. The degree of belief about these quantities can be iteratively updated using the famous Bayes' Theorem (see Equation (2.6)) when new data becomes available. When comparing different models this Bayesian inference process inherently incorporates Ockham's Razor effect (Jefferys & Berger, 1991), that is, it penalizes unnecessarily complex models.

Next we recapitulate the main concepts of Bayesian parameter inference and model comparison which are required for Chapter 6. More detailed introduction to Bayesian methods can be found in Jaynes (2003); Bernardo & Smith (2001); MacKay (2003) and specifically concerning the context of biology in Geris & Gomez-Cabrero (2015).

Let us consider a data set D and an ensemble of $\mathbf{m}$ candidate models M_i each with parametrisation θ_i, where $i \in \{1, 2, \ldots, \mathbf{m}\}$. We allow each model to include additional information I, for example, fixed parameters across all models.

Parameter inference. Through the Bayes' Theorem we can infer the probability over the parameters θ_i for a certain model M_i, given the data D and the additional information I. Namely, in this case, the Bayes' Theorem reads:

$$\Pr(\theta_i \mid D, M_i, I) = \frac{\Pr(D \mid \theta_i, M_i, I)\Pr(\theta_i \mid M_i, I)}{\Pr(D \mid M_i, I)}, \tag{2.6}$$

where the terms are identified as:

$\Pr(\theta_i \mid M_i, I)$ – the *prior*. The probability for the parametrisation θ_i of model M_i before observing the data D.

$\Pr(\theta_i \mid D, M_i, I)$ – the *posterior*. The probability of the model parametrisation θ_i obtained after taking into account the data D.

$\Pr(D \mid \theta_i, M_i, I)$ – the *likelihood*. The probability of the data D being generated by a model M_i with parametrisation θ_i.

$\Pr(D \mid M_i, I)$ – the *evidence*. The probability of observing the data D.

The evidence is a marginal distribution serving as a normalisation constant. It is given by the integral over the whole continuous parameter space Ω_i of model M_i:

$$\Pr(D \mid M_i, I) = \int_{\Omega_i} \Pr(D \mid \theta_i, M_i, I) \Pr(\theta_i \mid M_i, I) d\theta_i.$$

The calculation of this usually high-dimensional and analytically intractable integral can be neglected for parameter inference since it only acts as a normalisation constant.

We assume a log-uniform prior distribution of the parameters signifying our ignorance about their order of magnitude. Thus from the prior and by setting the likelihood we obtain a distribution proportional to the posterior which is sufficient to infer the distribution of the parameter vector θ_i.

Frequently the posterior density cannot be analytically derived and numerical methods to approximate it have to be employed. In particular, Markov Chain Monte Carlo (MCMC) techniques are used to produce a sequence of points in parameter space, whose density is proportional to the posterior probability density function (Gamerman & Lopes, 2006).

Model comparison. The posterior probability of a model M_i can also be expressed through the Bayes' Theorem as:

$$\Pr(M_i \mid D, I) = \frac{\Pr(D \mid M_i, I) \Pr(M_i \mid I)}{\Pr(D \mid I)}.$$

The terms in the formula have analogous interpretation as for parameter inference but have their parameters θ_i integrated out – $\Pr(M_i \mid I)$ is the prior model probability, $\Pr(D \mid I)$ is the probability of the data, and importantly the likelihood $\Pr(D \mid M_i, I)$ is exactly equal to the evidence integral we acquired for parameter inference.

To compare two models M_i and M_j we formulate their posterior odds ratio:

$$\frac{\Pr(M_i \mid D, I)}{\Pr(M_j \mid D, I)} = \frac{\Pr(D \mid M_i, I)}{\Pr(D \mid M_j, I)} \frac{\Pr(M_i \mid I)}{\Pr(M_j \mid I)} = B_{ij} \frac{\Pr(M_i \mid I)}{\Pr(M_j \mid I)},$$

where $\Pr(D \mid I)$ crosses out and the ratio $\frac{\Pr(D|M_i,I)}{\Pr(D|M_j,I)}$ is the so called *Bayes factor* B_{ij} (Kass & Raftery, 1995):

$$B_{ij} = \frac{\int_{\Omega_i} \Pr(D \mid \theta_i, M_i, I) \Pr(\theta_i \mid M_i, I) d\theta_i}{\int_{\Omega_j} \Pr(D \mid \theta_j, M_j, I) \Pr(\theta_j \mid M_j, I) d\theta_j}.$$

To calculate the posterior probability of a model M_i in the ensemble of $\mathbf{m}$ considered models we calculate the Bayes factors for all models with respect to

M_i to obtain (Sunnåker et al., 2013):

$$\Pr(M_i \mid D, I) = \left(1 + \sum_{j=1, i \neq j}^{m} B_{ji}\right)^{-1}.$$

The most challenging aspect of model comparison is to marginalise the likelihood to obtain the evidence and subsequently the Bayes factors. An approach to approximate the evidence proposed by Zamora-Sillero et al. (2011) is to identify the high-likelihood regions of the parameter space and sample them uniformly, while assuming that the rest of the parameter space contributes negligibly little to the likelihood. Then the evidence integrals is approximated by summing the contribution of the high-likelihood regions as (Sunnåker, 2013):

$$\Pr(D \mid M_i, I) \simeq \frac{Vol_i^{hl}}{Vol_i^{tot}} \left(\frac{1}{N} \sum_{s=1}^{N} \Pr(D \mid \theta_i^{(s)}, M_i, I)\right), \tag{2.7}$$

where Vol_i^{tot} is the total volume of the parameter space of model M_i, Vol_i^{hl} is the combined volume of its high-likelihood regions, and the N parameter points $\theta_i^{(s)}$ are uniformly sampled from the high-likelihood regions. The standard deviation of this evidence estimate under the assumption of Gaussian distributed error is expressed as (Zamora-Sillero et al., 2011):

$$\sigma = \frac{Vol_i^{hl}}{Vol_i^{tot}} \sqrt{\frac{1}{N} \left(\frac{1}{N} \sum_{s=1}^{N} \Pr(D \mid \theta_i^{(s)}, M_i, I)^2 - \left(\frac{1}{N} \sum_{s=1}^{N} \Pr(D \mid \theta_i^{(s)}, M_i, I)\right)^2\right)}. \tag{2.8}$$

An important implementational detail is that for parameter inference and model comparison we work with the negative log-likelihood functions of the considered models.

3

Prime Factorisation of the Kirchhoff Polynomial

3.1 Introduction

A spanning tree of an undirected graph G is a connected acyclic subgraph containing all vertices of G. As seen in Chapter 2, in a digraph G, the analogue is an *arborescence*. In this chapter by an arborescence we always mean an out-arborescence, i.e. a subdigraph of G spanning its vertex set such that all vertices are reachable from a root vertex along a unique directed path.

Recall that according to Tutte's Matrix-Tree Theorem (Theorem 2.4.1) summing up all (jj)-th minors of a Laplacian matrix results in a homogeneous polynomial, called the Kirchhoff polynomial (Equation (2.4)), in which each monomial represents an arborescence consisting of the edges corresponding to the labels appearing in the monomial. In general, there might be (super) exponentially many arborescences for a given G and thus explicitly computing the expanded representation of $\kappa(G)$ cannot be done in polynomial time.

In this chapter we investigate the algebraic properties of the Kirchhoff polynomial and their relation to the connectivity properties of the corresponding uniquely labelled digraph. More precisely, we are interested in finding an efficient graph theoretical procedure to test primality of Kirchhoff polynomials and to yield their prime factorisation.

To this end we present two decomposition rules for digraphs, and show that *every* factor of $\kappa(G)$ corresponds to a digraph obtained by applying one of the decomposition rules and is derived from some subdigraph of G. The first decomposition rule corresponds to finding a strongly connected component (SCC) of G together with all of its incoming edges e_{in} and subsequently contracting all source vertices of e_{in} into a single new vertex. The second decomposition rule is more involved and is based on *domination* and *immediate domination* of vertices (these terms are explained in Section 2.5). Our decomposition is closest to the decomposition in Nakamura & Iri (1980) that has been formulated in the language of principal partition of matroids.

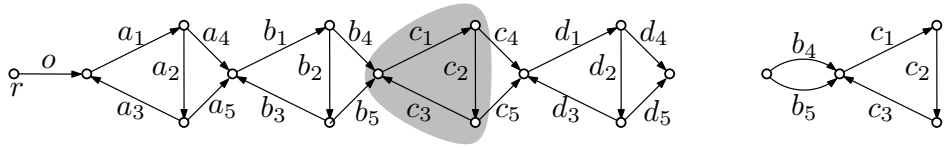

Figure 3.1: (left) A digraph with one trivial (the initial vertex) and four non-trivial strongly connected components (here cycles), each induced by the edges $\{x_1, x_2, x_3\}$, $x \in \{a, b, c, d\}$. The gray area depicts one such strongly connected component $G[V']$. (right) An illustration of $\widehat{G[V']}$.

To the best of our knowledge, the question of relating combinatorial features of a digraph to the algebraic properties of its Kirchhoff polynomial (such as its prime factorisation), although being a fundamental one, has not previously been investigated.

We illustrate the factorisation procedure on an example in Figure 3.1. Every arborescence in the example is rooted at r, contains the edge with label o, and contains the edges of type x_1 and x_2 from every SCC. The only freedom left is choosing whether edge x_4 or edge x_5 is part of an arborescence. These choices are mutually independent and, as a result, there are 2^4 arborescences, which results in 208 leaves (each leaf is a variable) in the expression tree. The factorized representation of the Kirchhoff polynomial (based on the SCC decomposition) is much shorter: $o(a_1a_2a_4+a_1a_2a_5)(b_1b_2b_4+b_1b_2b_5)(c_1c_2c_4+c_1c_2c_5)(d_1d_2d_4+d_1d_2d_5)$, and contains 25 explicitly written variables. We can further decompose each factor to finally obtain the prime factorization $oa_1a_2(a_4+a_5)b_1b_2(b_4+b_5)c_1c_2(c_4+c_5)d_1d_2(d_4+d_5)$, containing only 17 explicitly written variables.

An exhaustive application of the decomposition rules results in non-decomposable digraphs derived from subdigraphs of G, which correspond to prime factors of $\kappa(G)$. The prime decomposition provides a compressed form of $\kappa(G)$ which can be easily handled (evaluated) and manipulated (e.g. to find the greatest common divisor of two Kirchhoff polynomials). Moreover, the prime factorization of $\kappa(G)$ retains important connectivity properties of the original digraph and provides information about the type of digraphs with practically enumerable arborescences, which is beneficial for various practical applications such as symbolically deriving steady-states on digraphs governed by Laplacian dynamics. Furthermore, the decomposition/prime factorization can serve as a preprocessing step for the existing arborescence enumeration algorithms (such as Gabow & Myers (1978), Uno (1996), or Kapoor & Ramesh (2000)). Importantly, it is also a cornerstone for the development of the efficient Kirchhoff polynomial generation and manipulation procedures presented in Chapter 4.

3.2 Primality of Components

Observe that $\kappa(G)$ is a special homogeneous polynomial: every monomial of $\kappa(G)$ contains exactly $n-1$ variables, $n = |V|$, each with exponent equal to one.

Obviously, this property needs to also hold for factors of $\kappa(G)$ (recall that the monomials of $\kappa(G)$ represent an arborescence of G). Furthermore, observe that no variable $\ell(e)$ can appear in two factors of $\kappa(G)$.

Proposition 3.2.1. *If P is a factor of $\kappa(G)$, then all monomials of P have the same number of variables, each with exponent equal to one.*

Proposition 3.2.2. *If $\kappa(G) = P \cdot Q$, then $var(P) \cap var(Q) = \emptyset$.*

We observe that the partitioning of edges into P or Q under the factorization $\kappa(G) = P \cdot Q$ is induced by a partitioning of vertices.

Lemma 3.2.3. *If $\kappa(G) = P \cdot Q$ and $v \in V$, then either $\ell(in(v)) \subseteq var(P)$ or $\ell(in(v)) \subseteq var(Q)$.*

Proof. Assume that there are two incoming edges to v, e_1 and e_2, such that $\ell(e_1) \in \mathrm{var}(P)$ and $\ell(e_2) \in \mathrm{var}(Q)$. Then there exists a monomial in $\kappa(G)$ containing both $\ell(e_1)$ and $\ell(e_2)$. But such a monomial cannot represent an arborescence, a contradiction. □

Theorem 3.2.4. *Let G be a strongly connected digraph. Then $\kappa(G)$ is prime.*

Proof. Assume, on the contrary, that $\kappa(G) = P \cdot Q$, and P and Q are nontrivial factors. Let V_1 and V_2 be the set of vertices with incoming edges in $\mathrm{var}(P)$ and $\mathrm{var}(Q)$, respectively. By Proposition 3.2.2 and Lemma 3.2.3, $V_1 \cap V_2 = \emptyset$, and since P and Q are nontrivial, $V_1 \neq \emptyset$ and $V_2 \neq \emptyset$. Let v_1, v_2 be arbitrarily picked vertices such that $v_1 \in V_1$ and $v_2 \in V_2$.

Since G is strongly connected, for any $v \in V$ there exists an arborescence of G rooted at v. Let A_1, A_2 be two arborescences rooted at v_1 and v_2, respectively. Let p_1 and p_2 be the monomials from P corresponding to the arborescences A_1 and A_2, respectively. In A_1, every vertex from V_1, but the root v_1, has exactly one incoming edge in A_1. The label of every such edge necessarily belongs to P. Therefore, for A_1, the degree of the monomial p_1 in P is $\deg(p_1) = |V_1| - 1$. On the other hand, for A_2, all vertices from V_1 have an incoming edge whose label belongs to P and, therefore, the total degree of p_2 in P is $\deg(p_2) = |V_1|$. Then $\deg(p_1) \neq \deg(p_2)$, which contradicts Proposition 3.2.1. □

Theorem 3.2.5. *Let G be a digraph rooted at v, such that $G[V(G) \setminus \{v\}]$ is strongly connected, and G has no non-trivial dominators. Then $\kappa(G)$ is prime.*

To prove the above theorem, we use the following notion, and prove further auxiliary lemmas. Given a directed simple cycle $\mathcal{C} \subseteq G$, we say that a vertex $u \in \mathcal{C}$ is *independent* from $\mathcal{C}$, if there exists a simple path $\mathcal{P}$ connecting the root v to u, such that $\mathcal{P}$ and $\mathcal{C}$ are vertex-disjoint (except for u). We call any such $\mathcal{P}$ an *independent path* of u (with respect to $\mathcal{C}$).

Lemma 3.2.6. *Let G be a digraph as in Theorem 3.2.5. For any edge wu of G such that $u, w \neq v$, there exists a simple directed cycle $\mathcal{C}$ containing wu, such that $\mathcal{C}$ has at least two independent vertices, and w is one of those.*

Lemma 3.2.7. *Let G be a digraph as in Theorem 3.2.5, and let V_1 and V_2 be an arbitrary (non-trivial) partition of the vertices $V \setminus \{v\}$. There exists a simple directed cycle having an independent vertex from V_1 and an independent vertex from V_2.*

3.3 Decomposition

In this section we present two digraph decomposition rules corresponding to factorization steps of the Kirchhoff polynomial. The rules are based on the computation of SCCs and the dominator tree of a digraph. The exhaustive application of these rules yields digraphs that are prime factors of the Kirchhoff polynomial of the original digraph.

First, we need the following digraph construct.

Definition 3.3.1. *Let $G[V']$ be a SCC of G. By $\widehat{G[V']}$ we denote the digraph created from $G[V']$ as follows (see Figure 3.1):*

- *If $G[V']$ is the initial SCC, then $\widehat{G[V']} = G[V']$.*
- *Otherwise, we create a new vertex v_{aux}, and for every edge vu, such that $u \in V'$ and $v \notin V'$, we add an edge $v_{\mathsf{aux}}u$ with label $\ell(v_{\mathsf{aux}}u) = \ell(vu)$.*

Theorem 3.3.2. *Let $G[V_1], G[V_2], \ldots, G[V_k]$ be all strongly connected components of a connected digraph G. If G has exactly one initial component, then*

$$\kappa(G) = \kappa(\widehat{G[V_1]}) \cdot \kappa(\widehat{G[V_2]}) \cdot \ldots \cdot \kappa(\widehat{G[V_k]}). \tag{3.1}$$

Figure 3.2 presents an example on how SCC decomposition is employed to factorise $\kappa(G)$. The presented decomposition uncovers a fundamental property of arborescences. Namely, it shows that the arborescences of a digraph G are in a one-to-one correspondence with all combinations of subdigraphs of G obtained following the procedure: i) Pick an arborescence from the initial SCC of G. ii) For every non-initial SCC of G, pick as set W an arbitrary (nonempty) subset of all vertices with incoming edges from outside of this SCC, and pick the spanning forest of this SCC rooted in W.

An equivalent formulation (used in the proof of Theorem 3.3.2) is that any cycle can only be contained in a single SCC of G. This property allows us to relate the Kirchhoff polynomial of a digraph to the product of Kirchhoff polynomials of digraphs derived from its SCCs.

Theorem 3.3.2 allows us to factorize $\kappa(G)$ of any connected digraph G with at least two SCCs. Yet, it is not guaranteed that the obtained factorization is prime or non-trivial. Consider the case when the initial SCC is composed of a single vertex v, then the theorem states that $\kappa(G) = \kappa(G[\{v\}]) \cdot \kappa(G[\widehat{V \setminus \{v\}}])$. We can see that this is a trivial factorisation since $\kappa(G[\{v\}]) = 1$ and $\kappa(G[\widehat{V \setminus \{v\}}]) = \kappa(G)$ (here, $G[\widehat{V \setminus \{v\}}]$ renames the vertex v to v_{aux} but preserves the arborescences).

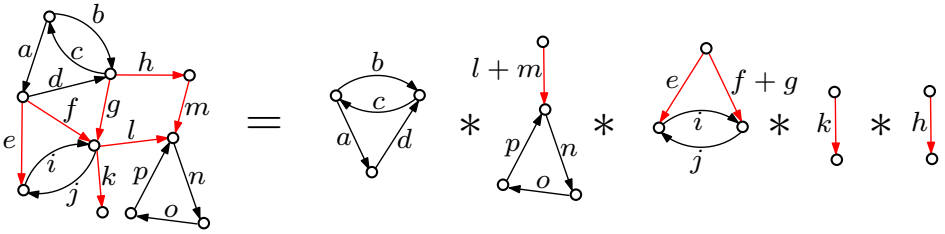

Figure 3.2: (left) An example of a digraph and (right) its decomposition using strongly connected components. The edges in black are part of a strongly connected component and the edges in red are connecting different SCCs.

In Theorem 3.2.4 we proved that the Kirchhoff polynomials of strongly connected digraphs are prime, which implies that the factor corresponding to the initial SCC is always prime. We note that the rest of the factors cannot be further non-trivially decomposed just using Theorem 3.3.2. Their primality is unsettled because they lack the property of strongly connected digraphs, namely, that any vertex of the digraph is the root of an arborescence, due to possessing a single root for all arborescences (the auxiliary vertex). Thereby, we proceed to studying the decomposability of non-initial SCC factors.

With Theorem 3.3.3 we specify a decomposition step for non-initial SCC factors. More precisely, we provide an additional factorization rule of $\kappa(G)$ by using vertex domination relations (with respect to the root vertex v_{aux}).

Theorem 3.3.3. *Let G be a digraph rooted at v and let u be an arbitrarily picked vertex of G. Denote $D = \mathsf{dom}_G(u)$. Then*

$$\kappa(G) = \kappa(\mathsf{rt}_u(G[D])) \cdot \kappa(G(D \to u)). \tag{3.2}$$

Similarly to SCC decomposition, one can interpret this result as either a one-to-one correspondence between arborescences of G and all combinations of the arborescences of its two factors, or as a statement on the structure of cyclic sets of edges in G (any cycle is either a cycle when restricted to D, or remains a cycle when D is contracted to u).

Applying Theorem 3.3.3 to all domination relations defined by the dominator tree $T(G)$ extends the decomposition to the whole dominator tree at once. An illustration of the dominator decomposition rule can be seen in Figure 3.3.

Corollary 3.3.4. *Let G be a digraph rooted at v. Then*

$$\kappa(G) = \prod_{u \in V} \kappa_u(H[\{u, u_1, \ldots, u_i\}]) \tag{3.3}$$

where $H = G(\mathsf{dom}_G(u_1) \to u_1; \ldots; \mathsf{dom}_G(u_i) \to u_i)$ and $\{u_1, \ldots, u_i\} = \mathsf{imm}_G(u)$.

Recall Theorem 3.2.5 which states that if there are no non-trivial domination relations in G (G being rooted at v for which no non-trivial decomposition by

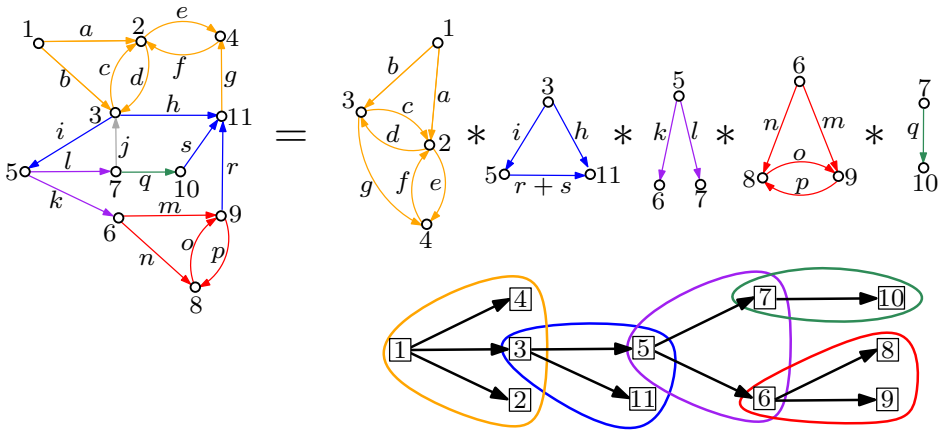

Figure 3.3: (above) Kirchhoff polynomial factorization of a digraph with respect to its dominator tree. (below) The dominator tree of the example digraph. Colour coding corresponds to immediate domination.

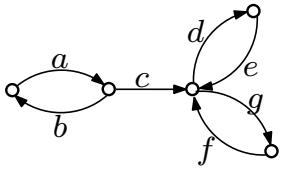

Figure 3.4: An example of a digraph that requires SCC decomposition followed by domination decomposition and another SCC decomposition to obtain the prime factorization of its corresponding Kirchhoff polynomial.

SCCs applies) then $\kappa(G)$ is prime. Corollary 3.3.4 ensures that all non-trivial dominator relations are eliminated but that cannot guarantee the primality of the decomposed factors since they can be SCC decomposable. Therefore, in order to obtain a complete prime factorization of the input digraph we need to use both rules of decomposition in an alternating fashion. One might expect that this process requires deep recursion. However, for any digraph a constant depth of recursion is needed. More precisely, it is enough to apply in sequence SCC factorization, dominators factorization, and SCC factorization to get prime components. This upper bound on the recursion depth is tight, as the example in Figure 3.4 shows.

Theorem 3.3.5. *If G is rooted at v, then any H being a factor obtained by the application of rule* (3.3) *has the following property: all factors of H obtained by applying* (3.1) *are prime.*

Pseudocode and time complexity. The pseudocode of the prime decomposition algorithm through SCCs and dominator relations can be found as Algorithm 1 in Section 8.1.2 from the appendix. Observe that obtaining the SCC decomposition

takes time $\mathcal{O}(|V| + |E|)$ by Tarjan's strongly connected components algorithm (Tarjan, 1972). Similarly, by the result of Alstrup et al. (1999), one can find the dominator tree of a digraph in time $\mathcal{O}(|V| + |E|)$.

Corollary 3.3.6. *There is an algorithm that finds the decomposition of G into prime components $G_1, \ldots, G_k$ in time $\mathcal{O}(|V| + |E|)$.*

3.4 Discussion

We studied the fundamental problem of factorising the Kirchhoff polynomial into irreducible factors. We provided a graph-theoretic structural characterization of digraphs corresponding to prime factors of $\kappa(G)$. Based on this we presented a linear-time digraph decomposition technique that corresponds to the prime factorization of $\kappa(G)$.

The presented decomposition technique has numerous uses, owing to its properties coming from the prime factorization of the Kirchhoff polynomial, preservation of structural properties, and compressed representation inherent to polynomial factorisation.

The fundamental insight provided by the decomposition is that practical arborescence enumeration and Kirchhoff polynomial generation is not directly dependent on the (super) exponentially growing number of arborescences but, rather, depends on digraph structure. The decomposition rules hint at what the structure of a digraph needs to be, in order to allow an effective (practical) enumeration of arborescences/Kirchhoff polynomial generation. An immediate example are digraphs, whose Kirchhoff polynomials factorize exclusively to small (say, constant size) prime factors. These digraphs (and others) form the class of *practically enumerable digraphs* – the class PE for short. In this thesis we do not aim to classify PE exactly. We note that the mechanics of the SCC decomposition (Theorem 3.3.2) and domination decomposition (Theorem 3.3.3) can be reversed to define a build-up procedure for generating non-trivial digraphs belonging to the class PE. For example, given two rooted digraphs $P, G \in \text{PE}$, we can obtain the digraph $P \circ G$ in which all vertices of G are dominated by one particular vertex p from P and $\kappa(P \circ G) = \kappa(P) \cdot \kappa(G)$. Additionally, G can be composed of multiple SCCs factorizing as $\kappa(G) = \kappa(P_1) \cdot \ldots \cdot \kappa(P_n)$, where $P_1, \ldots, P_n \in \text{PE}$. Interestingly, many digraphs obtained from real-life applications possess rich hierarchical and modular structure (Barabasi & Oltvai, 2004; Meunier et al., 2010), which could facilitate the practical enumeration of their arborescences.

The prime factorisation technique is central to this thesis since it establishes a theoretical basis for efficient generation and manipulation of Kirchhoff polynomials (Chapter 4) and a direct link between model topology and its dose-response function (Chapter 5) which are invaluable when modelling biological systems using steady-state Laplacian models (Chapter 6).

The decomposition can also find relevance in a wider context of applications. In many situations, one needs to enumerate/count only arborescences of certain type, e.g., those of minimum cost, or those of bounded degree. Our preliminary experimental investigation suggests that our decomposition technique might be of

practical/theoretical use. Also, note that we can sample, uniformly at random, an arborescence from the factorised form of $\kappa(G)$ as follows: pick a random monomial from each of the prime factors.

3.5 Contributions and Acknowledgements.

This chapter is based on the material originally published as Mihaľák et al. (2016) and developed in collaboration between M. Mihaľák (MM), P. Uznański (PU), and P. Yordanov (PY). PY conceived and initiated the study, and provided an initial proof about the SCC decomposition. PU devised the domination decomposition and the linear running time of the decomposition algorithm. PU and MM developed the combinatorial proofs. All authors wrote the manuscript.

We are grateful to Peter Widmayer and Jörg Stelling for the support and fruitful discussions. We thank Victor Chepoi for valuable suggestions regarding the proof of Lemma 3.2.6.

4

Manipulation and Generation of Expressions of Kirchhoff Polynomials

4.1 Introduction

The great significance of Kirchhoff polynomials stems from their instrumental role in understanding linear diffusion processes (of information, probabilities, concentrations) on (di)graph models which are abundant in science. Hence they have found essential applications and parallel developments in diverse disciplines, such as electrical engineering (Kirchhoff, 1847), probability theory (Leighton & Rivest, 1986; Anantharam & Tsoucas, 1989; Biane, 2015), and physics (Weinzierl, 2013).

Classically in biology, Kirchhoff polynomials are obtained as the (symbolic) expressions corresponding to King-Altman patterns which serve to derive steady-states and steady-state rate laws of enzyme reaction mechanisms (King & Altman, 1956). More precisely, King-Altman patterns are spanning trees/arborescences of biochemical reaction mechanisms represented as graphs/digraphs in which vertices denote biochemical species and edges mark the reactions between the species. As introduced in previous chapters we focus on biochemical networks represented as digraphs which allow for irreversible reactions. Recall that such biochemical mechanisms contain reactions exclusively governed by (pseudo) first- and zero-order mass-action kinetics (Poland, 1989), which we call *Laplacian models*. Models with this linear structure are frequently obtained when applying time-scale separation and have provided important insights to a wide spectrum of biological areas such as enzyme kinetics, allosteric enzymes, G-protein coupled receptors, ion channels, gene regulation, and post-translational modification (Gunawardena, 2012). Besides, they continue guiding us understand biological systems (Gunawardena, 2014), notably finding application when the widely used equilibrium assumption is inadequate and non-equilibrium steady-states have to be derived (Ahsendorf et al., 2014; Estrada et al., 2016).

In Chapter 2 we introduced a central property of Laplacian models, namely that they have a unique steady-state (in case their corresponding digraph is strongly

connected) , which can always be derived symbolically through the generation of appropriate Kirchhoff polynomials. Symbolic derivation of steady-states is invaluable when parameter values in a model are uncertain or unknown, as is commonly the case in biological models, and provides a direct link between model structure and its steady-state functional capabilities. Yet, despite their apparent mathematical simplicity, Laplacian models frequently suffer from the problem of exponential, and even super-exponential, growth of the size of their Kirchhoff polynomials and, respectively, their symbolic steady-state expressions. For example, an enzyme state transition model of Prostaglandin H Synthase 1 (PGHS-1) from Goltsov et al. (2010) with 30 vertices and 118 edges has 24 quadrillion arborescences which translates to a Kirchhoff polynomial of size 735 quadrillion. It is evident that symbolic steady-state expressions of such size are essentially impossible to derive and manipulate. Even when we are interested in the ratio between the steady-states of two species or their difference (as in steady-state rate laws), which can be far simpler than the original expressions due to algebraic simplifications, we have to generate complete Kirchhoff polynomials and symbolically manipulate and simplify them.

The inherent problem of practical generation and manipulation of steady-state expressions derived from Laplacian models was the primary incentive for King and Altman to develop their method as means to visually facilitate manual derivations instead of erroneously expanding determinants by hand. Their influential work triggered a prolific succession of methods and software (reviewed in Qi et al. (2009)) to derive steady-states and rate equations for Laplacian models of biological systems. Graph theoretical methods were proposed which provide rules and exploit symmetries to simplify derivations of steady-states and steady-state reaction rates (Volkenstein & Goldstein, 1966; Chou & Forsén, 1980). Other methods assume rapid equilibrium for some reactions (Cha, 1968) and employ systematic determinant expansion (Varon et al., 1997; Garcia-Sevilla et al., 2010). A particularly prominent approach is Wang algebra, a set of simple algebraic rules to determine unimodular discriminants (Duffin & Morley, 1978), since it allows to easily formulate Kirchhoff polynomials, although in a form which requires expression expansion and elimination of redundant terms (Fromm, 1970; Lam & Priest, 1972; Indge & Childs, 1976; Qi et al., 2009).

In the field of computer science developments have also been made to enumerate the set of all arborescences from which Kirchhoff polynomials are obtained. Gabow & Myers (1978) presented an algorithm for enumerating all arborescences with $O(|E| + N \cdot |E|)$ running time (N being the number of arborescences) and $O(|E|)$ space requirements. Later, this algorithm has been improved by the currently two state-of-the-art algorithms (Uno, 1996; Kapoor & Ramesh, 2000). Both algorithms start by computing an initial (arbitrary) arborescence, and then, iteratively, compute "close-by" arborescences by outputting only the edge-difference to the previously computed and listed arborescence. Uno (1996) uses a reverse search, while Kapoor & Ramesh (2000) use depth-first search in the space of all arborescences (represented as an undirected graph where a node corresponds to an arborescence and an edge denotes a single edge-swap between the two adjacent arborescences). The algorithm of Uno runs in $O(|E|+N \cdot \sqrt{|V|}\log(|E|/|V|))$ time

and has space complexity $O(|E|)$, and the algorithm of Kapoor and Ramesh runs in $O(N|V| + |V|^3)$ time and has a space complexity $O(|V|^2)$.

Despite the considerable progress the existing methods and algorithms all suffer from the "(super)exponential scaling curse" and only offer limited and *ad hoc* manipulation of steady-state expressions. The number of arborescences is present in the time and space complexity classes of all available algorithms and it is regarded as a hard bound on how well the algorithms can perform. This fact hinders the analysis of larger and more detailed models which follow from the advancement in experimental techniques such as phosphoproteomics to study posttranslational modification of proteins (Gnad et al., 2011).

Exponential scaling of the size of Kirchhoff polynomials seems insurmountable but any approach that mitigates it would greatly benefit the applications of Laplacian models in biology, namely would deepen structure-function understanding and allow analysis of larger models. An important step in the direction of taming the exponential growth is the realisation in Chapter 3 that Kirchhoff polynomials can be efficiently factorised into irreducible factors which provides a natural compact representation that is not directly dependent on the number of arborescences but is, rather, determined by digraph connectivity.

In this chapter, we employ the prime factorisation of Kirchhoff polynomials from Chapter 3 as a basis to efficiently manipulate and compactly generate them. We develop theory and algorithms to simplify expressions of Kirchhoff polynomials, bypassing expensive symbolic generation and manipulation of lengthy expressions by computer algebra systems. We achieve this by considering the prime components of all Kirchhoff polynomials in an expression as symbolic variables. The resulting coarse-grained expressions allow for symbolic simplification without the explicit generation of the polynomials. This is possible since we derive one necessary and one sufficient condition defining when different prime digraphs have equal Kirchhoff polynomials. Further, we study how to do arithmetic and calculus with Kirchhoff polynomials without explicitly generating them. We demonstrate the benefits of efficient manipulation for cases in which lengthy expressions of Kirchhoff polynomials can be significantly simplified.

To explicitly generate the Kirchhoff polynomials, e.g. as is needed for their repeated evaluation, we examine one recursive and one iterative algorithm inspired by algebraic simplification. The algorithms alternate between prime decomposition and edge deletion-contraction in every prime component which decomposes the irreducible component into a sum of desirably reducible digraphs. Although it is a hard and instance specific problem to decide which edges to delete-contract in order to obtain a maximally compressed Kirchhoff polynomial, we examine various compression heuristics. We achieve additional compression within the iterative algorithm since it identifies digraphs with identical Kirchhoff polynomials during runtime and thus avoids redundant Kirchhoff polynomial generation. We apply the algorithms to a collection of Laplacian models and observe that digraph connectivity aware heuristics prove to be useful in practice and achieve large compressions and short running times. The developed methods and algorithms are implemented in a Python package called *KirchPy*.

4.2 Efficient Manipulation of Expressions of Kirchhoff Polynomials

In Section 2.4 we have already seen that the steady-states of Laplacian models are ratios of Kirchhoff polynomials, or put more generally they are expressions of Kirchhoff polynomials. Similarly, any symbolic expressions derived from steady-state Laplacian models through arithmetic and calculus would also be expressions of Kirchhoff polynomials. Such examples are ratios of steady-states, steady-state rate equations, the, so called, differential expressions which are the main subject of study in Chapter 5, and differentiated steady-state expressions with respect to a reaction constant to determine parameter sensitivities.

Expressions of Kirchhoff polynomials appear to play a central role in the analysis of steady-state Laplacian models. Developing methods for their algebraic manipulation is important to understand when the expressions can be simplified. If simplification is possible, long expressions can be transformed into shorter and more comprehensible ones, and if simplification is impossible it is time-saving to know that additional manipulation would not be useful. For example, the steady-state of a Laplacian model, which is a ratio between Kirchhoff polynomials, can be simplified if the numerator and denominator share common factors. After all common factors are crossed out the numerator and denominator become relatively prime and further simplification is not possible. Non-trivial steady-states of closed systems can never be simplified since their denominators corresponds to Kirchhoff polynomials of strongly connected digraphs which are always prime. In contrast, it could be possible to simplify the steady-state of an open system since its numerator and denominator are both Kirchhoff polynomials of rooted digraphs. It could happen that the rooting operations delete edges which decompose the numerator and denominator into prime factors, some of which could be crossed out.

Despite its importance, symbolic simplification can prove impractical due to the (super) exponentially growing size of Kirchhoff polynomials. We show how to circumvent tedious symbolic manipulation by exploiting particular properties of Kirchhoff polynomials which allow their implicit manipulation, that is without explicitly generating polynomials in expanded form but working with the corresponding digraphs. More precisely, our approach is to:

(i) find the prime components corresponding to prime factors of all Kirchhoff polynomials in the expression, then

(ii) determine which prime components generate identical Kirchhoff polynomials, and

(iii) form a *coarse-grained representation* of the original expression by substituting prime components with symbolic variables, where prime components with identical Kirchhoff polynomials are assigned the same variable, and finally,

(iv) symbolically simplify the resulting coarse-grained expression.

Prime decomposition is performed in linear time as seen in Chapter 3 and we rely on available software for symbolic simplification. It remains to determine how to efficiently decide which prime components generate equal Kirchhoff polynomials without their explicit generation.

4.2.1 Prime Digraphs with Equal Kirchhoff Polynomials

We consider Kirchhoff polynomial equality in the algebraic sense, and not as a general isomorphism between polynomials in which the identity of the variables does not matter as long as they can be mapped through a bijection between the compared polynomials. Thus it is important to remark that by uniquely labelling a digraph we assign identity to each edge through its label, that is, a label defines a particular reaction. Applying the digraph operations of prime decomposition, edge deletion, edge contraction, and vertex rooting to a uniquely labelled digraph preserves the identity of the reactions while the names of the vertices can change. However, when comparing two Kirchhoff polynomials originating from different sources, e.g. when evaluating competing hypotheses expressed through Laplacian models with rearranged reactions, identical reactions between the sources need to carry the same label and different reactions – different labels, in order to have a meaningful comparison.

A necessary condition for two polynomials to be equal is to have the same set of variables corresponding to terms with non-zero coefficients. This condition cannot be transferred directly to compare the digraphs generating the Kirchhoff polynomials polynomials because it is possible that the digraphs contain *nuisance edges* which do not take part in any arborescence. Thereby, the set of labels of two digraphs generating equal Kirchhoff polynomials will be different when one or both of them contain nuisance edges. Next we show that if we concentrate on comparing only prime digraphs we can prove that they do not contain nuisance edges since every edge participates in, at least, one arborescence.

Theorem 4.2.1. *Let G be a prime digraph, then each edge in G participates in at least one arborescence.*

The non-existence of nuisance edges in *prime digraphs* (digraphs with prime Kirchhoff polynomials) allows us to formulate a necessary condition for Kirchhoff polynomial equality in Corollary 4.2.2.

Corollary 4.2.2. *Let G and H be two prime digraphs with equal Kirchhoff polynomials, then G and H have equal sets of edge labels, i.e. $\kappa(G) = \kappa(H) \Rightarrow \ell(G) = \ell(H)$.*

Proof. Follows directly from Theorem 4.2.1. □

The condition can be tested efficiently since it involves only a comparison between sets. It is also easy to show that it is not a sufficient condition for Kirchhoff polynomial equality. An example is given in Figure 4.1a depicting two digraphs with equal edge labels sets but different Kirchhoff polynomials.

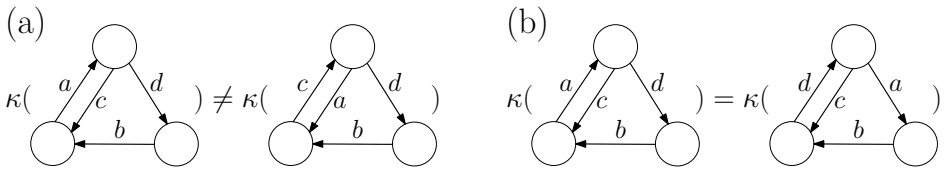

Figure 4.1: Examples for (a) two digraphs with equal edge label sets but different Kirchhoff polynomials and for (b) two non-λ-isomorphic prime digraphs with identical Kirchhoff polynomials.

We continue by presenting a digraph-based sufficient condition of Kirchhoff polynomial equality. We define the term *identical-label-isomorphism* (for short λ-*isomorphism*) to denote a vertex bijection which is edge-preserving and enforcing the corresponding edges to have identical labels.

Definition 4.2.3 (λ-isomorphism)**.** *Two labelled digraphs G and H are called identical-label-isomorphic (for short λ-isomorphic), denoted $G \simeq_\lambda H$, iff there exists a bijective mapping $\psi : V(G) \mapsto V(H)$, such that:*

1. *$uv \in E(G)$ iff $\psi(u)\psi(v) \in E(H)$ and*
2. *$\ell(uv) = \ell(\psi(u)\psi(v))$.*

It is evident that two λ-isomorphic digraphs give rise to identical Kirchhoff polynomials since the digraphs differ only by vertex names and otherwise have identical topology and labels.

Observation 4.2.4. *Let G and H be λ-isomorphic, then they generate identical Kirchhoff polynomials, i.e. $G \simeq_\lambda H \Rightarrow \kappa(G) = \kappa(H)$.*

To derive a condition testing for λ-isomorphism we need the definition of the, so called, *line digraph* $\mathscr{L}(G)$ associated to a given digraph G.

Definition 4.2.5 (Line digraph)**.** *The line digraph $\mathscr{L}(G)$ associated to the digraph G satisfies the conditions:*

1. *the vertices of $\mathscr{L}(G)$ are the* unique edge labels *of G, i.e. $V(\mathscr{L}(G)) \equiv \ell(G)$ and*
2. *two vertices $u, v \in V(\mathscr{L}(G))$ are joined by a directed edge uv iff $u = \ell(rs), v = \ell(st)$ for $r, s, t \in V(G)$.*

Theorem 4.2.6. *Two prime digraphs G and H are λ-isomorphic iff the edge sets of their line digraphs are equal, i.e. $G \simeq_\lambda H \Leftrightarrow E(\mathscr{L}(G)) = E(\mathscr{L}(H))$.*

Theorem 4.2.6 allows us to formulate a sufficient condition for prime Kirchhoff polynomial equality.

Corollary 4.2.7. *Let G and H be two uniquely labelled prime digraphs whose line digraphs have equal edge sets, then the Kirchhoff polynomials they generate are equal, i.e.* $E(\mathscr{L}(G)) = E(\mathscr{L}(H)) \Rightarrow \kappa(G) = \kappa(H)$

Proof. Follows directly from Observation 4.2.4 and Theorem 4.2.6. □

The sufficient condition for prime Kirchhoff polynomial equality presented in Corollary 4.2.7 is also cheap to evaluate since it only involves line digraph construction which has quadratic time complexity and the comparison of two sets. The condition is not necessary for prime Kirchhoff polynomial equality because two non-λ-isomorphic prime digraphs can generate identical Kirchhoff polynomials as presented in Figure 4.1b.

4.2.2 Formulation of Coarse-Grained Expressions and Their Algebraic Manipulation

We use the conditions from Corollary 4.2.2 and Corollary 4.2.7 to assign identical variable names to prime digraphs with equal Kirchhoff polynomials in order to formulate the coarse-grained description of an expression of Kirchhoff polynomials without their explicit generation. First we apply the necessary condition to filter possible matches and then the sufficient one to certify the equality. Pairs of prime digraphs which are non-λ-isomorphic but have the same label sets require special attention. If such are present we cannot guarantee that we have identified all digraphs with equal Kirchhoff polynomials. This uncertainty translates to lack of guarantees for maximal symbolic simplification of the coarse-grained description. On the other hand, when such pairs of digraphs are not present in the expression we can guarantee the exhaustive identification of prime digraphs with equal Kirchhoff polynomials. Further, the comparisons of prime digraphs can be sped up by realizing that each prime component of a digraph can be equal to at most one prime component of another digraph, since prime factorisation partitions the set of labels.

It is also important to note that although the conditions are not necessary and sufficient in general, they could be such in certain cases. For example, when we compare the Kirchhoff polynomials of two prime digraphs G_1 and G_2 obtained from the same digraph G by means of edge deletion and prime decomposition we can be sure that they have the same Kirchhoff polynomials iff they have equal edge label sets. This is due to the fact that starting from a common uniquely labelled digraph G, edge deletions (removal of edges) and prime decomposition (partition of edges) do not change the comparative topology of G_1 and G_2. An example for such expressions derived from a single digraph by means of edge deletion and prime decomposition are the steady-state expressions of open Laplacian models – their numerator and denominator contain Kirchhoff polynomials of rooted digraphs which could possibly be prime decomposable. On the other hand, edge contractions have the capacity to permute the edges and lead to the examples form Figure 4.1.

Once coarse-grained expressions are formulated they can be symbolically simplified with any computer algebra system, e.g. Python's SymPy or Mathematica.

For example, we can find the *greatest common divisor* between the numerator and denominator of a ratio like an open systems' steady-state expression and simplify it to an irreducible fraction, or take out a common factor from a sum of products of Kirchhoff polynomials to obtain a shorter form of the expression.

Note that there might be reasons different from incompletely identifying digraphs with equal Kirchhoff polynomials that do not guarantee full simplification. For example, simplification on a lower or higher level from the coarse-graining could be possible. One such instance is the difference between two prime Kirchhoff polynomials which share monomials (the corresponding digraphs share arborescences). The common monomials will cancel out if the Kirchhoff polynomials are written in explicit form but cannot be cancelled in the coarse-grained representation. Partially developing the prime Kirchhoff polynomials, e.g. using the edge deletion-contraction identity, to sums containing the shared monomials could often turn to be lengthy. Another instance is when the sum or difference can be reduced by combining Kirchhoff polynomials to form the Kirchhoff polynomial of another digraph. For example, according to the edge deletion-contraction identity if we identify digraphs $G \setminus e$ and G/e in the expression $\kappa(G \setminus e) + \ell(e)\kappa(G/e)$ we can simplify it to $\kappa(G)$. Other variations of this identity are also possible, e.g. the expression $\frac{\kappa(G)-\kappa(G\setminus e)}{\ell(e)}$ can be written simply as $\kappa(G/e)$.

Note that some proofs and derivations are constructed under the assumption that the digraph models have unique and irreducible expressions in their labels. If this assumption is not met, e.g. when different reactions are assumed to have the same rate constant, rate constants are expressions which can be simplified or contain symbols shared across different labels, then additional symbolic simplification might be required since the primality of the decomposition is not guaranteed and the manipulation formulas of the coarse-grained representation might not hold.

4.2.3 Calculus of Kirchhoff Polynomials

The study of steady-state Laplacian systems is not complete without an understanding of how to efficiently apply differentiation and integration to Kirchhoff polynomials. Frequently, we need to evaluate the sensitivities of steady-states to small changes in reaction-rate constants. Again, generating the full form of the contained Kirchhoff polynomials and differentiating could be difficult due to their length. We show that the properties of Kirchhoff polynomials allow to map differentiation and integration to digraph operations and thus work with the implicit coarse-grained representation.

Taking the partial derivative of a Kirchhoff polynomial with respect to a reaction rate constant $\ell(e)$ corresponding to the edge e is equivalent to edge contraction in the corresponding digraph as shown by Identity 4.2.8.

Identity 4.2.8.

$$\frac{\partial \kappa(G)}{\partial \ell(e)} = \kappa(G/e).$$

We can also derive a differentiation rule for digraphs with available prime decomposition. Then, since prime decomposition is a partition of labels, we need only contract the edge in a single prime component.

Identity 4.2.9.

$$\frac{\partial\kappa(G)}{\partial\ell(e)} = \kappa(P_1/e)\prod_{i=2}^{n}\kappa(P_i),$$

where P_1 is the single prime component of G containing e and P_i are the remaining $n-1$ prime components.

Along the same lines, we can derive a formula for the ratio of Kirchhoff polynomials composed of two digraphs G and H.

Identity 4.2.10. *Let the prime factorisation of the Kirchhoff polynomials $\kappa(G)$ and $\kappa(H)$ be $\kappa(G) = \prod_{i=1}^{n}\kappa(P_i)$ and $\kappa(H) = \prod_{j=1}^{m}\kappa(Q_j)$, then:*

$$\frac{\partial}{\partial\ell(e)}\frac{\kappa(G)}{\kappa(H)} = \frac{\prod_{i=2}^{n}\kappa(P_i)}{\kappa(Q_1)^2\prod_{j=2}^{m}\kappa(Q_j)}\left(\kappa(P_1/e)\kappa(Q_1) - \kappa(P_1)\kappa(Q_1/e)\right),$$

where P_1 and Q_1 are the prime components of G and H, correspondingly, containing e.

It could be possible to further factorise the derived expressions since edge contraction could change the connectivity of the digraphs.

Integrating a Kirchhoff polynomial with respect to a label $\ell(e)$ corresponding to the edge e is equivalent to multiplication by $\ell(e)$ and edge relabelling in the corresponding digraph as seen from Identity 4.2.11.

Identity 4.2.11.

$$\int \kappa(G)d\ell(e) = \ell(e)\kappa(G^{\ell(e)\leftarrow\frac{\ell(e)}{2}}) + C,$$

where C is the integration constant and $\ell(e) \leftarrow \frac{\ell(e)}{2}$ denotes a relabelling operation replacing the label of e by the same label divided by two, e.g. if the old label was $\ell(e) = r_1$ the new would be $\ell(e) = \frac{r_1}{2}$.

Note that integration does not change the factorisation properties of G since its connectivity remains unchanged and that the labels remain unique unless $\frac{\ell(e)}{2}$ is already labelling another edge in the digraph.

4.2.4 Results

To illustrate the manipulation of expressions of Kirchhoff polynomials in the coarse-grained representation, we first consider the simple open receptor trafficking model with a digraph G_1 shown in Figure 4.2a. It consists of species for an unbound surface receptor R, a cell surface ligand-receptor complex RL, their respective internalized counterparts R_i and RL_i, and a set of state transition,

(a) G_1

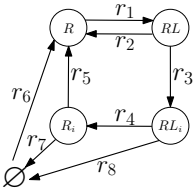

(b)

$$x^{SS}_{RL_i} = \frac{\kappa_{RL_i}(G_1)}{\kappa_{\varnothing}(G_1)} = \frac{r_6(r_5+r_7)}{r_7r_8+r_5r_8+r_4r_7}$$

(c) G_2

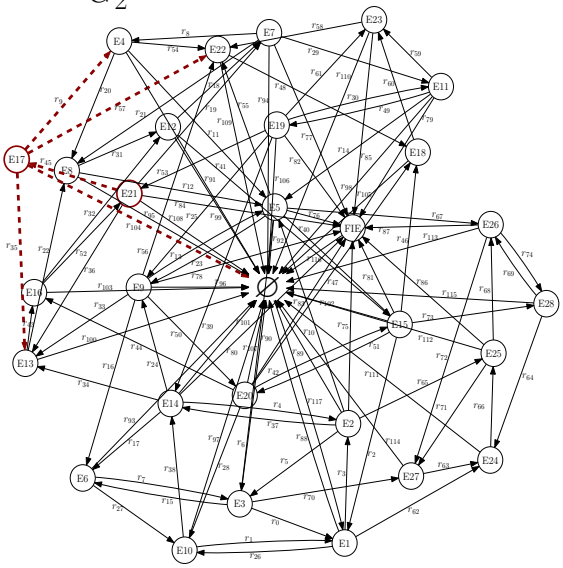

(d)

$$\frac{x^{SS}_{E21}}{x^{SS}_{E17}} = \frac{\kappa_{E21}(G_2)}{\kappa_{E17}(G_2)} = \frac{r_9+r_{35}+r_{104}+r_{57}}{r_{45}}$$

Figure 4.2: Simplification of expressions of Kirchhoff polynomials in the coarse-grained representation. (a) Simple receptor trafficking model G_1 and (b) the simplification of its steady-state expression. Prime components with equal Kirchhoff polynomials have the same colour. Note that vertex labels are not important since they can change during edge contractions. Also, the symbol κ is omitted in front of the digraphs for visual clarity. (c) A model of the PHGS catalytic cycle G_2 (see COX in Table 8.1) from Goltsov et al. (2010) and (d) the steady-states ratio of species $E21$ and $E17$ obtained through the coarse-grained representation. Coloured vertices denote the species of interest and the coloured dashed arrows denote reactions contained in the simplified ratio.

synthesis, and degradation reactions. In Figure 4.2b we derive the steady-state for RL_i by prime decomposing the digraphs in the steady-state ratio and crossing out the common factors. We see, without the complete generation of the polynomials $\kappa_{RL_i}(G_1)$ or $\kappa_{\varnothing}(G_1)$, that the resulting expression does not depend on the rate constants r_1 and r_3.

The advantage of the coarse-grained representation becomes more pronounced for expressions consisting of digraphs with numerous arborescences. Let us consider the model of the PHGS catalytic cycle from Goltsov et al. (2010) shown in Figure 4.2c as G_2 and derive the ratio of the steady-states of species $E21$ and $E17$. Taking the standard approach, we have to generate the Kirchhoff polynomials $\kappa_{E21}(G_2)$ and $\kappa_{E17}(G_2)$, and symbolically simplify their ratio. However, each of them consists of trillions of arborescences (respectively 280,420,755,225,601 and 2,336,839,626,880) which makes both generation and simplification impossible in practice. Adopting the digraph-based coarse-grained form implemented in *KirchPy* we obtain the resulting very short expression shown in Figure 4.2d instantly.

4.3 Compact Generation of Expressions of Kirchhoff Polynomials

After simplifying an expression of Kirchhoff polynomials in its coarse-grained form we can observe which labels have vanished (the corresponding reactions do not affect the expression) and which remain (the corresponding reactions might affect the function modelled by the expression). However, to symbolically obtain the simplified expression for further analysis or repeated evaluation, e.g. for parameter space exploration, we have to abandon the coarse-grained representation and explicitly generate full-length Kirchhoff polynomials. To do that, we can once more take advantage of the coarse-grained representation and only generate the Kirchhoff polynomials for prime components with dissimilar Kirchhoff polynomials. For this reason, in what follows, we focus on Kirchhoff polynomial generation for individual digraphs and not in expressions of Kirchhoff polynomials.

4.3.1 Problem Formulation

The standard approaches for Kirchhoff polynomial generation based on arborescence enumeration reviewed in the introduction provide us with (super) exponentially growing output and evaluation time due to the frequently (super) exponential growth of the number arborescences in digraphs. In order to lessen the exponential blow-up in Kirchhoff polynomial length, we take a new approach to Kirchhoff polynomial generation, namely, that of algebraic simplification – compression of the polynomial to an equivalent but more compact form. Thus we look for an algorithm C taking as an input a digraph G and producing an algebraically equivalent representation of its Kirchhoff polynomial $\Gamma_C(\kappa(G))$ with size as small as possible.

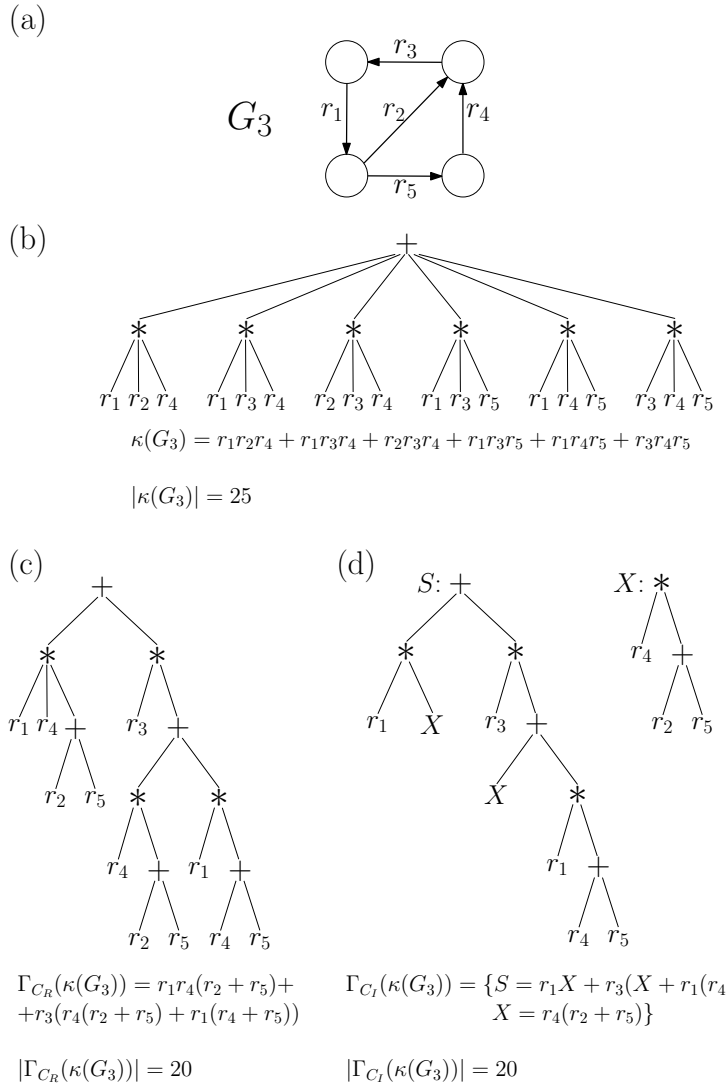

Figure 4.3: Algebraically equivalent Kirchhoff polynomials, their expression trees, and sizes for (a) an example digraph G_3 in (b) fully expanded form, (c) factorised form obtained by algorithm C_R, and (d) change of variables form (forest of expression trees) obtained by algorithm C_I. Note that the size of a Kirchhoff polynomial representation is the sum of the number of branch vertices and the number of leaves in its expression tree. Additionally, when change of variables is applied, each expression tree from the forest is assigned a pointer counting as 1 to the size of the representation and pointing to the leaves of other expression trees where it should be substituted to obtain the expression tree of the complete Kirchhoff polynomial. The pointer S denotes the "starting" expression tree.

An ideal algorithm C would take a digraph and generate its Kirchhoff polynomial in a maximally compact form, bypassing explicit generation and tedious simplification. It is hard to determine the best algorithm C and to even check if a Kirchhoff polynomial is fully simplified. For that reason, we aim to propose algorithms which, despite not giving guarantees for maximal compression, heuristically provide us with satisfactory results to practical problems.

Inspired from polynomial simplification, and more precisely by the well-known polynomial simplification techniques of factorisation, taking out a common factor, and change of variables, we find digraph operation counterparts to those symbolic manipulation techniques for Kirchhoff polynomials and use them to propose two greedy generation algorithms.

An important caveat is that the change of variables procedure requires an extension of the definition of Kirchhoff polynomial representation size since it produces a forest of expression trees instead of a single expression tree as can be seen in Figure 4.3. We define the size of a Kirchhoff polynomial for such a representation as the the total number of branch vertices and leaves in the forest plus the number of expression trees in the forest. It is necessary to account for the number of expression trees since each of them is given a unique pointer indicating its location within the other expression trees.

4.3.2 Recursive Algorithm C_R

The prime decomposition developed in Chapter 3 behaves as the ideal algorithm C for compression – it takes a digraph and, in linear time, produces a guaranteed maximally compact form due to the irreducibility of each prime component. However, it cannot be applied to prime digraphs, which can also have sizeable Kirchhoff polynomials. Thus we need an additional procedure to compress the Kirchhoff polynomials of the prime components. We achieve this by rearranging irreducible Kirchhoff polynomials, particularly by taking a factor out from part of their monomials, such that we can further factorise parts of them. Factoring out a variable in a Kirchhoff polynomial, without its explicit generation, is achieved through the deletion-contraction identity introduced by Proposition 2.5.2. To recall, after choosing an edge $e \in E(G)$, any Kirchhoff polynomial can be written as the sum:

$$\kappa(G) = \kappa(G \setminus e) + \ell(e)\kappa(G/e),$$

in which, for a prime G, the modified digraphs $G \setminus e$ and G/e could be amenable to further prime decomposition since e's deletion and contraction could change the connectivity of G.

With this insight, we formulate the algorithm C_R whose pseudocode can be found in Section 8.2.2 of the appendix as Algorithm 2. It takes a digraph G, and recursively alternates between prime decomposition and edge deletion-contraction in every prime component until digraphs are reduced to a single vertex or a single edge, whose polynomials are trivial to generate. The algorithm is easy to implement and produces an expression tree as in Figure 4.3c that is more compact than the expanded form of the Kirchhoff polynomial. Importantly, the compact

form can easily be evaluated and analysed, but multiple recursive calls could unnecessarily work on large digraphs having the same Kirchhoff polynomial.

4.3.3 Iterative Algorithm C_I with Change of Variables

We propose a second algorithm, C_I (for pseudocode see Section 8.2.2, Algorithm 3), employing the digraph comparisons certifying Kirchhoff polynomial equality developed in Section 4.2.1 to eliminate the potential redundancy of multiply generating identical Kirchhoff polynomials.

As in C_R, given a digraph G, C_I alternates between prime decomposition and edge deletion-contraction to reduce the Kirchhoff polynomial generation problem to several smaller ones. Differences to C_R are that a unique pointer is associated to every digraph, and that C_I adds the reduced digraphs to a queue for further reduction, simultaneously remembering the partial expression tree they participate in. A *partial expression tree* is such a tree in which leaves could correspond to Kirchhoff polynomials. For example, the deletion-contraction identity from Proposition 2.5.2 provides a partial expression tree in which two leaves are Kirchhoff polynomials, $\kappa(G \setminus e)$ and $\kappa(G/e)$, and one is an edge label $\ell(e)$. Thus this tree can be remembered after substituting $\kappa(G\setminus e)$ and $\kappa(G/e)$ with their pointers, and the digraphs corresponding to these Kirchhoff polynomials taken for further reduction. Additionally, during the reduction procedure every prime component is compared to all previously encountered prime components using the edge label and the λ-isomorphism tests from Corollary 4.2.2 and Corollary 4.2.7. If the equality of a prime component's Kirchhoff polynomial to a previously considered digraph's Kirchhoff polynomial cannot be certified, then the prime component is taken for further reduction. In contrast, if a prime component and a previously encountered digraph H have equal Kirchhoff polynomials, then the reduction of the prime component is discontinued and its Kirchhoff polynomial is substituted with the pointer of H, thus marking the identity. Algebraically this is equivalent to a change of variables – substituting identical parts of the Kirchhoff polynomial with identical symbols and explicitly generating them only once (see Figure 4.3d). The reduction procedure again continues until digraphs are reduced to a single vertex or a single edge and produces a set of partial expression trees.

The partial expression trees are then assembled. The assembly starts from the given digraph G (with pointer S) and its partial expression tree which is sequentially merged with the partial expression trees of its reduced digraphs. The merging proceeds if the current reduced digraph has not been matched with another digraph with identical Kirchhoff polynomial. If a match is present, then the partial expression tree of the reduced digraph is substituted with the pointer, e.g. X, (as a variable) of a predetermined digraph with equal Kirchhoff polynomial encountered during the reduction procedure (could be the current digraph itself) and merging is discontinued. Simultaneously, another assembly is initiated starting from X and its corresponding digraph to obtain a forest of expressions marked with the pointers of the initializing digraphs as in Figure 4.3 d. This forest of expression trees corresponds to a set of Kirchhoff polynomials, which after being substituted into each other give rise to the complete Kirchhoff polynomial of the

given digraph G.

Note that substitution is unnecessary when evaluating the Kirchhoff polynomial for a given set of edge label values. There exists a sequence obtainable in linear time in which the expression trees from the forest can be evaluated such that there are no uncalculated pointer variables during the evaluation. The reason is that the expression trees in the forest can be thought arranged in a directed acyclic graph, with vertices being the trees themselves and edges the change of variables directed relations, which can always be topologically sorted.

The resulting representation of the Kirchhoff polynomial is more compact than its expanded form and can still be easily evaluated and analysed. However, if there are few small digraphs with equal Kirchhoff polynomials encountered during the reduction, in comparison to C_R, C_I might consume more memory due to remembering pointers and already considered digraphs, have longer running time due to equality comparisons, and not provide significantly better compression (compare Figure 4.3c and d). On the other hand, if there are many large digraphs with equal Kirchhoff polynomials encountered during the reduction, only C_I could be capable to generate practically relevant Kirchhoff polynomials.

4.3.4 Heuristic Edge Deletion-Contraction

An important ingredient of both algorithms G_R and C_I is the choice of an edge for the deletion-contraction operation reducing the Kirchhoff polynomial of a prime digraph to the sum of the Kirchhoff polynomials of two smaller digraphs (function GetEdgeForDelContr in Algorithm 2 and Algorithm 3).

For us it is an open problem which edges to delete-contract in order to generate a maximally compressed Kirchhoff polynomial. Thus we resort to a heuristic approach, that is, we greedily select an edge to delete-contract such that a criterion on the decomposition properties, which we introduce later, is optimised. Since Kirchhoff polynomial generation results are instance specific we explore different heuristics to empirically look for rules leading to satisfactory compression.

The heuristics we consider follow a four-step procedure. For each step we propose several choices of *sub-heuristics*. Then the set of all heuristics we investigate contains all combinations of these sub-heuristics at the different steps of the procedure. More precisely, the procedure is (also see Box 8.1 in the appendix for a more concise description):

(i) Pre-select a subset of edges $E'(G) \subseteq E(G)$.

This subset could be a single randomly picked edge (leading to a random *connectivity-uninformed heuristic*), all edges, or a subset of edges connected to the digraph cycle structure (aiming to break open many or large cycles).

(ii) Apply edge deletion-contraction to G for each $e \in E'(G)$ and decide which branch of the deletion-contraction tree to consider, i.e. the edge deleted digraph $G \setminus e$, the edge contracted digraph G/e, or both $(G \setminus e, G/e)$.

This is required since edge contraction could also lead to edge deletions and thus to further prime decomposition.

(iii) Choose whether to decompose the digraphs in the considered edge deletion-contraction branch(es) to strongly connected components or to prime components.

SCC decomposition alone leads to Kirchhoff polynomial factorisation which is not guaranteed to be prime. Yet we include it as a sub-heuristic due to recent results in strong connectivity allowing to retrieve all strong bridges (Italiano et al., 2012), the total number of SCCs, and the size of the largest and of the smallest SCCs obtained after edge deletion in linear time (Georgiadis et al., 2015c). Note that, in order to have comparable running times when decomposing into prime components and SCCs, we naively delete-contract each considered edge and do not employ the mentioned recent advancements.

(iv) Calculate a score on the digraph decomposition and pick the edge producing an optimal score.

The score is based on the number, size distribution (in terms of number of vertices or edges), and *complexity* (number of arborescences) of components in the selected branch(es) of the deletion-contraction tree. The scores from the decompositions of $G \setminus e$ and G/e are summed when both branches are taken into account. We choose the edge whose deletion leads to a decomposition in which there are the largest number of SCCs/prime components, the largest component is the smallest, the total complexity is the smallest, or there are the largest number of components with the smallest total complexity.

We describe each heuristic by four integers, where each integer marks the choice of a sub-heuristic. See Box 8.1 from the appendix for the identifiers of each sub-heuristic we consider. For example, the heuristic $\mathcal{H} = 2205$ translates to a procedure in which we:

(i) **2:** Find the longest simple cycle S in the input digraph G and take its edges $E(S)$.

(ii) **2:** For every $e \in E(S)$ we apply deletion-contraction to obtain the digraphs from both branches of the deletion-contraction tree, $G \setminus e$ and G/e.

(iii) **0:** Obtain the strongly connected components for every $G \setminus e$ and G/e and add them to a list p_e.

(iv) **5:** Pick the edge producing the list p_e with the largest length and return the edge e. If there are several lists having the same length, we pick the one with the smallest total sum of component complexities and return the corresponding edge e.

We use the same heuristic throughout the whole reduction process of a given input digraph. Note that we denote the connectivity-uninformed heuristic (i) **0** as $\mathcal{H} = 0 * **$ since we need not apply the steps (ii), (iii), and (iv) having already chosen randomly an edge to delete-contract. Otherwise, we explore all 108

combinations of the different sub-procedures, which we call *connectivity-informed heuristics*. This amounts to 109 heuristics in total.

4.3.5 Results

We evaluated the running time and compression of the two Kirchhoff polynomial generation algorithms, C_R and C_I, employing the 109 described heuristics on a collection of biologically relevant examples (see Table 8.1 in the appendix for example description). We selected examples from literature having a wide spectrum of complexities – ten less complex digraph models with tens to millions of arborescences and two more complex models, HC4 and COXD, having tens of millions and quadrillions of arborescences, respectively. Although the collection may not be representative of all Laplacian models encountered in biology, it certainly is a diverse and challenging example set. Further, we define *compression* as the ratio between the size of the expanded representation of a Kirchhoff polynomial $|\Gamma_E(\kappa(G))|$ and the size of its representation produced by an algorithm C, $|\Gamma_C(\kappa(G))|$.

The first part of the analysis concerns the less complex examples and aims to shed light on relations and trade-off in performance between C_R and C_I, and the different heuristics. We obtained the compression and average running time (from 10 runs) for each example from this set using the 108 connectivity-informed heuristics with each algorithm, C_R and C_I. The connectivity-uninformed random heuristic $\mathcal{H} = 0 * **$ was run 20 times on each low complexity example for both C_R and C_I.

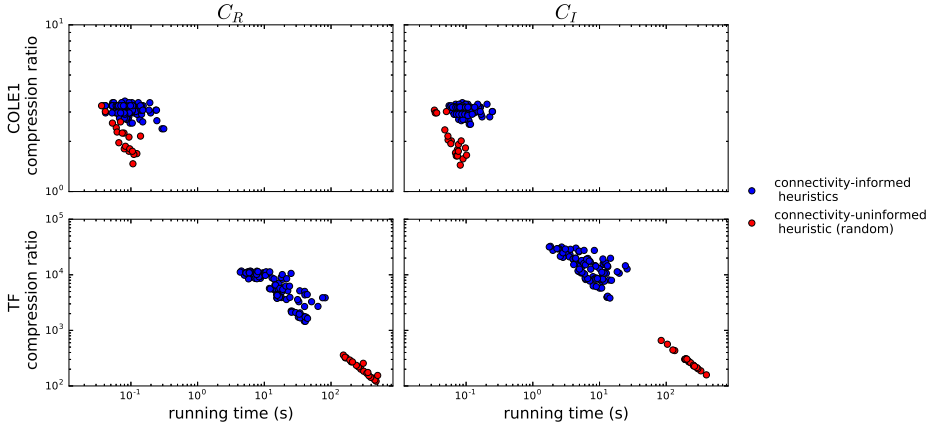

Figure 4.4: Scatter plots of running time versus compression obtained with each of the two Kirchhoff polynomial generation algorithms, (left column) C_R and (right column) C_I. The first row corresponds to COLE1, an example of low complexity (having 26 arborescences), the second row to an example with high complexity, TF (1.5 million arborescences). Blue points represent performance results for each of the 108 connectivity-informed heuristics and red points mark the results for the 20 runs of the uninformed random heuristic $\mathcal{H} = 0 * **$.

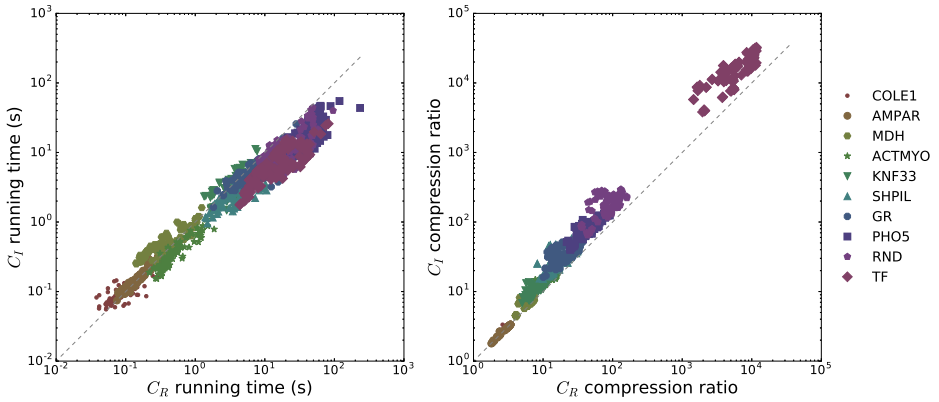

Figure 4.5: Scatter plots comparing the (left) running time and (right) compression of algorithms C_R and C_I on the collection of less complex examples described in Table 8.1. Each point represents the running time/compression for an example digraph obtained by C_R and C_I using the same connectivity-informed heuristic. The 45° dashed line marks equal running time/compression for C_R and C_I. The examples are sorted by complexity – COLE1 having the lowest complexity and TF the highest.

To understand how important the selection of the particular heuristic is we contrasted the performance of the algorithms run with the random uninformed heuristic $\mathcal{H} = 0 * **$ and with the informed heuristics incorporating digraph connectivity information on the collection of less complex examples. The results for an example with low complexity COLE1 and an example with high complexity TF are shown in Figure 4.4 (for results on all less complex examples see Figure 8.2 in the appendix). They indicate that several runs with the uninformed heuristic are enough to generate highly compressed Kirchhoff polynomials in short time for examples of low complexity, possibly due to the lack of computational overhead which is present for the informed heuristics. However, for digraphs with higher complexity, the performance of the random heuristic quickly deteriorates becoming orders of magnitude worse than the informed heuristics, as is evident from the results for example TF. This behaviour is expected since compressibility depends on digraph connectivity and it becomes less probable to randomly pick a set of edges for deletion-contraction in larger digraphs without any connectivity information. Additionally, we observe that running time and compression are inversely correlated (in log-log space) and the correlation becomes more pronounced when the complexity of the examples increases.

In Figure 4.5 we compare the performance of algorithms C_R and C_I for the connectivity-informed heuristics. The running time and compression results for examples of low complexity lie on or symmetrically around the 45° dashed line, which indicates that the two algorithms perform alike. The more complex the examples, the more apparent becomes the superiority of algorithm C_I over C_R. More points fall below the 45° line in the time comparison scatter plot indicating predominantly shorter running times for C_I on the same example instance and

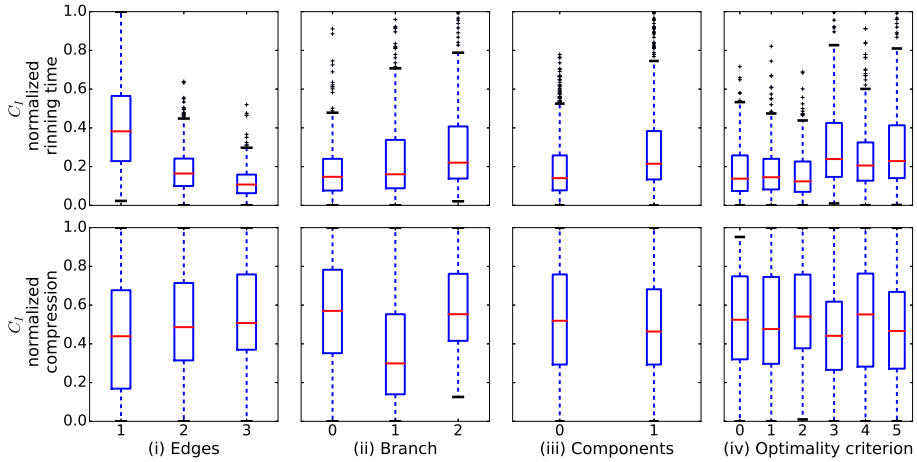

Figure 4.6: Comparison of the normalised running time and compression distributions on the set of less complex examples for algorithm C_I grouped by the different choices of each sub-heuristic - edges, branch, components, and optimality criterion. The running time and compression were normalized from 0 to 1, using the formula $\frac{x-min}{max-min}$, where x is the running time/compression for every heuristic and example, min is the shortest running time/smallest compression and max is the longest running time/largest compression among all heuristics for the particular example.

employing the same heuristic. In the compression comparison scatter plot the results are even more striking since all points lie above the 45° line implying that the change of variables benefits the compression of all less complex examples.

To assess the relative efficiency of the heuristics applied on the collection of less complex examples we normalized the performance measures over all heuristics separately for each example and divided them into groups. The resulting box plots for algorithm C_I can be seen in Figure 4.6. The results for C_R are similar and are presented in Figure 8.1 from the appendix. We observe that some sub-heuristics, on average, perform better both in running time and compression on the collection of examples. We performed the non-parametric Kruskal-Wallis H-test which showed that in every group there was at least one choice for a sub-heuristic dominating the others, with the exception of the compression results of group "(iii) Components" in which no sub-heuristic dominates. Post-hoc comparisons of sub-heuristic choices using the Wilcoxon signed-rank test revealed that focusing deletion-contraction to edges relevant to the cycle structure of the digraphs (sub-heuristics (i) **2** and (i) **3**), considering the edge deleted digraphs (sub-heuristic (ii) **0**) and strongly connected components (sub-heuristic (iii) **0**), and not picking sub-heuristic (iv) **2** leads to significantly shorter running time and larger compression on average (see Table 8.2 and Table 8.3 for results). A limitation in the significance analysis is the different skewness of the data and the dependency between the sub-heuristics, e.g. a good optimality criterion choice

Table 4.1: Performance results for algorithm C_I employing the heuristics leading to the largest compression among all 109 considered heuristics on a set of example digraph models (for example descriptions see Table 8.1 in the appendix). Shown are the size of the expression tree of the expanded Kirchhoff polynomial $|\Gamma_E(\kappa(G))|$, the size of the compressed expression tree $|\Gamma_{C_I}(\kappa(G))|$, the heuristic $\mathcal{H}$ producing the compression result, the compression calculated as the ratio $\frac{|\Gamma_E(\kappa(G))|}{|\Gamma_{C_I}(\kappa(G))|}$, and the average running time in seconds obtained from 10 runs (HC4 and COXD were run only once) of KirchPy on a Dell laptop with Intel i-7 CPU@2.10GHz and 8GB RAM.

G	$\lvert\Gamma_E(\kappa(G))\rvert$	$\lvert\Gamma_{C_I}(\kappa(G))\rvert$	$\mathcal{H}$	Compression	Time (s)
COLE1	157	46	2012	3.4	0.09
AMPAR	211	63	2102	3.3	0.07
MDH	1,270	141	2001	9.0	0.27
ACTMYO	3,561	142	3003	25.1	0.19
KNF33	15,553	940	3114	16.5	1.41
SHPIL	45,601	786	2204	58.0	1.58
GR	65,742	1,280	2102	51.4	1.63
PHO5	640,513	4,691	3215	136.5	10.61
RND	967,681	3,281	1011	294.9	7.53
TF	38,746,801	1,191	2002	32,533	1.84
HC4	679,477,249	333,599	1001	2,036	1,797
COXD	367,647,474, 647,060,221	89,532	1010	4.1e12	661

cannot remedy a bad edge subset choice. Thus we cannot conclude that a given heuristic, e.g. $\mathcal{H} = 3002$, always leads to fast running time and good compression.

The more complex models were run only once using only the connectivity-informed heuristics and algorithm C_I due to time and memory considerations. The results for the heuristics leading to the largest compression can be seen in Table 4.1. There we observe that different heuristics are optimal for different problem instances and thus we cannot determine a single heuristic that would give largest compression.

An important result that can be seen in Table 4.1 is that the compressed form is significantly shorter than the number of arborescences, which becomes more obvious for larger digraphs. Therefore, the number of arborescences is not a hard bound for Kirchhoff polynomial generation, but rather the property of algebraic compressibility. It is an open problem how to determine the compressibility of a digraph. However, we can get an impression by looking at the results for HC4 and COXD. COXD is a significantly more complex and larger model than HC4 but its compression is much higher. If we look at the topology of the corresponding digraphs we observe that COXD has a lower density of 0.13 and only 14 out of 117 reversible edges, while HC4 has a higher density of 0.25 and 56 out of 60 reversible edges. These observations are not surprising since it is difficult to uncover strong connectivity and domination during the digraph reduction procedure in dense

digraphs when many reversible edges are present and it is simpler to break open cycles in digraphs with low density and many unidirectional edges.

4.4 Discussion

The symbolic analysis of steady-state Laplacian models of biological systems amounts to the analysis of expressions of Kirchhoff polynomials. For applications, however, the manipulation of such expressions frequently becomes impractical for even relatively small model instances because the size of Kirchhoff polynomials frequently grows (super) exponentially with the size of their corresponding digraphs.

We developed a framework for the efficient manipulation of expressions of Kirchhoff polynomials without their explicit generation but by working directly with their corresponding digraphs. Namely, we first prime decompose all digraphs in an expression and determine the prime digraphs giving rise to equal Kirchhoff polynomials. This then allows us to form a coarse-grained variant of the expression which is suitable for symbolic simplification. The resulting coarse-grained representation permits the manipulation of otherwise symbolically intractable expressions of Kirchhoff polynomials. It also helps establish a structure-function relationship between a model and its steady-state response by identifying which reactions do not partake in the expression due to algebraic simplification and, in some cases, which reactions participate in it due to irreducibility. A limitation of the theory is that the presented Kirchhoff polynomial equality conditions are not simultaneously necessary and sufficient, such that we cannot, in general, guarantee that we have identified all digraphs giving rise to equal Kirchhoff polynomials in a coarse-grained expression.

It is curious that there is available theory establishing when two undirected graphs have isomorphic Kirchhoff polynomials (Bogner & Weinzierl, 2010), which is a more general property than Kirchhoff polynomial equality, but we are not aware of equivalent Kirchhoff polynomial isomorphism theory for digraphs. For the purpose of manipulation also less general conditions than isomorphism could be practically useful. For example, a necessary and sufficient condition for Kirchhoff polynomial equality of digraphs derived from a common digraph through edge deletion and edge contraction would apply to a large set of practically relevant expressions.

We introduced two algorithms, a recursive one C_R and an iterative one C_I, to explicitly generate individual Kirchhoff polynomials, once the coarse-grained expression is simplified. The algorithms are inspired by algebraic simplification of polynomials but operate on the corresponding digraphs. They produce compressed Kirchhoff polynomials which are algebraically equivalent to their fully expanded counterparts. Since maximum compression appears to be a hard problem, the algorithms employ greedy heuristics. We demonstrated the practical utility of the algorithms, and especially of C_I, to generate the Kirchhoff polynomials of a wide range of Laplacian models from literature. The large compression outcomes affirm the finding from Chapter 3 that Kirchhoff polynomial genera-

tion is dependent on digraph connectivity and not on the (super) exponentially growing number of arborescences. We observed that compression is instance and heuristic specific. This calls for a more in-depth characterisation of Kirchhoff polynomial *compressibility* based on digraph connectivity and an understanding of how to appropriately choose heuristics. Choosing appropriate and efficiently running heuristics is also a difficult challenge, which could be facilitated by the recent advances in strong connectivity and 2-connectivity (Georgiadis et al., 2015c, 2017).

It is important to note that additional properties not accounted for by the generation algorithms could help increase compression, and decrease running time and memory requirements. One such property is digraph symmetry. For example, we generated the Kirchhoff polynomial of HC4, the four dimensional hypercube digraph rooted at a vertex, because due to symmetry all its rooted Kirchhoff polynomials are isomorphic and can be obtained from each other through a simple change of variables.

The presented manipulation and generation theory and algorithms are implemented in the Python package KirchPy. We believe that KirchPy, together with the theoretical insights into manipulation and generation of Kirchhoff polynomials, would allow modelling efforts to catch up with the ever more comprehensive experimental data by promoting the construction and analysis of larger Laplacian models.

4.5 Contributions and Acknowledgements

This chapter is based on the manuscript Yordanov & Stelling (2017a) developed in collaboration between P. Yordanov (PY) and J. Stelling (JS). The original idea of the recursive Kirchhoff polynomial algorithm was presented in Mihaľák et al. (2016). PY conceived and initiated the study, developed the theory, and generated the results. PY wrote the manuscript. JS supervised the study.

We are grateful to Przemysław Uznański for fruitful discussions and insights.

5

Differential Dose-Response in Laplacian Models of Biological Systems

5.1 Introduction

Steady-state dose-response curves are a classical and ubiquitous tool to study input-output relationships in biochemical systems. They relate the dose of a biochemically active agent such as a ligand, enzyme, drug, or toxicant to a biochemical, physiological, or even population-level response this agent triggers, such as receptor activation in a cell, concentration of a chemical in a body compartment, or mortality (Tallarida & Jacob, 2012). Experimentally obtained dose-response curves often have a sigmoid shape and their standard analysis involves the fitting of an empirical model, such as the probit model or the Hill equation to retrieve the main characteristics of the dose-response relation as illustrated in Figure 5.1a. Characteristics of central interest are the baseline and maximal responses, as well as, the dose that produces a response halfway between baseline and maximum to measure the potency of the biochemically active agent, depending on the context denoted as effective concentration (EC_{50}), inhibitory concentration (IC_{50}), or infectious dose (ID_{50}).

Relevant information in basic science and applications is often obtained by comparing dose-response curves. One can, for example, compare how dose affects different system responses to find an optimal trade-off between therapeutic efficiency and toxicity via the therapeutic index (TI) (Muller & Milton, 2012). Often, it is of interest to understand how perturbations such as mutations, drugs, or "natural" variations due to ligands with different affinities affect dose-response relations. We focus on this aspect and use *differential response* (*differential* for short) to refer to the relative differences between a reference and a perturbed dose-response curve. The differential can be an experimental tool to probe the underlying functioning of a biological system, in particular, to identify mecha-

nisms guiding the system's steady-state behaviour. Differential responses are also exploited in natural systems. For example, membrane receptors in mammalian type I interferon signalling can recognize various ligands that are structurally similar but have different binding affinities to the receptor, and reliably trigger appropriate differential (anti-viral or anti-proliferative) responses (Schreiber & Piehler, 2015).

The differential between sigmoid dose-response curves is easily captured by shifts in baseline response, maximal response, and quantities such as the EC_{50}, but other dose-response relationships are also common. A prominent example are biphasic dose-response curves with low dose stimulation and high dose inhibition, so-called hormetic curves, which have received renewed attention (Calabrese & Baldwin, 2003; Mattson, 2008; Di Veroli et al., 2015). However, it is not established how a sigmoid curve can be compared to a hormetic one, or more generally how dose-response curves of any shape can be compared with each other (see Figure 5.1a).

In addition, relating the observed effects to biochemical mechanisms is a key challenge. Mathematical models in dose-response analysis are mostly empirical (for data interpolation to estimate the characteristics described above), and not mechanistic in the sense of incorporating relationships between biochemical entities that (are hypothesized to) give rise to the experimental data. Specifically, there exists no comprehensive mechanistic model-based theory to describe differential responses, despite their fundamental nature and importance in all fields of biology. The lack of mechanistic models, however, is not surprising: many relevant biological network models are non-linear and they cannot be analysed symbolically for non-trivial network sizes to derive design principles, such that differential effects can only be characterized through simulations, which in turn depend on frequently unknown network structures and parameter values.

To tackle such limitations and to extract general principles of biological systems, several parameter-free methods have been developed. For example, Chemical Reaction Network Theory aims to obtain a qualitative understanding of biological systems by determining what their capabilities in terms of number of steady-states are, solely by examining their reaction network (model) structure (Conradi et al., 2007; Craciun & Pantea, 2008). With respect to differential responses, however, we are interested in quantitative features (e.g., shifts in EC_{50}), for which these approaches are not directly applicable.

Instead, we concentrate on *Laplacian models* introduced in Section 2.1, for which steady-state symbolic derivations are possible in principle. Recall that Laplacian models are deterministic (ordinary differential equation, or linear algebraic for the steady-state) models of reactions endowed exclusively with zero- and first-order mass-action kinetics. They represent molecular state transitions but cannot account explicitly for binding events and non-linear kinetics (unless the kinetics do not depend on any of the species in the Laplacian model). Despite these limitations, Laplacian models have been invaluable for understanding enzyme kinetics, for example, via the systematic enumeration of patterns on reaction graphs dating back to King & Altman (1956). Recently, Laplacian models have received renewed interest after introducing mathematical rigour into the classical

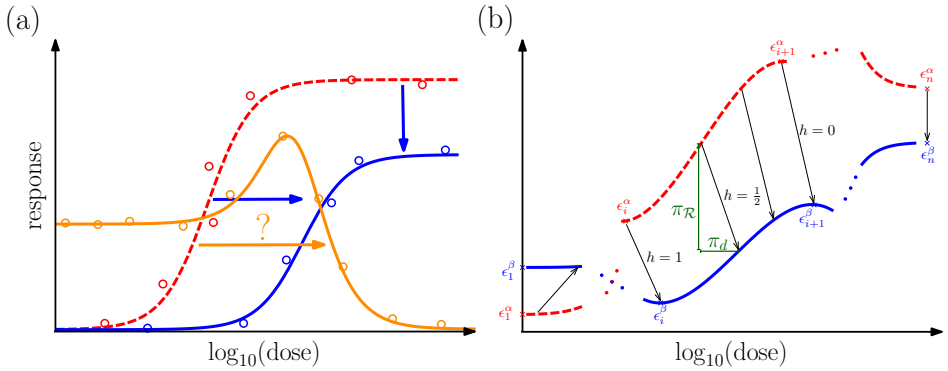

Figure 5.1: Relations between sigmoid reference (red) and perturbed (blue and orange) dose-response curves with exemplary experimental data (circles) and fitted empirical models (lines). (a) When perturbations preserve the shape of the dose-response curve (blue vs. red), the effect of a perturbation can be quantified by the shifts in baseline response and maximal response, and by the difference in the dose required for half-maximal response; such shifts are indicated by blue arrows. Corresponding measures are not defined when the perturbation yields a hormetic curve (orange) or for the general comparison of non-sigmoid dose response curves. (b) Definition of the differential response as the length of displacement of a reference dose-response curve A (red, dashed) to a perturbed dose-response curve B (blue, solid), generated by functions f^α and f^β, respectively, both with n critical points $\epsilon_{1\ldots n}^{\{\alpha,\beta\}}$. The curves are related through a map $\mathcal{M}$ that preserves the order of critical points and segments as well as the proportion of response $h \in [0,1]$ in each pair of mapped segments (corresponding points indicated by black arrows). The signed projections of the differential on the dose and response axes are denoted as $\pi_d(h)$ and $\pi_{\mathcal{R}}(h)$ and shown in green.

framework (Mirzaev & Gunawardena, 2013; Gunawardena, 2014) and providing multiple promising applications of the theory (Thomson & Gunawardena, 2009; Ahsendorf et al., 2014; Estrada et al., 2016). In particular, Gunawardena (2012) showed that time-scale separation analysis across many biological areas such as enzyme kinetics, G-protein coupled receptors, and gene regulation can be combined into a single linear graph-theoretic framework. It connects the symbolic derivation of steady-state expressions for Laplacian models to combinatorial objects on graphs, namely rooted directed spanning trees (arborescences). This relation between structure and function makes Laplacian models appealing for extracting general principles of the steady-state differential responses.

Although symbolic steady-state derivations are possible for Laplacian systems, their current practical application, for example in pharmacology, is limited because the length/size of the steady-state expressions increases exponentially with model size. One approach to circumvent this problem is to assume that the system is at equilibrium to simplify derivations. However, for systems far from equilibrium, such as cell signalling pathways and eukaryotic gene regulation Estrada

et al. (2016), the equilibrium assumption does not hold and the weaker steady-state assumption has to be considered—making even apparently "small" systems practically intractable.

Here, we develop a comprehensive theory and practically scalable computational methods for studying differential steady-state dose-response relationships to pinpoint the mechanisms leading to experimentally observed behaviours. First, we extend the classic comparison of sigmoid dose-response curves and formally define a general notion of the differential. In the framework of Laplacian models, we exploit the developments from Chapters 3 and 4 to address challenges such as to determine the reactions that affect differential responses, to identify equivalence classes of networks, and to reliably reject hypothetical models without needing to know parameter values. Specifically, the theory helps determine which reactions take part in the differential and how perturbations (such as variation of parameter values, deletions and additions of states and reactions) affect the differential. This is possible for practical applications because we do not actually need to derive complete steady-state expressions for quantitative symbolic analysis since our efficient algorithms for generation and manipulation of Kirchhoff polynomials from Chapter 4 produce compact, simplified steady-state expressions. We illustrate the application of the framework for insulin signalling, covering aspects such as model building and analysis, model rejection, model reduction, and (numerical) bounds on differential dose-response relations.

5.2 Formalizing the Steady-State Differential Response

Comparing general dose-response curves is not established in the biological literature and it is particularly ambiguous how comparison should be performed when non-monotone curves are involved (see Figure 5.1a). Here we provide a formal definition of the differential response that generalizes over dose-response curves of different functional form (sigmoid or multiphasic) and their characteristics such as maximal response and dose for half-maximal activation.

We define the differential response as the length of displacement between a point on a reference dose-response curve A and a corresponding point on a perturbed dose-response curve B. A map $\mathcal{M}$ relates points from monotone segments of both curves that have the same "local" characteristics to each other (see Figure 5.1b). It is evident that a closed form of the map $\mathcal{M}$ cannot be obtained in the general case. However, when functional relations between dose and response originate from the steady-state expressions of Laplacian models, the map can be analytically determined.

Briefly, the dose-response curves are generated by functions $\mathcal{R}^{\alpha}(d)$ and $\mathcal{R}^{\beta}(d)$ for reference and perturbed version, respectively (see Section 8.3.1 in the appendix for formal specifications). To segment the dose-response curves along the dose coordinate, we identify critical points of the respective responses such as suprema, infima, and extrema denoted by ϵ_i (omission of superscript indicates application to both curves). To provide the required generalization (also see Fig. 5.1b), we construct the map $\mathcal{M}$ (and correspondingly the mapping of segments) such that

it preserves the order of critical points and segments without omitting any of them, and that it preserves the proportion of response in each pair of mapped segments. To achieve the latter, we relate the doses that have the same proportion h ($h \in [0,1]$) of response between the minimal and maximal response in any given segment, as determined by the responses at the critical points that enclose the segment. This allows us to define the signed projections of the *dose differential* $\pi_d(h)$ and of the *response differential* $\pi_{\mathcal{R}}(h)$, which have clear biological interpretations, as:

$$\pi_d(h) := \log_{10} \frac{d^\alpha}{d^\beta} \text{ and } \pi_{\mathcal{R}}(h) := \mathcal{R}^\alpha - \mathcal{R}^\beta,$$

with respective doses d and responses $\mathcal{R}$. Note that the dose differential is expressed in log scale to easily identify fold differences in the dose.

5.3 Differential Laplacian Systems

To derive general expressions for the dose (π_d) and response ($\pi_{\mathcal{R}}$) dimensions of the differential, we need to define dose, response, and perturbation in Laplacian models, leading to the notion of differential Laplacian systems.

Here, we assume that the dose variable affects one or more reactions proportionally, which can be interpreted as an input changing the rate constant gradually, or as an input species with constant concentration binding to the educt of the reaction; for example, the effect of a ligand with constant external concentration that binds to a receptor incorporated in this way via the law of mass-action. Formally, the input dose variable d partakes in the mathematical expressions labeling w of the edges of the system's digraph G, $I(G) := \{e_{d,1}, \ldots, e_{d,w}\}$. We call members of the set $I(G)$ *dose edges* of G and their labels are expressions proportional to the input dose variable d:

$$\ell(e_{d,i}) = g_i(p)d,$$

where $g_i(p)$ are functions of the parameters in the corresponding edge label but they do not contain d (see Figure 5.2a for an example in which we assume that the dose affects receptor-ligand binding).

In our analysis, the response $\mathcal{R}$ is a linear combination of the steady-state concentrations at chosen output vertices (such as phosphorylated receptor-ligand complex RL_p in Figure 5.2a). The q species eliciting the response are associated with a set of output vertices $O(G) := \{v_1, \ldots, v_q\}$ ($O(\overline{G})$ for open systems). Then if we use Equation (2.5) to derive general expressions for the steady-state response for closed and open systems using Kirchhoff polynomials $\kappa(G)$, we obtain:

$$\mathcal{R}_{O(G)} = \frac{\sum_{v_i \in O(G)} a_i \kappa_{v_i}(G)}{\kappa(G)} x_t \qquad \text{and} \qquad \mathcal{R}_{O(\overline{G})} = \frac{\sum_{v_i \in O(\overline{G})} a_i \kappa_{v_i}(G)}{\kappa_{v_\varnothing}(G)},$$

where $a_i \geq 0$ designates the weight given to the steady-state concentration associated with vertex v_i. This implies that steady-state dose-response curves of Lapla-

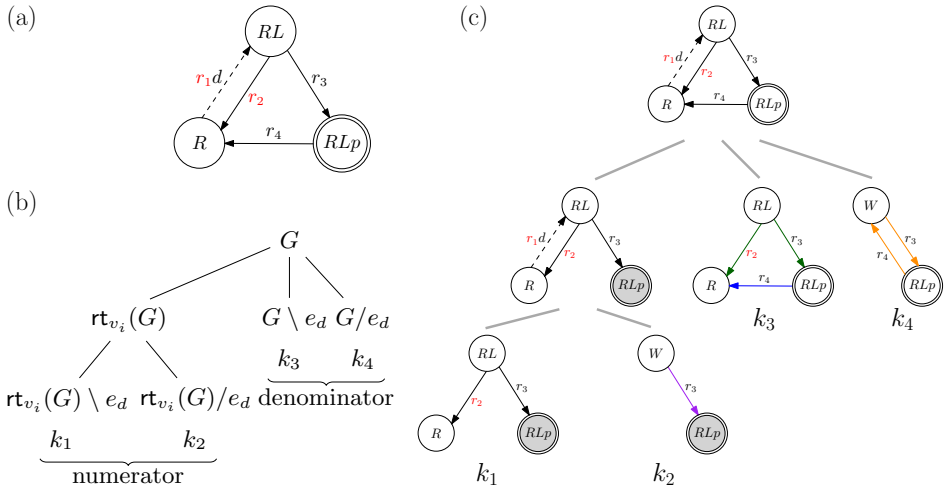

Figure 5.2: Differential analysis for a simple insulin receptor activation model (corresponding to the general receptor tyrosine kinase activation model from Figure 2.1a). (a) Digraph for the differential system. The dose edge is marked by a dashed arrow, red symbols correspond to differential parameters (those with different values in the reference and perturbed system), doubly-encircled vertices mark the output vertices. (b) Tree scheme for a general digraph G showing how to obtain the relevant digraphs participating in the coefficients k_i of the dose-response relationship in closed systems (for reference and perturbed systems through the digraph operations rooting, deletion, and contraction. Note that there are also additional terms contained in the steady-state coefficients. (c) The tree scheme for decomposition of the insulin receptor activation model. Gray-filled vertices denote that the digraphs are rooted at them, different edge color in the leaves of the tree mark the prime components (same color means same prime component also among different digraph leaves), black edges (when present) are not part of any prime component.

cian models are rational functions of the dose variable, for example, $\mathcal{R}_{O(G)}(d)$.

Perturbations are any changes in the model structure (additions and deletions of species and reactions), parameters (different values in the reference and perturbed model), number and position of the edges affected by the input variable, number and position of the output vertices, and parametrization of the output function. We capture these perturbations by defining two Laplacian systems for a reference (α) and a perturbed (β) condition, each of which consists of a digraph G, a set of parameters p (from G's labels), a set of dose edges I (whose labels contain the dose variable d), and a set of output vertices O the concentrations associated to which are weighted by a to obtain the observed response $\mathcal{R}$. Formally, a *steady-state Laplacian differential system* is then the tuple $\mathscr{D} = \big((G^\alpha, p^\alpha, I^\alpha, O^\alpha, a^\alpha), (G^\beta, p^\beta, I^\beta, O^\beta, a^\beta)\big)$.

In Figure 5.2a we use our example receptor tyrosine activation model from Figure 2.1a to define a first differential system $\mathscr{D}$. Let the receptor R transition to

its ligand-bound state RL upon activation by a ligand with constant concentration d. We account for the dose variable d in the transition rate by changing the label of edge $v_R v_{RL}$ to $r_1 d$. To construct a differential Laplacian system, we consider a reference system with digraph topology as the example digraph G, dose edge $e_d = v_R v_{RL}$, i.e. $I = \{e_d\}$ with $\ell(e_d) = r_1 d$, a single output vertex $O = \{v_{RLp}\}$ weighted by 1, and parameters $p = \{r_1, r_2, r_3, r_4\}$. The perturbed system is identical to the reference one, with the exception of the values of parameters r_1 and r_2, which we will denote as r_1^α, r_2^α (r_1^β and r_2^β) in the reference (perturbed) system. These differential parameters correspond to stimulation of the system with two different ligands that have different affinities to the receptor R. Since reference and perturbed system are identical except for their differential parameters, we can illustrate the differential system by a single digraph and highlight the differential parameters as shown in Figure 5.2a.

5.4 Symbolic Derivation of the Differential

For tractability, we are first interested in deriving analytical expressions for the differential of systems with a constant input that influences exactly one edge proportionally ($I(G) = \{e_d\}$ and $\ell(e_d) = g(p)d$) to model, for example, a ligand binding once to a receptor.

To express the steady-state response $\mathcal{R}$ for closed and open systems explicitly as a function of the dose variable d, we apply the deletion-contraction property from Proposition 2.5.2 to partition the set of arborescences from the numerator and denominator of the corresponding rational function into two categories—those that contain the dose d in one of their labels and those that do not. This is equivalent to factoring out the edge labels from the monomials in the corresponding Kirchhoff polynomial that contain the dose variable d. After simplification, we obtain the general form of dose-response expressions for closed and open systems with a digraph G:

$$\mathcal{R}_O(d) = \frac{k_1 + k_2 d}{k_3 + k_4 d}, \text{ where} \tag{5.1}$$

for closed systems:
$k_1 = x_t \sum_{v_i \in O(G)} a_{v_i} \kappa_{v_i}(G \backslash e_d)$,
$k_2 = x_t g(p) \sum_{v_i \in O(G)} a_{v_i} \kappa_{v_i}(G / e_d)$,
$k_3 = \kappa(G \backslash e_d)$,
$k_4 = g(p) \kappa(G / e_d)$,

for open systems:
$k_1 = \sum_{v_i \in O(\overline{G})} a_{v_i} \kappa_{v_i}(G \backslash e_d)$,
$k_2 = g(p) \sum_{v_i \in O(\overline{G})} a_{v_i} \kappa_{v_i}(G / e_d)$,
$k_3 = \kappa_{v_\varnothing}(G \backslash e_d)$,
$k_4 = g(p) \kappa_{v_\varnothing}(G / e_d)$.

We call $k_i, i \in \{1, 2, 3, 4\}$ *steady-state coefficients* although they are symbolic expressions involving parameters and Kirchhoff polynomials of specific digraphs obtained from the initial digraph G by applying edge deletions, edge contractions, and digraph rooting. The coefficients k might be zero if arborescences do not exist in the respective digraphs. For example, when $k_2 = k_4 = 0$ or when $k_1 = k_3 = 0$, the response does not depend on the dose.

How to obtain the relevant digraphs participating in the coefficients for closed systems can be seen in the tree scheme in Figure 5.2b (the tree scheme for open systems is shown in Figure 8.3 in the appendix) and an application to the example differential system in Figure 5.2c. With only one edge containing the dose d, the numerator and denominator have at most first degree in d and thus the tree schemes in Figure 5.2b,c have four leaves. Note that the tree scheme is the same for the reference and perturbed systems, except for the differential parameters. The coefficients for the example are $k_1 = x_t\kappa(\mathsf{rt}_{RLp}(G)\backslash e_d)$, $k_2 = x_t r_1\kappa(\mathsf{rt}_{RLp}(G)/e_d)$, $k_3 = \kappa(G\backslash e_d)$, and $k_4 = r_1\kappa(G/e_d)$. By generating the Kirchhoff polynomials in the respective digraphs, we obtain:

$$k_1 = 0,\ k_2 = r_1 r_3,\ k_3 = r_4\left(r_2 + r_3\right),\ \text{and}\ \ k_4 = r_1\left(r_3 + r_4\right).$$

To analyse the signed projections π_d and $\pi_{\mathcal{R}}$, we derive the map $\mathcal{M}$ (see Section 8.3.2 in the appendix) and recognize that the perturbed and reference dose-response curves are parametrized through the proportion variable h, which leads to:

$$\pi_d = \log_{10}\frac{k_3^{\alpha}k_4^{\beta}}{k_3^{\beta}k_4^{\alpha}} \qquad \text{and} \qquad \pi_{\mathcal{R}}\left(h\right) = h\left(\frac{k_1^{\alpha}}{k_3^{\alpha}} - \frac{k_1^{\beta}}{k_3^{\beta}}\right) + (1-h)\left(\frac{k_2^{\alpha}}{k_4^{\alpha}} - \frac{k_2^{\beta}}{k_4^{\beta}}\right). \tag{5.2}$$

The signed dose projection of the differential does not depend on h, in contrast to the response projection. In practice, we are often interested in the response projections that summarize the shift in the response for the maximum and the minimum of the dose-response in the corresponding segment, which depending on whether the segments are monotonically increasing or decreasing correspond to $h = 0$ and $h = 1$:

$$\pi_{\mathcal{R}}\left(h = 0\right) = \frac{k_2^{\alpha}}{k_4^{\alpha}} - \frac{k_2^{\beta}}{k_4^{\beta}} \qquad \text{and} \qquad \pi_{\mathcal{R}}\left(h = 1\right) = \frac{k_1^{\alpha}}{k_3^{\alpha}} - \frac{k_1^{\beta}}{k_3^{\beta}}.$$

For the example differential system, we find that:

$$\pi_d = \log_{10}\frac{r_1^{\beta}}{r_1^{\alpha}}\frac{r_2^{\alpha} + r_3}{r_2^{\beta} + r_3} \qquad \text{and} \qquad \pi_{\mathcal{R}}\left(h\right) = 0,$$

where the response component of the differential vanishes because $k_1 = 0$ and because the differential parameters r_1 in k_2 and k_4 cancel each other. Also, the dose differential is independent of the rate constant r_4.

The example illustrates that, by deriving the general form of the signed projections of the differential π_d and $\pi_{\mathcal{R}}$, we establish a direct connection between the structure of the differential system and its function. More generally, the steady-state expressions and projections of the differential in Laplacian models are algebraic expressions of Kirchhoff polynomials. It is a central task of the analysis to determine their constituent variables (reactions) and the effect of each variable (reaction). This is not trivial because some expressions might simplify, in

particular, for fractions of Kirchhoff polynomials as above. The full simplification of an algebraic expression translates to a *necessary and sufficient condition* for a variable (reaction) to influence the expression of interest. As a consequence, we can define equivalence classes of differential systems that have differing structure, but the same functional expressions with respect to their simplified differential or steady-state. However, it is a major challenge to efficiently generate and manipulate Kirchhoff polynomials due to the exponentially growing number of arborescences with increasing size of the model digraphs. This problem is reduced by the developed algorithms in Chapter 3 and Chapter 4 that allow for the factorization and compressed generation of Kirchhoff polynomials, and for the manipulation of algebraic expressions without explicit generation of the Kirchhoff polynomials.

5.5 Properties of the Differential

Remember that we consider closed and open systems with strongly connected digraphs G, and thus systems with prime (irreducible) Kirchhoff polynomials. The steady-state expressions for closed systems are always irreducible fractions because the denominator contains the Kirchhoff polynomial of the strongly connected G. By contrast, the denominator of the steady-state expression in open systems contains the strongly connected G rooted at the environment vertex $v_\varnothing$ which is obtained by deleting all synthesis edges s_i. These digraph rooting operations can yield digraphs with reducible Kirchhoff polynomials. Formally, we call an edge $e \in E(G)$ a *prime bridge* if the edge deleted digraph $G \setminus e$ has more non-trivial prime factors than the original digraph G. Hence, the Kirchhoff polynomial corresponding to $\mathsf{rt}_{v_\varnothing}(G)$ is non-trivially factorisable when any s_i is a prime bridge during the sequential deletion of s_i (s_1 might not be a prime bridge in G but in $G \setminus s_2 \ldots \setminus s_n$). Likewise, the numerator of the steady-state expression for open systems consists of the linear combination of rooted polynomials, each of which could be factorisable. In this case, there could exist reactions whose alteration (of rate) does not affect the steady-state. Thereby, in open systems there exist equivalence classes of models with different digraphs G but the same steady-state expressions. A necessary and sufficient condition for a reaction to take part in the steady-state expression is that it is part of a prime component that is not shared between the numerator and denominator.

The dose projection of the differential π_d for general systems with a single dose edge depends on the Kirchhoff polynomials contained in the coefficients k_3 and k_4 but not on k_1 and k_2 (Equation (5.2)). It is therefore independent of the choice of output vertices in O, of the vertex weights α for the reference and perturbed system, and of the total conserved amount x_t in closed systems (the synthesis reactions s_i in open systems). The dose differential can be simplified to the logarithm of an irreducible fraction by obtaining the prime factorizations of the numerator and denominator and dividing them by the greatest common divisor $\gcd(k_3^\alpha k_4^\beta, k_3^\beta k_4^\alpha)$ with the manipulation tools from Chapter 4. Then the necessary and sufficient condition for a reaction to participate in π_d is to be part of a prime component of the relevant digraphs that is different in the reference

and perturbed system, and not the same in the dose-edge deleted and dose-edge contracted digraphs of the same condition. To illustrate these points, consider π_d for closed systems:

$$\pi_d = \log_{10} \frac{\kappa(G^\alpha \backslash e_d^\alpha) g^\beta(p^\beta) \kappa(G^\beta / e_d^\beta)}{\kappa(G^\beta \backslash e_d^\beta) g^\alpha(p^\alpha) \kappa(G^\alpha / e_d^\alpha)}.$$

The polynomials $\kappa(G \backslash e_d)$ are factorisable if and only if e_d is a prime bridge. Edge contraction for $\kappa(G/e_d)$ could also lead to an increase of prime factors if any of the deleted edges during the procedure is a prime bridge. We will call an edge whose contraction increases the number of prime factors a *prime contraction bridge*. Hence, $\kappa(G/e_d)$ is factorisable when e_d is a prime contraction bridge. The factor $g(p)$ is prime since it is the label of a single edge. Overall, thus, if the dose differential is reducible depends exclusively on the perturbation, the connectivity of the dose edge e_d (in G^α and G^β), and the connectivity of the edges in e_d's immediate neighbourhood. Note that the reducibility characterization of π_d for open systems is analogous but includes an additional dependency on the location and connectivity of the synthesis edges in G^α and G^β.

The response projection of the differential $\pi_\mathcal{R}$ in single-dose systems is a sum of ratios dependent on all coefficients k_i, includes the conserved x_t in each ratio for closed systems, and the synthesis reactions in open systems (Equation (5.2)). However, it does not depend on the dose edge label function $g(p)$ because it always cancels in $\frac{k_2}{k_4}$ (for both reference and perturbed coefficients). For illustration, let us focus on the response differential for closed systems when $h = 0$:

$$\pi_\mathcal{R}\,(h=0) = \left(\frac{\sum_{v_i \in O^\alpha(G)} a_{v_i}^\alpha \kappa_{v_i}(G^\alpha / e_d^\alpha)}{\kappa(G^\alpha / e_d^\alpha)} - \frac{\sum_{v_i \in O^\beta(G)} a_{v_i}^\beta \kappa_{v_i}(G^\beta / e_d^\beta)}{\kappa(G^\beta / e_d^\beta)} \right) x_t.$$

To simplify the expression, first, the common factors between k_2 and k_4 are canceled (keeping in mind that k_2 is a linear combination of prime factorized Kirchhoff polynomials) to obtain $\overline{k_2}$ and $\overline{k_4}$. The response differential can be further reduced if $\gcd(\overline{k_4}^\alpha, \overline{k_4}^\beta) \neq 1$ by combining the fractions under a common denominator. Note that the response differential could be zero due to the minus sign. The characterization of the response differential in the general case for h not fixed and for open systems is analogous.

When either k_1 or k_2 is zero, the response differential $\pi_\mathcal{R}$ has a simpler form but the dose differential π_d is not affected. Note again that the differential can be degenerate or undefined. The differential is degenerate when $k_1 = k_2 = 0$ since the steady-state function $\mathcal{R}(d)$ is always zero, and it is undefined when k_3 or k_4 is zero since the steady-state function is either constant or unbounded.

5.6 Analysing the Insulin Receptor Life-Cycle

To illustrate the applications of the theory, we will extend the example model stepwise to a previously published model for insulin receptor signalling (Sedaghat

et al., 2002). Insulin receptor trafficking/recycling is a complex process and it is particularly important to find which reactions and species are essential in order to formulate an appropriate abstraction to model signalling. Again, for simplicity, we define the differential system by assuming that the reference and the perturbed model differ only in the values of a subset of parameters—the differential parameters—and that all other elements are identical.

We extend the example model (Figure 5.2) with two states: internalized phosphorylated ligand-bound receptor RLp_i and internalized receptor R_i (Figure 5.3). They can be reached by reversible reactions from their non-internalized (membrane) counterparts RLp and R to represent endocytosis and receptor recycling, and RLp_i can be dephosphorylated to R by an irreversible reaction. We assume two output species in the reference and perturbed system, the phosphorylated ligand-bound receptors, such that $O(G) = \{RLp_i, RLp\}$ with unit weights ($a_{RLp_i} = a_{RLp} = 1$).

The resulting differential system is what we call a *basic signalling system*. It is a differential system with a closed digraph that contains a reversible reaction for which the forward and reverse rates differ between the reference and perturbed model, and for which the forward rate is affected by the dose variable d. More precisely, we have a digraph G with $I(G) = \{e_{on}\}$, $\ell(e_{on}) = g_{\text{on}}(p)d$, and $\ell(e_{off}) = g_{\text{off}}(p)$. Also, reference and perturbed model have no structural differences, they differ only by the functions $g_{\text{on}}(p)$ and $g_{\text{off}}(p)$ (and the parameters contained in them). In such basic signalling models the dose edge contracted digraph G/e_{on} is the same for the reference and perturbed system, therefore, its Kirchhoff polynomial always cancels in the dose differential fraction. The dose differential for closed systems (results and definitions are analogous for open systems) is:

$$\pi_d = \log_{10} \frac{\kappa(G^\alpha \backslash e_{on})}{\kappa(G^\beta \backslash e_{on})} \frac{g^\beta_{\text{on}}(p^\beta)}{g^\alpha_{\text{on}}(p^\alpha)}.$$

The response projection of the differential for $h = 0$ will always be zero under the stated assumptions since $\frac{k_2^\alpha}{k_4^\alpha} = \frac{k_2^\beta}{k_4^\beta}$. When $h = 1$, the response projection is not affected by the assumptions for basic signalling systems.

Although the digraph of the extended system contains more states and reactions and the steady-state expression is more complicated (see Section 8.3.2.2 in the appendix), the differential is identical to that of our initial example without endocytosis because the newly added reactions take part in prime components that do not contain differential parameters and therefore cancel out (see Figure 5.3). The initial and the extended system belong to the same equivalence class with respect to their differential. The equivalence class is defined by structural properties of the differential system and the applied perturbation, namely, by which prime components are present and do not cancel out.

The concept of equivalence classes has direct applications for model selection and experimental design. For example, assume that we have experimental evidence that changes in the rate constant of a reaction such as r_4, in both the reference and perturbed model, affect the dose differential. If this reaction does

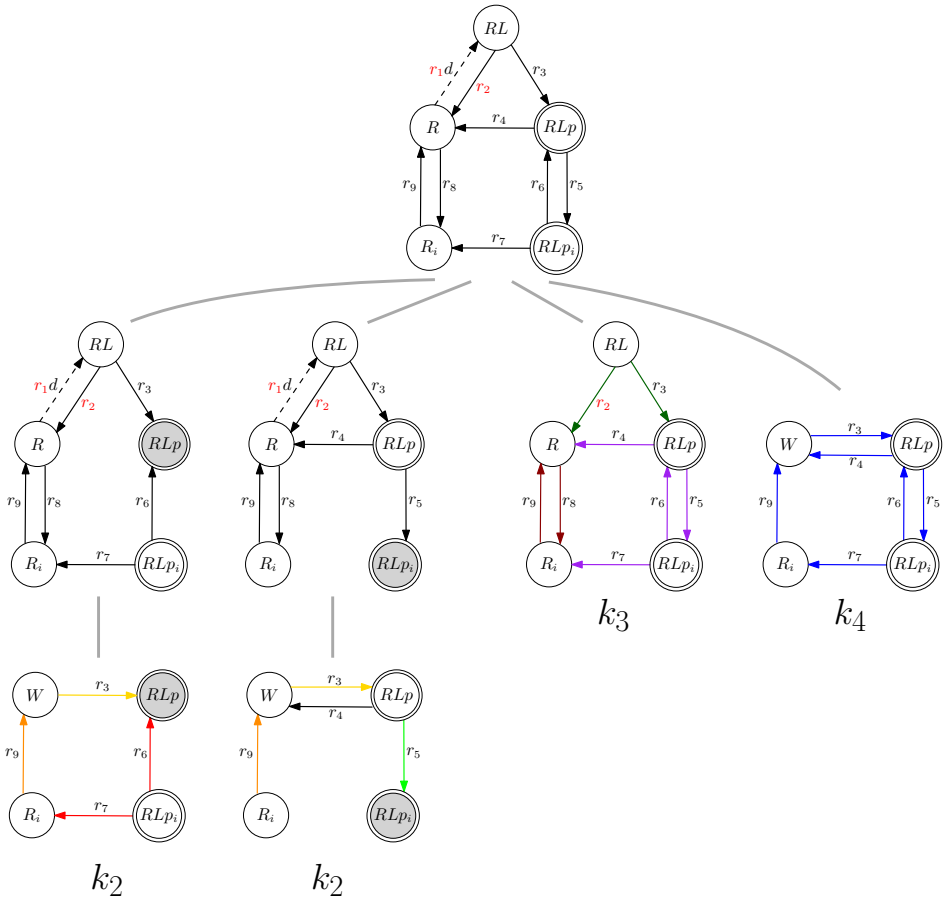

Figure 5.3: Tree scheme for a model extending the differential system from Figure 5.2a with internalized species RLp_i and R_i. Note that only digraphs belonging to non-zero coefficients are shown.

not take part in the dose differential expression of the equivalence class of models we are studying (as for the equivalence class for insulin signalling defined above), we can directly reject *all* members of the equivalence class because they are incompatible with the experimental observation.

Conversely, assume we know our current model is incompatible with the data on differential signalling, and we need to find model extensions that remedy this limitation. For example, when we are interested in the long-term effects of insulin receptor trafficking, we need to account for receptor synthesis and degradation. This converts the model from a closed system to an open system. Let us consider a model extension in which the non-internalized free receptor R is synthesized and degraded. Then, however, the differential is not defined because the steady-state coefficient k_4 is zero. Figure 5.4a shows that the contraction of the dose edge

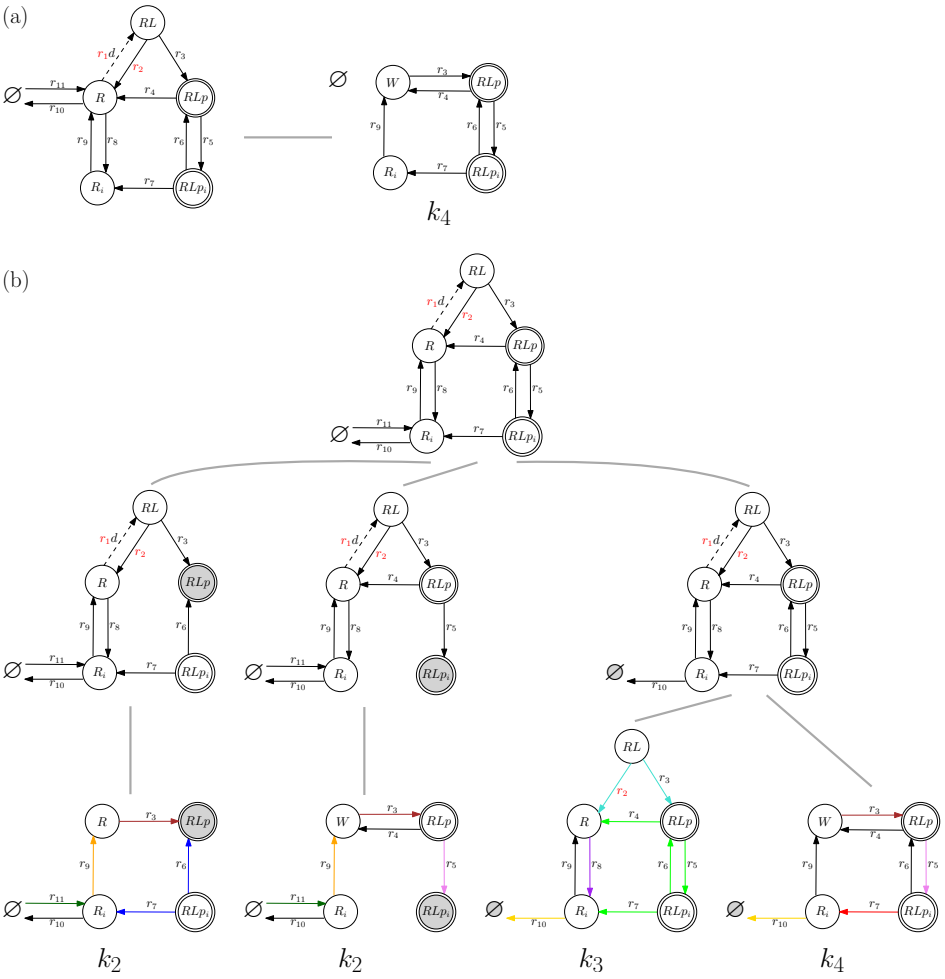

Figure 5.4: Extended insulin model with receptor degradation (open system). (a) The dose and response differential for the system with synthesis and degradation of membrane-bound receptor R (for reference and perturbed digraph) is not defined since the steady-state coefficient $k_4 = 0$ (the contained digraph is disconnected and therefore does not contain any in-arborescences). (b) Tree scheme for a differential system containing synthesis and degradation of the internalized receptor R_i. Digraphs with no in-arborescences are not shown.

eliminates the degradation edge $e_{r_{10}}$ and, additionally, the rooting at the environment vertex $v_\varnothing$ eliminates the synthesis edge $e_{r_{11}}$; this results in a disconnected digraph with no in-arborescences in k_4. Hence, we can reject this extension just based on structural considerations.

Let us consider adding only the synthesis and degradation reactions for R_i as a more biologically plausible way to capture receptor trafficking (Figure 5.4b).

but the differential is still identical to that of the initial example model from Figure 2.1; the extended model belongs to the same equivalence class due to cancellation of prime factors that do not contain differential parameters in both reference and perturbed model (see Figure 5.4b).

A logical next question is what second perturbation to design (or how to change the first perturbation) in order to differentiate between models in the same equivalence class. In other words, we want to divide the class into smaller equivalence classes, and ultimately identify a single model that represents the biological process. More specifically, a second perturbation could change the prime factors, for example, by adding or deleting new species and reactions, or by changing the input edge. We illustrate the theory's capabilities by deciding which reaction rate constant to alter in the perturbed system. For example, we could experimentally perturb r_8 and r_5 such that we have the largest effect in the dose differential. For the steady-state coefficient k_3 from Figure 5.4b, we observe that r_8 is alone in a prime component while r_5 has three more reaction constants in the same prime component. This means that, if we perturb r_8, we will obtain a factor in the dose differential corresponding to $\frac{k_3^\alpha}{k_3^\beta} = \frac{r_8^\alpha}{r_8^\beta}\frac{r_2^\alpha+r_3}{r_2^\beta+r_3}$ where our perturbation will have a multiplicative effect on the dose differential. On the other hand, if we perturb r_5 we obtain $\frac{k_3^\alpha}{k_3^\beta} = \frac{r_4(r_6+r_7)+r_5^\alpha r_7}{r_4(r_6+r_7)+r_5^\beta r_7}\frac{r_2^\alpha+r_3}{r_2^\beta+r_3}$, where the perturbation is dampened by the other reaction rates—the change in the dose differential upon this perturbation might become experimentally indistinguishable. Hence, perturbing elements of smaller factors has a more direct effect on the observed dose differential, and a corresponding experimental design is more likely to help determining whether the model under consideration is appropriate.

5.7 Extension: Numerical Analysis

The symbolic analysis can be augmented by numerical methods when quantitative prior knowledge or experimental data is available. Here, we consider the case when parameter values or bounds on those values are known (or can be estimated). Known parameter values (or ratios of parameter values) can be directly incorporated to simplify the symbolic expressions. If parameter values are uncertain, but we have knowledge on plausible intervals of parameter values, these intervals form the box in parameter space $\mathcal{I}$ that accounts for prior knowledge on the parameters. By bounding the range of the differential projections π_d and $\pi_{\mathcal{R}}$ over this box $\mathcal{I}$, we can determine the capacity of the model to produce a differential of a given (observed) magnitude and thereby assess if the model agrees with the observations.

Formally, let us denote the range of a differential projection to be the interval $\mathbb{D} = (a, b)$ ($\mathbb{D}_{\pi_d}$ for the dose and $\mathbb{D}_{\pi_{\mathcal{R}}}$ for the response projection), where $a, b \in \mathbb{R}$ and $a \leq \pi(p^\alpha, p^\beta) \leq b$, $p^\alpha, p^\beta \in \mathcal{I}$. We want to determine outer bounds $\hat{a}$ and $\hat{b}$ of $\mathbb{D}$ over the parameter box $\mathcal{I}$, where $\hat{\mathbb{D}} = (\hat{a}, \hat{b}) : \hat{a} \leq a$ and $\hat{b} \geq b$, which tightly enclose the set of all possible magnitudes of the differential projections. In systems with a single dose edge, with edge labels that contain rational expressions,

and regarding all parameters as variables, bounding the differential translates to finding the global minimum and maximum of a multivariate rational function.

In general, finding global optima of multivariate rational functions is NP-hard (Jibetean & de Klerk, 2006). However, there exist several numerical methods that give certificates for global optimality or find bounds based on polynomial optimization, such as fractional programming (Frenk & Schaible, 2009), interval arithmetic (Moore & Bierbaum, 1979), and Bernstein expansion of the numerator and denominator of rational functions (Narkawicz et al., 2012). Here, we focus on Bernstein expansions because multivariate polynomials expressed in Bernstein form possess the *interval enclosing property* according to which the range of a polynomial over an interval can be bounded by control points derived from their Bernstein coefficients. This property has recently been extended to bound the range of multivariate rational functions over an interval box (Narkawicz et al., 2012). The Bernstein expansion method is implemented in the Kodiak package (Smith et al., 2015). In Smith et al. (2015) it was demonstrated that the method produces tight outer bounds for a dose differential expression containing 12 free variables.

To illustrate the approach for the dose differential of the example model from Figure 5.2a, we assume that $x_t = 1$ nM, parameters lie in a parameter box $\mathcal{I}$ defined by $r_1, r_2, r_3, r_4 \in [1e\text{-}5, 1]$ with units per second (s^{-1}), and that we have experimentally determined the ratios of differential parameters as $\frac{r_1^\alpha}{r_1^\beta} = 100$ and $\frac{r_2^\alpha}{r_2^\beta} = 0.01$ With Kodiak we find the bounds $\widehat{\mathbb{D}_{\pi_d}} = (-4, -2)$. Additionally, one can check how the bounds of the differential change when a parameter is altered; we call the resulting plots *profile differential bounds*. For our example, we fix each of the free parameters taking part in the differential, namely r_2^β and r_3, for every value in their interval of definition, and calculate the bounds of the differential expression range (see Figure 5.5a). This analysis shows the capacity of individual parameters to control and constrain the possible magnitude of the differential. In Figure 5.5a one can see that, no matter what the value of the other free parameter is, r_2^β can significantly change the lower bound of the differential for values smaller than approximately $1e$-2 and for higher values it starts decreasing the upper bound. Such analysis can also be used for model rejection. For example, if the observed differential is outside the calculated bounds one can reliably reject the model and the parameter box $\mathcal{I}$ under consideration since the observed differential cannot be reproduced for any parametrisation in $\mathcal{I}$. Further, the profile differential bounds analysis can show how to confine $\mathcal{I}$ such that all considered parameter values are consistent with the observed magnitude of the differential.

The non-linear differential expressions' algebraic structures also imply that not every differential value is equally likely to occur when we sample parameter values uniformly from $\mathcal{I}$. Examples for the resulting distributions of dose differentials are shown in Figure 5.5a, b. This non-uniformity of the differential can be interpreted as parametric robustness because random changes of parameters may not lead to random magnitudes of the differential. On the other hand, these results imply that the differential system induces an important structural prior on the behaviour—system structures (and parameter intervals) define what magnitude

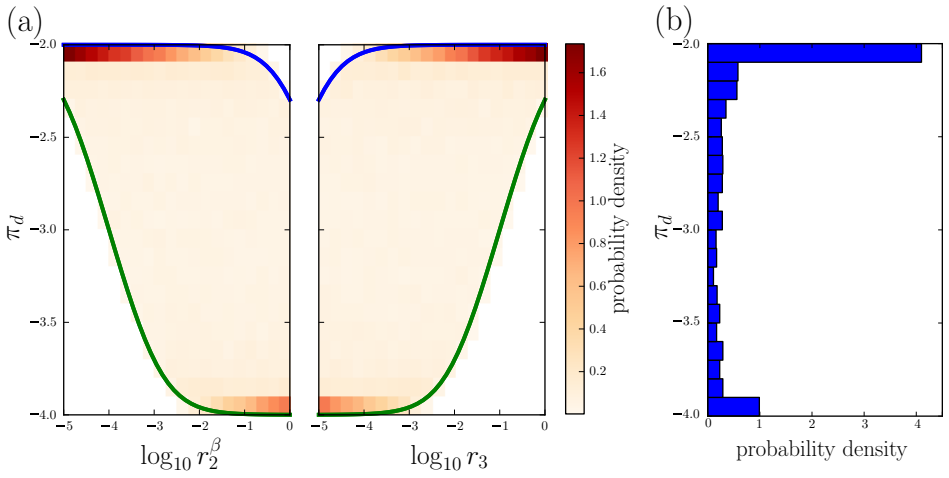

Figure 5.5: Numerical analysis of the example model from Figure 5.2a. (a) Profile bounds (blue – upper outer bound, green – lower outer bound) superimposed on the profile differential distribution (density) for the free parameters r_2^β and r_3. (b) Marginal probability distribution of the dose differential magnitude. Densities were obtained from uniform samples of the parameter box $\mathcal{I}$ defined by $r_1, r_2, r_3, r_4 \in [1e\text{-}5, 1]$ in units s^{-1}, assuming $x_t = 1$ nM, $\frac{r_1^\alpha}{r_1^\beta} = 100$, and $\frac{r_2^\alpha}{r_2^\beta} = 0.01$.

of the differential can be expected, and this prior information could be exploited for more detailed model selection against experimental data.

5.8 Extension: Two Dose Edges

To extend the framework to cases in which hormesis is possible, we consider that the input dose acts proportionally and simultaneously on two edges, i.e. $I(G) = \{e_{d,1}, e_{d,2}\}$, $\ell(e_{d,1}) = g_1(p)d$, and $\ell(e_{d,2}) = g_2(p)d$. To derive the general form of dose-response expressions for closed and open systems, we apply the deletion-contraction formula to partition the set of arborescences from the numerator and denominator of the response function $\mathcal{R}$ into four categories—those containing no input edges, those containing $e_{d,1}$ but not $e_{d,2}$, those containing $e_{d,2}$ but not $e_{d,1}$, and those containing both $e_{d,1}$ and $e_{d,2}$. After simplification, we obtain:

$$\mathcal{R}_O(d) = \frac{k_1 + k_{23}d + k_4 d^2}{k_5 + k_{67}d + k_8 d^2}, \tag{5.3}$$

where $k_{23} := k_2 + k_3$ and $k_{67} := k_6 + k_7$ (see Section 8.3.3 in the appendix for all details). For two dose edges, the numerator and denominator polynomials in the dose d can be at most of degree two; for an input acting on w edges simultaneously, these polynomials are at most of degree w. However, the arborescence

partitioning determines the digraphs contained in the coefficients k of the polynomials (see, for example, the tree scheme in Figure 8.4 from the appendix) and the exponential increase of the number of relevant digraphs with number of dose edges (2^w digraphs) is one of the main causes for complexity of systems with multiple inputs.

Depending on the coefficients k_i, two or three critical points define a sigmoid or a biphasic/hormetic dose-response relationship, respectively. A necessary and sufficient condition for a biphasic dose-response function, which we call the *Hormesis condition*, is:

$$(k_{67} = 0 \wedge k_{23} \neq 0) \vee \left(k_{67} \neq 0 \wedge U \geq 0 \wedge \left(\frac{k_{23}}{k_{67}} < \frac{k_4}{k_8} \leq \frac{k_1}{k_5} \vee \frac{k_{23}}{k_{67}} < \frac{k_1}{k_5} < \frac{k_4}{k_8} \vee \frac{k_4}{k_8} \leq \frac{k_1}{k_5} < \frac{k_{23}}{k_{67}} \vee \frac{k_1}{k_5} < \frac{k_4}{k_8} < \frac{k_{23}}{k_{67}} \right) \right).$$

where $U = (k_1k_8 - k_4k_5)^2 + (k_1k_{67} - k_5k_{23})\,(k_4k_{67} - k_8k_{23})$. Because the values of the coefficients k_i are not known in general, the number of critical points cannot be determined unambiguously, and we need to distinguish cases depending on the number of segments in A (σ^α) and B (σ^β) that are mapped to each other to derive the signed projections π_d and $\pi_{\mathcal{R}}$ (see Section 8.3.3 from the appendix for details).

The projections of the differential have a more complicated form (for example, the expressions are not necessarily rational functions since they involve square roots) and there are multiple conditions to be considered, but the expressions are symbolic and (more involved) symbolic analysis with efficient methods for the generation and manipulation of Kirchhoff polynomials is applicable. For example, general properties of the differentials in systems with two dose edges are: (i) in contrast to systems with a single dose edge, the dose differential π_d depends on the choice of output vertices and their weights; (ii) for closed systems, π_d does not depend on the conserved x_t, but potentially on the synthesis reactions and the proportion variable h; (iii) the response differential $\pi_{\mathcal{R}}$ depends on all eight partitions of the set of arborescences of G, and it includes x_t in closed systems; and (iv) the differential can also be degenerate or undefined, e.g. when $U < 0$.

To illustrate these concepts, we consider a more detailed model for insulin receptor trafficking that includes a second dose edge through binding of a second ligand molecule to the receptor as well as the relevant reactions and internalized species shown in Figure 5.6a. The model has been proposed as a realistic approximation of insulin signalling in Sedaghat et al. (2002). Assume that the receptor species on the cell surface that are bound by a single ligand molecule are our outputs of interest ($O = \{v_{RL}, v_{RLp}\}$) and we stimulate the cell with two ligands that differ in their affinity to the receptor (ligand α with reaction rate constants r_1^α, r_2^α, r_{12}^α, r_{13}^α, and ligand β with r_1^β, r_2^β, r_{12}^β, r_{13}^β). In this scenario, it is possible to use the *Hormesis condition* to find parametrizations such that the reference dose-response curve (for α) is sigmoidal, whereas the perturbed curve

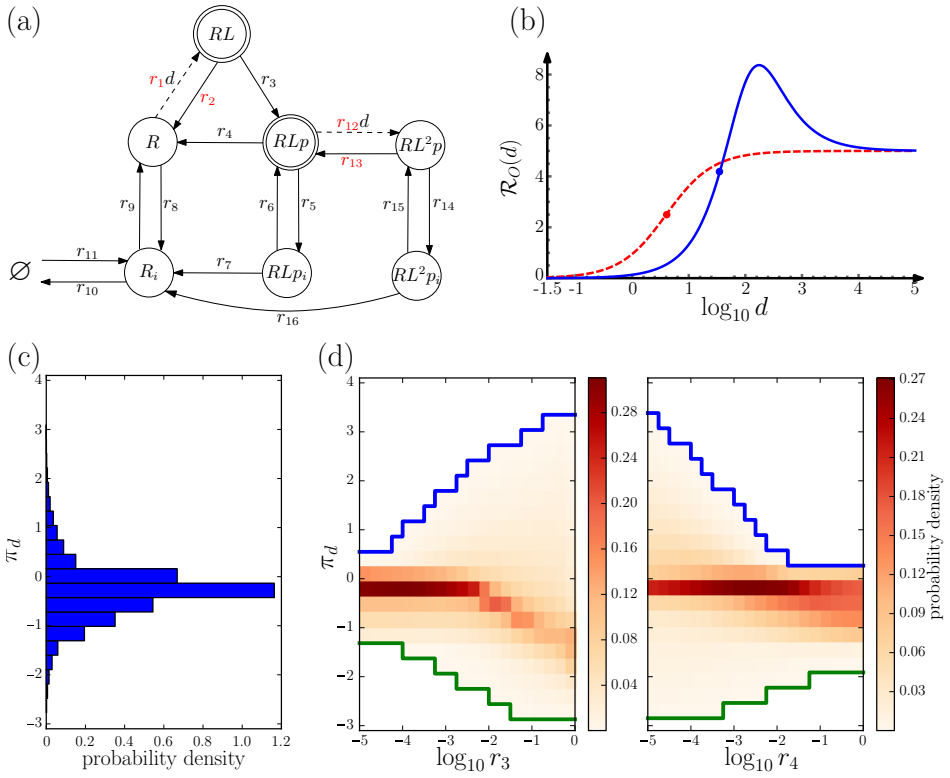

Figure 5.6: Extended insulin model with two dose edges. (a) Digraph of the model for receptor trafficking from Sedaghat et al. (2002) with notation as in Figure 5.2; differential parameters are shown in red. (b) Sigmoid reference (dashed red) and hormetic perturbed (blue) dose-response curves. The half-maximal response points ($h = 0.5$) for which the dose differential was analysed are marked with a red and a blue dot on the reference and the first segment of the perturbed curve, respectively. The differential parameters were fixed to $r_1^\alpha = 0.03$, $r_{12}^\alpha = 0.1$, $r_2^\alpha = 0.1$, $r_{13}^\alpha = 0.001$, $r_1^\beta = 0.002$, $r_{12}^\beta = 0.001$, $r_2^\beta = r_{13}^\beta = 0.01$. Other parameters were fixed to $r_9 = 0.5$, $r_4 = r_6 = r_{14} = 0.2$, $r_3 = r_7 = r_8 = r_{15} = r_{10} = r_{11} = r_{16} = 0.1$, and $r_5 = 0.01$. (c-d) Numerical analysis of the two dose edge insulin model. Densities were obtained using the fixed differential parameters from (b) and uniformly sampling the remaining n parameters from the parameter box $\mathcal{I} = [10e\text{-}5, 1]^n$; note that $n = 12$ in (c) and $n = 11$ in (d) since one additional parameter is fixed at a time. (c) Marginal probability distribution of the dose differential magnitude. (d) Profile differential distributions together with the inner profile bounds (blue, upper inner bound; green, lower inner bound) for the free parameters r_3 and r_4.

(for β) is hormetic (Figure 5.6b; see Section 8.3.3 from the appendix for details). Our symbolic analysis of the system shows the following: (i) the values of r_9, r_{10}, and r_{11} (free receptor externalization, degradation, and synthesis, respectively)

do not affect whether or not the response is hormetic; (ii) the first and last critical points of the reference and perturbed curves are identical; (iii) the last critical points depend only on the four reaction rates r_3, r_9, r_{10}, and r_{11}; (iv) the dose component of the second critical point of the perturbed system does not depend on r_9, r_{10}, and r_{11}; (v) the response differential between the reference curve and the second segment of the perturbed curve for $d \to \infty$ is always zero, independent of the magnitude of the perturbation and of the parameter values; and (vi) both the dose and the response differential are invariant with respect to the reaction rate constants r_9, r_{10}, and r_{11}.

Finally, we analyse the dose differential numerically, assuming the affinities of the two ligands to be known, while remaining uncertain about the rest of the reaction rate constants. Uniform sampling of the dose differential yields a few magnitudes of variability presented by the wide inner bounds $\widehat{\mathbb{D}_{\pi_d}} = [-2.8, 3.1]$ but a small region of most probable values illustrated by a marginal density peaked around -0.25 (Figure 5.6c). The profile differential distributions in Figure 5.6d show how the free parameters r_3 (receptor phosphorylation) and r_4 (receptor dephosphorylation) affect the upper and lower inner bounds and the peak of the marginal distribution, revealing their potential to control the differential.

5.9 Discussion

We developed a theory for steady-state dose-response relationships in Laplacian models of biochemical reaction networks that is analytic, and therefore also applicable under the realistic conditions that parameter values are largely unknown. In particular, we formalized the concept of differential responses to establish a comprehensive parameter-free framework for analysing differential responses in Laplacian systems. This framework helps to study system behaviours upon perturbations of many features of reaction networks, such as network topology, parameters, choice and number of inputs and outputs. In particular, the algebraic and numerical methods allow us to explore the space of network topologies and perturbations to arrive efficiently at a set of candidate models that are consistent with prior knowledge and experimental data. For example, if it is known from experiments that a particular perturbation leads to a significant dose differential, we can *reliably reject* all potential models for which the differential expression does not depend on the perturbed variable. Additionally, numerical bounding of the range of the differential expressions over a predefined region in parameter space provides us with limits for all possible differential magnitudes—we can use this knowledge as a certificate to reliably reject models that can never reproduce quantitative experimental data. Another application of the developed methodology is in experimental design, namely to determine (optimal) perturbations of a reference system that lead to a desired differential, to invalidate a model, to discriminate between equivalence classes of networks, or for applications such as finding optimal (combinations of) drug targets. Note also that we did not cover all aspects of the differential analysis framework in detail or through the application examples; in general, every element of the differential system can be perturbed

and labels for dose edges can be formulated in a more general form, making the framework applicable to a wide spectrum of perturbations.

The most obvious limitation of our framework is the restriction to Laplacian systems, that is, reaction networks with zero- and first-order chemical kinetics; it therefore has to rely on prior, often parameter- and state-dependent simplifications for higher-order kinetics, such as those obtained via time-scale separation. In terms of scalability, the exponential growth of the number of digraphs to be considered for the analysis and the resulting high degree polynomials with increasing number of reactions influenced by the dose is a challenge. Our examples demonstrate that systems with up to two dose edges can be analysed efficiently due to the linear scaling of the prime factorization algorithm and the few digraphs that have to be considered. According to the *Abel-Ruffini Theorem*, general algebraic solutions for the roots of polynomial equations of degree five or higher with arbitrary coefficients—corresponding to the dose acting proportionally on five or more edges—do not exist. However, depending on the particular digraph structure and form of the label expressions, such cases, or cases with labels that are non-linear functions of the dose, could be analytically tractable if the polynomials simplify to a lower degree. Similarly, obtaining exact bounds might be feasible for simple differential expressions with few variables and convex properties, but it is computationally costly to determine the exact bounds of arbitrary multivariate rational functions. In practice, therefore, bounding methods provide us with inner or outer bounds, which do not guarantee reliable model rejection. Because bounding approaches are often employed in control theory (Walter et al., 1996) and methods are being improved, for example, for bounding the range of rational functions in more complicated parameter spaces using Bernstein polynomials (Titi et al., 2015; Smith et al., 2015), these limitations could be reduced substantially.

Extensions of the framework could further build on the central insight that prime factors and components (and their similarity in perturbed digraphs) are the units, the very characterization, of the differential response function in steady-state Laplacian models. For example, perturbations that result from additions and deletions of vertices and edges in certain parts of both the reference and perturbed digraph may never have an effect on the differential if they belong to a prime component that always cancels in the differential expression. In general, the positions (connectivity) of additions and deletions within the digraph and the size distribution of the induced prime components play an important role in the change of the differential upon structural perturbations. This could be exploited to develop a notion of *structural robustness* of the differential to account for how the properties of the differential change when edges and vertices are (randomly) added or removed. We also note that many of the graph theoretical notions defined here subsume graph theoretical concepts such as distributions of sizes of SCCs, strong bridges, and strong articulation points that are actively studied in computer science; for example, efficient algorithms for their characterization (Italiano et al., 2012; Georgiadis et al., 2015a,b; Firmani et al., 2015) could help extending the scope of our framework.

In terms of applications, we envisage our framework to be most useful for the

systematic study of mechanisms underlying hormesis, a phenomenon in toxicology and cell signalling that receives increasing attention. For example, empirical evidence favoured hormetic over threshold models for dose-response relationships in a large-scale yeast anticancer drug screen (Calabrese et al., 2008) and hormetic phenomena are frequently observed in stress responses and their relations to ageing (Gems & Partridge, 2008). Corresponding theoretical work has only (re-)started very recently. One example study uses simple models of interacting linear pathways in cell signalling to show that non-monotonic dose-response relationships can arise through non-obvious pathway interactions, and that the network structure imposes fundamental constraints on options for pharmacological treatment (van Wijk et al., 2015). Our analysis of the insulin signalling network demonstrates first steps in a direction we believe to become increasingly important and that is enabled by our framework: a systematic analysis of hormesis in biochemical reaction networks despite prevailing uncertainties on the networks' quantitative features.

5.10 Contributions and Acknowledgements

This chapter is based on the manuscript Yordanov & Stelling (2017b) developed in collaboration between P. Yordanov (PY) and J. Stelling (JS). PY initiated the study, developed the theory, and generated the results. PY and JS conceived the study and wrote the manuscript. JS supervised the study.

6

A Minimal Model of Differential Type I Interferon Signalling

6.1 Introduction

A central property of cytokine signalling is the capacity of individual receptors to recognise different ligands and trigger the appropriate cellular responses (Moraga et al., 2014). Type I interferons (IFNs) are a prominent cytokine family displaying such functional plasticity. In humans, a total of 17 structurally similar interferon ligands bind to a common heterodimeric receptor composed of the subunits IFNAR1 and IFNAR2, thus leading to the assembly of a ternary receptor-ligand complex (De Weerd & Nguyen, 2012; Schreiber & Piehler, 2015). Ternary complex formation initiates the activation of various effector proteins, and particularly the Janus kinase/signal transducer and activator of transcription (JAK/STAT) signalling cascade, which ultimately elicit differential antiviral, immunomodulatory, and antiproliferative (apoptosis and cell cycle arrest) activities (Ivashkiv & Donlin, 2014; Schreiber & Piehler, 2015). The differential activities are determined by interferon concentration, binding affinity to the receptor subunits, and duration of stimulation (Kalie et al., 2008; De Weerd & Nguyen, 2012; Schreiber & Piehler, 2015). Importantly, they are exemplified by the observation that ligands with vastly differing affinities, i.e. low affinity IFNα2 and high affinity IFNβ, trigger similar early signalling events leading to nearly equipotent antiviral responses, while during late signalling IFNβ induces a much stronger antiproliferative effect than IFNα2 (Jaitin et al., 2006; Piehler et al., 2012).

Due to their important activities, interferons serve as a first line of defence against pathogens and malignancies (Hertzog & Williams, 2013; Schneider et al., 2014), and have found therapeutic application in treating multiple sclerosis, cancer, and hepatitis (Borden et al., 2007). It is essential to understand which molecular mechanisms govern the observed differential responses in order to extract general principles about cytokines' functional plasticity and design more effective therapies. An array of recent experimental studies have provided deep insight

into the probable major mechanisms of differential antiviral and antiproliferative signalling. It has been shown that thresholds in the number of activated ternary receptor-ligand complexes dictate the differential interferon activities (Kalie et al., 2008; Levin et al., 2011). Besides, the data indicates that the stability and abundance of ternary complexes is determined by (i) interferon affinity to each of the receptor subunits (Jaitin et al., 2006; Jaks et al., 2007), (ii) receptor trafficking including endocytosis, recycling, and degradation (Marchetti et al., 2006; Claudinon et al., 2007; Marijanovic et al., 2007), (iii) late negative expression feedback interfering with ternary complex assembly, specifically ubiquitin-specific protease 18 (USP18) binding to the cytosolic domain of IFNAR2 (Francois-Newton et al., 2012; Wilmes et al., 2015), and (iv) surface receptor number varying among cells due to stochastic gene expression (Moraga et al., 2009; Levin et al., 2011). It is hypothesized that the combination of these main determinants can explain differential IFN activities (Piehler et al., 2012; Schreiber & Piehler, 2015).

Previous mathematical modelling efforts of the type I interferon system have addressed the kinetic behaviour of IFNα signalling leading to accelerated antiviral response (Maiwald et al., 2010) and the inherent stochasticity in IFN signal transduction (Rand et al., 2012). Recently, bistability at the level of early STAT signalling has been theoretically detected using tools from Chemical Reaction Network Theory (Otero-Muras et al., 2016), which presents a possible hypothesis for the observed threshold behaviour.

Many important aspects of differential signalling, for which modelling efforts can markedly contribute, still remain uninvestigated. For instance, it is not clear if the mechanisms hypothesized to control interferon ternary complex stability are sufficient to achieve the observed population differential activities and how they functionally fit together. Formal elucidation of the essential determinants of differential signalling would provide vital insight into the functional plasticity of interferon signalling. However, such an analysis is challenged by the high topological and parametric uncertainty, as well as, cell-to-cell variability inherent to the interferon system.

In this chapter we develop a framework to evaluate the various posed hypotheses and find the minimal sufficient model constituents which can explain the differential responses as observed in the IFNα2 vs. IFNβ dose-response curves for antiviral and antiproliferative activities in WISH cells from Jaitin et al. (2006). Our framework accounts for (i) the cell-to-cell variability in IFNAR2 number by explicitly considering its distribution, (ii) parametric uncertainty by performing Bayesian parameter inference to determine the posterior parameter distribution, and (iii) uncertainty in model topology by exploring an ensemble of possible models through Bayesian model comparison.

More precisely, we consider the empirical IFNAR2 receptor distribution in a population of cells prior to interferon stimulation. We transform this distribution with a ternary complex stability (TCS) submodel to obtain the distribution of active ternary complexes in the population. Then, with regards to an activity specific threshold, i.e. one threshold for antiviral and one for antiproliferative activity, we determine the proportion of alive cells in the population. Particularly, in line with the observations from Levin et al. (2011), cells stay alive if they have

a sufficient number of active ternary complexes to trigger downstream signalling and counteract virus infection, or have an insufficient number of active ternary complexes to trigger apoptosis. Thus, depending on the population-wide receptor distribution, TCS submodel, and activity thresholds we obtain a model for generating population-level dose-response curves that can be compared to experimentally derived ones displaying differential responses. The described model can be classified as a threshold model (Cox, 1987; Viswanathan et al., 2002) and a generalised non-linear model (Lane, 1996). What is particular is the formulation of the TCS submodel as a (steady-state) differential Laplacian model as introduced in Chapter 5. It allows us to symbolically derive the expressions for the differential responses on the population level (in the sense of Chapter 5) for models with one and two dose edges, and to provide an explicit likelihood function for the model.

We study an ensemble of 290 models in which the TCS submodels comprise all biologically feasible combinations of the aforementioned hypothetical determinants of ternary complex stability. We rank those models using Bayesian model comparison, which naturally implements Ockham's razor permitting the selection of a minimal, least complex model reproducing the data sufficiently well. The top ranking model provides strong evidence that receptor assembly, receptor endocytosis and recycling, and USP18 inhibition with signalling originating from both the cell surface and endosomes are the minimal sufficient mechanisms to reproduce the experimental dose-response data. Additionally, we use Bayesian parameter inference to infer the posterior probability over the parameter space with respect to data for the considered models. The posterior distribution for the top model hints that fast irreversible ternary complex phosphorylation could be central to establishing the differential response.

6.2 Modelling Framework

We develop a modelling framework to study how the mechanisms affecting ternary complex stability differentially trigger key activities in the interferon signalling pathway. Specifically, by differential activity we understand the difference in antiviral and antiproliferative dose-response behaviour of populations of cells treated with IFNα2 and IFNβ ligands. For conciseness we denote IFNα2 and IFNβ, as α and β, and antiviral and antiproliferative activities, as AV and AP, respectively. Also, by writing χ, $\chi \in \{\alpha, \beta\}$ we mean either the ligand α or the ligand β and by ω, $\omega \in \{AV, AP\}$ we denote either the antiviral or the antiproliferative activity.

We look for the minimal sufficient determinants of differential signalling and for that reason we use only the essential theoretical tools allowing to account for the major experimental observations. As a result the modelling framework consists of three main parts:

1. A collection of TCS submodels which are steady-state Laplacian models. They represent different hypothetical mechanisms dictating the stability of the active ternary complex.

2. An intracellular signalling cascade empirically modelled as a threshold sensing mechanism of the active ternary complex concentration which results in a life/death event for a single cell.

3. A population-level model aggregating the life/death responses of single cells with heterogeneous number of receptors on the cell surface.

The resulting population models differ by their parameter values and TCS mechanisms. They can be compared and their parameters can be inferred through Bayesian model comparison and parameter inference by defining a likelihood function relating experimentally obtained dose-response curves to dose-response curves produced by the population model.

6.2.1 Ternary Complex Stability (TCS) Submodels

We examine receptor trafficking, assembly, and inhibition mechanisms with strong experimental evidence in controlling ternary complex stability. Pertinent questions are to model these mechanisms in a minimal, yet adequate way to explain the observations, and to combine them in order to form an ensemble of TCS submodels to analyse.

6.2.1.1 Modelling receptor assembly, trafficking, and inhibition

We focus on three main mechanisms controlling the stability of signalling interferon receptors – (i) ligand-induced ternary complex assembly on the cell surface, (ii) ternary complex endocytosis including receptor recycling and endosomal degradation, and (iii) inhibition of the free IFNAR2 receptor by USP18. We assume that interferon ligand concentration is constant and notice that all mechanisms of interest have IFNAR2 at their core (see Section 8.4.1 in the appendix for details). Thus we choose to describe the mechanisms as state transitions of IFNAR2 (R_2 for short), and consider IFNAR1 (with concentration R_1) and USP18 (denoted as U with concentration u) implicitly. Formally, we represent the reactions in each mechanism with (pseudo) first-order mass-action kinetics and also include a zero-order mass-action term to account for R_2's synthesis. For some mechanisms we construct multiple models of differing complexity, i.e. with different level of detail and parametrisation, with the aim to arrive at minimal but adequate representations. For instance, we build multiple variants of the ligand-induced ternary complex assembly mechanism – several detailed ones including intermediate states to obtain the ternary complex and a crude one containing a direct transition from R_2 to the active ternary complex. We call each such variant of a mechanism a *component*. All different components which we consider are described in Section 8.4.1 in the appendix.

6.2.1.2 Hypothesis space generation

The set of all reactions we consider are presented in the form of a *master model* in Figure 6.1. We combine these reactions through the components they constitute in

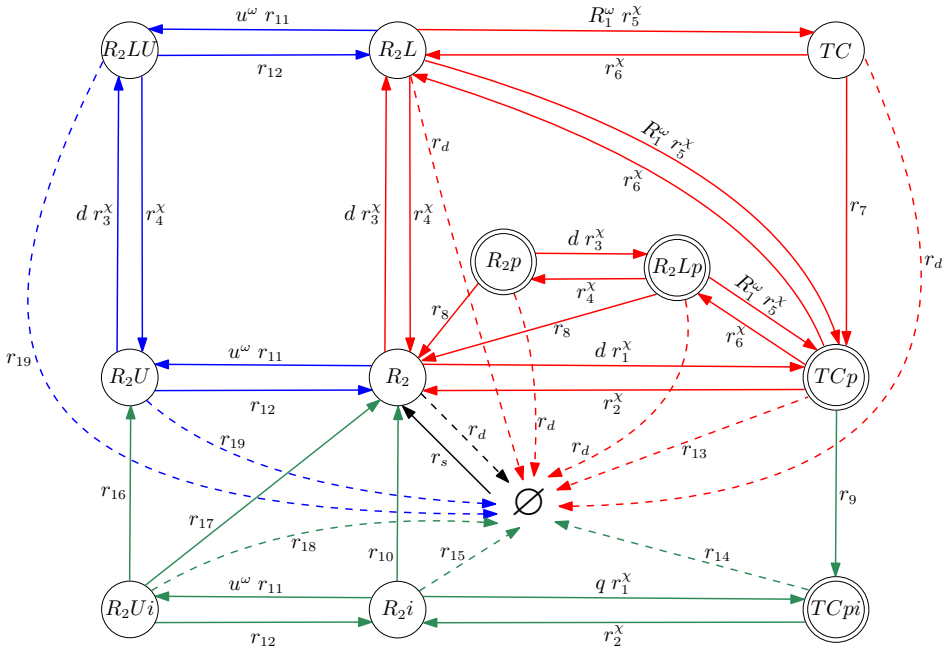

Figure 6.1: A master model for ternary complex stability regulation containing all reactions under consideration. Individual TCS submodel hypotheses are biologically meaningful subsets of the master model. Black arrows indicate basal synthesis and degradation reactions, red arrows – ligand-induced ternary complex assembly on the cell surface, blue arrows – inhibition of IFNAR2 by USP18 on the cell surface, and green arrows – ternary complex endocytosis along with ternary complex disassembly, endosomal degradation, receptor recycling, and inhibition inside endosomes. Dashed arrows denote degradation reactions, doubly encircled vertices represent species hypothesized to have signalling abilities. Superscripts indicate which parameters differ between interferon activities (superscript ω) and ligand types (superscript χ). The ternary complex is denoted as TC, IFNAR2 as R_2, the interferon ligand as L and its concentration with d, USP18 as U and its concentration as u, and IFNAR1's concentration as R_1. The letter p indicates a phosphorylated state and the letter i – an internalised state.

all possible biologically meaningful ways to obtain an ensemble of TCS submodels – our hypothesis space. When building the submodel ensemble we need to take into account biological feasibility. Namely, that some components can exist on their own or in combination with other components, e.g. a cell surface component is a meaningful model by itself but it can also be combined with an endocytic component. Other components require the presence of specific components, e.g. an endocytic component is not biologically meaningful by itself but requires a cell surface component. There are also components incompatible with certain other components, e.g. it is nonsensical to combine components modelling the

same mechanism but on different level of detail. Thus the master model itself is not part of the hypothesis space since it contains all components, even those of the same mechanism with different level of detail. The last ingredient when generating the hypothesis space is the choice of signalling species. We regard the phosphorylated states TCp, R_2Lp, R_2p, and $TCpi$, denoting respectively the phosphorylated ternary complex, the IFNAR2-ligand complex, the free IFNAR2, and the internalised ternary complex, as able to trigger downstream signalling with the same strength. Since there is experimental evidence that TCp is capable of signalling we include it in all models. Depending on which other species are present in a given combination of components, we consider the cases in which each of them, each pair of them, and all of them simultaneously are signalling competent. Finally, combining the components following the rules and assigning the signalling species we obtain the hypothesis space. It consists of a collection of 290 TCS submodels.

The generated TCS submodels are open Laplacian models with one, two, or three dose edges. We make the assumption that their steady-states are relevant for the stability of the signalling species in line with Kalie et al. (2008). We can express their steady-states for a given set of signalling species O as:

$$\rho_O(d) = \begin{cases} \dfrac{k_1 + k_2 d}{k_3 + k_4 d}, & \text{for single dose-edge submodels,} \\ \dfrac{k_1 + k_{23} d + k_4 d^2}{k_5 + k_{67} d + k_8 d^2}, & \text{for double dose-edge submodels,} \\ \dfrac{k_1 + k_{234} d + k_{567} d^2 + k_8 d^3}{k_9 + k_{101112} d + k_{131415} d^2 + k_{16} d^3}, & \text{for triple dose-edge submodels,} \end{cases} \tag{6.1}$$

where k_i are the steady-state coefficients as defined in Chapter 5.

All 290 TCS submodels in the ensemble we generate have $k_1 = 0$. The reason, which can also be observed in the master model, is that when deriving the numerator of any submodel steady-state expression for any of the output species TCp, $TCpi$, R_2p, or R_2Lp there does not exist an arborescence spanning vertex R_2 and simultaneously containing zero dose-edges.

We consider four different parametrisations of every submodel to account for the ligand types and activities which define differential signalling. We assume for simplicity that the differences between the submodels for α and β in AV and AP are only parametric and not topological. Thereby, each TCS submodel can be expressed as a quadruple of ligand and activity specific steady-states:

$$\left(\rho_O(d, k^{\alpha AV}), \rho_O(d, k^{\beta AV}), \rho_O(d, k^{\alpha AP}), \rho_O(d, k^{\beta AP})\right),$$

where the superscripts indicate the ligand and activity specific parametrisations. The ligand specific parametrisations differ by ligand affinity towards the receptor subunits and activity specific ones reflect the fact that AV and AP activities are separated in time – AV activity happens shortly after interferon stimulation while

AP activity requires longer continuous stimulation which establishes expression feedbacks, particularly USP18 expression.

6.2.1.3 Incorporating initial receptor concentration

Experimental measurements of the free cell surface receptor R_2 in unstimulated cells can readily be incorporated in the TCS steady-state expressions for a digraph model of interest G. Let r_0 be that quantified initial receptor concentration and consider the unstimulated digraph submodel G^U containing only the species and reactions present prior to stimulation with the interferon ligand. The unstimulated model in our case is the basal IFNAR2 synthesis and degradation mechanism $\varnothing \underset{r_d}{\overset{r_s}{\rightleftharpoons}} R_2$. Then we can derive the steady-state concentration of the measured species in the unstimulated submodel as:

$$\rho_{\{R_2\}} = \frac{\kappa_{v_{R_2}}(G^U)}{\kappa_{v_\varnothing}(G^U)} = \mathrm{r}_0.$$

Next, we notice that we only consider submodels containing a single synthesis reaction, i.e. $\varnothing \xrightarrow{r_s} R_2$ which we denote as the edge e_s. Hence, the Kirchhoff polynomial from the numerator of any submodel's steady-state can be expressed as $\kappa_v(G) = \ell(e_s)\kappa_v(G/e_s)$ since all arborescences it represents contain e_s as the only edge spanning the environmental vertex $v_\varnothing$. The Kirchhoff polynomial from the denominator never contains the synthesis rate due to the rooting operation at the environment vertex. Thus the synthesis rate (the label of the synthesis reaction) in the unstimulated submodel can be expressed as:

$$\ell(e_s) = \frac{\kappa_{v_\varnothing}(G^U)}{\kappa_{v_{R_2}}(G^U/e_s)}\mathrm{r}_0 \Rightarrow r_s = r_d \mathrm{r}_0.$$

Assuming the synthesis rate does not change after interferon stimulation, we can represent the steady-state of the stimulated submodels in terms of the initial measured IFNAR2 surface concentration r_0. For example, for single dose-edge submodels:

$$\rho_O(d; K, \mathrm{r}_0) = \frac{k_2^{\ell(e_s)\leftarrow r_d} d}{k_3 + k_4 d}\mathrm{r}_0, \tag{6.2}$$

where $\ell(e_s) \leftarrow r_d$ denotes a relabelling operation replacing the label of the synthesis edge e_s by the degradation rate constant r_d in the corresponding steady-state coefficient. Analogous relabelling applies to submodels with double and triple dose-edges. For conciseness we denote the relabelled steady-state coefficients as $K_i = k_i^{\ell(e_s)\leftarrow r_d}$ and the set of all steady-state coefficients, including the relabelled coefficients from the numerator and the coefficients from the denominator as K. Note that by writing $\rho_O(d; K)$ we mean the dose-response expression with applied edge relabelling operations but excluding the measured r_0, i.e. $\rho_O(d; K) = \frac{\rho_O(d;K,\mathrm{r}_0)}{\mathrm{r}_0}$.

6.2.2 Single-Cell Threshold Model

We assume, in line with Levin et al. (2011), that threshold sensing mechanisms in the steady-state magnitude of the cumulative signal $\rho_O(d; K, \mathrm{r}_0)$ originating from the TCS submodel determine the life/death fate of a single cell. For type I interferon signalling two threshold values are of main relevance:

τ^{AV} – a positive *antiviral threshold*, under which a cell does not express antiviral genes and cannot cope with viral infections which ultimately leads to its death, and above which a cell expresses antiviral genes thus remaining alive by counteracting the viral infection.

τ^{AP} – a positive *antiproliferative threshold*, under which a cell is alive, but above which apoptosis is triggered leading to cell death.

The thresholds serve as an abstraction of downstream JAK-STAT signalling, the ensuing gene expression, and the resulting antiviral and antiproliferative responses. A concrete mechanism implementing the threshold response could be bistability in early JAK-STAT signalling as hypothesized by Otero-Muras et al. (2016).

Let $y^{AV}(d)$ and $y^{AP}(d)$ be the binary variables describing the 1–life/0–death state of a cell with respect to the antiviral and antiproliferative activities of interferon, respectively. Formally, we can consider the cumulative signal $\rho_O(d; K, \mathrm{r}_0)$ as a latent variable and define the binary variables as:

$$y_{AV}(d) = \begin{cases} 1 & \text{if } \rho_O(d; K, \mathrm{r}_0) > \tau^{AV} \\ 0 & \text{if } \rho_O(d; K, \mathrm{r}_0) \leq \tau^{AV} \end{cases}, \qquad y_{AP}(d) = \begin{cases} 1 & \text{if } \rho_O(d; K, \mathrm{r}_0) \leq \tau^{AP} \\ 0 & \text{if } \rho_O(d; K, \mathrm{r}_0) > \tau^{AP}. \end{cases}$$

In Chapter 5 we defined the differential for continuous dose-response curves but it can also be derived for step dose-response functions. Let us denote by $y(d)$ and τ a binary variable and its threshold without specifying the interferon activity. Then the dose differential is the difference between the doses for which the reference α and the perturbed β system, $y^{\alpha}(d)$ and $y^{\beta}(d)$, reach the threshold τ.

Namely, for single dose-edge submodels $\rho_O(d; K, \mathrm{r}_0) = \frac{K_2 d}{k_3 + k_4 d}\mathrm{r}_0 = \tau \quad \Rightarrow \quad d = \frac{k_3}{k_4\tau - K_2 \mathrm{r}_0}$ leading to:

$$\pi_d = \log_{10} \frac{k_3^{\alpha}}{k_3^{\beta}} \frac{K_2^{\beta}\frac{\mathrm{r}_0}{\tau} - k_4^{\beta}}{K_2^{\alpha}\frac{\mathrm{r}_0}{\tau} - k_4^{\alpha}}.$$

We observe that the dose differential expression of the binary variable for single dose-edge submodels has the steady-state coefficient K_2 weighted by the ratio of the measured pre-stimulation surface receptor concentration r_0 and a threshold value (antiviral or antiproliferative). It differs form the differential of the latent variable $\rho_O(d; K, \mathrm{r}_0)$ shown in Chapter 5 since it incorporates K_2 and is identical to it only in the trivial case when $K_2 = 0$ or $\mathrm{r}_0 = 0$. The response differential $\pi_{\mathcal{R}}$ is 1 between the doses for which the response reaches the threshold and 0 otherwise.

The differential for the double dose-edge case can also be derived (see Section 8.4.2 from the appendix) but the one for three dose-edges, though symbolically derivable is tedious to analyse.

6.2.3 Population Threshold Model

Dose-response relations observed on the population level might be misleading for interpretation from the viewpoint of single-cell models because of cell-to-cell variation leading to non-trivial aggregation of single-cell effects. It has been shown in Moraga et al. (2009); Levin et al. (2011) that there exists single-cell variation in interferon receptor levels which is reproducible, maintained, due to stochastic expression, and key in determining the interferon signalling outcome. Therefore, we extend the single-cell model to a population model assuming that the main heterogeneous element in the cell population is the ratio between R_2's synthesis and degradation rate constants. Its variability is indirectly expressed through the variability of the measured cell surface R_2 number in unstimulated cells, r_0.

We model the distribution of r_0 in a cell population as the random variable R_0 having a log-normal distribution with a location parameter μ and a scale parameter σ:

$$\mathrm{R}_0 \sim \text{Log-}\mathcal{N}(\mu,\ \sigma).$$

Note that the choice of the distribution for R_0 is not limiting for the analysis. Other choices of distributions taking only positive values are also possible. For example, the Gamma distribution has been used to model the distribution of copy numbers of proteins (Friedman et al., 2006).

Recalling Equation 6.2, we can see that the dose d and the steady-state coefficients K are scalars, and r_0 is a particular realisation of the random variable R_0. Hence we can regard the signal from the TCS submodel $\rho_O(d; K, \mathrm{r}_0)$ as a particular realisation of a random variable, which we call $\mathcal{P}_O$, obtained by transforming R_0 by the scalar quantity $\rho_O(d; K)$. In general, the product between a scalar s and a log-normal random variable with a location parameter μ and a scale parameter σ is log-normally distributed with a location parameter $\mu + \ln s$ and the same scale parameter. Thus $\mathcal{P}_O$ also follows the log-normal distribution, although with a location parameter different from that of R_0, namely:

$$\mathcal{P}_O \sim \text{Log-}\mathcal{N}\left(\mu + \ln \rho_O(d; K),\ \sigma\right). \tag{6.3}$$

In other words, as depicted in Figure 6.2, the TCS submodel's topology and parameters, expressed through the steady-state coefficients and values of the dose variable, transform R_2's measured distribution to the distribution of the signalling species abundance within the population.

Analogously to the single-cell model, the total number of activated species $\mathcal{P}_O$ serves as a latent random variable rendering a dichotomous 1-life/0-death cell response. We model this response by the Bernoulli random variable Y_i for the i-th cell in the population and according to the antiviral and antiproliferative thresholds τ^{AV} and τ^{AP}. The probability of survival for an individual cell in

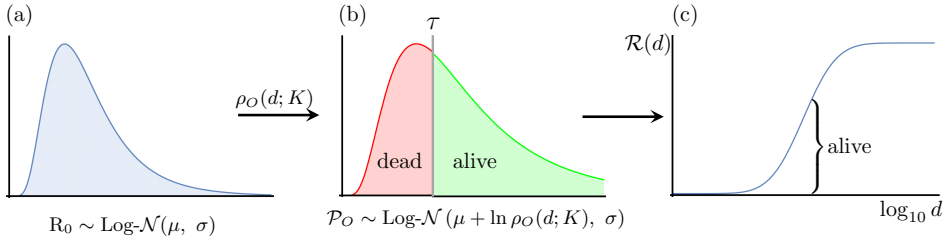

Figure 6.2: Population threshold model. (a) The distribution of the measured initial concentration of R_2 within a cell population, expressed through the probability density function of the random variable R_0 is transformed by a TCS submodel $\rho_O(d;K)$ to obtain (b) the steady-state population variation in the active signalling species modelled by the random variable $\mathcal{P}_0$. A threshold value τ operating on $\mathcal{P}_0$ determines the life/death fate of cells in the population. (c) The expected proportion of alive cells $\mathcal{R}(d)$ resulting from treatment with varying doses of interferon presents an experimentally testable dose-response relationship.

the population can then be expressed through the cumulative distribution function (CDF) of $\mathcal{P}_O$ for antiviral and apoptotic activities as:

$$\Pr\left(Y_i^{\chi AV} = 1 \mid \mu, \sigma, \tau^{AV}, d, K^{\chi AV}, O\right) = 1 - \Phi\left(\frac{\ln \frac{\tau^{AV}}{\rho_O(d;K^{\chi AV})} - \mu}{\sigma}\right),$$

$$\Pr\left(Y_i^{\chi AP} = 1 \mid \mu, \sigma, \tau^{AP}, d, K^{\chi AP}, O\right) = \Phi\left(\frac{\ln \frac{\tau^{AP}}{\rho_O(d;K^{\chi AP})} - \mu}{\sigma}\right),$$

where the CDF of $\mathcal{P}_O$ is expressed through $\Phi(.)$, the CDF of the standard normal distribution.

We assume that the life/death fates Y_i of single cells for a fixed interferon dose in a population of n cells are independent and identically distributed, thus the number of surviving cells in the population for a fixed ligand type and activity can be described by the binomially distributed random variable Z, $Z = \sum_{i=1}^{n} Y_i$. The expected proportion of alive cells in the population is then equal to the probability of a single cell being alive:

$$\mathcal{R}(d) = \frac{\mathrm{E}[Z]}{n} = \Pr\left(Y_i = 1 \mid \mu, \sigma, \tau, K, d, O\right), \tag{6.4}$$

The resulting model of interferon response reminds of the Probit model, but it is also quite different mainly due to the non-linear TCS submodel.

6.2.3.1 Population differential response

The population differential response can be derived from $\mathcal{R}(d)$, the expected fraction of living cells for the AV and AP activities.

We take the first derivative of $\mathcal{R}(d)$ to determine the critical points of the population dose-response relation obtaining:

$$D_d\mathcal{R}_{AP}(d) = -D_d\mathcal{R}_{AV}(d) = \frac{-k_3}{d(k_3+k_4d)\sigma\sqrt{2\pi}e^{\frac{\left(\ln\frac{(k_3+k_4d)\tau^\omega}{K_2d}-\mu\right)^2}{2\sigma^2}}},$$

where D_d denotes the first derivative with respect to the dose and $\tau^\omega \in \{\tau^{AV}, \tau^{AP}\}$. The first derivative is never zero for non-trivial dose-response relationships and thus $\mathcal{R}(d)$ defines a sigmoid curve which has only two critical points for both the antiviral and the antiproliferative threshold:

$$\mathcal{E}_{AV} = \left\{\epsilon_1 = (0,0), \epsilon_2 = \left(\infty, 1-\Phi\left(\frac{\ln\frac{k_4\tau^{AV}}{K_2}-\mu}{\sigma}\right)\right)\right\},$$
$$\mathcal{E}_{AP} = \left\{\epsilon_1 = (0,1), \epsilon_2 = \left(\infty, \Phi\left(\frac{\ln\frac{k_4\tau^{AP}}{K_2}-\mu}{\sigma}\right)\right)\right\}.$$

Now we can derive the dose and the response differential as described in Chapter 5. The dose differential π_d has the form:

$$\pi_d(h) = \log_{10}\frac{k_3^{\alpha\omega}}{k_3^{\beta\omega}}\,\frac{K_2^{\beta\omega}\,\eta_1\left(\tau^\omega,\mu,\sigma,h,\frac{k_4^{\beta\omega}}{K_2^{\beta\omega}}\right)-k_4^{\beta\omega}}{K_2^{\alpha\omega}\,\eta_1\left(\tau^\omega,\mu,\sigma,h,\frac{k_4^{\alpha\omega}}{K_2^{\alpha\omega}}\right)-k_4^{\alpha\omega}}, \text{ with}$$

$$\eta_1\left(\tau^\omega,\mu,\sigma,h,\frac{k_4^{\chi\omega}}{K_2^{\chi\omega}}\right) = \frac{1}{\tau^\omega}e^{\mu-\sigma\sqrt{2}\,\mathrm{erfc}^{-1}\left((1-h)\,\mathrm{erfc}\left(\frac{\mu-\ln\frac{k_4^{\chi\omega}\tau^\omega}{K_2^{\chi\omega}}}{\sigma\sqrt{2}}\right)\right)},$$

where we call $\eta_1(.)$ the *population receptor function* for single dose-edge models, $\mathrm{erfc}\,(.)$ is the complementary error function and $\mathrm{erfc}^{-1}\,(.)$ is its inverse.

We can also express the response differential as:

$$\pi_{\mathcal{R}}(h) = \begin{cases} (1-h)\left(\Phi\left(\frac{\ln\frac{k_4^{\beta AV}\tau^{AV}}{K_2^{\beta AV}}-\mu}{\sigma}\right)-\Phi\left(\frac{\ln\frac{k_4^{\alpha AV}\tau^{AV}}{K_2^{\alpha AV}}-\mu}{\sigma}\right)\right), & \text{for AV,} \\ (1-h)\left(\Phi\left(\frac{\ln\frac{k_4^{\alpha AP}\tau^{AP}}{K_2^{\alpha AP}}-\mu}{\sigma}\right)-\Phi\left(\frac{\ln\frac{k_4^{\beta AP}\tau^{AP}}{K_2^{\beta AP}}-\mu}{\sigma}\right)\right), & \text{for AP.} \end{cases}$$

Despite the complicated form of differential expressions we can easily isolate the effect of the TCS submodels on the population differential. We notice that two population models with identical parameters h,τ^ω,μ, and σ have the same response differential when they have the same ratio of steady-state coefficients $\frac{k_4^{\chi\omega}}{K_2^{\chi\omega}}$, and have the same dose differential when they have the same response

differential and the same expression $\frac{k_3^{\alpha\omega}}{k_3^{\beta\omega}} \frac{K_2^{\beta\omega}}{K_2^{\alpha\omega}} \frac{c^{\beta}-k_4^{\beta\omega}}{c^{\alpha}-k_4^{\alpha\omega}}$ where c^{χ} is the population receptor function regarded as a symbol.

The derivation of the differential for two dose edges can be found in Section 8.4.2 from the appendix, while that for three dose edges, although analytically derivable, is more difficult to interpret.

6.2.3.2 The single-cell differential is a limiting case of the population differential.

The single-cell and the population dose differential expressions have a similar form in which ratio $\frac{\mathrm{r}_0}{\tau}$ corresponds to the population receptor function $\eta(.)$. To check if the population differential reduces to the single-cell differential, we consider a limiting case initial receptor distribution R_0 with mean r_0 and variance approaching zero. The arithmetic mean and variance of a log-normal distribution can be expressed through the location and scale parameters as $\mathrm{E}[\mathrm{R}_0] = e^{\mu+\frac{1}{2}\sigma^2} = \mathrm{r}_0$ and $\lim_{\sigma\to 0} \mathrm{Var}[\mathrm{R}_0] = (e^{\sigma^2}-1)(\mathrm{E}[\mathrm{R}_0])^2 = 0$, leading to $\mu = \ln \mathrm{r}_0$ and $\sigma \to 0$. It can be seen that plugging the resulting μ and σ in the population receptor function we recover $\eta\left(\ln \mathrm{r}_0, \sigma \to 0, h, \frac{k_4^{\chi}}{K_2^{\chi}}\right) = \frac{\mathrm{r}_0}{\tau}$ and thus the single-cell dose differential is indeed a limiting case of the population dose differential. Analogously, it can be shown that the population double dose-edge dose differential reduces to the corresponding single-cell dose differential.

6.2.4 Bayesian Parameter Inference and Model Comparison

To apply Bayesian parameter inference and model comparison, as introduced in Chapter 2, we need to define the data of interest, the likelihood function, and the prior knowledge about the interferon system.

6.2.4.1 Data

Receptor-ligand interaction rate constants. In the presented TCS submodels we incorporate experimentally obtained kinetic constants for ligand-receptor interactions taken from Gavutis et al. (2006) and Jaks et al. (2007). The specific values and units of the constants can be found in Table 6.1.

Cell-to-cell variation of IFNAR2 receptor numbers. We parametrise the log-normally distributed random variable R_0 with an empirical IFNAR2 distribution for a population of unstimulated cells taken from Levin et al. (2011).

The raw distribution data originates from FACS measurements which we transform to receptor number per cell (number/cell). To do that we use the formula $\mathrm{r}_0 = \frac{f}{F}$, where f denotes the measured florescence and F is the florescence corresponding to a single receptor. We set $F = 7$ under the assumption that there are on average around 500 IFNAR2 receptor subunits per cell in WISH cells (Piehler et al., 2012).

Receptors can also be regarded in terms of concentration (e.g. nM) or density (e.g. number/m^2) but it has been established for most purposes to express them in

Table 6.1: Experimentally measured association and dissociation rate constants for IFNα2 and IFNβ binding to IFNAR1 (2D binding on the cell surface of IFNAR2-L to IFNAR1) and IFNAR2 (3D binding of L to IFNAR2) from Gavutis et al. (2006) and Jaks et al. (2007). Descriptions of the rate constants can be found in Section 8.4.1 from the appendix and also in the master model from Figure 6.1. Note that we consider these parameters as fixed and do not account for their variation.

Parameter	χ		Units	Description
	α	β		
$r_1^\chi = r_3^\chi$	0.003	0.01	$\frac{1}{nM\ s}$	3D association rate constant for the binding of L to IFNAR2
$r_2^\chi = r_4^\chi$	0.015	0.001	$\frac{1}{s}$	dissociation rate constant of L-IFNAR2
r_5^χ	16.5	16.5	$\frac{m^2}{nmol\ s}$	2D association rate constant for the binding of L-IFNAR2 to IFNAR1
r_6^χ	0.4	0.01	$\frac{1}{s}$	dissociation rate constant of L-IFNAR2-IFNAR1

number/cell as a positive continuous quantity (Lauffenburger & Linderman, 1993). For our purpose the number of active receptors is relevant since it determines the strength of downstream signalling. The experimental data is best fitted to a log-normal distribution with a location parameter $\mu = 6.18$ and a scale parameter $\sigma = 0.42$.

Dose-response curves. We use population-level antiviral and antiproliferative dose-response data in WISH cells resulting from IFNα and IFNβ treatment taken from Jaitin et al. (2006). The data comprise four dose-response datasets corresponding to the four ligand-activity conditions – αAV, βAV, αAP, βAP. The interferon dose in each of them is measured in nM and the response is measured in arbitrary units of cell density proportional to the number of living cells. We normalise the data such that when no cells are alive the response is 0 and when all cells are alive the response is 1, and intermediate responses correspond to a proportion of alive cells. During the normalisation special attention is given to the AP dose-response curves since only about 60% of the cells are able to respond to high interferon concentration and trigger antiproliferative response (Levin et al., 2011). For a given interferon dose each of the four datasets provides a mean response and standard deviation calculated from six independent experiments. Thus to reverse engineer the individual experimental outcomes we took six random samples from a normal distribution parametrised by the corresponding aggregate data. Additionally, we assume that there are $\widehat{n} = 2500$ cells in each experiment (Marijanovic et al., 2007). From the normalised proportions of alive cells and total number of cells we obtain the number of alive cells in each

of experiment, which we express in the form:

$$\widehat{Z}^{\chi\omega} = \left\{ \left(\widehat{d}_i^{\chi\omega}, \widehat{z}_i^{\chi\omega} \right) \right\}_{i=1}^{m^{\chi\omega}},$$

where $\widehat{z}_i^{\chi\omega}$ is the number of alive cells in a single experiment corresponding to the dose $\widehat{d}_1^{\chi\omega}$ when ligand χ was used and activity ω was measured. There are $m^{\chi\omega}$ measurements in total per ligand type and activity. By $\widehat{Z} = \{\widehat{Z}^{\alpha AV}, \widehat{Z}^{\beta AV}, \widehat{Z}^{\alpha AP}, \widehat{Z}^{\beta AP}\}$ we denote the dose-response data across the two ligand types and two activities.

6.2.4.2 Likelihood function

Recall that we model the number of alive cells in a population under specific ligand and activity conditions with the binomial random variable $Z^{\chi\omega}$. Then the probability to obtain $\widehat{z}^{\chi,\omega}$ alive cells in a population of $\widehat{n}$ cells for AV and AP activities is given by:

$$\Pr\left(Z^{\chi AV} = \widehat{z}_i^{\chi AV} \mid \mu, \sigma, \tau^{AV}, K^{\chi AV}, \widehat{d}_i^{\chi AV}, O, \widehat{n} \right) =$$
$$\binom{\widehat{n}}{\widehat{z}_i^{\chi AV}} \left(1 - \Phi\left(\frac{\ln \frac{\tau^{AV}}{\rho_O(\widehat{d}_i^{\chi AV}, K^{\chi AV})} - \mu}{\sigma} \right) \right)^{\widehat{z}_i^{\chi AV}} \Phi\left(\frac{\ln \frac{\tau^{AV}}{\rho_O(\widehat{d}_i^{\chi AV}, K^{\chi AV})} - \mu}{\sigma} \right)^{\widehat{n} - \widehat{z}_i^{\chi AV}},$$

$$\Pr\left(Z^{\chi AP} = \widehat{z}_i^{\chi AP} \mid \mu, \sigma, \tau^{AP}, K^{\chi AP}, \widehat{d}_i^{\chi AP}, O, \widehat{n} \right) =$$
$$\binom{\widehat{n}}{\widehat{z}_i^{\chi AP}} \Phi\left(\frac{\ln \frac{\tau^{AP}}{\rho_O(\widehat{d}_i^{\chi AP}, K^{\chi AP})} - \mu}{\sigma} \right)^{\widehat{z}_i^{\chi AP}} \left(1 - \Phi\left(\frac{\ln \frac{\tau^{AP}}{\rho_O(\widehat{d}_i^{\chi AP}, K^{\chi AP})} - \mu}{\sigma} \right) \right)^{\widehat{n} - \widehat{z}_i^{\chi AP}}.$$

We assume that the individual measurements for the same and different ligand doses, ligand types, and activities are independent and identically distributed. The likelihood of the dose-response data $\widehat{Z}$ for a given model can then be written as:

$$L(\theta) = \Pr(\widehat{Z} \mid \theta, \theta') =$$
$$\prod_{\omega \in \{AV, AP\}} \prod_{\chi \in \{\alpha, \beta\}} \prod_{i=1}^{m^{\chi\omega}} \Pr\left(Z^{\chi,\omega} = \widehat{z}_i^{\chi,\omega} \mid \mu, \sigma, \tau^{\omega}, K^{\chi\omega}, \widehat{d}_i^{\chi\omega}, O, \widehat{n} \right),$$

where $L(.)$ is the likelihood function, θ' is the set of fixed parameters – μ,σ,O,$\widehat{n}$, and the reaction rate constants taking part in the dose response coefficients K which are shown in Table 6.1, and $\theta \in \Omega$ is the set of free parameters over the continuous parameter space Ω consisting of activity dependent thresholds and the unknown reaction rate constants from $K^{\chi\omega}$ listed in Table 8.4 in Section 8.4.3

from the appendix.

The binomial coefficients in the likelihood function can be safely discarded since they are constant and do not alter the parameter inference and model comparison problems. We also, by convention, work with the negative log likelihood during the inference and comparison process.

Likelihood regularisation. The dose-response measurements normalized to the interval $[0, 1]$ do not represent genuine proportion data. Measurement errors and unaccounted-for variation in the total number of cells $\widehat{n}$ among experiments give rise to too big variation of measurements close to the proportions 0 and 1. Thus the available data does not fully exhibit the expected for proportion data heteroscedasticity originating from ceiling and floor effects. This observation has to be reckoned with since the developed model is by nature heteroscedastic and thus "stiff" close to the floor 0 and ceiling 1 proportions. Not accounting for this effect could lead to biased inference and numerical artefacts.

To aid the inference process we regularise the ligand and activity dependent functions $F(d) = \Phi\left(\frac{\ln \frac{\tau}{\rho_O(d;K)} - \mu}{\sigma}\right)$ comprising the likelihood. More precisely, we introduce an unknown parameter γ which decides how to scale $F(d)$ to obtain $\overline{F(d)}$, such that optimal floor and ceiling values with regards to the available data are chosen:

$$\overline{F(d)} = \gamma + (1 - 2\gamma)F(d),$$

where the parameter γ is to be estimated together with all other free parameters. Having completed the inference process we regard the estimated most probable new floor and ceiling values with regards to the data as corresponding to proportion 0 and 1. Thus we revert $\overline{F(d)}$ back to $F(d)$ in our models but scale the data as:

$$\overline{\widehat{z}_i^{\chi\omega}} = -\gamma + (1 + 2\gamma)\widehat{z}_i^{\chi\omega}.$$

This regularisation generates a data normalisation which mitigates the effect of data not being genuinely proportional. A consequence is that some data points have values below the proportion of 0 and above the proportion of 1.

6.2.4.3 Parameter and model priors.

We assume all models are equally probable prior to considering the experimental data. We regard each model's free parameters as log-uniformly distributed to express our ignorance about their order of magnitude. We incorporate available prior information to fix the minimum and maximum values, a and b, correspondingly, of some parameters and for the rest we set a wide interval of definition over several orders of magnitude as shown in Table 8.4, Section 8.4.3 from the appendix. Additionally, we work with $\log_{10}$ of the parameters and assume that their distributions are independent and identically distributed.

6.3 Results

6.3.1 Model Comparison

To rank the generated 290 models through Bayesian model comparison, as introduced in Chapter 2, we first identify the parameter point with the highest likelihood within each model's parameter space using the global optimization toolbox MEIGO (Egea et al., 2014), from which we initiate the exploration of the high-likelihood regions with HYPERSPACE (Zamora-Sillero et al., 2011) – a Matlab package to sample high-dimensional parameter spaces. As the threshold defining the high-likelihood regions we use the maximum likelihood of a model providing a poor fit to the data, and this value is orders of magnitude lower than the maximum likelihood achieved by the top ranking models. Having uniformly sampled the high likelihood regions of the parameter space we apply the estimator presented in Equation (2.7) to obtain an approximation of the evidence integral required for the calculation of Bayes factors and posterior model probabilities. The resulting ranking for the top 10 models is shown in Table 6.2.

The ranking from Table 6.2 reveals a top model with a TCS submodel (also see Figure 6.3) consisting of a cell surface component, an endocytosis component, and an inhibition component. The model contains 16 free parameters, and the inhibition and endocytosis components are the least detailed in their class hinting at the minimality of the model. More precisely, the inhibition component includes only the binding of USP18 to the cell surface R_2 and the endocytosis component does not have an inhibitory element. The cell-surface component is detailed indicating

Table 6.2: Ranking of the candidate models determined through Bayesian model comparison. The top 10 models out of the 290 models in the ensemble are shown, each with its specific TCS Laplacian submodel defined through its submodel components and signalling species, posterior probability, Bayes factor calculated with respect to the highest ranking model, and number of free parameters. The standard deviation of the estimator, as defined in Equation (2.8), is not shown since it is negligibly small and does not have an effect on the ranking, posterior model probabilities, and Bayes factors.

Rank	TCS submodel		Posterior	Bayes	No. free
	components	signalling species	probability	factor	params
1	S,I,E	TCp,R_2p,$TCpi$	approx. 1.0	–	16
2	S,I_1,E	TCp,R_2Lp,R_2p,$TCpi$	3.5e-43	97.7	16
3	S,E	TCp,R_2p,$TCpi$	8.6e-67	152.1	12
4	S,E	TCp,R_2Lp,R_2p,$TCpi$	2.7e-73	167.1	12
5	S,I_1,E	TCp,R_2p,$TCpi$	9.1e-92	209.6	16
6	S^ω,EI,$EIrS$	TCp,R_2p	2.3e-106	243.2	18
7	S,I,EI,$EIrI$	TCp,R_2p,$TCpi$	3.2e-108	247.5	18
8	S^ω,I_1,E	TCp,R_2p,$TCpi$	2.6e-117	268.4	17
9	S,EI,$EIrS$	TCp,R_2p,$TCpi$	1.9e-119	273.4	17
10	S^ω,E	TCp,R_2p	3.5e-121	277.3	13

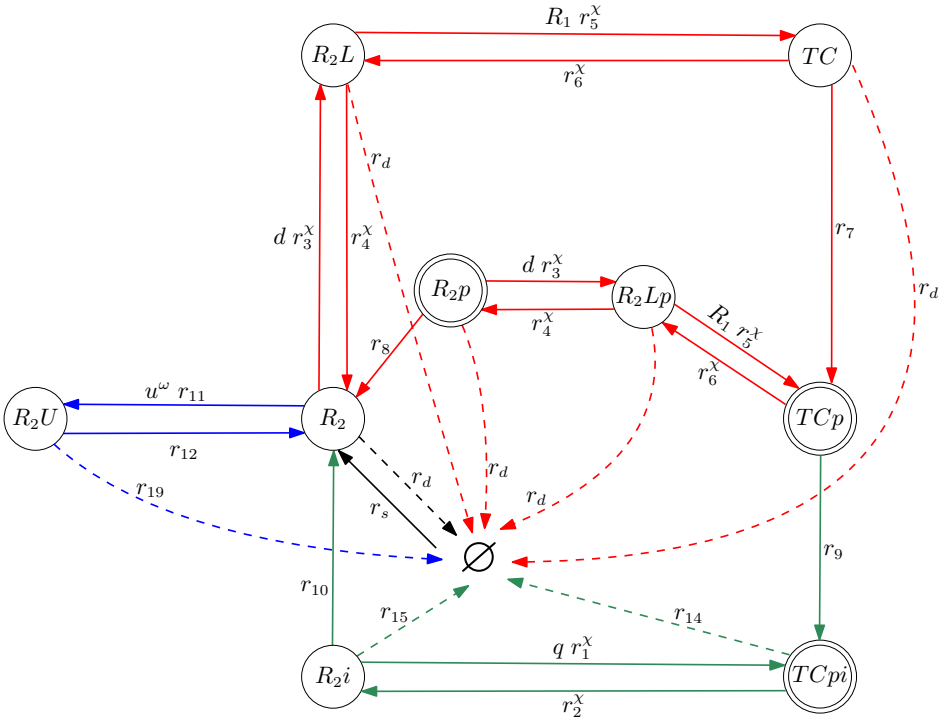

Figure 6.3: Reaction scheme of the differential TCS submodel belonging to the highest ranking model.

the importance of the different receptor assembly stages, but does not incorporate activity dependence of R_1. Thus, overall, the model complies with the hypothesis that receptor assembly, together with endocytosis, and USP18 inhibition are the minimal sufficient ingredients to reproduce the observed differential dose-response data (Schreiber & Piehler, 2015). Furthermore, signalling in the model happens through, both, species on the cell surface and within the endosomal compartment, pointing at the hypothesized importance of receptors signalling from the endosome (Schreiber & Piehler, 2015).

A striking result is the large posterior probability of the top ranking model of almost 1, especially in comparison to the low posterior probability of the second ranking model which is topologically similar and has the same number of free parameters. The greater topological complexity of the second model could be a reason for this discrepancy. Namely, its additional reactions in I_1 and more signalling species might make it more functionally constrained and thus having a smaller volume of its parameter space with high likelihood. However, caution has also to be given to the difficulty of approximating the high-dimensional evidence integral since the obtained two million samples might give a rough approximation.

The third and fourth ranking models present a curious result – they do not

incorporate an inhibitory component. Thus the only parameters differentiating between the AV and the AP activities are the threshold parameters τ^{AV} and τ^{AP}. These simple models contain only 12 free parameters, granting them high ranking through the Bayesian framework. However, although they feature a noteworthy differential mechanism explaining the experimental dose-response data, they would surely lead to inadequate results when additional data is incorporated, e.g. such showing that perturbations in USP18 greatly affect the differential (Francois-Newton et al., 2012).

6.3.2 Parameter Inference

To numerically obtain samples from the posterior and determine the posterior parameter distribution we employ DRAM – a Matlab toolbox implementing an adaptive Metropolis-Hastings MCMC algorithm with delayed rejection introduced in Haario et al. (2006). The efficiency of the DRAM algorithm has previously been shown on a variety of examples, and especially for high-dimensional posteriors with correlated components that we expect to see for our models with high parameter uncertainty.

We focus on the highest ranking model and obtain 20 million samples to reconstruct its posterior probability distribution. The resulting well mixed chains supply us with one dimensional marginal parameter distributions which can be seen in Figure 6.4, as well as, with two dimensional densities which are presented in Figure 6.5. From these results we see that the distributions for some parameters are peaked around a single value, while for others they are more spread out. Specifically, the threshold parameters τ^{AV} and τ^{AP} are peaked around the upper and lower boundary of their intervals of definition and thus correspond to the biologically feasible 10 and 100 receptors. The regularisation parameter γ is strongly peaked around the value 0.056 and indicates the small scaling needed to be incorporated to account for the non-proportionality properties of the dose-response data. The concentration of IFNAR1, R_1, is highly peaked around a value corresponding to approximately 80 thousand receptor units which is much more than the physiological expression of the receptor amounting to a couple of hundred units. We do not expect this parameter's value to have a strict interpretation since IFNAR1's variability and activity dependence are not explicitly incorporated in the model. It, however, shows that this omission does not have a strong effect on the minimal sufficient determinants of interferon differential signalling. Further, the low value of r_8 indicating slow dephosphorylation of R_2p presents an interesting observation worthwhile to be experimentally tested.

A hypothesis to explain the similar antiviral activity of interferons with vastly different receptor binding affinities is that the endocytosis rate, in our case r_9, should significantly exceed the IFNAR1 unbinding rate r_6^χ, so that the α vs β affinity difference cannot exert its differential effect (Schreiber & Piehler, 2015). We observe a similar effect between the irreversible phosphorylation of the ternary complex TC with reaction rate constant r_7 and the off-rate constant r_6^χ, namely $r_7 >> r_6^\chi$. However, we do not observe the same relation between the internalisation rate constant r_9 and r_6^χ but $r_6^\beta < r_7 < r_6^\alpha$. This does not reject the

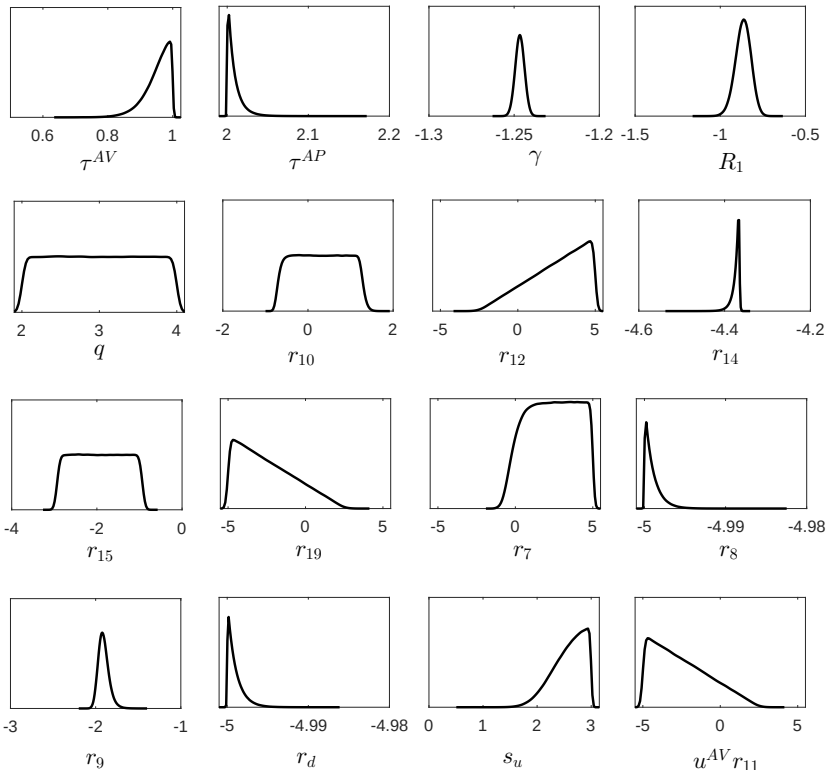

Figure 6.4: Marginal posterior probability densities for the 16 free parameters of the highest ranking model. Note that the posterior distributions are presented in log space but $\log_{10}$ was omitted in front of the parameters for visual clarity. The most probable values, distribution means, and standard deviations can be found in Table 8.5 from the appendix.

hypothesis for fast internalisation, but rather demonstrates that fast irreversible phosphorylation could also serve the purpose to decrease the differential for the AV activity.

The group of parameters q,r_{10}, and r_{15} shows high covariance (see Figure 6.5). It is composed by reactions outgoing from the species R_2i. Their uncertainty leads to lack of identifiability, which highlights them as candidates for experimental measurement. A second group of parameters, $u^{AV}r_{11}$,r_{12}, and r_{19} consisting of reactions incoming to and outgoing from the species R_2U also exhibits correlation and occupies a large high-posterior region. Their identification also requires subsequent experimental measurements. It is worth to note that $u^{AV}r_{11}$ has a small value as is expected for the AV activity time-scale when USP18's expression has not yet culminated, and $u^{AP}r_{11}$, expressed through the proportionality parameter s_u, is orders of magnitude higher hinting at the strong effect of UPS18

expression for the differential response. Finally, we note that the degradation of cell-surface species, with rate constant r_d, is slower than the degradation from the endocytic component (r_{14} and r_{15}) which is also biologically feasible.

The posterior parameter distribution was sampled to obtain a predictive envelope for the proportion of alive cells $\mathcal{R}^{\omega}(d)$ in a population when α and β ligands are employed and the responses are the AV and AP activities. The results are shown in Figure 6.6 and indicate that the top model successfully reproduces all features of the dose-response data with very little variation.

6.3.3 Symbolic Derivation of the Differential

The top ranking model has two dose edges and thus its population-level differential response can be derived symbolically. Recalling the derivations from Section 8.4.2, we study the expressions of Kirchhoff polynomials that define the dependence of the population differential on the TCS submodel parameters. Namely, the expression isolating the effect of the TCS model on the population response differential

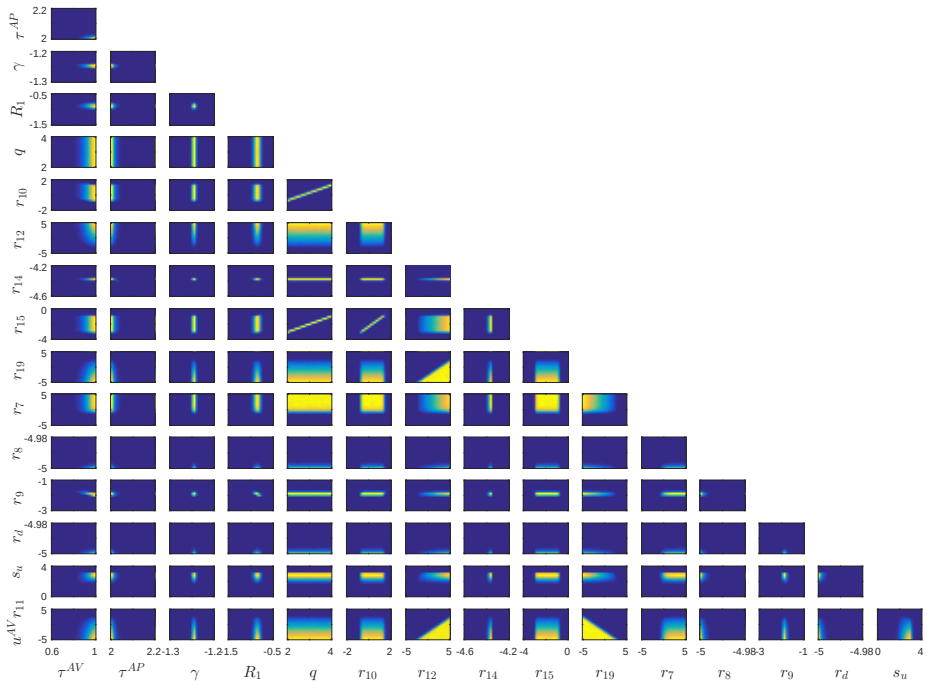

Figure 6.5: Two dimensional marginal posterior probability densities for the 16 free parameters of the highest ranking model. Note that the posterior distributions are presented in log space but $\log_{10}$ was omitted in front of the parameters for visual clarity. Low densities are represented by blue colour and high densities with yellow.

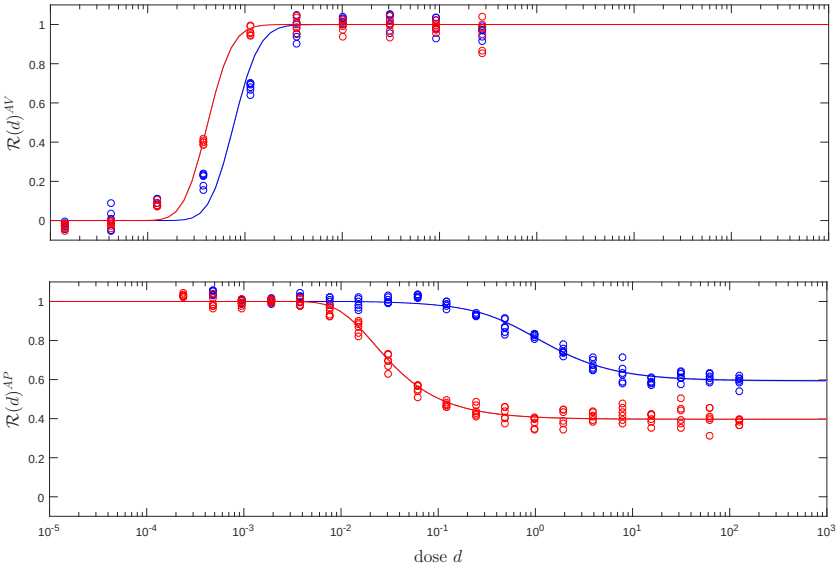

Figure 6.6: Predictive dose-response envelopes for the top ranking model contrasted to dose-response data from Jaitin et al. (2006). Results in the upper panel are for antiviral activity (AV) and in the lower panel for antiproliferative activity (AP). Red colour designates dose-response for IFNβ and blue for IFNα2. Circles represent samples from an experimentally determined aggregate dose-response data as introduced in Section 6.2.4.1, and solid curves represent predicted mean response. Note that the 95% posterior regions which indicate the prediction uncertainty are coloured in grey but are barely visible.

for the top model reads:

$$\frac{k_8^{\chi\omega}}{K_4^{\chi\omega}} = \frac{F_{K_8}^{\chi}}{F_{k_4}^{\chi} R_1 r_5^{\chi} r_7 r_d (R_1 r_5^{\chi} + r_d)},$$

where $F_{K_8}^{\chi\omega}$ and $F_{k_4}^{\chi\omega}$ are irreducible expressions which can be seen in Section 8.4.4. We see that the parameters R_1, r_5^{χ}, r_7, and r_d, respectively denoting the concentration of IFNAR1, the 2D association rate constant for the binding between L-IFNAR2 and IFNAR1, the ternary complex phosphorylation rate, and the cell surface receptor degradation rate, are present as single factors in the expression and thereby perturbations in their values have potentially a strong effect on the response differential. Further, we determine that important parameters such as the interferon-IFNAR2 binding and unbinding rate constants r_3^{χ} and r_4^{χ}, the USP18 related reaction rate constants $u^{\omega} r_{11}$, r_{12}, and r_{19}, as well as, r_8, the irreversible dephosphorylation of $R_2 p$ are not present in the expression which implies that perturbing them does not affect the population response differential.

The effect of the TCS submodel on the population-level dose differential is

defined by the response differential expression which we already derived and the expression:

$$\frac{K_4^{\beta\omega}c^{\beta\omega}-k_8^{\beta\omega}}{K_4^{\alpha\omega}c^{\alpha\omega}-k_8^{\alpha\omega}}\frac{k_{67}^{\alpha\omega}-K_{23}^{\alpha\omega}c^{\alpha\omega}\pm\sqrt{(k_{67}^{\alpha\omega}-K_{23}^{\alpha\omega}c^{\alpha\omega})^2+4k_5^{\alpha\omega}(K_4^{\alpha\omega}c^{\alpha\omega}-k_8^{\alpha\omega})}}{k_{67}^{\beta\omega}-K_{23}^{\beta\omega}c^{\beta\omega}\pm\sqrt{(k_{67}^{\beta\omega}-K_{23}^{\beta\omega}c^{\beta\omega})^2+4k_5^{\beta\omega}(K_4^{\beta\omega}c^{\beta\omega}-k_8^{\beta\omega})}}=$$
$$\frac{r_3^{\beta}}{r_3^{\alpha}}\frac{\left(c^{\beta\omega}F_{k_4}^{\beta}R_1r_5^{\beta}r_7r_d(R_1r_5^{\beta}+r_d)-F_{K_8}^{\beta}\right)}{\left(c^{\alpha\omega}F_{k_4}^{\alpha}R_1r_5^{\alpha}r_7r_d(R_1r_5^{\alpha}+r_d)-F_{K_8}^{\alpha}\right)}\cdot$$
$$\cdot\frac{F_{k_{67}}^{\alpha\omega}-c^{\alpha\omega}F_{K_{23}}^{\alpha}R_1(r_{12}+r_{19})r_5^{\alpha}r_7r_d\pm\sqrt{\begin{array}{r}\left(F_{k_{67}}^{\alpha\omega}-c^{\alpha\omega}F_{K_{23}}^{\alpha}R_1(r_{12}+r_{19})r_5^{\alpha}r_7r_d\right)^2+\\+4k_5^{\alpha\omega}(r_{12}+r_{19})\\\left(c^{\alpha\omega}F_{k_4}^{\alpha}R_1r_5^{\alpha}r_7r_d(R_1r_5^{\alpha}+r_d)-F_{K_8}^{\alpha}\right)\end{array}}}{F_{k_{67}}^{\beta\omega}-c^{\beta\omega}F_{K_{23}}^{\beta}R_1(r_{12}+r_{19})r_5^{\beta}r_7r_d\pm\sqrt{\begin{array}{r}\left(F_{k_{67}}^{\beta\omega}-c^{\beta\omega}F_{K_{23}}^{\beta}R_1(r_{12}+r_{19})r_5^{\beta}r_7r_d\right)^2+\\+4k_5^{\beta\omega}(r_{12}+r_{19})\\\left(c^{\beta\omega}F_{k_4}^{\beta}R_1r_5^{\beta}r_7r_d(R_1r_5^{\beta}+r_d)-F_{K_8}^{\beta}\right)\end{array}}},$$

where $k_5^{\chi\omega}$,$F_{K_{23}}^{\chi}$, and $F_{k_{67}}^{\chi\omega}$ are expressions defined in Section 8.4.4 in the appendix. It is evident that the values of the interferon-IFNAR2 binding reaction constant r_3^{χ} have a large effect on the differential since it is a multiplicative factor of the whole expression. However, the expression is more involved and depends on all model parameters. Thus it is not straightforward to understand the effects of individual parameters on the differential, such as the activity specific values of the USP18 inhibition rate constant $u^{\omega}r_{11}$ which should drive the larger differential in the AP activity.

6.4 Discussion

In this chapter we presented a modelling framework tailored to type I interferon signalling. It has the aim to identify the minimal sufficient combination of mechanisms reproducing experimental IFNα2 vs IFNβ population-level dose-response curves for antiviral and antiproliferative activities. The framework accounts for the uncertainty in the combinations of mechanisms capable of generating the observed differential by considering an ensemble of hypothetical models and ranking them through Bayesian model comparison. It further addresses the problem that many kinetic rate constants in interferon signalling are unknown by performing Bayesian parameter inference to quantify this inherent parameter uncertainty. Each model from the ensemble is a simple multi-scale model consisting of three parts whose importance in determining the differential response has been experimentally demonstrated. The first part concerns the different hypothetical controls of the active ternary complex stability and is thus the main distinction between the models from the ensemble. Said stability can be affected by interferon-induced

receptor assembly, receptor internalisation and recycling, as well as receptor inhibition mechanisms, and is modelled by a steady-state Laplacian system which determines the amount of signal propagated through the interferon pathway. The second part abstracts the downstream signalling cascade through an activity specific threshold in the number of active ternary complexes which renders a cell dead or alive. The third part accounts for the cell-to-cell variability of the number of IFNAR2 receptor subunits in a population of cells. It serves to extend the single-cell models to population-level models capable to relate interferon dose to the proportion of living cells in a population resulting from antiviral or antiproliferative interferon activity.

A particular strength of the resulting models is that an analytical formula for their likelihood functions can be derived, obviating the need to obtain approximations when applying Bayesian inference methods. Hence, we are able to rank the models using standard Bayesian model comparison and determine the ternary complex stability regulation hypothesis for which the data provides largest evidence. Our results indicate that there is a large evidence for the mechanisms of detailed cell-surface receptor assembly, simple endocytosis and recycling, and simple USP18 inhibition, with signalling originating from the cell surface and endosomal compartments, comprise the minimal sufficient combination of mechanisms able to explain the experimentally observed differential responses. This finding agrees with the state-of-the-art hypothesis of interferon differential signalling (Schreiber & Piehler, 2015). Still, in light of the difficulty of approximating the evidence integral required for the comparison, models with lower evidence should not be completely dismissed but ideally also analysed.

The availability of the likelihood function also facilitates Bayesian parameter inference. The parameter posterior distribution for the top ranking model pinpoints groups of unidentifiable free parameters, namely those associated to reactions containing the species R_2U and R_2i. It also provides an alternative to the hypothesis that fast ternary complex endocytosis equalizes the IFNα2 and IFNβ responses in antiviral signalling (Schreiber & Piehler, 2015), which is that fast irreversible phosphorylation of the ternary complex could serve the same purpose.

Additionally, the dose and response differential expressions explicating the relationship between system perturbations and the resulting relative difference between dose-response curves (as introduced in Chapter 5) can also be derived for the population models. Their population form is more complicated than that of their single-cell counterparts but is still amenable to symbolic analysis. Specifically, it reveals the effect of individual parameters on the dose differential, such as the large effect of the IFNAR2-interferon association constant, and which parameters might and which ones do not affect the response differential, thus generating candidate hypotheses for experimental validation.

Possible extensions of the current framework with the aim to obtain more quantitative understanding of differential signalling is to explicitly consider the cell-to-cell variability of IFNAR1 and the activity specific thresholds, and to incorporate the uncertainty of the fixed parameters. This would require the availability of adequate experimental data, complicate the analysis, and might not lead to significantly different insights, but could adjust the biologically infeasible values we

currently obtain for IFNAR1's steady-state concentration. Another possible extension is to increase the size of the model space by considering more ternary complex stability submodels. Note, however, that we generate all combinations of submodel components to define our submodel space which leads to a combinatorial explosion in the number of submodels, prompting that a different approach is necessary when accounting for more submodel components.

The dose-response data has a central role in the model comparison and parameter inference processes. The typical data, however, constitutes cell density measurements with only approximate knowledge on the total number of cells in each experiment. Thus the data cannot reliably be transformed into proportional as is required in our framework. This is not a major limitation since we regularise the likelihood to account for this effect but precise knowledge on the number of cells in each experiment could improve our inference procedure. Further, affinity and dose-response data for different natural and mutant interferon ligands could be used to test the predictability of the top ranking model.

The modelling framework offers qualitative understanding of the sufficient mechanisms giving rise to the observed differential activities, compare different model hypotheses, and connect receptor stability to population responses. However, to quantitatively understand the dynamics of the differential signalling phenomenon and to incorporate time-course data we need to build detailed dynamical models. The minimal model could serve as the backbone in the development of such models. It is important to note that the detailed dynamical models could achieve quantitative understanding on the single-cell level, however, their analysis would suffer from the lack of analytical tractability, more involved model comparison and parameter inference, as well as computationally expensive incorporation of cell heterogeneity.

6.5 Contributions and Acknowledgements

This chapter is based on the manuscript Yordanov et al. (2017) developed in collaboration between P. Yordanov (PY), I. Otero-Muras (IOM), and J. Stelling (JS). JS and IOM initiated the study. PY, IOM, and JS conceived the study. PY developed the theory and generated the results. JS and IOM supervised the study. PY wrote the manuscript.

We are grateful to the members of the EU FP7 project IFNAction for fruitful discussions.

7

Concluding Remarks and Outlook

This thesis introduced theory and methods to study the effect of perturbations on structure-function relationships in the domain of steady-state Laplacian models of biological systems. We approached this fundamental question from the viewpoint of algebraic graph theory and highlighted the deep connection between digraph connectivity and relative responses resulting from model perturbations. Importantly, we accounted for challenging properties of biological systems and data leading to heterogeneity, topological and parametric uncertainty, and complexity of the developed models, simultaneously keeping a grasp on their analytical tractability.

In Chapter 3 we laid the theoretical foundation for the rest of the chapters in the thesis by uncovering an important property of the main object of interest for the structure-function mapping in Laplacian models, namely prime factorisation of Kirchhoff polynomials. We exploited the strong connectivity and vertex domination concepts to propose an efficient decomposition algorithm taking as an input a digraph G and producing digraph components that are prime factors of the Kirchhoff polynomial corresponding to G. Due to the important role of Kirchhoff polynomials in a wide spectrum of scientific disciplines we believe that the prime factorisation algorithm would find applications also in other fields of science. Interestingly, we noticed that by reversing the decomposition rules to composition rules we can hierarchically construct digraphs with innumerable arborescences which can be factorised in linear time. We called the class of such digraphs – practically enumerable (PE) – but did not provide its characterisation. Thereby, a logical next step would be to study properties like information transmission on PE digraphs and determine if there are real-life networks with such or similar topology. Another sensible extension is to derive a similar factorisation relevant for the transient phase derivations of Laplacian models. However, it would involve working with cycles and paths on a phase graph in the sense of Chou (1993) which might require a different insight and set of theoretical tools.

In Chapter 4 we exploited the factorisation theory to devise methods to manipulate and generate expressions of Kirchhoff polynomials that dramatically ease the handling of larger and more complicated steady-state Laplacian models. We

derived criteria for Kirchhoff polynomial equality which allowed us to formulate a coarse-grained representation for an expression of Kirchhoff polynomials thereby making its simplification manageable by standard symbolic algebra tools. A weakness of the manipulation method is that it cannot, in general, certify that all digraphs with equal Kirchhoff polynomials have been identified since the developed criteria are not simultaneously necessary and sufficient. Thus, an important next step would be to find sufficient and necessary conditions for Kirchhoff polynomials equality. One such condition is Kirchhoff polynomial isomorphism which, to the best of our knowledge, is not developed for digraphs. Unfortunately, finding digraphs with isomorphic Kirchhoff polynomials appears to be a more complicated and computationally expensive problem than the already developed Kirchhoff polynomial isomorphism theory for undirected graphs, which is equivalent in complexity to the graph isomorphism problem (Bogner & Weinzierl, 2010; Raghavendra Rao & Jayalal Sarma, 2011). Regarding the explicit generation of Kirchhoff polynomials, we proposed two heuristic algorithms that perform sequential Kirchhoff polynomial simplification steps through the corresponding digraphs and output compressed Kirchhoff polynomials. The algorithm employing the change of variables technique works well in practice even for some of the largest Laplacian models of biological systems we found in literature having quadrillions of arborescences, namely the catalytic cycle of PGHS (Goltsov et al., 2010). Thus we explicitly demonstrated that connectivity properties, rather than the (super) exponentially growing number of arborescences, determine if Kirchhoff polynomials can be manipulated and generated. The generation algorithms can be further improved by accounting for digraph symmetry or by using more efficient connectivity-informed heuristics incorporating the recent developments in strong connectivity and 2-connectivity (Georgiadis et al., 2015c, 2017). Further, Kirchhoff polynomial isomorphism can also find application in the compressed generation of Kirchhoff polynomials by generating the polynomial for only one digraph in an isomorphism class and obtaining the rest of the Kirchhoff polynomials through a simple change of variables. However, the central questions of how to measure Kirchhoff polynomial compressibility, and more importantly, how to maximally compress Kirchhoff polynomials, remain open.

In Chapter 5, armed with the theory and methods devised by the previous chapters, we proceeded to formally define the notion of differential response as the difference between a reference and a perturbed dose-response curve, and investigate how it is affected by perturbations in steady-state Laplacian models. Besides, our definition of differential response accounts for non-sigmoid dose-response curves which are also frequently observed (Mattson & Calabrese, 2009). The developed theory is analytic. Thereby, it can determine the differential response capabilities of a given Laplacian model in the context of unknown parameters, solely from its topology. The main insight brought by the theory is that in steady-state Laplacian models prime digraph components and their relation to exerted perturbations are the determinants of the differential response. It is curious that reactions and species with important roles in a model, i.e. whose deletion significantly affects the differential, subsume the graph theoretical concepts of strong bridges and strong articulation points (Italiano et al., 2012). Thus we expect our

theory further to benefit from the algorithmic developments in graph theory and computer science. We demonstrated on a set of insulin signalling model examples how these structural insights allow us to deeply understand the effect of various perturbations, explore the space of possible model topologies, reliably reject models whose differential responses do not comply with desired perturbations, and design perturbations of interest. An important limitation of the theory is that analytical power gets lost for models containing five or more dose edges due to analytical intractability of polynomials of fifth and higher degree. For that reason, developments for high number of dose edges have no alternative but to employ numerical methods. In this chapter we incorporated numerical methods for another reason – to bound the range of the differential. Bounding plays an important role to determine the possible differential magnitude when knowledge on the parameters, that is intervals of definition, is available. Reliable bounding of multivariate rational functions is difficult, but fortunately methods like those based on Bernstein polynomials (Titi et al., 2015) are efficient and currently under active research. A natural extension of the theory is to study the differential response in cascades of steady-state Laplacian models. Perturbation of cascades is of profound importance to cell signalling and their analysis thorough the tools of Laplacian systems could reveal important insights into the roles of the different cascade layers.

Finally, in Chapter 6 we developed a modelling framework to elucidate the minimal sufficient combination of mechanisms that can explain experimental data on how "natural" perturbations, that is ligands with different affinities, trigger differential responses in the type I interferon signalling pathway. The framework serves as a testbed to study the topological and parameter uncertainty inherent to cell signalling by employing Bayesian model comparison and parameter inference. More precisely, it infers the parameters and compares different simple multiscale models incorporating a steady-state Laplacian model of interferon ternary complex stability, a threshold abstracting downstream signalling and subsequent life/death cell fates, and the population variation of the receptor IFNAR2. The primary difference between the resulting models is their ternary complex stability (TCS) submodels. We investigated 290 TCS submodels comprising different combinations of stability control mechanisms and signalling species for whose significance in differential signalling there is experimental evidence. Namely, the mechanisms are receptor assembly on the cell surface, receptor endocytosis and recycling, and receptor inhibition by the USP18 factor. Our results indicate that these three mechanisms along with signalling from the cell surface and the endosomal compartment are the minimal sufficient constituents capable to explain the dose-response data we used. A strong advantage of the framework, in comparison to other threshold models such as (Viswanathan et al., 2002), is that various mechanistic hypotheses constructed as steady-state Laplacian models can be tested benefiting from the theory and tools for model structure to function mapping developed in the previous chapters. More precisely, Laplacian models with undesired functional properties can be efficiently spotted solely on the basis of their topology and, consequently, unpromising submodels can be easily discarded. Another remarkable characteristic of the framework is that it accounts

for cell-to-cell-variability, and topological and parameter uncertainty, while at the same time preserves the analytical tractability of the differential response expressions and the likelihood function. This feature allows to understand in-depth how perturbations on single-cell level translate to differences in population response. Limitations of the present framework include all limitations of the differential Laplacian system such as the analytical intractability of systems with more than a small number of dose-edges. An additional limitation is the combinatorial explosion of possible TCS submodels since currently we consider all combinations of mechanisms. This problem can be remedied by assigning submodels to equivalence classes depending on their steady-state and differential expressions, and discarding impossible models on the basis of topological properties as previously mentioned. A paths for future development includes the investigation of how hormetic responses of single-cells translate to population activities. We would also like to emphasize the generality of the framework and its direct extensibility to other signalling pathways exhibiting threshold behaviour in the concentration of active receptor species.

In conclusion, we believe that the developed theory and analysis toolbox for Laplacian models would prove useful in the study of biological systems, especially in light of uncertainty and structure to function mapping under perturbations, and in applications to analytically investigate the core mechanisms behind complex biological processes.

8

Appendix

8.1 Supplement to Chapter 2

8.1.1 Omitted Proofs

8.1.1.1 Proofs from 3.2 Primality of Components

For a directed path $\mathcal{P}$ and vertices $x, y \in \mathcal{P}$ appearing on $\mathcal{P}$ in this order, we define a *slice* $\mathcal{P}[x : y]$ as the sub-path of P having x as a starting vertex and y as an ending vertex. Similarly, for a directed cycle $\mathcal{C}$ and $u, v \in \mathcal{C}$, we define a slice $\mathcal{C}[u : v]$ as the directed path from u to v using the edges of the cycle C.

Lemma 3.2.6. *Let G be a digraph as in Theorem 3.2.5. For any edge wu of G such that $u, w \neq v$, there exists a simple directed cycle $\mathcal{C}$ containing wu, such that $\mathcal{C}$ has at least two independent vertices, and w is one of those.*

Proof. Strong connectivity of $G \setminus \{v\}$ implies the existence of a simple directed path from u to w. This path and the edge wu form a directed cycle $\mathcal{C}'$ containing edge wu. By Menger's Theorem, there are two directed vertex-disjoint paths $\mathcal{P}_1, \mathcal{P}_2$ from the root v to vertex w. The paths are not necessarily disjoint with $\mathcal{C}'$. Let us denote, in reverse order on the cycle $\mathcal{C}'$, starting from w, all intersections $c_1, c_2, \ldots, c_k$ of $\mathcal{C}'$ with $\mathcal{P}_1$ or $\mathcal{P}_2$. Assume, without loss of generality, that $c_k \in \mathcal{P}_1$. We construct the cycle $\mathcal{C} = \mathcal{P}_1[c_k : w] \cup \mathcal{C}'[w : c_k]$. Observe that $\mathcal{P}_2$ is vertex-disjoint with $\mathcal{P}_1$, and with $\mathcal{C}'[w : c_k]$, since all intersections with $\mathcal{C}$ are between c_k and w. Thus, $\mathcal{P}_2$ is an independent path for w with respect to $\mathcal{C}$. Similarly, $\mathcal{P}_1[v : c_k]$ is an independent path for c_k with respect to $\mathcal{C}$. □

Lemma 3.2.7. *Let G be a digraph as in Theorem 3.2.5, and let V_1 and V_2 be an arbitrary (non-trivial) partition of the vertices $V \setminus \{v\}$. There exists a simple directed cycle having an independent vertex from V_1 and an independent vertex from V_2.*

Proof. Since $G \setminus \{v\}$ is strongly connected, there exists an edge wu with $u \in V_1$ and $w \in V_2$. By Lemma 3.2.6, there is a cycle $\mathcal{C}$ and a vertex x such that x and

w are independent from $\mathcal{C}$. Without loss of generality, we can assume that there are no independent vertices on $\mathcal{C}$ between w and x (as we can always pick x to be closer to w). If $x \in V_1$, C satisfies the statement of the Lemma and we are done. Assume therefore that $x \in V_2$ from now on.

Let $\mathcal{P}_1$ and $\mathcal{P}_2$ be the independent paths of w and x, respectively. Since w is not dominating u, there exists a v-u path $\mathcal{P}$ omitting w. We can assume that $\mathcal{P}$ intersects $\mathcal{C}$, as otherwise $\mathcal{P}$ is an independent path for u, and the Lemma follows. Moreover, $\mathcal{P}$ must intersect $\mathcal{C}[x : w]$, as otherwise the first intersection z of $\mathcal{P}$ with $\mathcal{C}$ is an independent vertex (with $\mathcal{P}[v : z]$ its independent path) that lies between w and x, a contradiction.

Let y be the last intersection of $\mathcal{P}$ with $\mathcal{C}[x : w]$. We show that after y, $\mathcal{P}$ does not intersect $\mathcal{P}_1$ nor $\mathcal{P}_2$. Assume for contradiction that $\mathcal{P}[y : u]$ intersects path $\mathcal{P}_1$ or $\mathcal{P}_2$, and let y' be the last such intersection. Let $\bar{u}$ be the first intersection of $\mathcal{P}[y' : u]$ with $\mathcal{C}$. Observe that $\bar{u}$ always exists (it is, at the latest, the vertex u), and that, by our definition of y and y', $\bar{u} \in \mathcal{C}[w : x] \setminus \{x\}$. Let $i \in \{1, 2\}$ be the index of the path such that $y' \in \mathcal{P}_i$. Observe that $\mathcal{P}_i[v : y'] \cup \mathcal{P}[y' : \bar{u}]$ is an independent path from $\mathcal{C}$ and thus $\bar{u}$ is an independent vertex between w and x (note that $\bar{u} \neq w$), a contradiction.

Let $s_0 = u, s_1, s_2, \ldots, s_k$ be all the intersection vertices of $\mathcal{P}[y : u]$ and $\mathcal{C}[w : x] \setminus \{w, x\}$. We now iteratively define the sequence $c_0, c_1, c_2, \ldots, c_{2d}$ as follows. We set $c_0 = u$ and $c_1 = s_1$. Then, for every $\ell = 1, 2, \ldots$, we do: If $s_k \in \mathcal{C}[w : c_{2\ell-1}]$, then we set $c_{2\ell} = s_k$ and terminate the creation of the sequence. Else, let s_i be the value of $c_{2\ell-1}$, and we set $c_{2\ell} = s_j$, where j is the largest $j \geq i$ such that $s_j \in \mathcal{C}[w : s_i]$. Note that it is possible that $c_{2\ell} = c_{2\ell-1}$. We also set $c_{2\ell+1} = s_j + 1$. Observe that $c_{2d} = s_k$. Now, one of the following two cases happen:

$c_{2d} \in V_1$**:** Consider a cycle $\mathcal{C}' = \mathcal{C}[c_{2d} : y] \cup \mathcal{P}[y : c_{2d}]$. Observe that $\mathcal{C}[w : c_{2d}] \cup \mathcal{P}_1$ is an independent path for c_{2d}, and $\mathcal{P}_2$ is an independent path for x (with respect to $\mathcal{C}'$), and the Lemma follows.

$c_{2i} \in V_2$ **and** $c_{2i-2} \in V_1$ **for some** i**:** Consider a cycle $\mathcal{C}'' = \mathcal{P}[c_{2i-1} : c_{2i-2}] \cup \mathcal{C}[c_{2i-2} : c_{2i-1}]$. Observe that $\mathcal{C}[w : c_{2i-2}] \cup \mathcal{P}_1$ is an independent path for c_{2i-2}, and $\mathcal{P}[c_{2i+1} : c_{2i}] \cup \mathcal{C}[c_{2i+2} : c_{2i+1}] \cup \mathcal{P}[c_{2i+3} : c_{2i+2}] \cup \ldots \cup \mathcal{C}[c_{2d} : c_{2d-1}] \cup \mathcal{P}[y : c_{2d}] \cup \mathcal{C}[x : y] \cup \mathcal{P}_2$ is an independent path for c_{2i} (with respect to $\mathcal{C}''$), and the Lemma follows.

□

Theorem 3.2.5. *Let G be a digraph rooted at v, such that $G[V(G) \setminus \{v\}]$ is strongly connected, and G has no non-trivial dominators. Then $\kappa(G)$ is prime.*

Proof. As in the proof of Theorem 3.2.4, assume that $\kappa(G) = P \cdot Q$, and P and Q are nontrivial factors. Let V_1 and V_2 be the set of vertices with incoming edges in $\mathrm{var}(P)$ and $\mathrm{var}(Q)$, respectively. Due to Lemma 3.2.3, V_1 and V_2 define a partition of $V \setminus \{v\}$.

Let us choose $\mathcal{C}$ and two vertices x, y according to the statement of Lemma 3.2.7, with $\mathcal{P}_x$ being an independent path of a vertex $x \in V_1$, and $\mathcal{P}_y$ being an indepen-

dent path of a vertex $y \in V_2$. Also, let e_x and e_y be the edges from $\mathcal{C}$ ending at x and y, respectively.

Thus, $(\mathcal{C} \setminus \{e_x\}) \cup \mathcal{P}_x$ is a simple path from v to x and there exists an arborescence A_x containing this path as a subdigraph. Respectively, there exists an arborescence A_y with path $(\mathcal{C} \setminus \{e_y\}) \cup \mathcal{P}_y$ as a subdigraph. Thus, the polynomial P has to contain a monomial corresponding to $A_x[V_1]$ and $A_y[V_1]$, and the polynomial Q has to contain a monomial corresponding to $A_x[V_2]$ and $A_y[V_2]$. Thus, there exists a monomial in the product of P and Q which corresponds to the set of edges $A = A_y[V_1] \cup A_x[V_2]$. However, $\mathcal{C} \subseteq A$, and that contradicts the definition of an arborescence, since A has to be acyclic. □

8.1.1.2 Proofs from 3.3 Decomposition

We start with the following two observations that relate the unrooted Kirchhoff polynomial $\kappa(G)$ and its rooted version $\kappa_v(G)$:

Proposition 8.1.1.

$$\kappa(G) = \sum_{v \in V} \kappa_v(G) \qquad \textit{and} \qquad \kappa_v(G) = \kappa(\mathsf{rt}_v(G)).$$

The next observation comes from the fact that in order to construct an arborescence in a digraph, it is necessary and sufficient to pick exactly one incoming edge for each vertex except the root.

Proposition 8.1.2. *For an arbitrary G, $v \in V(G)$, and $\{v_1, v_2, \ldots, v_{n-1}\} = V(G) \setminus \{v\}$:*

$$\kappa_v(G) = \sum_{\substack{e_1 \in in(v_1),\\ \ldots,\\ e_{n-1} \in in(v_{n-1})}} [\{e_1, \ldots, e_{n-1}\} \textit{ is acyclic}] \cdot \ell(e_1) \cdot \ldots \cdot \ell(e_{n-1}), \tag{8.1}$$

where [.] denotes the characteristic function.

Theorem 3.3.2. *Let $G[V_1], G[V_2], \ldots, G[V_k]$ be all strongly connected components of a connected digraph G. If G has exactly one initial component, then*

$$\kappa(G) = \kappa(\widehat{G[V_1]}) \cdot \kappa(\widehat{G[V_2]}) \cdot \ldots \cdot \kappa(\widehat{G[V_k]}). \tag{3.1}$$

Proof. W.l.o.g. we can assume that $G[V_1]$ is the only initial component of G. Thus $\kappa(G) = \sum_{v \in V_1} \kappa_v(G)$ and it is enough to show that for any $v \in V_1$:

$$\kappa_v(G) = \kappa_v(\widehat{G[V_1]}) \cdot \kappa(\widehat{G[V_2]}) \cdot \ldots \cdot \kappa(\widehat{G[V_k]}). \tag{8.2}$$

Let us set $V_i = \{v_1^i, v_2^i, \ldots, v_{n_i}^i\}$ for $i = 2, \ldots, k$ and $V_1 = \{v_1^1, v_2^1, \ldots, v_{n_1-1}^1\} \cup \{v\}$. Additionally, we denote by u_i the auxiliary vertex of $\widehat{G[V_i]}$ (for $i = 2, \ldots, k$).

Observe that for $i = 2, \ldots, k$ each $\widehat{G[V_i]}$ is rooted at u_i. Thus we can rewrite the right side of Equation (8.2) as:[1]

$$\begin{aligned}
&\kappa_v(\widehat{G[V_1]}) \cdot \kappa(\widehat{G[V_2]}) \cdot \ldots \cdot \kappa(\widehat{G[V_k]}) = \\
&= \kappa_v(\widehat{G[V_1]}) \cdot \kappa_{u_2}(\widehat{G[V_2]}) \cdot \ldots \cdot \kappa_{u_k}(\widehat{G[V_k]}) \overset{\text{Prop. 8.1.2}}{=} \\
&= \left(\sum_{\substack{e_1^1 \in \mathrm{in}(v_1^1), \\ \ldots, \\ e_{n_1-1}^1 \in \mathrm{in}(v_{n_1-1}^1)}} [\{e_1^1, \ldots, e_{n_1-1}^1\} \text{ is acyclic}] \cdot \ell(e_1^1) \cdot \ldots \cdot \ell(e_{n_1-1}^1) \right) \cdot \\
&\cdot \left(\sum_{\substack{e_1^2 \in \mathrm{in}(v_1^2), \\ \ldots, \\ e_{n_2}^2 \in \mathrm{in}(v_{n_2}^2)}} [\{e_1^2, \ldots, e_{n_2}^2\} \text{ is acyclic}] \cdot \ell(e_1^2) \cdot \ldots \cdot \ell(e_{n_2}^2) \right) \cdot \ldots \\
&\ldots \cdot \left(\sum_{\substack{e_1^k \in \mathrm{in}(v_1^k), \\ \ldots, \\ e_{n_k}^k \in \mathrm{in}(v_{n_k}^k)}} [\{e_1^k, \ldots, e_{n_k}^k\} \text{ is acyclic}] \cdot \ell(e_1^k) \cdot \ldots \cdot \ell(e_{n_k}^k) \right) = \\
&= \sum_{\substack{e_1^1 \in \mathrm{in}(v_1^1), \\ \ldots, \\ e_{n_1-1}^1 \in \mathrm{in}(v_{n_1-1}^1)}} \ldots \sum_{\substack{e_1^k \in \mathrm{in}(v_1^k), \\ \ldots, \\ e_{n_k}^k \in \mathrm{in}(v_{n_k}^k)}} \Big([\{e_1^1, \ldots, e_{n_1-1}^1\} \text{ is acyclic}] \cdot \ldots \cdot [\{e_1^k, \ldots, e_{n_k}^k\} \text{ is acyclic}] \cdot \\
&\qquad \cdot \big(\ell(e_1^1) \cdot \ldots \cdot \ell(e_{n_1-1}^1)\big) \cdot \ldots \cdot \big(\ell(e_1^k) \cdot \ldots \cdot \ell(e_{i_k}^k)\big) \Big). \quad (8.3)
\end{aligned}$$

Since $\{v_1, v_2, \ldots, v_{n-1}\} = V(G) \setminus \{v\} = (V_1 \setminus \{v\}) \cup V_2 \cup \ldots \cup V_k = \{v_1^1, \ldots, v_{n_1-1}^1, \ldots, v_1^k, \ldots, v_{n_k}^k\}$, both Equation (8.1) and Equation (8.3) are summing over the same ranges (in a permuted order). Thus it is enough to prove that

$$\{e_1, \ldots, e_{n-1}\} \text{ is acyclic in } G$$
$$\text{iff}$$
$$\Big(\{e_1^1, \ldots, e_{n_1-1}^1\} \text{ is acyclic in } G[V_1]\Big) \text{ and } \Big(\{e_1^k, \ldots, e_{n_k}^k\} \text{ is acyclic in } G[V_k]\Big),$$

[1] For any $x \in V_i$, $\widehat{G[V_i]}$ preserves the labels of its incoming edges from the rest of G, thus we can safely write $\mathrm{in}(x)$ without explicitly specifying the digraph.

where $\{e_1^1, \ldots, e_{n_1-1}^1\}, \ldots, \{e_1^k, \ldots, e_{n_k}^k\}$ is the partitioning of $\{e_1, e_2, \ldots, e_{n-1}\}$ by the strongly connected component to which the target vertex belongs. However, it is enough to notice that any cycle in G can only span vertices from a single strongly connected component. □

Theorem 3.3.3. *Let G be a digraph rooted at v and let u be an arbitrarily picked vertex of G. Denote $D = \mathsf{dom}_G(u)$. Then*

$$\kappa(G) = \kappa(\mathsf{rt}_u(G[D])) \cdot \kappa(G(D \to u)). \tag{3.2}$$

Proof. Observe that (3.2) is equivalent to:

$$\kappa_v(G) = \kappa_u(G[D]) \cdot \kappa_v(G(D \to u)).$$

Let us denote $D \setminus \{u\} = \{v_1, v_2, \ldots, v_{i-1}\}$, and let $V \setminus D \setminus \{v\} = \{v_{i+1}, \ldots, v_{n-1}\}$. Thus, $V = \{v_1, \ldots, v_{i-1}, u, v_{i+1}, \ldots, v_{n-1}, v\}$.

Observe, that in G there are no edges going from any vertex from $V \setminus D$ to any vertex from $D \setminus \{u\}$, as otherwise u would not dominate said vertices. If we denote for short $\mathrm{in}_1(u) = \mathrm{in}_G(u)$ (all incoming edges to u) and $\mathrm{in}_2(u) = \mathrm{in}_{G(D \to u)}(u)$ (edges incoming from $V \setminus D$), we have that $\mathrm{in}_2(u) \subseteq \mathrm{in}_1(u)$. Thus:

$$\kappa_v(G(D \to u)) = \sum_{e_i \in \mathrm{in}_2(u)} \sum_{\substack{e_{i+1} \in \mathrm{in}(v_{i+1}), \\ \ldots, \\ e_{n-1} \in \mathrm{in}(v_{n-1})}} [\{e_i, \ldots, e_{n-1}\} \text{ is acyclic}] \cdot \ell(e_i) \ldots \ell(e_{n-1}).$$

Observe that any arborescence of G rooted at v cannot use an edge from $\mathrm{in}_1(u) \setminus \mathrm{in}_2(u)$, as that would create disconnected digraph (as any path going from v to D has to go through u). Thus:

$$\kappa_v(G) = \sum_{\substack{e_1 \in \mathrm{in}(v_1), \\ \ldots, \\ e_{i-1} \in \mathrm{in}(v_{i-1})}} \sum_{e_i \in \mathrm{in}_2(u)} \sum_{\substack{e_{i+1} \in \mathrm{in}(v_{i+1}) \\ \ldots, \\ e_{n-1} \in \mathrm{in}(v_{n-1})}} [\{e_1, \ldots, e_{n-1}\} \text{ is acyclic}] \cdot \ell(e_1) \ldots \ell(e_{n-1}).$$

Additionally, in $G[D]$, all vertices from $D \setminus \{u\}$ have the same incoming edges as in G (as taking induced subdigraph removes edges coming from outside, but there were no such edges). Thus by Proposition 8.1.2:

$$\kappa_u(G[D]) = \sum_{\substack{e_1 \in \mathrm{in}(v_1), \\ \ldots \\ e_{i-1} \in \mathrm{in}(v_{i-1})}} [\{e_1, \ldots, e_{i-1}\} \text{ is acyclic}] \cdot \ell(e_1) \cdot \ldots \cdot \ell(e_{i-1}).$$

Thus, it is enough to prove that, for $e_i \in \mathrm{in}_2(u), e_1 \in \mathrm{in}(v_1), \ldots, e_{i-1} \in$

$\mathrm{in}(v_{i-1}), e_{i+1} \in \mathrm{in}(v_{i+1}), \ldots, e_{n-1} \in \mathrm{in}(v_{n-1})$:

$$\{e_1, \ldots, e_{n-1}\} \text{ is acyclic in } G$$
$$\text{iff}$$
$$\Big(\{e_1, \ldots, e_{i-1}\} \text{ is acyclic in } \mathsf{rt}_u(G[D])\Big)$$
$$\text{and}$$
$$\Big(\{e_i, \ldots, e_{n-1}\} \text{ is acyclic in } G(D \to u)\Big).$$

To prove it in one direction, observe that any cycle in $G[D]$ remains a cycle in G. Similarly, any cycle in $G(D \to u)$ remains a cycle in G. To prove it in the other direction, observe that any cycle in G (with constrains on $e_i \in \mathrm{in}_2(u)$) either spans vertices only from $D \setminus \{u\}$ thus remains a cycle in $G[D]$, or spans at least one vertex from $G \setminus (D \setminus \{u\})$. In the latter case, the digraph remains cyclic when contracting whole D into u. □

Theorem 3.3.5. *If G is rooted at v, then any H being a factor obtained by the application of rule* (3.3) *has the following property: all factors of H obtained by applying* (3.1) *are prime.*

Proof. Let H be a digraph obtained through the application of rule (3.3), that is

$$H = \mathsf{rt}_u\Big(G(\mathsf{dom}_G(u_1) \to u_1; \ldots; \mathsf{dom}_G(u_i) \to u_i)[\{u, u_1, \ldots, u_i\}]\Big).$$

First, observe that in digraph $F = \mathsf{rt}_u(G[\mathsf{dom}_G(u)])$ the domination relation between vertices (with respect to vertex u) is the same as is in G (with respect to vertex v). Thus, as we have that

$$H = F(\mathsf{dom}_G(u_1) \to u_1; \ldots; \mathsf{dom}_G(u_i) \to u_i),$$

there are no non-trivial dominance relations in H.

What is now left to prove is that for any strongly connected component $V_j \neq \{u\}$ of H, the digraph $\widehat{H[V_j]}$ has no non-trivial dominators (with respect to v_{aux}, its root). However, for any vertex $w \in V_j$ and for any path going from u to w in H, there is a path from v_{aux} to w in $\widehat{H[V_j]}$ corresponding to the suffix of the former one. Thus, if there is any vertex w' dominating (non-trivially) w in $\widehat{H[V_j]}$, then w' dominates (non-trivially) w in H, a contradiction. □

8.1.2 Pseudocode for the Prime Decomposition Algorithm

The pseudocode of the prime decomposition algorithm through SCCs and dominator relations is presented in Algorithm 1.

Algorithm 1 Digraph decomposition corresponding to Kirchhoff polynomial prime factorization.

```
 1: function SCCFactors(G)
 2:     Factors ← []
 3:     for all S ∈ SCCs(G) do                          ▷ strongly connected components
 4:         H ← G[S]                                    ▷ induced component
 5:         if ∃vu ∈ E(G) : v ∉ S ∧ u ∈ S then          ▷ non-initial SCC
 6:             H.addVertex(v_aux)
 7:             for all vu ∈ E(G) : v ∉ S ∧ u ∈ S do
 8:                 H.addEdge(v_aux u)
 9:             end for
10:         end if
11:         Factors.append(H)
12:     end for
13:     return Factors
14: end function
15:
16: function DominationFactors(G)
17:     if ¬isRooted(G) then                            ▷ G has to be rooted
18:         return [G]
19:     end if
20:     T ← DominatorTree(G, getRoot(G))
21:     Factors ← []
22:     H ← G                                           ▷ copy of G
23:     for u ∈ postorder(T) do
24:         S ← T.successors(u)
25:         Factors.append(MakeRooted(H[S ∪ {u}], u))
26:         H.contract(S, u)                            ▷ contract all of S into u
27:     end for
28:     return Factors
29: end function
30:
31: function GetPrimeDecomposition(G)
32:     Factors ← []
33:     for all G1 ∈ SCCFactors(G) do
34:         for all G2 ∈ DominationFactors(G1) do
35:             for all G3 ∈ SCCFactors(G2) do
36:                 Factors.append(G3)
37:             end for
38:         end for
39:     end for
40:     return Factors
41: end function
```

8.2 Supplement to Chapter 3

8.2.1 Omitted Proofs and Derivations

Theorem 4.2.1. *Let G be a prime digraph, then each edge in G participates in at least one arborescence.*

Proof. For this proof we consider out-arborescences.

The theorem statement is equivalent to the statement that there are no nuisance edge, or formally $\nexists e \in E(G)$ such that $\mathsf{arb}(G/e) = \emptyset$. Let $e = uv$ be such that $\mathsf{arb}(G/e) = \emptyset$ and let us investigate the two classes of prime digraphs:

- **G is strongly connected.**
  A digraph with no arborescences (G/e) from this class is either disconnected or has more than one initial SCC. Normal edge contraction, by itself, cannot disconnect a connected digraph or introduce a new initial SCC in a strongly connected G. However, edge contraction (w.r.t. out-arborescences) additionally deletes in-coming edges to v, which we call w_iv. Deleting w_iv cannot disconnect G since there exist paths from v to w_i (not including w_iv) due to strong connectivity. Deleting w_iv also cannot lead to more than one initial SCC but only new terminal SCCs (w_i could become part of a new terminal SCC when w_i connects back to v only through w_iv). Therefore, $\mathsf{arb}(G/e) \neq \emptyset$.

- **G is a digraph rooted at v_{aux}, such that $G[V(G) \setminus \{v_{aux}\}]$ is strongly connected and G has no non-trivial dominators.**
  Notice that the edges $v_{aux}u_i$, where $u_i \in V(G) \setminus \{v_{aux}\}$, always participate in at least one arborescence of G since there exists at least one arborescence A rooted at u_i in the strongly connected $G[V(G) \setminus \{v_{aux}\}]$ and, further, adding $v_{aux}u_i$ to A produces an arborescence of G. Also, notice that in this class of prime digraphs (apart from the trivial case when the digraph is a single edge) v_{aux} always connects to at least two different vertices, e.g. $u_1, u_2 \in V(G) \setminus \{v_{aux}\}$. If it connected to a single one, e.g. u_1, u_1 would dominate $V(G) \setminus \{v_{aux}, u_1\}$ and thus we have non-trivial domination.Therefore, e cannot be any of $v_{aux}u_i$. Thus let $e = uv$, $u, v \in V(G) \setminus \{v_{aux}\}$. Again, this means that contracting e either disconnects G or creates more than one initial SCC in it (currently the only one is v_{aux}). Edge contraction (w.r.t. out-arborescences) deletes in-coming edges to v, which we call w_iv. Deleting w_iv cannot disconnect G since there exists a path from v to w_i due to the strong connectivity of $G[V(G) \setminus \{v_{aux}\}]$ and if any w_i happens to be v_{aux} there exists an alternative path to v from v_{aux} due to the structure of this class prime digraphs. More precisely, v_{aux} connects to at least two vertices from $V(G) \setminus \{v_{aux}\}$ and if $u_1 = v$ then a path through $v_{aux}u_2$ to u_1 exists due to strong connectivity. Deleting w_iv also cannot create more than one initial SCC but only terminal SCCs. In $G[V(G) \setminus \{v_{aux}\}]$, as before, some or all of w_i could become part of new terminal SCCs when w_i connects back to v only through w_iv. When $v = u_i$

and $v_{aux}u_i$ is one of the edges deleted during the contraction there would still be a single initial SCC v_{aux}. Therefore, $\mathsf{arb}(G/e) \neq \emptyset$.

□

Theorem 4.2.6. *Two prime digraphs G and H are λ-isomorphic iff the edge sets of their line digraphs are equal, i.e. $G \simeq_\lambda H \Leftrightarrow E(\mathscr{L}(G)) = E(\mathscr{L}(H))$.*

Proof. The proof follows from Aigner (1967), Theorem 2, which states that there is a one-to-one correspondence between the set of all digraphs with at most one vertex of out-degree zero and at most one vertex of in-degree zero and no isolated vertices, and the set of all line digraphs. Prime digraphs are either strongly connected or have a single vertex of in-degree zero when considering out-arborescences (and a single vertex of out-degree zero for in-arborescences). Therefore, there is a one-to-one correspondence between prime digraphs and the set of all line digraphs. This means λ-isomorphic prime digraphs bijectively map to the same line digraph (defined by the set of its edges). □

Identity 4.2.8.

$$\frac{\partial\kappa(G)}{\partial\ell(e)} = \kappa(G/e).$$

Derivation.

$$\frac{\partial\kappa(G)}{\partial\ell(e)} = \frac{\partial}{\partial\ell(e)}(\kappa(G \setminus e) + \ell(e)\kappa(G/e)) =$$
$$= \frac{\partial}{\partial\ell(e)}\kappa(G \setminus e) + \frac{\partial}{\partial\ell(e)}(\ell(e)\kappa(G/e)) = \kappa(G/e).$$

□

Identity 4.2.10. *Let the prime factorisation of the Kirchhoff polynomials $\kappa(G)$ and $\kappa(H)$ be $\kappa(G) = \prod_{i=1}^{n}\kappa(P_i)$ and $\kappa(H) = \prod_{j=1}^{m}\kappa(Q_j)$, then:*

$$\frac{\partial}{\partial\ell(e)}\frac{\kappa(G)}{\kappa(H)} = \frac{\prod_{i=2}^{n}\kappa(P_i)}{\kappa(Q_1)^2\prod_{j=2}^{m}\kappa(Q_j)}\left(\kappa(P_1/e)\kappa(Q_1) - \kappa(P_1)\kappa(Q_1/e)\right),$$

where P_1 and Q_1 are the prime components of G and H, correspondingly, containing e.

Derivation.

$$\frac{\partial}{\partial e}\frac{\kappa(G)}{\kappa(H)} = \frac{\kappa(P_1/e)\prod_{i=2}^{n}\kappa(P_i)\prod_{j=1}^{m}\kappa(Q_j) - \kappa(Q_1/e)\prod_{i=1}^{n}\kappa(P_i)\prod_{j=2}^{m}\kappa(Q_j)}{[\prod_{j=1}^{m}\kappa(Q_j)]^2}$$
$$= \frac{\prod_{i=2}^{n}\kappa(P_i)\prod_{j=2}^{m}\kappa(Q_j)}{[\prod_{j=1}^{m}\kappa(Q_j)]^2}\left(\kappa(P_1/e)\kappa(Q_1) - \kappa(P_1)\kappa(Q_1/e)\right)$$
$$= \frac{\prod_{i=2}^{n}\kappa(P_i)}{\kappa(Q_1)^2\prod_{j=2}^{m}\kappa(Q_j)}\left(\kappa(P_1/e)\kappa(Q_1) - \kappa(P_1)\kappa(Q_1/e)\right).$$

□

Identity 4.2.11.

$$\int \kappa(G)d\ell(e) = \ell(e)\kappa(G^{\ell(e)\leftarrow\frac{\ell(e)}{2}}) + C,$$

where C is the integration constant and $\ell(e) \leftarrow \frac{\ell(e)}{2}$ denotes a relabelling operation replacing the label of e by the same label divided by two, e.g. if the old label was $\ell(e) = r_1$ the new would be $\ell(e) = \frac{r_1}{2}$.

Derivation.

$$\int \kappa(G)d\ell(e) = \int (\kappa(G \setminus e) + \ell(e)\kappa(G/e))d\ell(e) =$$

$$= \int \kappa(G \setminus e)d\ell(e) + \int \ell(e)\kappa(G/e)d\ell(e) =$$

$$= \ell(e)\kappa(G\setminus e)+C_1+\kappa(G/e)\int \ell(e)d\ell(e) = \ell(e)\kappa(G\setminus e)+C_1+\frac{\ell(e)^2}{2}\kappa(G/e)+C_2 =$$

$$= \ell(e)\left(\kappa(G \setminus e) + \frac{\ell(e)}{2}\kappa(G/e)\right) + C_1 + C_2 = \ell(e)\kappa(G^{\ell(e)\leftarrow\frac{\ell(e)}{2}}) + C.$$

□

8.2.2 Pseudocode for the Kirchhoff Polynomial Generation Algorithms

Algorithm 2 Recursive compressed generation of Kirchhoff polynomials through prime decomposition and edge deletion-contraction.

```
1: function C_R(G)
2:     if κ(G) == 0 then
3:         return 0
4:     end if
5:     if |V(G)| ≤ 2 then
6:         return GenKirchPolBaseCase(G)
7:     end if
8:     F ← []
9:     for all primeComponent ∈ GetPrimeDecomposition(G) do
10:        H ← GenKirchPolInPrimeComponent(primeComponent)
11:        F.append(H)
12:    end for
13:    return Multiply(F)                          ▷ n-ary multiplication
14: end function
15:
16: function GenKirchPolInPrimeComponent(G)
17:    if |V(G)| ≤ 2 then
18:        return GenKirchPolBaseCase(G)
19:    end if
20:    e ← GetEdgeForDelContr(G)
21:    kirchPolEdgeDelDigraph ← C_R(G \ e)
22:    kirchPolEdge ← GenKirchPolBaseCase(e)
23:    kirchPolEdgeContrDigraph ← C_R(G/e)
24:    return Add(kirchPolEdgeDelDigraph,
                  Multiply(kirchPolEdge, kirchPolEdgeContrDigraph))
25: end function
26:
27: function GenKirchPolBaseCase(G)
28:    if κ(G) == 0 then
29:        return 0
30:    end if
31:    if |V(G)| == 1 then
32:        return 1
33:    end if
34:    F ← []
35:    for all e ∈ E(G) do
36:        F.append(ℓ(e))
37:    end for
38:    return Add(F)                               ▷ n-ary addition
39: end function
```

Algorithm 3 Iterative compressed generation of Kirchhoff polynomials through prime decomposition, edge deletion-contraction, and change of variables.

```
1: function C_I(G)
2:     G.POINTER ← startPointer                ▷ every digraph has a unique pointer
3:     (P, R) ← GENIMPLICITKIRCHPOL(G)
4:     Q ← QUEUE()
5:     Q.ENQUEUE(startPointer)
6:     result ← []
7:     while Q not empty do
8:         currPointer ← Q.DEQUEUE()
9:         currExpr ← R.RETRIEVEEXPRESSION(currPointer)        ▷ currExpr is an
   expression tree
10:        result.APPEND((currPointer, ASSEMBLE(P, R, Q, currExpr))) ▷ pass Q by
   reference
11:    end while
12:    return result
13: end function
14:
15: function ASSEMBLE(P,R, Q, currExpr)
16:    if currExpr is MULTIPLY or ADD then
17:        newChildren ← []
18:        for all childExpr ∈ currExpr.CHILDREN do
19:            newChildren.APPEND(ASSEMBLE(P, R, Q, childExpr))
20:        end for
21:        currExpr.CHILDREN ← newChildren
22:    else if currExpr is a POINTER then
23:        if ∃i : currExpr == P_{i,0}.POINTER then
24:            Q.ENQUEUE(currExpr)
25:        else if ∃p and j : p ∈ P_{j,1} and currExpr == p then
26:            currExpr ← P_{j,0}.POINTER
27:        else
28:            newExpr ← R.RETRIEVEEXPRESSION(currExpr)
29:            return ASSEMBLE(P,R, Q, newExpr)
30:        end if
31:    end if
32:    return currExpr
33: end function
```

Algorithm 3 Continued.

```
34: function GenImplicitKirchPol(G)
35:     Q ← Queue()
36:     Q.enqueue(G)
37:     (P, R) ← ([], [])    ▷ P remembers already processed digraphs and R holds the results
38:     while Q not empty do
39:         H ← Q.dequeue()
40:         primeComps ← GetPrimeDecomposition(H)
41:         if H not prime OR κ(H) == 0 OR κ(H) == 1 then
42:             pointers ← GetPointers(primeComps)    ▷ list of primeComps's pointers; returns 0 or 1 if κ(H) == 0 or κ(H) == 1, respectively; calls base case labelsum
43:             expr ← Multiply(pointers)
44:             R.append((H.pointer, expr))
45:         end if
46:         if κ(H) ≠ 0 AND κ(H) ≠ 1 then
47:             for all D ∈ primeComponents do
48:                 if |V(D)| ≤ 2 then                                    ▷ base case
49:                     R.append((D.pointer, GenKirchPolBaseCase(D)))
50:                 else
51:                     if ∃ i: EQL(D,P_{i,0}) then    ▷ EQL() tests Kirchhoff polynomial equality
52:                         P_{i,1}.append(D.pointer)
53:                     else                                    ▷ digraph not investigated yet
54:                         P.append((D, []))
55:                         e ← GetEdgeForDelContr(D)
56:                         (DDelE, E, DContrE) ← (D \ e,
                                GenKirchPolBaseCase(e),D/e)
57:                         expr ←Add(DDelE.pointer,
                                Multiply(E, DContrE.pointer))
58:                         R.append((D.pointer, expr))
59:                         Q.enqueue(DDelE, DContrE)
60:                     end if
61:                 end if
62:             end for
63:         end if
64:     end while
65:     P ← RemoveUnmatchedDigarphs(P)
66:     return (P, R)
67: end function
```

8.2.3 Descriptions of Used Heuristics and Laplacian Models.

Box 8.1 Heuristics.

i.) Edges $E'(G)$:

0. A single randomly selected edge e, $E'(G) = \{e\}$.
1. All edges, $E'(G) = E(G)$.
2. Edges participating in the longest simple cycle.
3. The $|E(G)|/n, n = 3$ edges participating in the largest number of simple cycles.

ii.) Branch:

0. Edge deleted digraph, $G \setminus e$.
1. Edge contracted digraph, G/e.
2. Edge deleted and edge contracted digraph, $(G \setminus e, G/e)$.

iii.) Components:

0. Strongly connected components.
1. Prime components.

iv.) Optimality criterion:

0. Largest number of components.
1. Largest component (in terms of number of vertices) is smallest.
2. Largest component (in terms of number of edges) is smallest.
3. Smallest total complexity (number of arborescences) of the components.
4. Smallest total complexity with the largest (same) number of components.
5. Largest number of components with the (same) smallest total complexity.

Table 8.1: A collection of example digraph models, ordered by their complexity (number of arborescences). Shown are the digraph aliases (under G), number of vertices $|V|$, number of edges $|E|$, number of arborescences $|\mathsf{arb}(G)|$, and a short description for each digraph.

G	$\lvert V\rvert$	$\lvert E\rvert$	$\lvert\mathsf{arb}(G)\rvert$	Description
COLE1	6	10	26	Kinetic scheme of the ColE1 replication control mechanism from Shin et al. (2000).
AMPAR	7	14	30	Schematic diagram of the AMPA receptor trafficking model from Nakano et al. (2010).
MDH	9	18	141	Proposed kinetic mechanism for the reaction cycle of *M.methylotrophus* methanol dehydrogenase (MDH) with ammonium as activator from Hothi et al. (2005).
ACTMYO	10	20	356	State diagram detailing the interaction of actin and myosin from Sachse et al. (2003).
KNF33	9	24	1,728	Three by three classical KNF (Koshland, Nemethy, and Filmer) model for allosteric regulation of enzymes (Koshland Jr et al., 1966).
SHPIL	10	26	4,560	Model describing early IL-6 induced signaling. Model M0 from Dittrich et al. (2012).
GR	13	32	5,057	Scheme for the catalytic mechanism of glutathione reductase (GR) from Pannala et al. (2013).
PHO5	12	35	53,376	Regulation of yeast PHO5 gene from Ahsendorf et al. (2014).
RND	14	36	69,120	Random Ter-Ter mechanism from Garcia-Sevilla et al. (2010).
TF	25	49	1,549,872	Largest strongly connected component of the transcription factor network of *Saccharomyces cerevisiae* from Jeong & Berman (2008).
HC4	16	60	42,467,328	Four dimensional hypercube digraph rooted at a vertex (the specific rooting does not matter due to symmetry). It represents a generic transcription regulation model for a gene with promoter containing four transcription factor binding sites (Estrada et al., 2016).
COXD	30	117	12,254,915,821,568,674	COX rooted at the environment vertex, i.e. $\mathsf{rt}_{\varnothing}(\mathrm{COX})$, which is the digraph in the denominator of the steady-state expression for COX.
COX	30	118	24,509,831,643,137,316	Scheme of the catalytic cycle of PGHS considering inhibition by NSAID from Goltsov et al. (2010).

8.2.4 Additional Results

Table 8.2: Significance levels (p-values) of the different choices of sub-heuristics for the running time results of algorithm C_I on the less complex set of Laplacian model examples. The non-parametric Kruskal-Wallis H-test was applied along with post hoc pair comparisons using the Wilcoxon signed-rank test to determine whether the samples originate from the same distribution.

Test	(i) Edges		(ii) Branch		(iii) Components		(iv) Optimality	
	pair	p-value	pair	p-value	pair	p-value	pair	p-value
Kruskal-Wallis H-test	–	1.37e-88	–	2.91e-14	–	1.30e-16	–	1.14e-19
Wilcoxon signed-rank test	(1,2)	3.87e-55	(0,1)	5.39e-07	(0, 1)	5.50e-72	(0,1)	7.35e-01
	(1,3)	4.10e-58	(0,2)	1.64e-34			(0, 2)	4.94e-03
	(2,3)	3.38e-28	(1,2)	4.08e-09			(0, 3)	8.47e-21
							(0,4)	4.99e-17
							(0,5)	5.30e-20
							(1,2)	2.60e-03
							(1,3)	6.47e-20
							(1,4)	1.19e-14
							(1,5)	3.59e-19
							(2,3)	3.59e-28
							(2,4)	3.39e-23
							(2,5)	1.26e-27
							(3,4)	4.61e-10
							(3,5)	1.44e-02
							(4,5)	5.38e-07

Table 8.3: Significance levels (p-values) of the different choices of sub-heuristics for the compression results of algorithm C_I on the less complex set of Laplacian model examples.

Test	(i) Edges		(ii) Branch		(iii) Components		(iv) Optimality	
	pair	p-value	pair	p-value	pair	p-value	pair	p-value
Kruskal-Wallis H-test	–	4.15e-05	–	4.55e-33	–	1.01e-01	–	2.13e-02
Wilcoxon signed-rank test	(1,2)	9.08e-07	(0,1)	9.41e-18	(0,1)	1.78e-04	(0,1)	7.75e-01
	(1,3)	4.47e-08	(0,2)	9.03e-01			(0,2)	4.87e-01
	(2,3)	5.14e-02	(1,2)	8.67e-36			(0,3)	1.77e-03
							(0,4)	4.61e-01
							(0,5)	7.73e-02
							(1,2)	2.85e-02
							(1,3)	8.33e-03
							(1,4)	5.49e-01
							(1,5)	2.01e-01
							(2,3)	2.35e-10
							(2,4)	7.08e-01
							(2,5)	5.21e-05
							(3,4)	7.52e-08
							(3,5)	8.66e-04
							(4,5)	8.69e-05

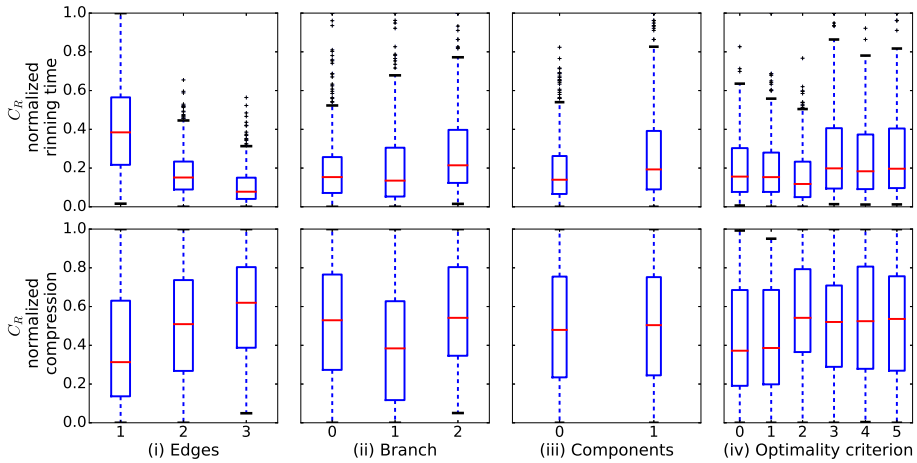

Figure 8.1: Comparison of the normalised running time and compression distributions on the set of less complex examples for algorithm C_R grouped by the different choices of each sub-heuristic - edges, branch, components, and optimality criterion.

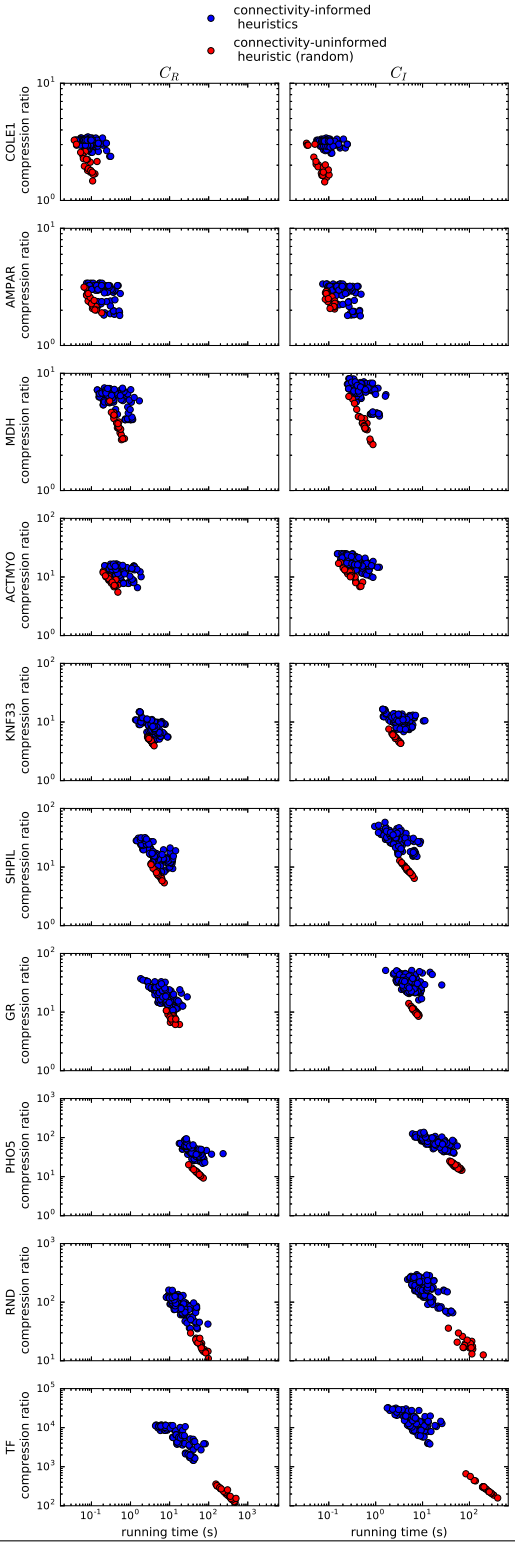

Figure 8.2: Scatter plots of running time versus compression obtained with each of the two algorithms C_R (left column) and C_I (right column) on the collection of less complex examples. Each row corresponds to a Laplacian model example and the examples are sorted by increasing digraph complexity. Blue points represent performance results for each of the 108 connectivity-informed heuristics and red points mark the results for the 20 runs of the uninformed random heuristic $\mathcal{H} = 0 * **$.

8.3 Supplement to Chapter 4

8.3.1 Formalizing the Steady-State Differential Response

Our formal definition of the differential comprises: (i) a metric space (X, μ), in which $X = \{\chi_1, \ldots, \chi_n\}$ is the set of all possible dose-response tuples $\chi_i := (d_i, \mathtt{R}_i)$, where $d_i \geq 0$ denotes the dose components, $\mathtt{R}_i \geq 0$ the response components, and $\mu : X \times X \to \mathbb{R}_{\geq 0}$ is a distance measure, (ii) a pair of steady-state dose-response sets (A, B), where $A \subset X$ and $B \subset X$, and (iii) a map $\mathcal{M} : A \mapsto B$.

The differential is expressed through distances between points on two dose-response curves A and B, i.e. $\mu : A \times B \to \mathbb{R}_{\geq 0}$ and it is a function of the *correspondence coordinate* defined by $\mathcal{M}$. Let us assume, w.l.o.g., that A is the reference curve and B is the perturbed one. We will use the superscripts α and β to denote the specific dissimilar (parametric and structural) features of the systems generating A and B, correspondingly. Further, when we do not explicitly specify α or β we refer to both identifiers at the same time.

We assume that the dose-response sets are generated by functions $\mathcal{R} : \mathbb{R}_{\geq 0} \to \mathbb{R}_{\geq 0}$, that are continuous, smooth, available in closed form, and bounded on the interval $d \in [0, \infty)$ (unbounded responses are not biologically feasible). We denote the functions generating A and B as $\mathcal{R}^\alpha(.)$ and $\mathcal{R}^\beta(.)$, respectively, to account for the *differential structure* of the underlying models. Formally,

$$A := \{(d_i, \mathtt{R}_i) | \mathtt{R}_i = \mathcal{R}^\alpha(d_i; p^\alpha)\} \text{ and } B := \{(d_i, \mathtt{R}_i) | \mathtt{R}_i = \mathcal{R}^\beta(d_i; p^\beta)\},$$

where p^α and p^β are the sets of parameters contained in the functions generating A and B. We call the parameters that differ between p^α and p^β *differential parameters*.

Assume that $\mathcal{R}^\alpha(.)$ and $\mathcal{R}^\beta(.)$ have, respectively, n and m critical points (suprema, infima, extrema, and stationary points of inflection that are identified by the functions' first derivatives) and denote them by $\epsilon_i \in \mathcal{E}$, where $\mathcal{E}$ is the set of all critical points for the relevant function ($\mathcal{E}^\alpha \subset A$ and $\mathcal{E}^\beta \subset B$) and i is their index ($i \in \{1, \ldots, n\}$ for ϵ_i^α and $i \in \{1, \ldots, m\}$ for e_i^β). Due to the functional relation between dose and response and by considering any two or more identical critical points as a single one, the critical points follow a strict total order in their dose component d_{ϵ_i} (e.g. for A, $d_{\epsilon_1} < \ldots < d_{\epsilon_n}$), which we use to define a strict total order of the critical points (e.g. for A, $\epsilon_1 < \ldots < \epsilon_n$).

From the boundedness requirement on $\mathcal{R}(.)$ it follows that the first and the last critical points are reached when the dose goes to zero and infinity, respectively. The intermediate critical points are defined by doses for which the first derivative of $\mathcal{R}(.)$ is zero. Thus the critical points of $\mathcal{R}^\alpha(.)$ are:

$$\epsilon_1^\alpha := \left(0, \lim_{d \to 0} \mathcal{R}^\alpha(d; p)\right), \epsilon_i^\alpha := \{(d_{\epsilon_i}, \mathcal{R}^\alpha(d_{\epsilon_i}; p)) | D_d \mathcal{R}^\alpha(d_{\epsilon_i}; p) = 0\}, \text{ and}$$

$$\epsilon_n^\alpha := \left(\infty, \lim_{d \to \infty} \mathcal{R}^\alpha(d; p)\right),$$

where $i \in \{2, \ldots, n-1\}$ indexes the intermediate critical points and D_d denotes the first derivative with respect to the dose variable d.

The critical points of $\mathcal{R}^\alpha(.)$ partition its domain into $n-1$ monotone segments σ_j, $j \in \{1, \ldots, n-1\}$. Each segment is defined by two consecutive critical points:

$$\sigma_j^\alpha := \left\{ (d, \mathcal{R}^\alpha(d;p)) | d \in \left(d_{\epsilon_j^\alpha}, d_{\epsilon_{j+1}^\alpha} \right) \right\}.$$

Let us denote the set of all segments as Σ. The definitions of critical points and segments for $\mathcal{R}^\beta(.)$ are analogous.

To derive a map $\mathcal{M}$ that preserves the order (and succession, i.e. no critical point is missed out) of critical points and segments let us assume, w.l.o.g., that $\mathcal{R}^\alpha(.)$ has less or equal critical points than $\mathcal{R}^\beta(.)$ ($n \leq m$). Then, we define $\mathcal{M}$ to map all critical points of $\mathcal{R}^\alpha(.)$ to all possible n consecutive critical points of $\mathcal{R}^\beta(.)$, which induces the mapping of the segments, namely:

$$\mathcal{M}(i; \mathcal{E}^\alpha, \mathcal{E}^\beta) : \begin{cases} \epsilon_1^\alpha \mapsto \epsilon_i^\beta \\ \epsilon_2^\alpha \mapsto \epsilon_{i+1}^\beta \\ \quad \vdots \\ \epsilon_n^\alpha \mapsto \epsilon_{i+n-1}^\beta \end{cases} \quad \text{and} \quad \mathcal{M}(i; \Sigma^\alpha, \Sigma^\beta) : \begin{cases} \sigma_1^\alpha \mapsto \sigma_i^\beta \\ \sigma_2^\alpha \mapsto \sigma_{i+1}^\beta \\ \quad \vdots \\ \sigma_{n-1}^\alpha \mapsto \sigma_{i+n-2}^\beta \end{cases},$$

where $i \in \{1, 2, \ldots, 1+m-n\}$. Notice that in the case when $n = m$ the map is bijective and it does not depend on the index $i = 1$.

To preserve the proportion of response in each pair of mapped segments $\sigma_i^\alpha \mapsto \sigma_j^\beta$, the mapping should relate the doses having the same proportion h ($h \in [0,1]$) of response between the minimal and maximal response in the segment, which are determined by the response components of the critical points that enclose it. Let this intra-segmental mapping be determined by the *proportional response function* $\zeta(h; x, y)$. Then, formally:

$$\mathcal{M}_{\mathtt{R}}(\sigma_i^\alpha, \sigma_j^\beta) : \zeta\left(h; \mathtt{R}_{\epsilon_i^\alpha}, \mathtt{R}_{\epsilon_{i+1}^\alpha}\right) \mapsto \zeta\left(h; \mathtt{R}_{\epsilon_j^\beta}, \mathtt{R}_{\epsilon_{j+1}^\beta}\right),$$

where the subscript in $\mathcal{M}_{\mathcal{R}}$ indicates that the definition is only for the response component of the mapping.

The proportional response function ζ has to parametrize the response component of a monotone segment in a dose-response curve. The following two definitions satisfy this requirement:

$$\zeta_1(h; x, y) := \begin{cases} hx + (1-h)y, & \text{if } x \neq y \\ x, & \text{when } x = y \end{cases},$$

and

$$\zeta_2(h; x, y) := \begin{cases} hx + (1-h)y, & \text{if } x > y \\ (1-h)x + hy, & \text{if } x < y \\ x, & \text{when } x = y \end{cases},$$

which are simplifications, respectively, of:

$$\zeta_1(h;x,y) := \frac{1}{2}\left(\left(1+\frac{x-y}{|x-y|}\right)h + \left(1-\frac{x-y}{|x-y|}\right)(1-h)\right)|x-y| + \min(x,y)$$

and

$$\zeta_2(h;x,y) := h\,|x-y| + \min(x,y)\,,$$

where $h \in [0,1]$ is the correspondence variable and x and y are the response coordinates (corresponding to dose coordinates d_x and d_y, $d_x < d_y$) defining a segment σ. Note also that we are not interested in the case when $x = y$ in a segment since it leads to a trivial differential expression.

The differences between these very similar definitions become evident when one of the mapped segments is monotonically increasing and the other one is monotonically decreasing; otherwise the definitions are identical up to the parametrisation of h. In the main text, we chose to use ζ_1, hence, calling it only ζ, due to the simpler expressions it yields in our subsequent derivations. Note that $\zeta_1(0;x,y) = y$ and $\zeta_1(1;x,y) = x$, which means that for $h = 1$ the response coordinates of smaller dose coordinates are mapped to each other while for $h = 0$ the mapping is between the response coordinates of larger dose coordinates.

Once the mapping of the response component is determined within a pair of corresponding segments, the mapping of their dose components can be recovered from the dose-response relation:

$$\mathcal{M}_d(\sigma_i^\alpha, \sigma_j^\beta) : d_{\sigma_i^\alpha,h} \mapsto d_{\sigma_j^\beta,h},$$

where $d_{\sigma_i^\alpha,h}$ is the solution of $\mathcal{R}^\alpha(d_{\sigma_i^\alpha,h};p) = \zeta\left(h;\mathtt{R}_{\epsilon_i^\alpha},\mathtt{R}_{\epsilon_{i+1}^\alpha}\right)$ in the interval $\left(d_{\epsilon_i^\alpha}, d_{\epsilon_{i+1}^\alpha}\right)$. The doses $d_{\sigma_i^\beta,h}$ are derived analogously.

The last ingredient to the formalization of the differential is the definition of μ. Instead of the Euclidean distance between the tuples $\chi^\alpha \in A$ and $\chi^\beta \in B$ mapped through $\mathcal{M} : \chi^\alpha \mapsto \chi^\beta$, we take into account that in dose-response analysis the dose is often plotted in log scale to identify fold differences in the dose variable. Formally, the differential is expressed as (also see Figure 5.1b):

$$\mu\left(\chi^\alpha,\chi^\beta\right) := \sqrt{\pi_d\left(\chi^\alpha,\chi^\beta\right)^2 + \pi_{\mathcal{R}}\left(\chi^\alpha,\chi^\beta\right)^2},$$

where

$$\pi_d\left(\chi^\alpha,\chi^\beta\right) := \log_{10}\frac{d^\alpha}{d^\beta} \text{ and } \pi_{\mathcal{R}}\left(\chi^\alpha,\chi^\beta\right) := \mathtt{R}^\alpha - \mathtt{R}^\beta.$$

8.3.2 Differential Response for a Single Dose Edge

Figure 8.3 shows the tree scheme for generation of the steady-state coefficients for open systems.

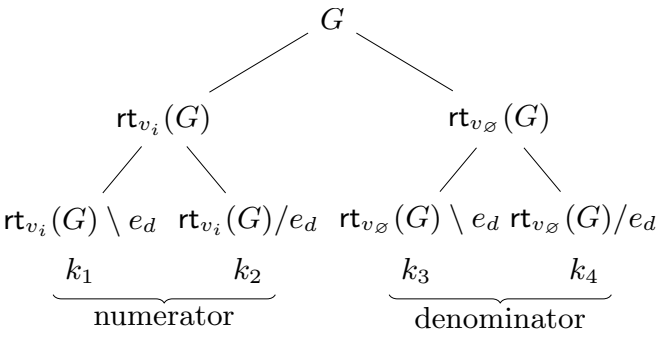

Figure 8.3: Tree scheme for a general digraph G for obtaining the relevant digraphs participating in the coefficients k_i of the dose-response relationship in open systems (for reference and perturbed systems) through the digraph operations rooting, deletion, and contraction. Note that there are also additional terms contained in the coefficients

.

8.3.2.1 Differential mapping

To derive the differential response for the defined dose-response relations first we have to determine the map $\mathcal{M}$. We derive the mapping for dose-response curves A and B both generated by functions of the form of Equation (5.1).

The steady-state function $\mathcal{R}_O(d)$ does not have extrema when varying the dose d since the first derivative is nowhere zero (apart from infinity and the dose independent case when $k_2k_3 = k_1k_4$). There are only two critical points and the dose-response curve is a sigmoid. The critical points are:

$$\mathcal{E} = \left\{ \epsilon_1 = \left(0, \frac{k_1}{k_3}\right), \epsilon_2 = \left(\infty, \frac{k_2}{k_4}\right) \right\}.$$

There exists only one segment defined between the dose components of ϵ_1 and ϵ_2, which we call σ. Every dose-response vector in this segment from A is mapped to its counterpart in B when employing the differential parameters and possibly different digraph topology.

The mapping for the response component in the segment σ is:

$$\mathcal{M}_{\mathcal{R}}(\sigma^\alpha, \sigma^\beta) : \zeta\left(h; \frac{k_1^\alpha}{k_3^\alpha}, \frac{k_2^\alpha}{k_4^\alpha}\right) \mapsto \zeta\left(h; \frac{k_1^\beta}{k_3^\beta}, \frac{k_2^\beta}{k_4^\beta}\right),$$

where the superscripts α and β indicate that the coefficients k have been obtained from the reference or perturbed system, respectively. Remember that we have only fixed $|I^\alpha| = |I^\beta|$, all other features of the reference and perturbed systems can be arbitrary.

The mapping of the dose component in the segment σ, $\mathcal{M}_d(\sigma^\alpha, \sigma^\beta) : d_{\sigma^\alpha,h} \mapsto d_{\sigma^\beta,h}$, where $d_{\sigma^\alpha,h}$ and $d_{\sigma^\beta,h}$ are obtained by solving $\mathcal{R}(d_{\sigma,h}; p) = \zeta\left(h; \frac{k_1}{k_3}, \frac{k_2}{k_4}\right)$

for $d_{\sigma,h}$ in the reference and perturbed dose-response system, correspondingly. In general,

$$d_{\sigma,h} = \frac{k_1 - \zeta\left(h; \frac{k_1}{k_3}, \frac{k_2}{k_4}\right) k_3}{\zeta\left(h; \frac{k_1}{k_3}, \frac{k_2}{k_4}\right) k_4 - k_2}, \text{which reduces to } d_{\sigma,h} = \begin{cases} \frac{1-h}{h}\frac{k_3}{k_4} & \text{if } \frac{k_1}{k_3} \neq \frac{k_2}{k_4}, \\ \text{not defined} & \text{if } \frac{k_1}{k_3} = \frac{k_2}{k_4}. \end{cases} \tag{8.4}$$

Ignoring the trivial case when $\frac{k_1}{k_3} = \frac{k_2}{k_4}$, the dose and the response mappings read:

$$\mathcal{M}_d(\sigma^\alpha, \sigma^\beta) : \frac{1-h}{h}\frac{k_3^\alpha}{k_4^\alpha} \mapsto \frac{1-h}{h}\frac{k_3^\beta}{k_4^\beta}$$

and

$$\mathcal{M}_\mathcal{R}(\sigma^\alpha, \sigma^\beta) : h\frac{k_1^\alpha}{k_3^\alpha} + (1-h)\frac{k_2^\alpha}{k_4^\alpha} \mapsto h\frac{k_1^\beta}{k_3^\beta} + (1-h)\frac{k_2^\beta}{k_4^\beta}.$$

8.3.2.2 Steady-state expressions for the investigated models

The steady-state expression for the reference and perturbed systems before plugging in the differential parameters for the example from Figure 5.3 is:

$$\mathcal{R}_O(d) = \frac{r_1 r_3 r_9 \left(r_5 + r_6 + r_7\right) d}{\begin{array}{l}\left(r_2 + r_3\right)\left(r_8 + r_9\right)\left(r_4\left(r_6 + r_7\right) + r_5 r_7\right) + \\ \quad + r_1\left(r_5\left(r_3 r_9 + r_7\left(r_3 + r_9\right)\right) + r_9\left(r_3 + r_4\right)\left(r_6 + r_7\right)\right) d\end{array}} x_t.$$

The steady-state expression for the example from Figure 5.4b reads:

$$\mathcal{R}_O(d) = \frac{r_1\left(r_3 r_5 r_9 r_{11} + r_3\left(r_6 + r_7\right) r_9 r_{11}\right) d}{r_8 r_{10}\left(r_2 + r_3\right)\left(r_4\left(r_6 + r_7\right) + r_5 r_7\right) + r_1 r_3 r_5 r_7 r_{10} d}.$$

8.3.3 Differential Response for Two Dose Edges

We consider the case in which the input dose acts proportionally and simultaneously on two edges, i.e. $I(G) = \{e_{d,1}, e_{d,2}\}$, $\ell(e_{d,1}) = g_1(p)d$, and $\ell(e_{d,2}) = g_2(p)d$.

8.3.3.1 General form of the dose-response.

We apply the deletion-contraction formula to partition the set of arborescences from the numerator and denominator of the response function $\mathcal{R}$ into four categories – those containing no input edges, those containing $e_{d,1}$ but not $e_{d,2}$, those containing $e_{d,2}$ but not $e_{d,1}$, and those containing both $e_{d,1}$ and $e_{d,2}$. Simplifying, we obtain the general form of dose-response expressions for closed and open systems:

$$\mathcal{R}_O(d) = \frac{k_1 + k_{23} d + k_4 d^2}{k_5 + k_{67} d + k_8 d^2}, \tag{8.5}$$

where $k_{23} := k_2 + k_3$ and $k_{67} := k_6 + k_7$, $\mathcal{R}_O(d)$ is bounded (the degree of the numerator is not higher than the degree of the denominator) and of second degree, and the coefficients are:

for closed systems
$k_1 = x_t \sum_{v_i \in O(G)} a_{v_i} \kappa_{v_i}(G \backslash e_{d,1} \backslash e_{d,2})$,
$k_2 = x_t g_2(p) \sum_{v_i \in O(G)} a_{v_i} \kappa_{v_i}(G \backslash e_{d,1} / e_{d,2})$,
$k_3 = x_t g_1(p) \sum_{v_i \in O(G)} a_{v_i} \kappa_{v_i}(G / e_{d,1} \backslash e_{d,2})$,
$k_4 = x_t g_1(p) g_2(p) \sum_{v_i \in O(G)} a_{v_i} \kappa_{v_i}(G / e_{d,1} / e_{d,2})$,
$k_5 = \kappa(G \backslash e_{d,1} \backslash e_{d,2})$,
$k_6 = g_2(p) \kappa(G \backslash e_{d,1} / e_{d,2})$,
$k_7 = g_1(p) \kappa(G / e_{d,1} \backslash e_{d,2})$,
$k_8 = g_1(p) g_2(p) \kappa(G / e_{d,1} / e_{d,2})$,

for open systems
$k_1 = \sum_{v_i \in O(\overline{G})} a_{v_i} \kappa_{v_i}(G \backslash e_{d,1} \backslash e_{d,2})$,
$k_2 = g_2(p) \sum_{v_i \in O(\overline{G})} a_{v_i} \kappa_{v_i}(G \backslash e_{d,1} / e_{d,2})$,
$k_3 = g_1(p) \sum_{v_i \in O(\overline{G})} a_{v_i} \kappa_{v_i}(G / e_{d,1} \backslash e_{d,2})$,
$k_4 = g_1(p) g_2(p) \sum_{v_i \in O(\overline{G})} a_{v_i} \kappa_{v_i}(G / e_{d,1} / e_{d,2})$,
$k_5 = \kappa_{v_\varnothing}(G \backslash e_{d,1} \backslash e_{d,2})$,
$k_6 = g_2(p) \kappa_{v_\varnothing}(G \backslash e_{d,1} / e_{d,2})$,
$k_7 = g_1(p) \kappa_{v_\varnothing}(G / e_{d,1} \backslash e_{d,2})$,
$k_8 = g_1(p) g_2(p) \kappa_{v_\varnothing}(G / e_{d,1} / e_{d,2})$

The arborescence partitioning determines the digraphs contained in the coefficients k, which can be seen in the tree scheme from Figure 8.4. The numerator and denominator polynomials in the dose variable d can be at most of degree two, where the highest degree corresponds to arborescences containing both $e_{d,1}$ and $e_{d,2}$. We see that even though the degree of the polynomials grows by one, the number of digraphs to consider grows exponentially. In the general case, for an input acting on w edges simultaneously, the numerator and denominator are at most of degree w and the digraphs giving rise to the coefficients of the polynomials are 2^w and, therefore, the tree scheme has 2^{w+1} leaves. Again, it could happen that arborescences do not exist for some digraphs resulting to simpler, trivial, or unbounded dose-response relationships.

8.3.3.2 Differential mapping.

We derive the mapping $\mathcal{M}$ for the reference and perturbed dose-response curves A and B, both being generated by functions having the form of Equation 8.5.

We are interested in deriving conditions guaranteeing positivity of an extremum and thus ensuring that Hormesis is present. The steady-state response function $\mathcal{R}_O(d)$ could have, in principle, at most two extrema when varying the dose vari-

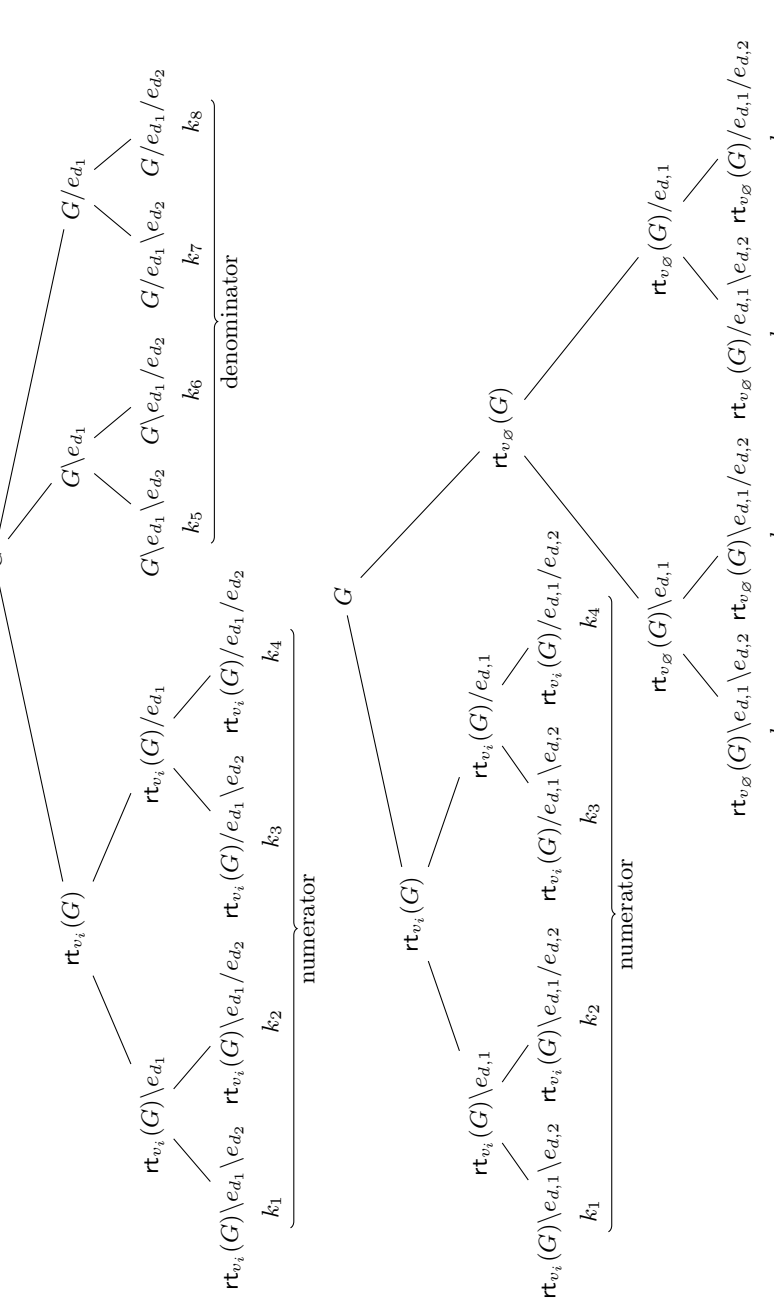

Figure 8.4: Tree scheme for obtaining the relevant digraphs generating the coefficients k in the dose-response relationship when the dose acts simultaneously on two edges for (above) closed and (below) open systems through the digraph operations rooting, deletion, and contraction. Note that there are also additional terms contained in the coefficients.

able since its first derivative can become zero for two values of d.

$$D_d \frac{k_1 + k_{23}d + k_4 d^2}{k_5 + k_{67}d + k_8 d^2} = 0 \Leftrightarrow$$

$$\frac{k_5 k_{23} - k_1 k_{67} + 2(k_4 k_5 - k_1 k_8)d + (k_4 k_{67} - k_8 k_{23})d^2}{(k_5 + k_{67}d + k_8 d^2)^2} = 0.$$

The denominator of the condition is never zero for positive doses d and k_is leading to non-degenerate systems (not all k_is being zero). The doses for which the numerator equals zero are the ones corresponding to extrema in the dose response, namely:

$$d_\epsilon^{(1,2)} = \frac{k_1 k_8 - k_4 k_5 \pm \sqrt{U}}{k_4 k_{67} - k_8 k_{23}},$$

where $U = (k_1 k_8 - k_4 k_5)^2 + (k_1 k_{67} - k_5 k_{23})\,(k_4 k_{67} - k_8 k_{23})$ and $k_4 k_{67} \neq k_8 k_{23}$.

Of interest are only the positive real roots since they are the extrema of the dose response relationships we study. The two roots can never be positive at the same time for non-negative values of the coefficients k_i. This fact becomes clear after employing Vieta's formulas for second degree polynomials and requiring that the sum and the product of the roots are positive, namely:

$$d^{(1)} + d^{(2)} = \frac{-2(k_4 k_5 - k_1 k_8)}{k_4 k_{67} - k_8 k_{23}} > 0 \quad \wedge \quad d^{(1)} d^{(2)} = \frac{k_5 k_{23} - k_1 k_{67}}{k_4 k_{67} - k_8 k_{23}} > 0,$$

which is equivalent to:

$$\left(\frac{k_{23}}{k_{67}} < \frac{k_4}{k_8} < \frac{k_1}{k_5} \vee \frac{k_1}{k_5} < \frac{k_4}{k_8} < \frac{k_{23}}{k_{67}}\right) \wedge \left(\frac{k_1}{k_5} < \frac{k_1}{k_5} < \frac{k_4}{k_8} \vee \frac{k_4}{k_8} < \frac{k_{23}}{k_{67}} < \frac{k_1}{k_5}\right).$$

It is evident that for non-negative coefficients k_i there exists no solution for the logical expression of the set of inequalities. More precisely, according to Vietta's formula sum condition the ratio $\frac{k_4}{k_8}$ needs to have a value between the ratios $\frac{k_1}{k_5}$ and $\frac{k_{23}}{k_{67}}$, and according to Vietta's product condition $\frac{k_4}{k_8}$ has to be either the largest or the smallest among the ratios. The two conditions can clearly not hold simultaneously and thus the two roots cannot be positive at the same time. However, we still need to derive the conditions for which a root is positive. All these considerations are important when deciding which extrema to include and how to order them when deriving the differential.

To derive criteria for the positivity of the real roots, $d^{(1,2)} > 0$ ($d^{(1,2)} = 0$ is not of interest since $0 < d < \infty$) and $U \geq 0$ needs to hold, i.e.:

$$\left(\frac{k_{23}}{k_{67}} < \frac{k_4}{k_8} < \frac{k_1}{k_5} \pm \frac{\sqrt{U}}{k_5 k_8} \vee \frac{k_1}{k_5} \pm \frac{\sqrt{U}}{k_5 k_8} < \frac{k_4}{k_8} < \frac{k_{23}}{k_{67}}\right) \wedge U \geq 0.$$

However, the condition $\frac{k_{23}}{k_{67}} < \frac{k_4}{k_8} < \frac{k_1}{k_5} - \frac{\sqrt{U}}{k_5 k_8}$ never holds. To see why, we can

restructure its inequalities to the equivalent form:

$$\frac{k_{23}}{k_{67}} < \frac{k_4}{k_8} \wedge \sqrt{\left(\frac{k_1}{k_5} - \frac{k_4}{k_8}\right)^2 + \left(\frac{k_1}{k_5}\frac{k_{67}}{k_8} - \frac{k_{23}}{k_8}\right)\left(\frac{k_4}{k_8}\frac{k_{67}}{k_5} - \frac{k_{23}}{k_5}\right)} < \frac{k_1}{k_5} - \frac{k_4}{k_8}$$

and realize that the condition holds iff $\frac{k_4}{k_8} < \frac{k_1}{k_5}$ and $\left(\frac{k_1}{k_5}\frac{k_{67}}{k_8} - \frac{k_{23}}{k_8}\right)\left(\frac{k_4}{k_8}\frac{k_{67}}{k_5} - \frac{k_{23}}{k_5}\right) < 0$ (but $U \geq 0$). This is equivalent to:

$$\frac{k_{23}}{k_{67}} < \frac{k_4}{k_8} < \frac{k_1}{k_5} \wedge \left(\frac{k_1}{k_5} < \frac{k_{23}}{k_{67}} < \frac{k_4}{k_8} \vee \frac{k_4}{k_8} < \frac{k_{23}}{k_{67}} < \frac{k_1}{k_5}\right),$$

and obviously never holds for the definition of the steady-state coefficients. The condition $\frac{k_1}{k_5} + \frac{\sqrt{U}}{k_5 k_8} < \frac{k_4}{k_8} < \frac{k_{23}}{k_{67}}$ can be analogously shown false.

The remaining root positivity conditions can be put in a simpler form, for example $\frac{k_{23}}{k_{67}} < \frac{k_4}{k_8} < \frac{k_1}{k_5} + \frac{\sqrt{U}}{k_5 k_8}$ is equivalent to:

$$\frac{k_{23}}{k_{67}} < \frac{k_4}{k_8} \wedge \frac{k_4}{k_8} - \frac{k_1}{k_5} < \sqrt{\left(\frac{k_1}{k_5} - \frac{k_4}{k_8}\right)^2 + \left(\frac{k_1}{k_5}\frac{k_{67}}{k_8} - \frac{k_{23}}{k_8}\right)\left(\frac{k_4}{k_8}\frac{k_{67}}{k_5} - \frac{k_{23}}{k_5}\right)},$$

where the second inequality always holds when $\frac{k_4}{k_8} \leq \frac{k_1}{k_5}$. When $\frac{k_1}{k_5} < \frac{k_4}{k_8}$ the inequality holds if $\left(\frac{k_1}{k_5}\frac{k_{67}}{k_8} - \frac{k_{23}}{k_8}\right)\left(\frac{k_4}{k_8}\frac{k_{67}}{k_5} - \frac{k_{23}}{k_5}\right) > 0$, i.e. if $\frac{k_{23}}{k_{67}} < \frac{k_1}{k_5}$ (keeping in mind we are in the case when $\frac{k_{23}}{k_{67}} < \frac{k_4}{k_8}$). This is equivalent to:

$$\frac{k_{23}}{k_{67}} < \frac{k_4}{k_8} \leq \frac{k_1}{k_5} \vee \frac{k_{23}}{k_{67}} < \frac{k_1}{k_5} < \frac{k_4}{k_8}.$$

Analogous analysis can be applied to $\frac{k_1}{k_5} - \frac{\sqrt{U}}{k_5 k_8} < \frac{k_4}{k_8} < \frac{k_{23}}{k_{67}}$ to obtain the equivalent form:

$$\frac{k_4}{k_8} \leq \frac{k_1}{k_5} < \frac{k_{23}}{k_{67}} \vee \frac{k_1}{k_5} < \frac{k_4}{k_8} < \frac{k_{23}}{k_{67}}.$$

When $\frac{k_{23}}{k_{67}} = \frac{k_4}{k_8}$ ($k_{67} \neq 0$) but $\frac{k_1}{k_5} \neq \frac{k_4}{k_8}$, the root is

$$d_\epsilon = \frac{k_1 k_{67} - k_5 k_{23}}{2(k_4 k_5 - k_1 k_8)},$$

which is positive for $\frac{k_{23}}{k_{67}} < \frac{k_1}{k_5} < \frac{k_4}{k_8} \vee \frac{k_4}{k_8} < \frac{k_1}{k_5} < \frac{k_{23}}{k_{67}}$. The conditions are never satisfied due to incompatibility with $\frac{k_{23}}{k_{67}} = \frac{k_4}{k_8}$ and $\frac{k_1}{k_5} \neq \frac{k_4}{k_8}$. Also, when $\frac{k_1}{k_5} = \frac{k_{23}}{k_{67}} = \frac{k_4}{k_8}$ ($k_{67} \neq 0$) the first derivative is constant (not dependent of the input variable). In these cases Hormesis cannot be present.

When $k_{67} = 0$ and $k_{23} \neq 0$ (which is not possible in closed systems but only open ones), $d^{(1)}d^{(2)} = -\frac{k_5}{k_8} > 0$ is never satisfied and it is, again, not possible to

have two positive roots. In this case the roots are:

$$d_\epsilon^{(1,2)} = \frac{k_1k_8 - k_4k_5 \pm \sqrt{(k_1k_8 - k_4k_5)^2 + k_5k_8k_{23}^2}}{-k_8k_{23}}.$$

The criteria for a positive root are:

$$\frac{k_1}{k_5} \pm \frac{\sqrt{U}}{k_5k_8} < \frac{k_4}{k_8},$$

and it can be shown that $\frac{k_1}{k_5} - \frac{\sqrt{U}}{k_5k_8} < \frac{k_4}{k_8}$ is always valid and $\frac{k_1}{k_5} + \frac{\sqrt{U}}{k_5k_8} < \frac{k_4}{k_8}$ is never valid. Hormesis will always be present since one root is always positive and real ($U \geq 0$ and for all positive steady-state coefficients).

In the case when $k_{67} = k_{23} = 0$, the steady-state response function $\mathcal{R}_O(d)$ has no non-trivial extrema, and thus can never generate a hormetic dose-response.

We summarize the derived necessary and sufficient conditions for having a positive extremum of the dose-response function, which we call *Hormesis condition* as:

$$(k_{67} = 0 \wedge k_{23} \neq 0) \vee \Bigg(k_{67} \neq 0 \wedge U \geq 0 \wedge \left(\frac{k_{23}}{k_{67}} < \frac{k_4}{k_8} \leq \frac{k_1}{k_5} \vee \frac{k_{23}}{k_{67}} < \frac{k_1}{k_5} < \frac{k_4}{k_8} \vee \frac{k_4}{k_8} \leq \frac{k_1}{k_5} < \frac{k_{23}}{k_{67}} \vee \frac{k_1}{k_5} < \frac{k_4}{k_8} < \frac{k_{23}}{k_{67}} \right) \Bigg). \tag{8.6}$$

If the inequalities for the respective conditions on the coefficients k_{23} and k_{67} are not satisfied or when $k_{23} = k_{67} = 0$, the model is not capable of generating hormetic dose-response curves. Note that even when the hormesis conditions are satisfied the biphasic behaviour might be weak and experimentally not evident.

Combining the critical points at zero and infinite dose with the positive extremum we obtain a set of critical points $\mathcal{E}$:

$$\mathcal{E} = \left\{ \epsilon_1 = \left(0, \frac{k_1}{k_5}\right), \epsilon_2 = \left(\frac{k_1k_8 - k_4k_5 \pm \sqrt{U}}{k_4k_{67} - k_8k_{23}}, \frac{k_{23}k_{67} - 2(k_1k_8 + k_4k_5) \pm 2\sqrt{U}}{k_{67}^2 - 4k_5k_8} \right), \epsilon_3 = \left(\infty, \frac{k_4}{k_8}\right) \right\},$$

where the sign in front of $\sqrt{U}$ in ϵ_2 depends on the steady-state coefficients:

$$\begin{array}{ll} k_{67} = 0 \wedge k_{23} \neq 0 \wedge : & -, \\ k_{67} \neq 0 \wedge \left(\frac{k_{23}}{k_{67}} < \frac{k_4}{k_8} \leq \frac{k_1}{k_5} \vee \frac{k_{23}}{k_{67}} < \frac{k_1}{k_5} < \frac{k_4}{k_8} \right) : & +, \\ k_{67} \neq 0 \wedge \left(\frac{k_4}{k_8} \leq \frac{k_1}{k_5} < \frac{k_{23}}{k_{67}} \vee \frac{k_1}{k_5} < \frac{k_4}{k_8} < \frac{k_{23}}{k_{67}} \right) : & -. \end{array}$$

When the Hormesis conditions are satisfied all three critical points are relevant (depending on the conditions, the roots with the appropriate sign have to be selected), thus each dose-response curve has two segments – σ_1 (defined by ϵ_1 and ϵ_2) and σ_2 (defined by ϵ_2 and ϵ_3). When the Hormesis conditions do not hold, we consider only ϵ_1 and ϵ_3 which define the single segment σ. In general, the values of the coefficients k_i are not known and the number of critical points cannot be determined unambiguously. Thus, three cases, depending on the number of segments in the reference and perturbed curves (A and B) mapped to each other, need to be considered (assuming, w.l.o.g., that A has less or equal critical points than B), namely:

Case 1: Hormesis conditions hold neither for A nor for B.
Hence, the single segment σ^α of A is mapped to the single segment σ^β of B, i.e. $n = m = 2$:

$$\mathcal{M}(i=1;\mathcal{E}^\alpha,\mathcal{E}^\beta):\left\{\begin{array}{l}\epsilon_1^\alpha\mapsto\epsilon_1^\beta\\ \epsilon_3^\alpha\mapsto\epsilon_3^\beta\end{array}\right.,\qquad \mathcal{M}(i=1;\Sigma^\alpha,\Sigma^\beta):\sigma^\alpha\mapsto\sigma^\beta.$$

Case 2: Hormesis conditions do not hold for A but hold for B.
Hence, the single segment σ^α of A is mapped to the two segments σ_1^β and σ_2^β of B, i.e. $n = 2$ and $m = 3$:

$$\mathcal{M}(i=1;\mathcal{E}^\alpha,\mathcal{E}^\beta):\left\{\begin{array}{l}\epsilon_1^\alpha\mapsto\epsilon_1^\beta\\ \epsilon_2^\alpha\mapsto\epsilon_2^\beta\end{array}\right.,\qquad \mathcal{M}(i=2;\mathcal{E}^\alpha,\mathcal{E}^\beta):\left\{\begin{array}{l}\epsilon_1^\alpha\mapsto\epsilon_2^\beta\\ \epsilon_2^\alpha\mapsto\epsilon_3^\beta\end{array}\right.,$$

$$\mathcal{M}(i=1;\Sigma^\alpha,\Sigma^\beta):\sigma_1^\alpha\mapsto\sigma_1^\beta,\qquad \mathcal{M}(i=2;\Sigma^\alpha,\Sigma^\beta):\sigma_1^\alpha\mapsto\sigma_2^\beta.$$

Case 3: Hormesis conditions hold for both A and B.
Hence, the two segments σ_1^α and σ_2^α of A are mapped to the two segments σ_1^β and σ_2^β of B, i.e. $n = m = 3$:

$$\mathcal{M}(i=1;\mathcal{E}^\alpha,\mathcal{E}^\beta):\left\{\begin{array}{l}\epsilon_1^\alpha\mapsto\epsilon_1^\beta\\ \epsilon_2^\alpha\mapsto\epsilon_2^\beta\\ \epsilon_3^\alpha\mapsto\epsilon_3^\beta\end{array}\right.,\qquad \mathcal{M}(i=1;\Sigma^\alpha,\Sigma^\beta):\left\{\begin{array}{l}\sigma_1^\alpha\mapsto\sigma_1^\beta\\ \sigma_2^\alpha\mapsto\sigma_2^\beta\end{array}\right..$$

The respective response component of the segment mapping in all three cases is obtained by plugging in the appropriate arguments in the proportion function. The derivation of the dose component is, however, more involved since it includes the solution of $\mathcal{R}(d_{\sigma,h};p)=\zeta(h;x,y)$ for $d_{\sigma,h}$ when the differential parameters, differential structure, and the appropriate segment are considered. Thus, in the general case, the parametrised dose component inside a segment ($h\neq 0,1$) reads:

$$\frac{k_1+k_{23}d+k_4d^2}{k_5+k_{67}d+k_8d^2}=\zeta(h;x,y)\Leftrightarrow$$

$$k_1-k_5\zeta(h;x,y)+(k_{23}-k_{67}\zeta(h;x,y))d+(k_4-k_8\zeta(h;x,y))d^2=0\Leftrightarrow$$

$$d_{\sigma,h}^{(1,2)} = \frac{k_{67}\zeta\left(h;x,y\right) - k_{23} \pm \sqrt{W(h;x,y)}}{2\left(k_4 - k_8\zeta\left(h;x,y\right)\right)},$$

where $W(h;x,y) = \left(k_{67}\zeta\left(h;x,y\right) - k_{23}\right)^2 - 4\left(k_1 - k_5\zeta\left(h;x,y\right)\right)\left(k_4 - k_8\zeta\left(h;x,y\right)\right)$, $d_{\sigma,h}^{(1)}$ is the root with $+\sqrt{W(h;x,y)}$ and $d_{\sigma,h}^{(1)}$ with $-\sqrt{W(h;x,y)}$.

When deriving the projections of the differential the relevant solution should be be positive for all $h \in (0,1)$ and belong to the dose interval of definition of the desired segment σ (defined by the doses corresponding to x and y) when $W(h;x,y) \geq 0$. Root positivity leads to:

$$\frac{k_{23}}{k_{67}} \mp \frac{\sqrt{W(h;x,y)}}{k_{67}} > \zeta\left(h;x,y\right) > \frac{k_4}{k_8} \vee \frac{k_{23}}{k_{67}} \mp \frac{\sqrt{W(h;x,y)}}{k_{67}} < \zeta\left(h;x,y\right) < \frac{k_4}{k_8}.$$

8.3.3.3 Projections of the differential.

Depending on the particular mapped segments σ_i^{α} and σ_j^{β}, the signed projections π_d and $\pi_{\mathcal{R}}$ have the general form:

$$\pi_d\left(h\right) = \log_{10}\frac{k_4^{\beta} - k_8^{\beta}\zeta\left(h;x^{\beta},y^{\beta}\right)}{k_4^{\alpha} - k_8^{\alpha}\zeta\left(h;x^{\alpha},y^{\alpha}\right)}\frac{k_{67}^{\alpha}\zeta\left(h;x^{\alpha},y^{\alpha}\right) - k_{23}^{\alpha} \pm \sqrt{W^{\beta}(h;x^{\alpha},y^{\alpha})}}{k_{67}^{\beta}\zeta\left(h;x^{\beta},y^{\beta}\right) - k_{23}^{\beta} \pm \sqrt{W^{\beta}(h;x^{\beta},y^{\beta})}}$$

and

$$\pi_{\mathcal{R}}\left(h\right) = \zeta\left(h;x^{\alpha},y^{\alpha}\right) - \zeta\left(h;x^{\beta},y^{\beta}\right).$$

Note that when $h = 0$ or $h = 1$ the dose differential is derived by mapping the dose components of the respective extrema.

In particular, the differential expression are different with respect to the number of segments in each dose-response curve:

Case 1: The conditions for positivity of the dose component solutions for all $h \in (0,1)$ when $W(h;\frac{k_1}{k_5},\frac{k_4}{k_8}) \geq 0$ can be reduced to:

$$\frac{k_{23}}{k_{67}} + \frac{\sqrt{W(h;\frac{k_1}{k_5},\frac{k_4}{k_8})}}{k_{67}} > h\frac{k_1}{k_5} + (1-h)\frac{k_4}{k_8} > \frac{k_4}{k_8} \vee$$
$$\frac{k_{23}}{k_{67}} - \frac{\sqrt{W(h;\frac{k_1}{k_5},\frac{k_4}{k_8})}}{k_{67}} < h\frac{k_1}{k_5} + (1-h)\frac{k_4}{k_8} < \frac{k_4}{k_8},$$

which correspond to the non-hormesis conditions $\frac{k_4}{k_8} \leq \frac{k_{23}}{k_{67}} \leq \frac{k_1}{k_5}$ and $\frac{k_1}{k_5} \leq \frac{k_{23}}{k_{67}} \leq \frac{k_4}{k_8}$, and the roots $d_{\sigma,h}^{(2)}$ and $d_{\sigma,h}^{(1)}$, respectively.

To see why, let us show that $\frac{k_{23}}{k_{67}} - \frac{\sqrt{W(h;\frac{k_1}{k_5},\frac{k_4}{k_8})}}{k_{67}} > \zeta\left(h;\frac{k_1}{k_5},\frac{k_4}{k_8}\right) > \frac{k_4}{k_8}$ never

holds. We rearrange the inequality to:

$$\frac{k_{23}}{k_{67}} - \zeta\left(h; \frac{k_1}{k_5}, \frac{k_4}{k_8}\right) > \sqrt{\left(\frac{k_{23}}{k_{67}} - \zeta\left(h; \frac{k_1}{k_5}, \frac{k_4}{k_8}\right)\right)^2 - 4\frac{\left(k_1 - k_5\zeta\left(h; \frac{k_1}{k_5}, \frac{k_4}{k_8}\right)\right)\left(k_4 - k_8\zeta\left(h; \frac{k_1}{k_5}, \frac{k_4}{k_8}\right)\right)}{k_{67}^2}},$$

and notice that due to the non-hormesis, $\frac{k_4}{k_8} < \zeta\left(h; \frac{k_1}{k_5}, \frac{k_4}{k_8}\right) < \frac{k_1}{k_5}$, which means the inequality never holds since

$$\left(k_1 - k_5\zeta\left(h; \frac{k_1}{k_5}, \frac{k_4}{k_8}\right)\right)\left(k_4 - k_8\zeta\left(h; \frac{k_1}{k_5}, \frac{k_4}{k_8}\right)\right) < 0.$$

The considerations are analogous for the other inequality in the positivity condition. This simplification shows that, depending on which positivity condition is met after α and β specifics are applied, only one root is relevant for the differential.

Now, ignoring the trivial case when $\frac{k_1}{k_5} = \frac{k_4}{k_8}$ for any differential structure and value of the differential parameters, the dose and the response mappings read:

$$\mathcal{M}_d(\sigma^\alpha, \sigma^\beta) : d_{\sigma,h}^{(1,2),\alpha} \mapsto d_{\sigma,h}^{(1,2),\beta}$$

and

$$\mathcal{M}_{\mathcal{R}}(\sigma^\alpha, \sigma^\beta) : h\frac{k_1^\alpha}{k_5^\alpha} + (1-h)\frac{k_4^\alpha}{k_8^\alpha} \mapsto h\frac{k_1^\beta}{k_5^\beta} + (1-h)\frac{k_4^\beta}{k_8^\beta}.$$

In this case, we have already expressed the relevant critical points through the dose-response coefficients. Thus we can write the differential as:

$$\pi_d(h) = \log_{10}\frac{k_8^\beta}{k_8^\alpha}\frac{k_4^\beta k_5^\beta - k_1^\beta k_8^\beta}{k_4^\alpha k_5^\alpha - k_1^\alpha k_8^\alpha} \frac{k_5^\alpha k_8^\alpha\left(-k_{23}^\alpha \pm \sqrt{W(h; \frac{k_1^\alpha}{k_5^\alpha}, \frac{k_4^\alpha}{k_8^\alpha})}\right) + k_{67}^\alpha\left(hk_1^\alpha k_8^\alpha + (1-h)k_4^\alpha k_5^\alpha\right)}{k_5^\beta k_8^\beta\left(-k_{23}^\beta \pm \sqrt{W(h; \frac{k_1^\beta}{k_5^\beta}, \frac{k_4^\beta}{k_8^\beta})}\right) + k_{67}^\beta\left(hk_1^\beta k_8^\beta + (1-h)k_4^\beta k_5^\beta\right)}$$

and

$$\pi_{\mathcal{R}}(h) = h\left(\frac{k_1^\alpha}{k_5^\alpha} - \frac{k_1^\beta}{k_5^\beta}\right) + (1-h)\left(\frac{k_4^\alpha}{k_8^\alpha} - \frac{k_4^\beta}{k_8^\beta}\right).$$

Note that the sign in front of the square root can be determined only by the positivity conditions, i.e. if it is not known which one is satisfied for A and B all combinations have to be considered.

Case 2: The dose and response projections of the differential for the different segment mappings are:

$$\pi_d\left(h; i=1\right) = \log_{10} \frac{k_4^\beta - k_8^\beta \zeta\left(h; \frac{k_1^\beta}{k_5^\beta}, \mathcal{R}_{\epsilon_2}^\beta\right)}{k_4^\alpha - k_8^\alpha \zeta\left(h; \frac{k_1^\alpha}{k_5^\alpha}, \frac{k_4^\alpha}{k_8^\alpha}\right)} \frac{k_{67}^\alpha \zeta\left(h; \frac{k_1^\alpha}{k_5^\alpha}, \frac{k_4^\alpha}{k_8^\alpha}\right) - k_{23}^\alpha \pm \sqrt{W(h; \frac{k_1^\alpha}{k_5^\alpha}, \frac{k_4^\alpha}{k_8^\alpha})}}{k_{67}^\beta \zeta\left(h; \frac{k_1^\beta}{k_5^\beta}, \mathcal{R}_{\epsilon_2}^\beta\right) - k_{23}^\beta \pm \sqrt{W(h; \frac{k_1^\beta}{k_5^\beta}, \mathcal{R}_{\epsilon_2}^\beta)}}$$

and

$$\pi_{\mathcal{R}}\left(h; i=1\right) = \zeta\left(h; \frac{k_1^\alpha}{k_5^\alpha}, \frac{k_4^\alpha}{k_8^\alpha}\right) - \zeta\left(h; \frac{k_1^\beta}{k_5^\beta}, \mathcal{R}_{\epsilon_2}^\beta\right).$$

$$\pi_d\left(h; i=2\right) = \log_{10} \frac{k_4^\beta - k_8^\beta \zeta\left(h; \mathcal{R}_{\epsilon_2}^\beta, \frac{k_4^\beta}{k_8^\beta}\right)}{k_4^\alpha - k_8^\alpha \zeta\left(h; \frac{k_1^\alpha}{k_5^\alpha}, \frac{k_4^\alpha}{k_8^\alpha}\right)} \frac{k_{67}^\alpha \zeta\left(h; \frac{k_1^\alpha}{k_5^\alpha}, \frac{k_4^\alpha}{k_8^\alpha}\right) - k_{23}^\alpha \pm \sqrt{W(h; \frac{k_1^\alpha}{k_5^\alpha}, \frac{k_4^\alpha}{k_8^\alpha})}}{k_{67}^\beta \zeta\left(h; \mathcal{R}_{\epsilon_2}^\beta, \frac{k_4^\beta}{k_8^\beta}\right) - k_{23}^\beta \pm \sqrt{W(h; \mathcal{R}_{\epsilon_2}^\beta, \frac{k_4^\beta}{k_8^\beta})}}$$

and

$$\pi_{\mathcal{R}}\left(h, i=2\right) = \zeta\left(h; \frac{k_1^\alpha}{k_5^\alpha}, \frac{k_4^\alpha}{k_8^\alpha}\right) - \zeta\left(h; \mathcal{R}_{\epsilon_2}^\beta, \frac{k_4^\beta}{k_8^\beta}\right).$$

Choosing the relevant root from $d_{\sigma,h}^{(1,2)}$ when deriving the dose differential depends on the hormesis conditions and the particular dose-response segment (the root need to be in the dose domain of the segment).

Case 3: The dose and response projections of the differential for the corresponding segments are:

$$\pi_d\left(h\right) = \begin{cases} \log_{10} \frac{k_4^\beta - k_8^\beta \zeta\left(h; \frac{k_1^\beta}{k_5^\beta}, \mathcal{R}_{\epsilon_2}^\beta\right)}{k_4^\alpha - k_8^\alpha \zeta\left(h; \frac{k_1^\alpha}{k_5^\alpha}, \mathcal{R}_{\epsilon_2}^\alpha\right)} \frac{k_{67}^\alpha \zeta\left(h; \frac{k_1^\alpha}{k_5^\alpha}, \mathcal{R}_{\epsilon_2}^\alpha\right) - k_{23}^\alpha \pm \sqrt{W(h; \frac{k_1^\alpha}{k_5^\alpha}, \mathcal{R}_{\epsilon_2}^\alpha)}}{k_{67}^\beta \zeta\left(h; \frac{k_1^\beta}{k_5^\beta}, \mathcal{R}_{\epsilon_2}^\beta\right) - k_{23}^\beta \pm \sqrt{W(h; \frac{k_1^\beta}{k_5^\beta}, \mathcal{R}_{\epsilon_2}^\beta)}} \\ \log_{10} \frac{k_4^\beta - k_8^\beta \zeta\left(h; \mathcal{R}_{\epsilon_2}^\beta, \frac{k_4^\beta}{k_8^\beta}\right)}{k_4^\alpha - k_8^\alpha \zeta\left(h; \mathcal{R}_{\epsilon_2}^\alpha, \frac{k_4^\alpha}{k_8^\alpha}\right)} \frac{k_{67}^\alpha \zeta\left(h; \mathcal{R}_{\epsilon_2}^\alpha, \frac{k_4^\alpha}{k_8^\alpha}\right) - k_{23}^\alpha \pm \sqrt{W(h; \mathcal{R}_{\epsilon_2}^\alpha, \frac{k_4^\alpha}{k_8^\alpha})}}{k_{67}^\beta \zeta\left(h; \mathcal{R}_{\epsilon_2}^\beta, \frac{k_4^\beta}{k_8^\beta}\right) - k_{23}^\beta \pm \sqrt{W(h; \mathcal{R}_{\epsilon_2}^\beta, \frac{k_4^\beta}{k_8^\beta})}} \end{cases},$$

and

$$\pi_{\mathcal{R}}(h) = \begin{cases} \zeta\left(h; \frac{k_1^\alpha}{k_5^\alpha}, \mathcal{R}_{\epsilon_2}^\alpha\right) - \zeta\left(h; \frac{k_1^\beta}{k_5^\beta}, \mathcal{R}_{\epsilon_2}^\beta\right) \\ \zeta\left(h; \mathcal{R}_{\epsilon_2}^\alpha, \frac{k_4^\alpha}{k_8^\alpha}\right) - \zeta\left(h; \mathcal{R}_{\epsilon_2}^\beta, \frac{k_4^\beta}{k_8^\beta}\right) \end{cases}.$$

Again, when choosing the appropriate root from $d_{\sigma,h}^{(1,2)}$ it has to be accounted for the hormesis conditions and the relevant segment.

It is evident that the obtained projections of the differential have a more complicated form than in the case for a single dose edge. Also, multiple conditions depending on the ratios between the dose-response coefficients have to be considered. However, the expressions are symbolic and symbolic analysis can be applied.

8.3.4 Two Dose Edge Example: Insulin Receptor Trafficking

For the analysis of the detailed model for insulin receptor trafficking from Sedaghat et al. (2002) (Figure 5.6a), we assume that we measure the singly ligand-bound receptor species on the cell surface, RL and RLp, thus $O = \{v_{RL}, v_{RLp}\}$, and obtain two dose-response curves by stimulating the system with two ligands that differ in their affinity to the receptor— ligand α with reaction rate constants r_1^α, r_2^α, r_{12}^α, r_{13}^α, and ligand β with r_1^β, r_2^β, r_{12}^β, r_{13}^β. Suppose that the dose-response curve for α (reference) is sigmoidal and the curve for β (perturbed) is hormetic (biphasic) (differential as in *Case 2*). We aim to derive the dose differential between the reference curve and the first segment of the perturbed curve at $h = 0.5$, as well as, the response differential between the reference curve and the second segment of the perturbed curve at $d \to \infty$, i.e. $h = 0$.

8.3.4.1 Steady-state coefficients.

For conciseness, we analyse the steady-state coefficients in polynomial form instead of digraph form:

$$\begin{aligned}
k_1 &= 0,\\
k_{23} &= r_1 r_9 r_{11}((r_3 + r_4)(r_6 + r_7) + r_5 r_7)(r_{13}(r_{15} + r_{16}) + r_{14} r_{16}),\\
k_4 &= r_1(r_6 + r_7) r_9 r_{11}\, r_{12}\, r_{14} r_{16},\\
k_5 &= (r_2 + r_3) r_8 r_{10}(r_4(r_6 + r_7) + r_5 r_7)(r_{13}(r_{15} + r_{16}) + r_{14} r_{16}),\\
k_{67} &= r_{10}((r_2 + r_3)(r_6 + r_7) r_8\, r_{12}\, r_{14} r_{16} + r_1 r_3 r_5 r_7(r_{13}(r_{15} + r_{16}) + r_{14} r_{16})),\\
k_8 &= r_1 r_3(r_6 + r_7) r_{10}\, r_{12}\, r_{14} r_{16},
\end{aligned}$$

where the differential parameters are marked in red.

Due to $k_1 = 0$, the only non-hormesis condition holding for the reference curve α is $\frac{k_1}{k_5} = 0 \leq \frac{k_{23}^\alpha}{k_{67}^\alpha} \leq \frac{k_4^\alpha}{k_8^\alpha}$ and the only hormesis condition holding for the perturbed curve β is $\frac{k_1}{k_5} = 0 < \frac{k_4^\beta}{k_8^\beta} < \frac{k_{23}^\beta}{k_{67}^\beta}$. This indicates that the perturbation should flip the inequality sign between the non-zero steady-state coefficient ratios. Also noting

that $\frac{k_4^\alpha}{k_8^\alpha} = \frac{k_4^\beta}{k_8^\beta}$, these conditions enforce the following condition on the parameters:

$$\frac{r_1^\alpha r_3((r_3+r_4)(r_6+r_7)+r_5r_7)(r_{13}^\alpha(r_{15}+r_{16})+r_{14}r_{16})}{(r_2^\alpha+r_3)(r_6+r_7)r_8r_{12}^\alpha r_{14}r_{16}+r_1^\alpha r_3r_5r_7(r_{13}^\alpha(r_{15}+r_{16})+r_{14}r_{16})} \leq 1$$
$$< \frac{r_1^\beta r_3((r_3+r_4)(r_6+r_7)+r_5r_7)(r_{13}^\beta(r_{15}+r_{16})+r_{14}r_{16})}{(r_2^\beta+r_3)(r_6+r_7)r_8r_{12}^\beta r_{14}r_{16}+r_1^\beta r_3r_5r_7(r_{13}^\beta(r_{15}+r_{16})+r_{14}r_{16})}. \quad (8.7)$$

This implies that the values of r_9, r_{10}, and r_{11} (free receptor externalisation, degradation, and synthesis, respectively) do not affect whether or not the response is hormetic.

8.3.4.2 Differential mapping.

We derive the two critical points of the non-hormetic reference curve as:

$$\mathcal{E}^\alpha = \left\{ \epsilon_1^\alpha = (0,0), \epsilon_2^\alpha = \left(\infty, \frac{r_9r_{11}}{r_3r_{10}}\right) \right\}.$$

When deriving the second critical point of the perturbed hormetic curve we comply with the hormesis condition by choosing the root that contains $-\sqrt{U}$, leading to:

$$\mathcal{E}^\beta = \left\{ \epsilon_1^\beta = (0,0), \epsilon_2^\beta = \left(\frac{r_{13}^\beta(r_{15}+r_{16})+r_{14}r_{16}}{r_{12}^\beta r_{14}r_{16}(r_6+r_7)}, \right.\right.$$
$$\frac{r_{12}^\beta r_{14}r_{16}r_8(r_2^\beta+r_3)(r_4(r_6+r_7)+r_5r_7)+\sqrt{U}}{r_1^\beta r_3(r_3+r_4)(r_{13}^\beta(r_{15}+r_{16})+r_{14}r_{16})-r_{12}^\beta r_{14}r_{16}r_8(r_2^\beta+r_3)},$$
$$\frac{r_{11}r_1^\beta r_9(r_{13}^\beta(r_{15}+r_{16})+r_{14}r_{16})}{r_{10}}$$
$$\left.\left. \frac{\begin{array}{r}(r_7(r_3+r_4+r_5)+r_6(r_3+r_4))\Big(r_{12}^\beta r_{14}r_{16}r_8(r_2^\beta+r_3)(r_6+r_7) \\ +r_1^\beta r_3r_5r_7(r_{13}^\beta(r_{15}+r_{16})+r_{14}r_{16})\Big)-2(r_6+r_7)\sqrt{U} \\ -2r_{12}^\beta r_{14}r_{16}r_8(r_2^\beta+r_3)(r_6+r_7)(r_4(r_6+r_7)+r_5r_7)\end{array}}{\Big(r_{12}^\beta r_{14}r_{16}r_8(r_2^\beta+r_3)(r_6+r_7)+r_1^\beta r_3r_5r_7\big(r_{13}^\beta(r_{15}+r_{16})+r_{14}r_{16}\big)\Big)^2-4r_{12}^\beta r_{14}r_{16}r_1^\beta r_3r_8(r_2^\beta+r_3)(r_6+r_7)\big(r_{13}^\beta(r_{15}+r_{16})+r_{14}r_{16}\big)(r_4(r_6+r_7)+r_5r_7)} \right), \right.$$
$$\left. \epsilon_3^\beta = \left(\infty, \frac{r_9r_{11}}{r_3r_{10}}\right) \right\},$$

where $\underline{U}$ denotes U with squared factors taken out of the square root and has the form:

$$\underline{U} = r_{12}^{\beta} r_{14} r_{16} r_3 r_8 (r_2^{\beta} + r_3)(r_4(r_6 + r_7) + r_5 r_7)\Big(- r_{12}^{\beta} r_{14} r_{16} r_8 (r_2^{\beta} + r_3)(r_6 + r_7) + r_1^{\beta}(r_3 + r_4)(r_{13}^{\beta}(r_{15} + r_{16}) + r_{14} r_{16})(r_7(r_3 + r_4 + r_5) + r_6(r_3 + r_4))\Big).$$

This leads to the following observations: (i) the first and last critical points of the reference and perturbed curves are identical; (ii) the last critical points depend only on the four reaction rates r_3, r_9, r_{10}, and r_{11}; and (iii) the dose component of the second critical point of the perturbed system ϵ_2^{β} does not depend on r_9, r_{10}, and r_{11}.

8.3.4.3 Dose and response differentials.

It is straightforward to see that the response differential between the reference curve and the second segment of the perturbed curve at $d \to \infty$ is always zero, independent of the magnitude of the perturbation and of the reaction constants' values:

$$\pi_{\mathcal{R}}\left(h = 0, i = 2\right) = \zeta\left(h = 0; 0, \frac{k_4^{\alpha}}{k_8^{\alpha}}\right) - \zeta\left(h = 0; \mathcal{R}_{\epsilon_2}^{\beta}, \frac{k_4^{\beta}}{k_8^{\beta}}\right) = \frac{r_9 r_{11}}{r_3 r_{10}} - \frac{r_9 r_{11}}{r_3 r_{10}} = 0.$$

The expressions in the previous section also allow us to identify feasible perturbations to alter the dose-response behaviour. For example. if we were to design a new perturbation, different from applying a ligand with modified affinity, that again leads to a hormetic perturbed dose-response, but to a non-zero response differential, it has to target parameters r_9, r_{11},r_3, or r_{10}. However, since hormesis is not affected by r_9, r_{11}, and r_{10}, r_3 needs to be perturbed.

To find the dose differential between the reference curve and the first segment of the perturbed curve with $h = 0.5$, we need to select the appropriate roots from $d_{\sigma,h}^{(1,2)}$. The relevant root for the reference curve is $d_{\sigma,h}^{(1)}$ since it corresponds to non-hormesis condition $\frac{k_1}{k_5} \leq \frac{k_{23}}{k_{67}} \leq \frac{k_4}{k_8}$. Furthermore, when choosing the relevant root, there are two cases of interest: (i) when the roots have different signs we take the larger (positive) root, and (ii) when the two roots are positive we consider the smaller root, which corresponds to the first segment of the hormetic curve. According to the Vietta's formulas, the roots have different signs when $\frac{-k_5^{\beta}\zeta(h;x,y)}{k_4^{\beta} - k_8^{\beta}\zeta(h;x,y)} < 0$, which translates to $k_4^{\beta} - k_8^{\beta}\zeta\left(h; x, y\right) > 0$, indicating that the relevant larger root is $d_{\sigma,h}^{(1)}$. Accordingly, both roots are positive when $-\frac{k_{23}^{\beta} - k_{67}^{\beta}\zeta(h;x,y)}{k_4^{\beta} - k_8^{\beta}\zeta(h;x,y)} > 0$ and $\frac{-k_5^{\beta}\zeta(h;x,y)}{k_4^{\beta} - k_8^{\beta}\zeta(h;x,y)} > 0$, implying $k_4^{\beta} - k_8^{\beta}\zeta\left(h; x, y\right) < 0$ and $k_{23}^{\beta} - k_{67}^{\beta}\zeta\left(h; x, y\right) > 0$. This satisfies the hormesis condition and settles the smaller positive root to be $d_{\sigma,h}^{(1)}$ again.

Thus, we select the root $d^{(1)}_{\sigma,h}$ for the reference and the perturbed curve, which gives:

$$\pi_d\left(h=\frac{1}{2};i=1\right)=\log_{10}\frac{2k_4^\beta-k_8^\beta\mathcal{R}_{\epsilon_2}^\beta}{k_4^\alpha k_8^\alpha}\frac{k_4^\alpha k_{67}^\alpha-2k_{23}^\alpha k_8^\alpha+2k_8^\alpha\sqrt{W(\frac{1}{2};0,\frac{k_4^\alpha}{k_8^\alpha})}}{k_{67}^\beta\mathcal{R}_{\epsilon_2}^\beta-2k_{23}^\beta+2\sqrt{W(\frac{1}{2};0,\mathcal{R}_{\epsilon_2}^\beta)}},$$

with $W(\frac{1}{2};0,y)=\left(\frac{k_{67}y}{2}-k_{23}\right)^2+k_5y\,(2k_4-k_8y)$.

After substituting the steady-state coefficients, we find the symbolic expression for the dose differential. By looking at the greatest common divisor of the separate terms in the numerator and denominator of the expression, again the reaction rate constants r_9, r_{10}, and r_{11} cross out. Therefore, both the dose and the response differential are invariant with respect to these parameters.

8.4 Supplement to Chapter 5

8.4.1 Ternary Complex Stability (TCS) Submodel Components

Below are presented and described the reactions we consider. The reactions are grouped by the mechanisms and the components they comprise.

Basal IFNAR2 synthesis and degradation.

$\varnothing \underset{r_d}{\overset{r_s}{\rightleftharpoons}} R_2$

IFNAR2 (R_2) basal synthesis and degradation reactions. They represent the unstimulated system and are part of every receptor trafficking submodel. Thus their participation in every submodel is implied and not explicitly stated. We assume that the reactions originate from an intracellular compartment different from the later described compartments harbouring the internalised ternary complexes and the receptors dissociated from them.

Ligand-induced ternary complex assembly on the cell surface.

Component id: S^{ω}

$R_2 \underset{r_4^{\chi}}{\overset{d\, r_3^{\chi}}{\rightleftharpoons}} R_2L$

$R_2L \underset{r_6^{\chi}}{\overset{R_1^{\omega}\ r_5^{\chi}}{\rightleftharpoons}} TC$

$TC \xrightarrow{r_7} TCp$

$R_2Lp \underset{r_6^{\chi}}{\overset{R_1^{\omega}\ r_5^{\chi}}{\rightleftharpoons}} TCp$

$R_2p \underset{r_4^{\chi}}{\overset{d\, r_3^{\chi}}{\rightleftharpoons}} R_2Lp$

$R_2p \xrightarrow{r_8} R_2$

$R_2p \xrightarrow{r_d} \varnothing$

$R_2L \xrightarrow{r_d} \varnothing$

$R_2Lp \xrightarrow{r_d} \varnothing$

$TC \xrightarrow{r_d} \varnothing$

Two-step ligand-induced ternary complex assembly and activation as reviewed in Schreiber & Piehler (2015). Usually, the ligand binding affinity to IFNAR2 is high and to IFNAR1 it is low. Thus, interferon ligands (denoted by L and having constant concentration d) predominantly bind to IFNAR2 to form the binary complex R_2L. Then, IFNAR1 (with concentration R_1) is recruited on the membrane to form the ternary complex TC. TC is irreversibly phosphorylated to obtain the active ternary complex TCp. Signalling from the active TCp stops upon dissociation of IFNAR1. However, as hypothesized in Moraga et al. (2009), dissociated binary complexes, here R_2Lp, might continue signalling. We account for IFNAR1's dynamics implicitly by modelling its binding as a pseudo-first order reaction in which R_1 takes a value depending on the type of activity ω. Note that we assume the concentration of R_1 is only activity specific but not ligand specific. This consideration is required to isolate mechanisms causing the α vs β differential since free ligand specific parameters would allow to trivially reproduce it. Further, ligand dependent discrepancies in IFNAR1 levels might be secondary and caused by the mechanisms controlling ternary complex stability. Also, in the modelling framework we account for the cell-to-cell variability of IFNAR2 but not IFNAR1. Note that r_3 and r_4 are the 3D association and dissociation rate constants of the extracellular ligand to IFNAR2 and are thus ligand specific, which is indicated by the dependence on χ. The constants r_5 and r_6 are also ligand specific but describe the 2D association and dissociation rate of the IFNAR2-L binary complex to the free IFNAR1 receptor both located on the cell membrane. We also assume that all species in this component have the same degradation rate constant apart from TCp to whose degradation we refer later.

	Component id: S This component contains the same reactions as component S^{ω} but not the dependence of R_1 on ω.
$R_2 \underset{r_4^{\chi}}{\overset{d\ r_3^{\chi}}{\rightleftharpoons}} R_2L$ $R_2L \underset{r_6^{\chi}}{\overset{R_1^{\omega}\ r_5^{\chi}}{\rightleftharpoons}} TC$ $TC \xrightarrow{r_7} TCp$ $R_2Lp \underset{r_6^{\chi}}{\overset{R_1^{\omega}\ r_5^{\chi}}{\rightleftharpoons}} TCp$ $R_2Lp \xrightarrow{r_8} R_2$ $R_2L \xrightarrow{r_d} \varnothing$ $R_2Lp \xrightarrow{r_d} \varnothing$ $TC \xrightarrow{r_d} \varnothing$	**Component id:** S_1^{ω} This component differs from S^{ω} with regards to the assumption that R_2Lp dephosphorylates and dissociates from the ligand at a single step to obtain free R_2.
	Component id: S_1 This component contains the same reactions as component S_1^{ω} but not the dependence of R_1 on ω.
$R_2 \underset{r_4^{\chi}}{\overset{d\ r_3^{\chi}}{\rightleftharpoons}} R_2L$ $R_2L \underset{r_6^{\chi}}{\overset{R_1^{\omega}\ r_5^{\chi}}{\rightleftharpoons}} TCp$ $R_2L \xrightarrow{r_d} \varnothing$	**Component id:** S_2^{ω} This component assumes a simple two state activation of the ternary complex – first, binding of R_2 to the ligand L to obtain R_2L and subsequent binding to R_1 which directly results to the active ternary complex TCp.
	Component id: S_2 This component contains the same reactions as component S_2^{ω} but not the dependence of R_1 on ω.
$R_2 \underset{r_2^{\chi}}{\overset{d\ r_1^{\chi}}{\rightleftharpoons}} TCp$	**Component id:** S_3 Direct ternary complex activation represented by a single abstract reaction. We assume that ternary complex assembly happens fast after IFNAR2 binds to the ligand and $r_1^{\chi} = r_3^{\chi}, r_2^{\chi} = r_4^{\chi}$. With this component we test whether the crudest ternary complex assembly mechanism has the capacity to explain the observed differential responses.

$TCp \xrightarrow{r_{13}} \varnothing$	**Component id:** $dTCp$ Degradation of the active ternary complex. It is part of the ternary complex assembly mechanisms whenever TCp internalisation in not present.

Inhibition by USP18.

$R_2 \underset{r_{12}}{\overset{u^\omega\ r_{11}}{\rightleftharpoons}} R_2U$ $R_2U \xrightarrow{r_{19}} \varnothing$	**Component id:** I USP18 serves as a late negative expression feedback which inhibits ternary complex formation by binding to the cytoplasmic domain of IFNAR2 (Francois-Newton et al., 2012; Wilmes et al., 2015). We denote USP18 by U and assume its concentration, u, is activity specific. More precisely, u's concentration is low during early signalling events leading to AV and high during late signalling events leading to AP (Schreiber & Piehler, 2015). We assume that IFNAR2 bound to USP18 (species R_2U) is possibly degraded with a different rate than the free R_2.
$R_2L \underset{r_{12}}{\overset{u^\omega\ r_{11}}{\rightleftharpoons}} R_2LU$ $R_2LU \xrightarrow{r_{19}} \varnothing$	**Component id:** I_1 This component contains all reactions from component I plus inhibition reactions for the ligand bound IFNAR2 state R_2L and a degradation reaction of the inhibited state R_2LU. The component can be combined with any surface component apart from component S_3 since it does not contain and intermediate state leading to ternary complex assembly and activation which is to be inhibited.
$R_2U \underset{r_4^\chi}{\overset{d\ r_3^\chi}{\rightleftharpoons}} R_2LU$	**Component id:** I_2 This component contains all reactions from component I_1 plus ligand association and dissociation of the USP18 bound receptor. We assume extracellular ligand affinity to IFNAR2 is not affected by intracellular USP18 binding. The component can also be combined with all surface components apart from S_3.

Ternary complex endocytosis, receptor recycling, endosomal degradation.

$TCp \xrightarrow{r_9} TCpi$ $R_2i \xrightarrow{r_{10}} R_2$ $R_2i \underset{r_2^\chi}{\overset{q\, r_1^\chi}{\rightleftharpoons}} TCpi$ $TCpi \xrightarrow{r_{14}} \varnothing$ $R_2i \xrightarrow{r_{15}} \varnothing$	**Component id:** E Activated ternary complex endocytosis, recycling, and degradation. The activated ternary complex is internalised as $TCpi$ and the free endosomal IFNAR2 receptor R_2i can recycle to the cell surface. We model ternary complex assembly and disassembly in the endosomal compartment, analogously to component S_3, as a one-step reaction. The one-step assembly is a reasonable approximation in the context of the small surface area and volume of individual endosomes which has the capacity to highly concentrate the receptors and lead to instant 2D interactions, e.g. between endosomal IFNAR2-L and IFNAR1. Additionally, we assume a constant ligand concentration q as can be expected in the constant environment within early endosomes (Villaseñor et al., 2015; Schreiber & Piehler, 2015). Endocytosis leads to degradation of R_2i and $TCpi$ and it is also possible that $TCpi$ continues signalling in early endosomes (Marchetti et al., 2006; Claudinon et al., 2007; Marijanovic et al., 2007).
$R_2i \underset{r_{12}}{\overset{u^\omega\, r_{11}}{\rightleftharpoons}} R_2Ui$ $R_2Ui \xrightarrow{r_{18}} \varnothing$	**Component id:** EI Includes the reactions from E plus USP18 inhibition of the free endocytosed IFNAR2 and degradation of the inhibited species.
$R_2Ui \xrightarrow{r_{16}} R_2U$	**Component id:** $EIrI$ Endocytosed USP18-bound receptor recycling to the cell surface.
$R_2Ui \xrightarrow{r_{17}} R_2$	**Component id:** $EIrS$ Endocytosed USP18-bound receptor recycling to the cell surface relevant for submodels which do not incorporate USP18 inhibition at the cell surface.

8.4.2 Two Dose Edge Differential

Single cell threshold model. Analogously to the single dose-edge case we derive the double dose-edge dose differential to be:

$$\pi_d = \log_{10} \frac{K_4^\beta \frac{r_0}{\tau} - k_8^\beta}{K_4^\alpha \frac{r_0}{\tau} - k_8^\alpha} \frac{k_{67}^\alpha - K_{23}^\alpha \frac{r_0}{\tau} \pm \sqrt{(k_{67}^\alpha - K_{23}^\alpha \frac{r_0}{\tau})^2 + 4k_5^\alpha (K_4^\alpha \frac{r_0}{\tau} - k_8^\alpha)}}{k_{67}^\beta - K_{23}^\beta \frac{r_0}{\tau} \pm \sqrt{(k_{67}^\beta - K_{23}^\beta \frac{r_0}{\tau})^2 + 4k_5^\beta (K_4^\beta \frac{r_0}{\tau} - k_8^\beta)}}.$$

Note that hormetic behaviour is possible and thus there could be up to four relevant dose differential expressions.

Population threshold model. We take the first derivative of $\mathcal{R}(d)$ to determine the critical points of the population dose-response relation.

$$D_d\mathcal{R}_{AP}(d) = -D_d\mathcal{R}_{AV}(d) = \frac{-K_{23}k_5 - 2K_4k_5d + (K_{23}k_8 - K_4k_{67})d^2}{d(K_{23}+K_4d)(k_5+k_{67}d+k_8d^2)\sigma\sqrt{2\pi}e^{\frac{\left(\ln\frac{(k_5+k_{67}d+k_8d^2)\tau}{K_{23}d+K_4d^2}-\mu\right)^2}{2\sigma^2}}}.$$

We observe that the numerators of the first derivatives of the population model and of the TCS submodel have identical roots. This indicates the population model and the TCS submodel have the same critical points. As will become clear later, the experimentally obtained population dose-response curves are sigmoid, which suggests that the TCS submodel's dose-response curves should also be sigmoid. Lack of hormesis in the TCS submodel is expressed through the condition $\frac{K_4}{k_8} > \frac{K_{23}}{k_{67}}$ and leads to two critical points:

$$\mathcal{E}_{AV} = \left\{\epsilon_1 = (0,0), \epsilon_2 = \left(\infty, 1-\Phi\left(\frac{\ln\frac{k_8\tau^{AV}}{K_4}-\mu}{\sigma}\right)\right)\right\},$$
$$\mathcal{E}_{AP} = \left\{\epsilon_1 = (0,1), \epsilon_2 = \left(\infty, \Phi\left(\frac{\ln\frac{k_8\tau^{AP}}{K_4}-\mu}{\sigma}\right)\right)\right\}.$$

With only two critical points the dose differential for two-dose edge models has the form:

$$\pi_d = \log_{10}\frac{K_4^\beta\eta_2^{\chi\omega}-k_8^\beta}{K_4^\alpha\eta_2^{\chi\omega}-k_8^\alpha}\frac{k_{67}^\alpha - K_{23}^\alpha\eta_2^{\chi\omega} \pm \sqrt{(k_{67}^\alpha - K_{23}^\alpha\eta_2^{\chi\omega})^2 + 4k_5^\alpha(K_4^\alpha\eta_2^{\chi\omega}-k_8^\alpha)}}{k_{67}^\beta - K_{23}^\beta\eta_2^{\chi\omega} \pm \sqrt{(k_{67}^\beta - K_{23}^\beta\eta_2^{\chi\omega})^2 + 4k_5^\beta(K_4^\beta\eta_2^{\chi\omega}-k_8^\beta)}},$$

where $\eta_2^{\chi\omega}$ is a concise notation for the population receptor function for double dose-edge models:

$$\eta_2\left(\tau^\omega, \mu, \sigma, h, \frac{k_8^{\chi\omega}}{K_4^{\chi\omega}}\right) = \frac{1}{\tau^\omega}e^{\mu-\sigma\sqrt{2}\,\mathrm{erfc}^{-1}\left((1-h)\,\mathrm{erfc}\left(\frac{\mu-\ln\frac{k_8^{\chi\omega}\tau^\omega}{K_4^{\chi\omega}}}{\sigma\sqrt{2}}\right)\right)}.$$

We can also express the response differential as:

$$\pi_{\mathcal{R}}(h) = \begin{cases} (1-h)\left(\Phi\left(\frac{\ln\frac{k_8^{\beta AV}\tau^{AV}}{K_4^{\beta AV}}-\mu}{\sigma}\right) - \Phi\left(\frac{\ln\frac{k_8^{\alpha AV}\tau^{AV}}{K_4^{\alpha AV}}-\mu}{\sigma}\right)\right), & \text{for AV,} \\ (1-h)\left(\Phi\left(\frac{\ln\frac{k_8^{\alpha AP}\tau^{AP}}{K_4^{\alpha AP}}-\mu}{\sigma}\right) - \Phi\left(\frac{\ln\frac{k_8^{\beta AP}\tau^{AP}}{K_4^{\beta AP}}-\mu}{\sigma}\right)\right), & \text{for AP.} \end{cases}$$

Again, in spite of the complicated form of differential expressions we can isolate the effect of the TCS submodels on the population differential. Precisely, two models have the same response differential when they have equal reduced ratios $\frac{k_8^{\chi\omega}}{K_4^{\chi\omega}}$ and have the same dose differential when they have the equal response differential along with equal expressions

$$\frac{K_4^{\beta\omega}c^{\beta\omega} - k_8^{\beta\omega}}{K_4^{\alpha\omega}c^{\alpha\omega} - k_8^{\alpha\omega}} \frac{k_{67}^{\alpha\omega} - K_{23}^{\alpha\omega}c^{\alpha\omega} \pm \sqrt{(k_{67}^{\alpha\omega} - K_{23}^{\alpha\omega}c^{\alpha\omega})^2 + 4k_5^{\alpha\omega}(K_4^{\alpha\omega}c^{\alpha\omega} - k_8^{\alpha\omega})}}{k_{67}^{\beta\omega} - K_{23}^{\beta\omega}c^{\beta\omega} \pm \sqrt{(k_{67}^{\beta\omega} - K_{23}^{\beta\omega}c^{\beta\omega})^2 + 4k_5^{\beta\omega}(K_4^{\beta\omega}c^{\beta\omega} - k_8^{\beta\omega})}},$$

for a fixed activity and where c^χ is regarded as a symbol.

8.4.3 Parameter Prior Information

Table 8.4: Free model parameters and their intervals of definition. Presented are the logarithm of the minimal and maximal bound, denoted as a and b correspondingly, the units, and a short description for each estimated parameter.

	$\log_{10} a$	$\log_{10} b$	Units	Notes
γ	-10	-1	–	On the basis of the available data we assume that the new floor and ceiling values could maximally differ by 10% from the current ones.
τ^{AV}	0	1	number	Few active receptors can trigger AV response (Levin et al., 2011).
τ^{AP}	2	3	number	Most receptors have to be active to trigger AP response (Levin et al., 2011).
R_1^{AV}	-6	0	$\frac{nmol}{m^2}$	The minimum and the maximum R_1^{AV} concentrations correspond to approximately 1 and 6e5 receptors for assumed cell surface area of 1e-9 $\frac{m^2}{cell}$ (Puck et al., 1956).
s_{R_1}	-2	0	$\frac{nmol}{m^2}$	A scaling constant defined through $R_1^{AP} = R_1^{AV} s_{R_1}$ and enforcing $R_1^{AV} \geq R_1^{AP}$ as experimentally observed (Schreiber & Piehler, 2015).
R_1	-6	0	$\frac{nmol}{m^2}$	Activity independent IFNAR1 concentration.
q	2	4	nM	Assuming early endosome volume of 8.2e-18 litres (Howe, 2005) and approx. 1 to 100 interferon ligands per endosome.
$u^{AV} r_{11}$	-6	6	$\frac{1}{s}$	The product of USP18's concentration resulting from the AV activity and the rate constant r_{11} are regarded as a single rate constant with a wide interval of definition.
s_u	0	3	$\frac{1}{s}$	A scaling constant defined through $u^{AP} r_{11} = u^{AV} r_{11} s_u$ and enforcing $u^{AV} r_{11} \leq u^{AP} r_{11}$ as experimentally observed (Schreiber & Piehler, 2015)
r_d,r_7,r_8,r_9, r_{10},r_{12},r_{13}, r_{14},r_{15},r_{16}, r_{17},r_{18},r_{19}	-5	5	$\frac{1}{s}$	Parameters with a wide interval of definition.

8.4.4 Supplementary Results

Table 8.5: The most probable values (MPV), means, standard deviations, and intervals of definition (in logarithmic scale) of the marginal posterior distributions for the 16 free parameters belonging to the highest ranking model. The minimal and maximal bound of the parameter interval of definition are denoted as a and b, correspondingly. Parameter units are shown in Table 8.4.

	$\log_{10}$MPV	$\log_{10}$Mean	$\log_{10}$Std. dev.	$\log_{10} a$	$\log_{10} b$
γ	−1.247	−1.247	0.003	−10	−1
τ^{AV}	0.999	0.951	0.040	0	1
τ^{AP}	2.000	2.009	0.010	2	3
R_1	−0.869	−0.866	0.045	−6	0
q	3.024	3.000	0.577	2	4
$u^{AV} r_{11}$	−3.997	−2.473	1.792	−5	5
s_u	2.999	2.581	0.296	0	3
r_d	−5.000	−4.999	0.001	−5	5
r_7	4.363	2.385	1.541	−5	5
r_8	−5.000	−4.999	0.001	−5	5
r_9	−1.959	−1.906	0.063	−5	5
r_{10}	0.243	0.301	0.581	−5	5
r_{12}	1.241	2.475	1.790	−5	5
r_{14}	−4.366	−4.374	0.010	−5	5
r_{15}	−1.931	−1.933	0.579	−5	5
r_{19}	−2.493	−2.468	1.796	−5	5

Omitted expressions. Symbolic expression for the factors omitted from the derivation of the dose and response population differentials for the top ranking model:

$$F^{\chi}_{K_{23}} = (qr^{\chi}_1 r_{14}+(r_{10}+r_{15})(r_{14}+r^{\chi}_2))r^{\chi}_4 r^{\chi}_6+(qr^{\chi}_1+r_{10}+r_{15})r_9(r^{\chi}_4+R_1 r^{\chi}_5+r_d)(r_8+r_d) + (qr^{\chi}_1 r_{14} + (r_{10} + r_{15})(r_{14} + r^{\chi}_2))(r^{\chi}_4 + R_1 r^{\chi}_5 + r_d)(r_8 + r_d),$$

$$F^{\chi}_{k_4} = qr^{\chi}_1(r_{14}+r_9)+(r_{10}+r_{15})(r_{14}+r^{\chi}_2+r_9),$$

$$F^{\chi\omega}_{k_{67}} = (r_{12} + r_{19}) \Bigg((qr^{\chi}_1 r_{14}+(r_{10}+r_{15})(r_{14}+r^{\chi}_2))r_d(r^{\chi}_6+r_7+r_d)(r_8+r_d)(R_1 r^{\chi}_5 r_9+(r^{\chi}_6+r_9)(r^{\chi}_4+r_d))+ + R_1 r^{\chi}_5 \Big((qr^{\chi}_1 r_14+(r_{10}+r_{15})(r_{14}+r^{\chi}_2))r_d(r_8+r_d)(R_1 r^{\chi}_5 r_9+(r^{\chi}_6+r_9)(r^{\chi}_4+r_d))+ + r_7 \Big(r_{14}(qr^{\chi}_1 + r_{10} + r_{15})(r_9(r^{\chi}_4 + R_1 r^{\chi}_5 + r_d)(r_8 + r_d) + r^{\chi}_6 r_d(r^{\chi}_4 + r_8 + r_d))+ + r^{\chi}_2(r_{15}r_9(r^{\chi}_4 + R_1 r^{\chi}_5 + r_d)(r_8 + r_d) + (r_{10} + r_{15})r^{\chi}_6 r_d(r^{\chi}_4 + r_8 + r_d)) \Big) \Big) \Bigg) + + (qr^{\chi}_1 r_{14} + (r_{10} + r_{15})(r_{14} + r^{\chi}_2))(R_1 r^{\chi}_5 r_9 + (r^{\chi}_6 + r_9)r_d) \Big(R_1 r^{\chi}_5(r_7 + r_d)+ + (r^{\chi}_4 + r_d)(r^{\chi}_6 + r_7 + r_d) \Big)(r_{12}r_d + r_{19}(r_d + u^{\omega}r_{11})),$$

$$F^{\chi}_{K_8} = (qr^{\chi}_1 r_{14} + (r_{10} + r_{15})(r_{14} + r^{\chi}_2))r_d(r^{\chi}_6 + r_7 + r_d)(R_1 r^{\chi}_5 r_9 + (r^{\chi}_6 + r_9)r_d)+ + R_1 r^{\chi}_5 \Bigg(r_{14}(qr^{\chi}_1 + r_{10} + r_{15})(r_7 + r_d)(R_1 r^{\chi}_5 r_9 + (r^{\chi}_6 + r_9)r_d)+ + r^{\chi}_2((r_{10}+r_{15})r_d(R_1 r^{\chi}_5 r_9+(r^{\chi}_6+r_9)r_d)+r_7(R_1 r_{15} r^{\chi}_5 r_9+(r_{10}r^{\chi}_6+r_{15}(r^{\chi}_6+r_9))r_d)) \Bigg),$$

$$k^{\chi\omega}_5 = (r_8 + r_d)(qr^{\chi}_1 r_{14} + (r_{10} + r_{15})(r_{14} + r^{\chi}_2))(R_1 r^{\chi}_5 r_9 + (r^{\chi}_6 + r_9)(r^{\chi}_4 + r_d))\cdot \cdot (R_1 r^{\chi}_5(r_7 + r_d) + (r^{\chi}_4 + r_d)(r^{\chi}_6 + r_7 + r_d))(r_{12}r_d + r_{19}(r_d + u^{\omega}r_{11})).$$

Bibliography

Ahsendorf, T., Wong, F., Eils, R., & Gunawardena, J. (2014). A Framework for Modelling Gene Regulation Which Accommodates Non-Equilibrium Mechanisms. *BMC Biology* 12, 102.

Aigner, M. (1967). On the Linegraph of a Directed Graph. *Mathematische Zeitschrift* 102, 56–61.

Alstrup, S., Harel, D., Lauridsen, P. W., & Thorup, M. (1999). Dominators in Linear Time. *SIAM Journal on Computing* 28, 2117–2132.

Anantharam, V. & Tsoucas, P. (1989). A Proof of the Markov Chain Tree Theorem. *Statistics & Probability Letters* 8, 189–192.

Barabasi, A.-L. & Oltvai, Z. N. (2004). Network Biology: Understanding the Cell's Functional Organization. *Nature Reviews Genetics* 5, 101–113.

Bernardo, J. M. & Smith, A. F. (2001). *Bayesian theory*. IOP Publishing.

Bhalla, U. S. & Iyengar, R. (1999). Emergent Properties of Networks of Biological Signaling Pathways. *Science* 283, 381–387.

Biane, P. (2015). Polynomials Associated with Finite Markov Chains. *In Memoriam Marc Yor-Séminaire de Probabilités XLVII*, 249–262. Springer.

Bogner, C. & Weinzierl, S. (2010). Feynman Graph Polynomials. *International Journal of Modern Physics A* 25, 2585–2618.

Borden, E. C., Sen, G. C., Uze, G., Silverman, R. H., Ransohoff, R. M., Foster, G. R., & Stark, G. R. (2007). Interferons at Age 50: Past, Current and Future Impact on Biomedicine. *Nature Reviews Drug Discovery* 6, 975–990.

Busetto, A. G., Hauser, A., Krummenacher, G., Sunnker, M., Dimopoulos, S., Ong, C. S., Stelling, J., & Buhmann, J. M. (2013). Near-optimal Experimental Design for Model Selection in Systems Biology. *Bioinformatics* 29, 2625.

Calabrese, E., Stanek, E., Nascarella, M., & Hoffmann, G. (2008). Hormesis Predicts Low-Dose Responses Better Than Threshold Models. *International Journal of Toxicology* 27, 369–378.

Calabrese, E. J. & Baldwin, L. A. (2003). Hormesis: the Dose-response Revolution. *Annual Review of Pharmacology and Toxicology* 43, 175–197.

Cha, S. (1968). A Simple Method for Derivation of Rate Equations for Enzyme-catalyzed Reactions under the Rapid Equilibrium Assumption or Combined Assumptions of Equilibrium and Steady State. *Journal of Biological Chemistry* 243, 820–825.

Chou, K.-C. (1993). Graphic Rule for Non-steady-state Enzyme Kinetics and Protein Folding Kinetics. *Journal of Mathematical Chemistry* 12, 97–108.

Chou, K. C. & Forsén, S. (1980). Graphical Rules for Enzyme-catalysed Rate Laws. *Biochemical Journal* 187, 829–835.

Chung, F. & Yang, C. (2000). On Polynomials of Spanning Trees. *Annals of Combinatorics* 4, 13–25.

Claudinon, J., Monier, M., & Lamaze, C. (2007). Interfering with Interferon Receptor Sorting and Trafficking: Impact on Signaling. *Biochimie* 89, 735–743.

Conradi, C., Flockerzi, D., Raisch, J., & Stelling, J. (2007). Subnetwork Analysis Reveals Dynamic Features of Complex (Bio)Chemical Networks. *Proceedings of the National Academy of Sciences USA* 104, 19175–19180.

Cox, C. (1987). Threshold Dose-Response Models in Toxicology. *Biometrics* 43, 511–523.

Craciun, G. & Pantea, C. (2008). Identifiability of Chemical Reaction Networks. *Journal of Mathematical Chemistry* 44, 244–259.

Danos, V., Feret, J., Fontana, W., Harmer, R., & Krivine, J. (2007). *Rule-Based Modelling of Cellular Signalling*, 17–41. Springer Berlin Heidelberg, Berlin, Heidelberg. doi:10.1007/978-3-540-74407-8_3.

De Weerd, N. A. & Nguyen, T. (2012). The Interferons and Their Receptors–Distribution and Regulation. *Immunology and Cell Biology* 90, 483–491.

Di Veroli, G. Y., Fornari, C., Goldlust, I., Mills, G., Koh, S. B., Bramhall, J. L., Richards, F. M., & Jodrell, D. I. (2015). An Automated Fitting Procedure and Software for Dose-response Curves with Multiphasic Features. *Scientific Reports* 5.

Dittrich, A., Quaiser, T., Khouri, C., Görtz, D., Mönnigmann, M., & Schaper, F. (2012). Model-driven Experimental Analysis of the Function of SHP-2 in IL-6-induced Jak/STAT Signaling. *Molecular BioSystems* 8, 2119–2134.

Duffin, R. & Morley, T. (1978). Wang Algebra and Matroids. *IEEE Transactions on Circuits and Systems* 25, 755–762.

Egea, J. A., Henriques, D., Cokelaer, T., Villaverde, A. F., MacNamara, A., Danciu, D.-P., Banga, J. R., & Saez-Rodriguez, J. (2014). MEIGO: an Open-source Software Suite Based on Metaheuristics for Global Optimization in Systems Biology and Bioinformatics. *BMC Bioinformatics* 15, 136.

Elowitz, M. B., Levine, A. J., Siggia, E. D., & Swain, P. S. (2002). Stochastic Gene Expression in a Single Cell. *Science* 297, 1183–1186.

Estrada, J., Wong, F., DePace, A., & Gunawardena, J. (2016). Information Integration and Energy Expenditure in Gene Regulation. *Cell* 166, 234 – 244.

Fersht, A. (1999). *Structure and mechanism in protein science: a guide to enzyme catalysis and protein folding*. Macmillan.

Firmani, D., Georgiadis, L., Italiano, G. F., Laura, L., & Santaroni, F. (2015). Strong Articulation Points and Strong Bridges in Large Scale Graphs. *Algorithmica* 1–25.

Francois-Newton, V., Livingstone, M., Payelle-Brogard, B., Uzé, G., & Pellegrini, S. (2012). USP18 Establishes the Transcriptional and Anti-proliferative Interferon α/β Differential. *Biochemical Journal* 446, 509–516.

Frenk, H. & Schaible, S. (2009). Fractional Programming. *Encyclopedia of Optimization, Second Edition*, 1080–1091. doi:10.1007/978-0-387-74759-0_189.

Friedman, N., Cai, L., & Xie, X. S. (2006). Linking Stochastic Dynamics to Population Distribution: An Analytical Framework of Gene Expression. *Physical Review Letters* 97, 168302.

Fromm, H. J. (1970). A Simplified Schematic Method for Deriving Steady-state Rate Equations Using a Modification of the "Theory of Graphs" Procedure. *Biochemical and Biophysical Research Communications* 40, 692–697.

Gabow, H. N. & Myers, E. W. (1978). Finding All Spanning Trees of Directed and Undirected Graphs. *SIAM Journal on Computing* 7, 280–287.

Gamerman, D. & Lopes, H. F. (2006). *Markov Chain Monte Carlo: Stochastic Simulation for Bayesian Inference*. CRC Press.

Garcia-Sevilla, F., Arribas, E., Bisswanger, H., Garcia-Moreno, M., Garcia-Canovas, F., de Guevara, R. G.-L., Duggleby, R., Yago, J., & Varon, R. (2010). wREFERASS: Rate Equations for Enzyme Reactions at Steady State under MS-Windows. *MATCH Communications in Mathematical and in Computer Chemistry* 63, 553–571.

Gavutis, M., Jaks, E., Lamken, P., & Piehler, J. (2006). Determination of the Two-dimensional Interaction Rate Constants of a Cytokine Receptor Complex. *Biophysical Journal* 90, 3345–3355.

Gems, D. & Partridge, L. (2008). Stress-Response Hormesis and Aging: "That which Does Not Kill Us Makes Us Stronger". *Cell Metabolism* 7, 200–203.

Georgiadis, L., Italiano, G. F., Laura, L., & Parotsidis, N. (2015a). 2-edge Connectivity in Directed Graphs. *Proceedings of the Twenty-Sixth Annual ACM-SIAM Symposium on Discrete Algorithms*, 1988–2005. SIAM.

Georgiadis, L., Italiano, G. F., Laura, L., & Parotsidis, N. (2015b). 2-Vertex Connectivity in Directed Graphs. *Automata, Languages, and Programming*, 605–616. Springer Berlin Heidelberg.

Georgiadis, L., Italiano, G. F., & Parotsidis, N. (2015c). A New Framework for Strong Connectivity and 2-Connectivity in Directed Graphs. *arXiv preprint arXiv:151102913* .

Georgiadis, L., Italiano, G. F., & Parotsidis, N. (2017). *Strong Connectivity in Directed Graphs under Failures, with Applications*, 1880–1899. Proceedings of the Twenty-Eighth Annual ACM-SIAM Symposium on Discrete Algorithms. doi:10.1137/1.9781611974782.123.

Geris, L. & Gomez-Cabrero, D. (2015). *Uncertainty in Biology: a Computational Modeling Approach*, vol. 17. Springer.

Gnad, F., Gunawardena, J., & Mann, M. (2011). PHOSIDA 2011: the Posttranslational Modification Database. *Nucleic Acids Research* 39, D253–D260.

Goentoro, L. & Kirschner, M. W. (2009). Evidence that Fold-Change, and Not Absolute Level, of -Catenin Dictates Wnt Signaling. *Molecular Cell* 36, 872 – 884.

Goltsov, A., Lebedeva, G., Humphery-Smith, I., Goltsov, G., Demin, O., & Goryanin, I. (2010). In Silico Screening of Nonsteroidal Anti-inflammatory Drugs and their Combined Action on Prostaglandin H Synthase-1. *Pharmaceuticals* 3, 2059–2081.

Gunawardena, J. (2012). A Linear Framework for Time-Scale Separation in Nonlinear Biochemical Systems. *PloS ONE* 7, e36321.

Gunawardena, J. (2014). Time-scale Separation–Michaelis and Menten's Old Idea, Still Bearing Fruit. *FEBS Journal* 281, 473–488.

Haario, H., Laine, M., Mira, A., & Saksman, E. (2006). DRAM: Efficient Adaptive MCMC. *Statistics and Computing* 16, 339–354.

Hertzog, P. J. & Williams, B. R. (2013). Fine Tuning Type I Interferon Responses. *Cytokine & Growth Factor Reviews* 24, 217 – 225. Special Issue: CGFR Focus on Research in Australia.

Hothi, P., Sutcliffe, M., & Scrutton, N. (2005). Kinetic Isotope Effects and Ligand Binding in PQQ-Dependent Methanol Dehydrogenase. *Biochemical Journal* 388, 123–133.

Howe, C. (2005). Modeling the Signaling Endosome Hypothesis: Why a Drive to the Nucleus is Better than a (Random) Walk. *Theoretical Biology and Medical Modelling* 2, 43.

Indge, K. J. & Childs, R. (1976). A New Method for Deriving Steady-state Rate Equations Suitable for Manual or Computer Use. *Biochemical Journal* 155, 567–570.

Italiano, G., Laura, L., & Santaroni, F. (2012). Finding Strong Bridges and Strong Articulation Points in Linear Time. *Theoretical Computer Science* 447, 74–84.

Ivashkiv, L. B. & Donlin, L. T. (2014). Regulation of Type I Interferon Responses. *Nature Reviews Immunology* 14, 36–49.

Jaitin, D., Roisman, L., Jaks, E., Gavutis, M., Piehler, J., Van der Heyden, J., Uze, G., & Schreiber, G. (2006). Inquiring into the Differential Action of Interferons (IFNs): an IFN-α 2 Mutant with Enhanced Affinity to IFNAR1 is Functionally Similar to IFN-β. *Molecular and Cellular Biology* 26, 1888.

Jaks, E., Gavutis, M., Uzé, G., Martal, J., & Piehler, J. (2007). Differential Receptor Subunit Affinities of Type I Interferons Govern Differential Signal Activation. *Journal of Molecular Biology* 366, 525–539.

Jaynes, E. T. (2003). *Probability Theory: The Logic of Science*. Cambridge University Press.

Jefferys, W. H. & Berger, J. O. (1991). Sharpening Ockham's Razor on a Bayesian Strop. *Dept Statistics, Purdue Univ, West Lafayette, IN, Tech Rep* .

Jeong, J. & Berman, P. (2008). On Cycles in the Transcription Network of Saccharomyces Cerevisiae. *BMC Systems Biology* 2, 1–11.

Jibetean, D. & de Klerk, E. (2006). Global Optimization of Rational Functions: a Semidefinite Programming Approach. *Mathematical Programming* 106, 93–109.

Kalie, E., Jaitin, D., Podoplelova, Y., Piehler, J., & Schreiber, G. (2008). The Stability of the Ternary Interferon-receptor Complex Rather Than the Affinity to the Individual Subunits Dictates Differential Biological Activities. *Journal of Biological Chemistry* 283, 32925.

Kapoor, S. & Ramesh, H. (2000). An Algorithm for Enumerating All Spanning Trees of a Directed Graph. *Algorithmica* 27, 120–130.

Kass, R. E. & Raftery, A. E. (1995). Bayes Factors. *Journal of the American Statistical Association* 90, 773–795.

King, E. L. & Altman, C. (1956). A Schematic Method of Deriving the Rate Laws for Enzyme-catalyzed Reactions. *The Journal of Physical Chemistry* 60, 1375–1378.

Kirchhoff, G. (1847). Über die Auflösung der Gleichungen, auf welche man bei der Untersuchung der linearen Verteilung galvanischer Ströme geführt wird. *Annalen der Physik* 148, 497–508.

Kirk, P., Thorne, T., & Stumpf, M. P. (2013). Model Selection in Systems and Synthetic Biology. *Current Opinion in Biotechnology* 24, 767 – 774. Nanobiotechnology Systems biology.

Kitano, H. (2002). Systems Biology: A Brief Overview. *Science* 295, 1662–1664.

Koshland Jr, D., Nemethy, G., & Filmer, D. (1966). Comparison of Experimental Binding Data and Theoretical Models in Proteins Containing Subunits. *Biochemistry* 5, 365–385.

Kreutz, C. & Timmer, J. (2009). Systems Biology: Experimental Design. *FEBS Journal* 276, 923–942.

Lam, C. & Priest, D. (1972). Enzyme Kinetics: Systematic Generation of Valid King-Altman Patterns. *Biophysical Journal* 12, 248–256.

Lane, P. (1996). Generalized Nonlinear Models. Prat, A. (editor), *COMPSTAT*, 331–336. Physica-Verlag HD. doi:10.1007/978-3-642-46992-3_42.

Lauffenburger, D. A. & Linderman, J. (1993). *Receptors: Models for Binding, Trafficking, and Signaling*. Oxford University Press.

Leighton, F. & Rivest, R. (1986). The Markov Chain Tree Theorem. Tech. rep., MIT/LCS/TM-249, Laboratory for Computer Science, MIT, Cambridge, Mass., 1983. Also in IEEE Transactions on Information Theory, IT-37 (6).

Levin, D., Harari, D., & Schreiber, G. (2011). Stochastic Receptor Expression Determines Cell Fate Upon Interferon Treatment. *Molecular and Cellular Biology* 31, 3252.

Levine, L. (2011). Sandpile groups and spanning trees of directed line graphs. *Journal of Combinatorial Theory, Series A* 118, 350–364.

MacKay, D. J. (2003). *Information Theory, Inference and Learning Algorithms*. Cambridge University Press.

Maiwald, T., Schneider, A., Busch, H., Sahle, S., Gretz, N., Weiss, T. S., Kummer, U., & Klingmüller, U. (2010). Combining Theoretical Analysis and Experimental Data Generation Reveals IRF9 as a Crucial Factor for Accelerating Interferon α-induced Early Antiviral Signalling. *FEBS Journal* 277, 4741–4754.

Marchetti, M., Monier, M., Fradagrada, A., Mitchell, K., Baychelier, F., Eid, P., Johannes, L., & Lamaze, C. (2006). Stat-mediated Signaling Induced by Type I and Type II Interferons (IFNs) is Differentially Controlled Through Lipid Microdomain Association and Clathrin-dependent Endocytosis of IFN Receptors. *Molecular Biology of the Cell* 17, 2896–2909.

Marijanovic, Z., Ragimbeau, J., Uze, G., & Pellegrini, S. (2007). Comparable Potency of IFNα2 and IFNβ on Immediate JAK/STAT Activation but Differential Down-regulation of IFNAR2. *The Biochemical Journal* 407, 141.

Mattson, M. & Calabrese, E. (2009). *Hormesis: A Revolution in Biology, Toxicology and Medicine*. SpringerLink: Springer e-Books. Humana Press.

Mattson, M. P. (2008). Hormesis Defined. *Ageing research reviews* 7, 1–7.

Meunier, D., Lambiotte, R., & Bullmore, E. T. (2010). Modular and Hierarchically Modular Organization of Brain Networks. *Frontiers in Neuroscience* 4.

Mihaľák, M., Uznański, P., & Yordanov, P. (2016). Prime Factorization of the Kirchhoff Polynomial: Compact Enumeration of Arborescences. *Proceedings of the Thirteenth Workshop on Analytic Algorithmics and Combinatorics (ANALCO 2016)*, 93–105. Society for Industrial and Applied Mathematics Publications, Philadelphia, PA.

Mirzaev, I. & Bortz, D. M. (2015). Laplacian Dynamics with Synthesis and Degradation. *Bulletin of Mathematical Biology* 77, 1013–1045.

Mirzaev, I. & Gunawardena, J. (2013). Laplacian Dynamics on General Graphs. *Bulletin of Mathematical Biology* 75, 2118–2149.

Molinelli, E. J., Korkut, A., Wang, W., Miller, M. L., Gauthier, N. P., Jing, X., Kaushik, P., He, Q., Mills, G., Solit, D. B., Pratilas, C. A., Weigt, M., Braunstein, A., Pagnani, A., Zecchina, R., & Sander, C. (2013). Perturbation Biology: Inferring Signaling Networks in Cellular Systems. *PLOS Computational Biology* 9, 1–23.

Moore, R. E. & Bierbaum, F. (1979). *Methods and Applications of Interval Analysis*, vol. 2. SIAM.

Moraga, I., Harari, D., Schreiber, G., Uzé, G., & Pellegrini, S. (2009). Receptor Density is Key to the $\alpha 2/\beta$ Interferon Differential Activities. *Molecular and Cellular Biology* 29, 4778–4787.

Moraga, I., Spangler, J., Mendoza, J. L., & Garcia, K. C. (2014). Chapter One - Multifarious Determinants of Cytokine Receptor Signaling Specificity. vol. 121 of *Advances in Immunology*, 1 – 39. Academic Press. doi:http://dx.doi.org/10.1016/B978-0-12-800100-4.00001-5.

Muller, P. Y. & Milton, M. N. (2012). The determination and interpretation of the therapeutic index in drug development. *Nature reviews Drug discovery* 11, 751–761.

Nakamura, M. & Iri, M. (1980). On the Decomposition of a Directed Graph with Respect to Arborescences and Related Problems (Graphs and Combinatorics III). *RIMS Kokyuroku* 397, 104–118.

Nakano, T., Doi, T., Yoshimoto, J., & Doya, K. (2010). A Kinetic Model of Dopamine- and Calcium-dependent Striatal Synaptic Plasticity. *PLOS Computational Biology* 6, e1000670.

Narkawicz, A., Garloff, J., Smith, A. P., & Munoz, C. A. (2012). Bounding the Range of a Rational Function Over a Box. *Reliable Computing* 17, 35.

Otero-Muras, I., Yordanov, P., & Stelling, J. (2016). Chemical Reaction Network Theory Elucidates Sources of Multistability in Interferon Signaling. *PLOS Computational Biology, accepted* .

Pannala, V. R., Bazil, J. N., Camara, A. K. S., & Dash, R. K. (2013). A Biophysically Based Mathematical Model for the Catalytic Mechanism of Glutathione Reductase. *Free Radical Biology and Medicine* 65, 1385–1397.

Piehler, J., Thomas, C., Garcia, K. C., & Schreiber, G. (2012). Structural and Dynamic Determinants of Type I Interferon Receptor Assembly and Their Functional Interpretation. *Immunological Reviews* 250, 317–334.

Poland, D. (1989). King-Altman-Hill Diagram Method for Open Systems. *The Journal of Physical Chemistry* 93, 3605–3612.

Puck, T., Marcus, P., & Cieciura, S. (1956). Clonal Growth of Mammalian Cells In Vitro: Growth Characteristics of Colonies from Single HeLa Cells with a "Feeder Layer". *The Journal of Experimental Medicine* 103, 273–284.

Qi, F., Dash, R. K., Han, Y., & Beard, D. A. (2009). Generating Rate Equations for Complex Enzyme Systems by a Computer-assisted Systematic Method. *BMC Bioinformatics* 10, 238.

Raghavendra Rao, B. & Jayalal Sarma, M. (2011). On the Complexity of Matroid Isomorphism Problem. *Theory of Computing Systems* 49, 246–272.

Rand, U., Rinas, M., Schwerk, J., Nöhren, G., Linnes, M., Kröger, A., Flossdorf, M., Kály-Kullai, K., Hauser, H., Höfer, T. et al. (2012). Multi-layered Stochasticity and Paracrine Signal Propagation Shape the Type-I Interferon Response. *Molecular Systems Biology* 8, 584.

Sachse, F. B., Glänzel, K., & Seemann, G. (2003). Modeling of Protein Interactions Involved in Cardiac Tension Development. *International Journal of Bifurcation and Chaos* 13, 3561–3578.

Schneider, W. M., Chevillotte, M. D., & Rice, C. M. (2014). Interferon-stimulated Genes: a Complex Web of Host Defenses. *Annual Review of Immunology* 32, 513.

Schreiber, G. & Piehler, J. (2015). The Molecular Basis for Functional Plasticity in Type I Interferon Signaling. *Trends in Immunology* 36, 139 – 149.

Sedaghat, A. R., Sherman, A., & Quon, M. J. (2002). A Mathematical Model of Metabolic Insulin Signaling Pathways. *American Journal of Physiology-Endocrinology and Metabolism* 283, E1084–E1101.

Shin, I., Kim, J., Cantor, C., & Kang, C. (2000). Effects of Saturation Mutagenesis of the Phage SP6 Promoter on Transcription Activity, Presented by Activity Logos. *Proceedings of the National Academy of Sciences* 97, 3890–3895.

Smith, A. P., Muñoz, C. A., Narkawicz, A. J., & Markevicius, M. (2015). Kodiak: An Implementation Framework for Branch and Bound Algorithms .

Sunnåker, M., Zamora-Sillero, E., Dechant, R., Ludwig, C., Busetto, A. G., Wagner, A., & Stelling, J. (2013). Automatic Generation of Predictive Dynamic Models Reveals Nuclear Phosphorylation as the Key Msn2 Control Mechanism. *Science Signaling* 6, ra41–ra41.

Sunnåker, M. A. (2013). *Computational Methods for Automated Construction and Analysis of Dynamical Models of Biochemical Systems*. Ph.D. thesis, Diss., Eidgenössische Technische Hochschule ETH Zürich, Nr. 21485, 2013.

Tallarida, R. & Jacob, L. S. (2012). *The DoseResponse Relation in Pharmacology*. Springer Science & Business Media.

Tarjan, R. (1972). Depth-first Search and Linear Graph Algorithms. *SIAM Journal on Computing* 1, 146–160.

Thomson, M. & Gunawardena, J. (2009). The Rational Parameterisation Theorem for Multisite Post-translational Modification Systems. *Journal of Theoretical Biology* 261, 626–636.

Titi, J., Hamadneh, T., & Garloff, J. (2015). *Modelling, Computation and Optimization in Information Systems and Management Sciences: Proceedings of the 3rd International Conference on Modelling, Computation and Optimization in Information Systems and Management Sciences - MCO 2015 - Part I*, chap. Convergence of the Simplicial Rational Bernstein Form, 433–441. Springer International Publishing, Cham. doi:10.1007/978-3-319-18161-5_37.

Toni, T. & Stumpf, M. P. (2010). Simulation-based Model Selection for Dynamical Systems in Systems and Population Biology. *Bioinformatics* 26, 104–110.

Tutte, W. T. (1948). The Dissection of Equilateral Triangles into Equilateral Triangles. *Mathematical Proceedings of the Cambridge Philosophical Society*, vol. 44, 463–482. Cambridge University Press.

Uno, T. (1996). An Algorithm for Enumerating All Directed Spanning Trees in a Directed Graph. Asano, T., Igarashi, Y., Nagamochi, H., Miyano, S., & Suri, S. (editors), *Algorithms and Computation*, vol. 1178 of *LNCS*, 166–173. Springer. doi:10.1007/BFb0009492.

van Wijk, R., Tans, S. J., ten Wolde, P. R., & Mashaghi, A. (2015). Non-monotonic Dynamics and Crosstalk in Signaling Pathways and Their Implications for Pharmacology. *Scientific Reports* 5, 11376.

Varon, R., Garcia-Sevilla, F., Garcia-Moreno, M., Garcia-Canovas, F., Peyro, R., & Duggleby, R. G. (1997). Computer Program for the Equations Describing the Steady State of Enzyme Reactions. *Computer Applications in the Biosciences: CABIOS* 13, 159–167.

Villaseñor, R., Nonaka, H., Del Conte-Zerial, P., Kalaidzidis, Y., & Zerial, M. (2015). Regulation of EGFR Signal Transduction by Analogue-to-digital Conversion in Endosomes. *Elife* 4, e06156.

Viswanathan, S., Benatar, T., Rose-John, S., Lauffenburger, D. A., & Zandstra, P. W. (2002). Ligand/Receptor Signaling Threshold (LIST) Model Accounts for gp130-Mediated Embryonic Stem Cell Self-Renewal Responses to LIF and HIL-6. *Stem Cells* 20, 119–138.

Volkenstein, M. & Goldstein, B. (1966). A New Method for Solving the Problems of the Stationary Kinetics of Enzymological Reactions. *Biochimica et Biophysica Acta (BBA) - General Subjects* 115, 471 – 477.

Vyshemirsky, V. & Girolami, M. A. (2008). Bayesian Ranking of Biochemical System Models. *Bioinformatics* 24, 833–839.

Walter, E., Norton, J., Piet-Lahanier, H., & Milanese, M. (1996). *Bounding Approaches to System Identification*. Perseus Publishing.

Weinzierl, S. (2013). *Feynman Graphs*, 381–406. Springer Vienna, Vienna. doi: 10.1007/978-3-7091-1616-6_16.

Wilkinson, D. J. (2007). Bayesian Methods in Bioinformatics and Computational Systems Biology. *Briefings in Bioinformatics* 8, 109–116.

Wilmes, S., Beutel, O., Li, Z., Francois-Newton, V., Richter, C. P., Janning, D., Kroll, C., Hanhart, P., Hötte, K., You, C., Uzé, G., Pellegrini, S., & Piehler, J. (2015). Receptor Dimerization Dynamics as a Regulatory Valve for Plasticity of Type I Interferon Signaling. *The Journal of Cell Biology* 209, 579–593.

Yordanov, P., Otero-Muras, I., & Stelling, J. (2017). A Minimal Model of Differential Type I Interferon Signalling. *Working Paper* .

Yordanov, P. & Stelling, J. (2017a). Kirchpy: Efficient Manipulation and Compact Generation of Expressions of Kirchhoff polynomials. *Working Paper* .

Yordanov, P. & Stelling, J. (2017b). Steady-State Differential Dose-Response in Laplacian Models of Biological Systems. *Working Paper* .

Zamora-Sillero, E., Hafner, M., Ibig, A., Stelling, J., & Wagner, A. (2011). Efficient Characterization of High-dimensional Parameter Spaces for Systems Biology. *BMC Systems Biology* 5, 142.